Exploring structural/functional relationship in Type II NADH:quinone oxidoreductases

Filipa Vaz Sena

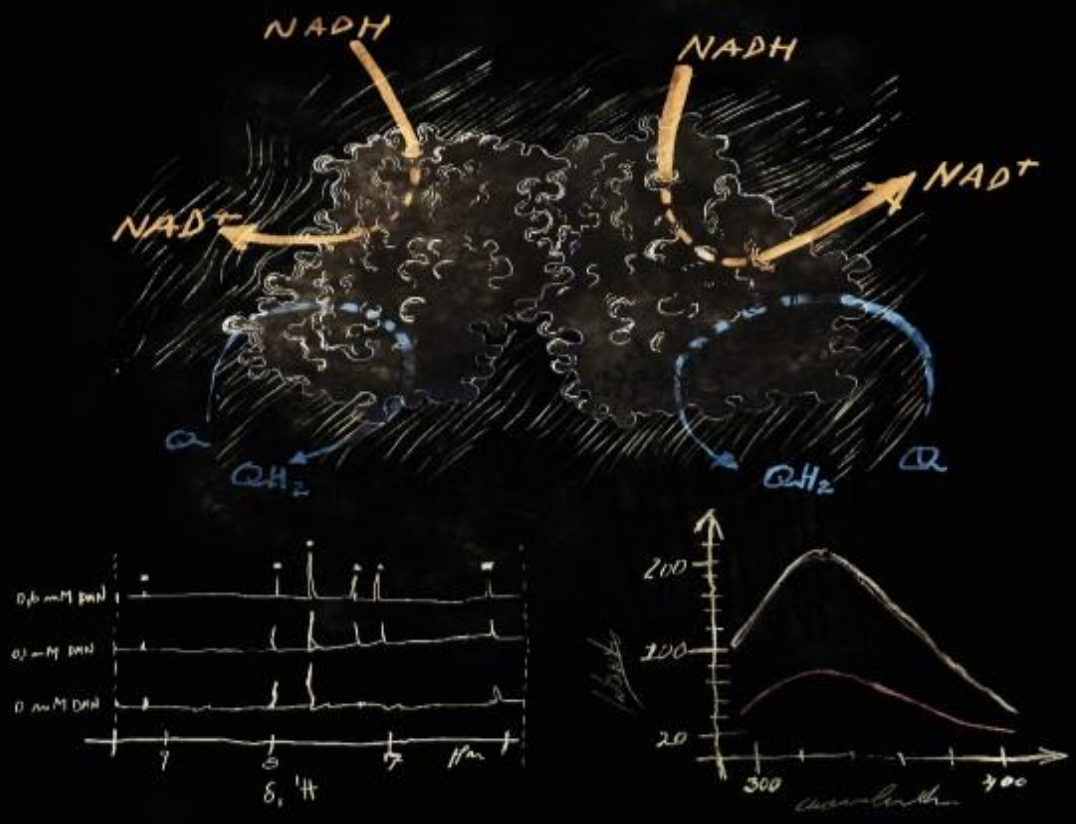

Dissertation presented to obtain the Ph.D degree in Molecular Biosciences

Instituto de Tecnologia Química e Biológica António Xavier | Universidade Nova de Lisboa

Oeiras,
October, 2020

UNIVERSIDADE NOVA DE LISBOA

Exploring structural/functional relationship in Type II NADH:quinone oxidoreductases

Filipa Vaz Sena

Dissertation presented to obtain the Ph.D degree in Molecular Biosciences

Instituto de Tecnologia Química e Biológica António Xavier | Universidade Nova de Lisboa

Oeiras, October, 2020

Financial support from *Fundação para a Ciência e a Tecnologia* through grant PD/BD/113985/2015 awarded to Filipa Sena under the auspices of the MolBioS PhD program (PD/00133/2012).

Cover image: *Paulo Alcobia*

Protein-substrate interactions in *Staphylococcus aureus* NDH-2. This cartoon was the cover image of the Molecular Microbiology Journal, Volume 98, Number 2.

Supervisor: *Prof. Manuela M. Pereira*

Acknowledgments

This Ph.D would not have been possible without the contribution of several people who accompanied me during this journey and whom I want to thank.

Among the people who contributed most to this work, there is undoubtedly my supervisor Prof. Manuela Pereira, without whom none of this would be possible. Thank you for receiving me in your laboratory, for your trust and friendship, for taking me to the scientists' “vacation camp” in the United States but most of all thank you for the patience and availability to teach, support, always pushing me to be a better scientist and person.

To Prof. Miguel Teixeira for welcoming me in the laboratory, for the shared knowledge, advices, and scientific discussions.

To Prof. Teresa Catarino for all the hours spent in the stopped flow room, "shooting" and discussing electron transfer but also rambling about life and laughing out loud. Thank you for your friendship and for the endless scientific discussions and for the enzymology classes even in pandemic times.

To Dr. Mariana Pinho for her interest towards my work, for hosting me in her laboratory, *Bacterial Cell Biology*, a period that it should have been a couple of months, but it ended in a strong collaboration with very profitable scientific discussions. A special thanks to Raquel Pereira for her availability and sympathy, who taught me the hard work of cloning *Staphylococcus aureus*.

To Prof. Eurico Cabrita for explaining me all the details about NMR and for showing me how “scary” techniques can be surprising. To Prof. Margarida Bastos for welcoming me in her laboratory at *Faculdade de Ciências Universidade do Porto*, helpful scientific inputs, and discussions regarding protein-substrate interactions.

To the members of the PhD dissertation committee Dr. Mariana Pinho and Dr. Lígia Martins for generously offering their time and guidance.

To Isabel Pacheco for all the help in protein purification, for saving my days when the anaerobic chamber was full of oxygen and for her kind words in our daily routine.

To João Carita, for growing infinite liters of cells and doing the hard part of breaking the cells and for his friendship.

To former colleagues and friends of the Metalloproteins and Bioenergetics Unit. A special thanks to Ana Paula who welcomed me into the laboratory as her student and with whom I learned a lot, her dedication, intelligence, commitment, and friendship will never be forgotten. To Bruno Marreiros for the great moments in the laboratory, for the sports and beers outside the ITQB, but mainly for his continuous scientific criticism and for his "Chinese" helping in bioinformatics.

To all "my" students, with whom I have shared my passion for science and who helped me in my project but above all contributed to my growth as a person and as a scientist. Thank you Joana Gonçalves, Tatiana Pires, Gonçalo Piedade, Mariana Carmona and Hugo Ferreira.

To my present friends and colleagues from the Bioenergetics Lab: Filipe Sousa, Patricia Refojo, Filipa Calisto, Diana Duarte, Inna Uliyakina, and Andreia Barreto. A special thanks to Patrícia for her critical spirit, for all the lunches together and for all the good moments shared about our girls. To Filipe Sousa, my partner in crime, who started out as "my" student, and I ended up learning a lot from him. Thank you for always look to our results with criticism, for the endless scientific and non-scientific discussions and for always having time to listen to my complaints.

To my friends from the MolBioS classes, Eleonora, Maika, Joana, Catarina and Sara for sharing with me the best moments of this journey, I will never forget that weekend in Foz do Arelho. To Eleonora the best of this Ph.D, a colleague who quickly became a close friend, thank you for all the moments we shared, for being a drama queen like me, for the best carbonara I've ever eaten, grazie mille e non dimenticare che andrà tutto bene.

To all my friends far from the science world: Blanca, Ana, Filipa, Margarida, Vaz, Pipa, Maria Inês, Sara, Teresinha, Hélia, Tété, Ju, Leonor e Maia, obrigada por estarem sempre aí, nos bons e nos maus momentos, por fazerem parte deste meu percurso e me ensinarem a viver a vida.

Por fim quero agradecer à minha família, o meu pilar, aos presentes e aos ausentes. Obrigada Tia Margarida pelos conselhos, pela ajuda na escrita, pelo apoio incondicional e pela amizade que nos une. Ao meu irmão, Miguel, o meu melhor amigo, que mesmo longe e no meio dos oceanos esteve sempre por perto, sempre atento e disponível para me ajudar.

Aos meus pais, as pessoas a quem eu devo tudo o que tenho, obrigada por me apoiarem, por sobretudo me ouvirem e por acreditarem em mim, sou fruto da educação que me deram e do que construímos juntos.

Ao Pedro e à Carlota, a minha família, obrigada Pedro por me ouvires, por seres o meu porto seguro, por seres um marido e pai incrível e por me ajudares a ultrapassar os momentos difíceis e sempre apoiares todas as minhas decisões.

Thesis Publications

This thesis is based on the following publications:

- ✓ Rosário AL*, **Sena FV***, Batista AP, Athayde D, Oliveira TF, Pereira MM, Brito JA, Archer M. Expression, purification, crystallization and preliminary X-ray diffraction analysis on a type-II NADH:quinone oxidoreductase from the human pathogen *Staphylococcus aureus*. *Acta Crystallogr F Struct Biol Commun.* (2015) Apr; 71(Pt 4):477-82. Doi: 10.1107/S2053230X15005178.

- ✓ **Sena FV**, Batista AP, Catarino T, Brito JA, Archer M, Viertler M, Madl T, Cabrita EJ, Pereira, MM. Type-II NADH:quinone oxidoreductase from *Staphylococcus aureus* has two distinct binding sites and is rate limited by quinone reduction. *Mol Microbiol.* 98 (2015) 272–288. Doi: 10.1111/mmi.13120.

- ✓ Marreiros CM, Calisto F, Castro PJ, Duarte AM, **Sena FV,** Silva AF, Sousa FM, Teixeira M, Refojo PN, Pereira MM. Exploring membrane respiratory chains. *BBA bioenergetics*. (2016). Doi: 10.1016/j.bbabio.2016.03.028.

- ✓ Marreiros BC, **Sena FV**, Sousa FM, Batista AP, Pereira MM. Type II NADH:quinone oxidoreductase family: phylogenetic distribution, structural diversity and evolutionary divergences. *Environ Microbiol*. (2016). Doi: 10.1111/1462-2920.13352.

- ✓ Marreiros BC, **Sena FV**, Sousa FM, Oliveira AS, Soares CM, Batista AP, Pereira MM. Structural and Functional insights into the catalytic mechanism of the Type II NADH:quinone oxidoreductase family. *Sci Rep.* 7 (2017) 42303. Doi: 10.1038/srep42303.

- ✓ Sousa FM, **Sena FV**, Batista AP, Athayde D, Brito JA, Archer M, Oliveira ASF, Soares CM, Catarino T, Pereira MM. The key role of glutamate 172 in the mechanism of type II NADH:quinone oxidoreductase of Staphylococcus aureus. *Biochim. Biophys. Acta - Bioenerg*. 1858 (2017) 823–832. Doi: 10.1016/j.bbabio.2017.08.002.

- ✓ **Sena FV**, Sousa FM, Oliveira ASF, Soares CM, Catarino T, Pereira MM. Regulation of the mechanism of Type-II NADH: Quinone oxidoreductase from *S. aureus*. *Redox Biol*. (2018) 16:209-214. Doi: 10.1016/j.redox.2018.02.004

- ✓ Refojo PN*, **Sena FV***, Calisto F*, Sousa FM*, Pereira MM. The plethora of membrane respiratory chains in the phyla of life. *Adv Microb Physiol.* (2019). Doi: 10.1016/bs.ampbs.2019.03.002.

Publications not included in this thesis:

- ✓ Salewski J, Batista AP, **Sena FV**, Millo D, Zebger I, Pereira MM, Hildebrandt P. Substrate-Protein Interactions of Type II NADH:Quinone Oxidoreductase from Escherichia coli. *Biochemistry*. (2016). Doi: 10.1021/acs.biochem.6b00070

- ✓ Stevanović S, Perdih A, Senćanski M, Glišić S, Duarte M, Tomás AM, **Sena FV**, Sousa FM, Pereira MM, Solmajer T. In Silico Discovery of a Substituted 6-Methoxy-quinalidine with Leishmanicidal Activity in Leishmania infantum. *Molecules.* (2018). Doi: 10.3390/molecules23040772.

* Equally contributing authors.

Thesis outline

This thesis covers six chapters detailing studies on the Type II NADH:quinone oxidoreductases (NDH-2s) from *Staphylococcus aureus*.

The first chapter provides an overview on respiratory chains once NDH-2s are enzymes that are part of it in several organisms. Some representative respiratory chains are illustrated and discussed based on bioinformatic analyses and on the available biochemical studies. Emphasis on *S. aureus* respiratory chain is given since the NDH-2s under study are from this pathogen. A brief introduction is made to NDH-2 family, the object of study of this work.

The expression, purification, and biochemical characterization of the two NDH-2s from *S. aureus* (NDH-2A and NDH-2B) is described in chapter two. Briefly both genes coding for the NDH-2s were individually cloned and expressed in *Escherichia coli* under aerobic conditions. The recombinant proteins were purified and biochemically characterized through distinct methodologies including sequence analysis, cyclic voltammetry, circular dichroism and UV visible spectroscopy.

Structural insights into both type II NAD(P)H:quinone oxidoreductases are given in chapter three by the crystal and solution structures of NDH-2A enzyme, obtained by X-ray crystallography and small-angle X-ray scattering. Since the crystal structure of NDH-2B still remains to be obtained, the structural model of this protein is presented, and structural features are compared with those of NDH-2A. Additionally, protein-substrate interaction studies of the two NDH-2s, with NAD(P)H/$NAD(P)^+$ or quinones, were analyzed by fluorescence and saturation transfer difference NMR spectroscopies.

The catalytic mechanism of NDH-2 is controversially discussed within the Bioenergetics community. In the fourth chapter we investigate the catalytic mechanism of both NDH-2s from *S. aureus*, the reaction transfer rates are

discussed, and reaction intermediates identified. An extensive kinetic study is shown, using steady-state and fast kinetics methodologies. Moreover, the mechanism of NDH-2s is further explored by investigating the common elements of all NDH-2s, based on the rationale that conservation of such elements reflects their structural/functional importance. Based on this last data, site-directed mutagenesis of glutamate 172 in NDH-2A protein was performed and the biochemical characterization of the enzyme's variants is presented.

The cellular role of the two NDH-2s is described in chapter five, which was investigated by constructing knockout mutants of the genes coding for both enzymes (Δ*ndh-2a* and Δ*ndh-2b*). Cell growth analysis and NMR-based metabolomics were used to study the generated mutants and to inspect whether the absence of each enzyme have the same impact in *S. aureus* metabolism. Moreover, to study NDH-2A and NDH-2B localization *S. aureus* strains were constructed expressing a *ndh-2a*-mNeonGreen and a *ndh-2b*-mNeonGreen and these fusions were analyzed by microscopy.

In Chapter 6 the main conclusions will be described, and future perspectives will be discussed.

Abbreviations and Acronyms

ACIII	Alternative complex III
Ag/AgCl	Silver chloride electrode
AIF-M2/AMID	Apoptosis-inducing factor-homologous mitochondrion-associated inducer of death
AOX	Alternative oxygen reductase
ATP	Adenosine triphosphate
BCA	Bicinchoninic Acid Protein Assay
BLAST	Basic local alignment search tool
BN-PAGE	Blue native polyacrylamide gel electrophoresis
BSA	Bovine serum albumin
Complex I	Type I NADH:quinone oxidoreductase
Complex II	Succinate:quinone oxidoreductase
Complex III	Cytochrome bc_1/b_6f complex
Complex IV	Cytochrome *c* oxidase
CV	Cyclic voltammetry
Cyt c	Cytochrome *c*
DDB	2,3-Dimethoxy-5,6-dimethyl-p-benzoquinone
DHOQO	Dihydroorotate:quinone oxidoreductase
DMN	2,3-Dimethyl-1,4-naphthoquinone
DMSO	Dimethyl sulfoxide
DQ	2,3,5,6-Tetramethyl-1,4-benzoquinone
ΔF	Change in emission at 330 nm
Δ*ndh-2a*	Strain with *ndh-2a* gene deleted
Δ*ndh-2b*	Strain with *ndh-2b* gene deleted
$\Delta\tilde{\mu}$	Difference in transmembrane electrochemical potential
ETC	Electron transport chain
ETF-QO	Electron transfer flavoprotein:ubiquinone oxidoreductase
FAD	Flavin adenine dinucleotide
$FADH_2$	Reduced flavin adenine dinucleotide
Fd	Ferredoxin
FMN	Flavin mononucleotide
Fdn-N	Formate:quinone oxidoreductase
G3P	Glycerol-3 phosphate
G3PQO	Glycerol 3-phosphate:quinone oxidoreductase
HPLC	High performance liquid chromatography

HQNO	2-n-Hepthyl-4-hydroxyquinoline-N-oxide
IPTG	Isopropyl-β-D-thiogalactosidase
K_D	Dissociation constant
KEGG	Kyoto encyclopedia of genes and genomes
LQO	Lactate:quinone oxidoreductase
MDH	Malate: NAD^+ oxidoreductase
MQO	Malate:quinone oxidoreductase
MRSA	Methicillin resistant *S. aureus*
MS	Mass spectrometry
NAD^+	Oxidized nicotinamide adenine dinucleotide
NADH	Reduced nicotinamide adenine dinucleotide
$NADP^+$	Oxidized Nicotinamide adenine dinucleotide Phosphate
NADPH	Reduced Nicotinamide adenine dinucleotide Phosphate
NDH-2	Type II NADH:quinone oxidoreductase
NQR	Sodium translocating NADH:quinone oxidoreductase
N-side	Negative side of the membrane
OD_{600}	Optical density at 600 nm
PCR	Polymerase Chain Reaction
PDB	Protein data bank
PQ	Plastoquinone
PQO	Pyruvate:quinone oxidoreductase
P-side	Positive side of the membrane
PTOX	Plastid terminal oxidase
Q	Quinone
QH_2	Quinol
SDH	Succinate:quinone oxidoreductase
SDS	Sodium dodecyl sulphate
SDS-PAGE	Sodium dodecyl sulphate – polyacrylamide gel electrophoresis
SHE	Standard hydrogen electrode
SQR	Sulfide:quinone oxidoreductase
TCA	Tricarboxylic acid
tDBDF	Two-dinucleotide binding domains flavoproteins
TSB	Tryptic soy broth
UniProt	Universal protein resource
UQ	Ubiquinone
V_{MAX}	Maximal velocity

WT	Wild type
X-Gal	5-bromo-4-chloro-3-indolyl-β-galactopyranoside

A. tumefaciens	*Agrobacterium tumefaciens*
B. pseudofirmus	*Bacillus pseudofirmus*
B. subtilis	*Bacillus subtilis*
C. thermarum	*Caldalkalibacillus thermarum*
C. reinhardtii	*Chlamydomonas reinhardtii*
C. glutamicum	*Corynebacterium glutamicum*
E. histolytica	*Entamoeba histolytica*
E. coli	*Escherichia coli*
E. gracilis	*Euglena gracilis*
F. oxysporum	*Fusarium oxysporum*
G. intestinalis	*Giardia intestinalis*
G. oxydans	*Gluconobacter oxydans*
H. pylori	*Helicobacter pylori*
H. sapiens	*Homo sapiens*
M. capsulatus	*Methylococcus capsulatus*
M. smegmatis	*Mycobacterium smegmatis*
M. tuberculosis	*Mycobacterium tuberculosis*
N. gruberi	*Naegleria gruberi*
N. crassa	*Neurospora crassa*
P. falciparum	*Plasmodium falciparum*
P. biforma	*Pygsuia biforma*
S. aureus	*Staphylococcus aureus*
S. cerevisiae	*Saccharomyces cerevisiae*
T. vaginalis	*Trichomonas vaginalis*
T. gondii	*Toxoplasma gondii*
T. brucei	*Trypanosoma brucei*
U. maydis	*Ustilago maydis*
Y. lipolytica	*Yarrowia lipolytica*

Summary

Type II NADH:quinone oxidoreductases (NDH-2s) are membrane bound enzymes involved in respiratory chains. They contribute to the regeneration of $NAD(P)^+$, allowing several metabolic pathways to proceed. These enzymes do not translocate charges across the membrane and thus do not contribute directly to the generation of the transmembrane difference in the electrochemical potential. NDH-2s are members of the so-called two-dinucleotide binding domain flavoprotein (tDBDF) superfamily, which are characterized by having NAD(P)H- and flavin-binding domains, with identical structural Rossmann folds.

NDH-2s are monotopic enzymes recognized as suitable targets for novel antimicrobial therapies, as these are the only enzymes with NAD(P)H:quinone oxidoreductase activity expressed in many pathogenic organisms. *Staphylococcus aureus*, a worldwide problem in clinical medicine due to its multiple drug resistant forms, has two genes encoding NDH-2s.

This work aimed at investigating deeply type II NADH:quinone oxidoreductases in functional, structural and cellular terms. It was our goal to explore their catalytic mechanism and intermediates, as well as the interaction with the substrates. The specific addressed questions were: How does the catalytic mechanism proceed? What are the structural/functional determinants for substrate specificity among NDH-2s? Why do *S. aureus* contain more than one gene of NDH-2? And do these two genes, code for two proteins with the same cellular role?

We obtained structural insights into NDH-2A by resolving both its crystal and solution structures, which showed that it is a dimer in solution. Studies on protein–substrate interactions by fluorescence and STD-NMR spectroscopies, indicated that NAD(P)H and the quinone bind to different sites.

Moreover, these data also showed that HQNO, a quinone inhibitor, interacts with NDH-2s in a different way from those of NAD(P)H or DMN, suggesting that the inhibitor binds to a distinct site, stabilizing a conformation with less affinity for quinone.

Additionally, we carried out functional studies, including pre-steady-state and steady-state kinetic assays of the two NDH-2s. These revealed the presence of a charge-transfer (CT) complex formed between NAD^+ and the reduced flavin which is dissociated by the quinone in NDH-2A enzyme, leading to the conclusion that NDH-2A establishes a ternary complex during catalysis. Such CT complex is not observed in NDH-2B, which was shown to be a NADPH:quinone oxidoreductase, with maximal activity at pH 5.5. Furthermore, the rate-limiting step in NDH-2A is the reduction of the quinone and in NDH-2B enzyme the opposite occurs, NADPH oxidation is rate-limited. Here we hypothesize both enzymes from *S. aureus* organism resort to two different strategies/processes, the formation of the CT complex or the limiting step being the reduced, to obtain the same effect, the protein does not form a stable reduced state. As consequently, a long flavin reduced state is avoided, which might react nonspecifically with O_2. In this way the two processes prevent the production of ROS in vivo.

The study of NDH-2s at the cellular level was explored throught the construction of the green fluorescent mNeonGreen labelled NDH-2s and knockout strains. The first indicated NDH-2A-mNeonGreen localizes at the membrane and NDH-2B-mNeonGreen seems to localize mostly in the cytoplasm, reflecting the weak interactions that these enzymes may have with the membrane. Fluorescence microscopy of Δ*ndh-2a* and Δ*ndh-2b* strains showed an increase in cell volume in both mutants when compared with wild-type cells that were confirmed by calculating the volume of each cell in each

phase (P1, P2 and P3) of *S. aureus* cell cycle. Δ*ndh-2a* presented more cells in P2 and P3 phases meaning that cell division may be compromised in this mutant. Our NMR-based metabolomics unravel a strong phenotype for Δ*ndh-2a* with high levels of lactate excretion, 4 times higher when comparing with the WT and Δ*ndh-2b* strains. We hypothesize that in the absence of NDH-2A, *S. aureus* may have opted a fermentation metabolism by oxidizing glucose to lactate, in which NAD^+ regeneration occurs through NADH:pyruvate oxidoreductase, with production of lactate, to maintain the glycolytic flux.

Altogether, our work provides a thorough investigation of NDH-2s, where the two NAD(P)H:quinone oxidoreductases in *Staphylococcus aureus* are positioned to play important roles in the respiratory chain of this pathogen, and contributing to the regeneration of $NAD(P)^+$, a critical oxidant for numerous biochemical reactions. Furthermore, and knowing that these NDH-2s may be the only enzymes with NAD(P)H:quinone oxidoreduction activity in many pathogenic organisms, including *S. aureus*, this work may also contribute to pave the way for rational design of novel antibiotics that target these enzymes.

Sumário

NADH:quinona oxidoredutases tipo II (NDH-2s) são enzimas associados à membrana envolvidos nas cadeias respiratórias. Estes contribuem para a regeneração de $NAD(P)^+$, permitindo que várias vias metabólicas prossigam. Estes enzimas não translocam cargas através da membrana e, portanto, não contribuem diretamente para o estabelecimento de diferença de potencial eletroquímico transmembranar. NDH-2s são membros da superfamília dos *two-dinucleotide binding domain flavoprotein* (tDBDF), caracterizados por possuir domínios que interagem com NAD(P)H e flavina, com estruturas idênticas a um *Rossmann fold*.

Os NDH-2 são enzimas monotópicos reconhecidos como alvos adequados para novas terapias antimicrobianas, sendo os únicos enzimas com atividade NAD(P)H:quinona oxidoredutase expressa em muitos organismos patogénicos. O *Staphylococcus aureus*, um problema mundial na medicina clínica devido às suas múltiplas formas resistentes a medicamentos, possuí dois genes que codificam para NDH-2s.

Este trabalho teve como objetivo investigar de forma aprofundada os enzimas NADH:quinona oxidoredutases tipo II, em termos funcionais, estruturais e celulares. O nosso objetivo foi explorar o mecanismo catalítico, os intermediários e a interação com os substratos. As perguntas específicas abordadas foram: Como se prossessa o mecanismo catalítico? Quais são os determinantes estruturais/ funcionais da especificidade do substrato entre os NDH-2s? Por que razão o *S. aureus* possui mais do que um gene do NDH-2? E estes dois genes, codificam para duas proteínas com o mesmo papel celular?

Foram obtidas informações estruturais sobre NDH-2A, resolvendo as estruturas cristalina e em solução, mostrando que o enzima é um dímero em solução. Estudos de interação proteína-substrato por espectroscopia de

fluorescência e STD-RMN, indicaram que NAD(P)H e quinona se ligam a diferentes locais. Além disso, estes dados também mostraram que o HQNO, um inibidor da quinona, interage com NDH-2s de forma diferente do NAD(P)H ou DMN, sugerindo que o inibidor se liga a um local distinto, estabilizando uma conformação com menor afinidade para a quinona.

Além disso, foram realizados estudos funcionais, incluíndo ensaios pré cinéticos e no estado estacionário dos dois NDH-2s. Estes estudos revelaram a presença de um complexo de transferência de cargas (CT), formado entre o NAD^+ e a flavina reduzida, que é dissociado pela quinona no enzima NDH-2A, levando à conclusão de que o NDH-2A estabelece um complexo ternário durante a catálise. Este complexo CT não é observado no NDH-2B, que mostrou ser uma NADPH:quinona oxidoredutase, com atividade máxima a pH 5.5. Para além disso, o passo limitante de NDH-2A é a redução da quinona e no enzima NDH-2B ocorre o contrário, a oxidação do NADPH é o passo limitante. Aqui hipotetizamos que os dois enzimas do organismo *S. aureus* recorrem a duas estratégias/processos diferentes, a formação do complexo CT ou o passo limitante a reação de redução da flavina, para obter o mesmo efeito, a proteína não forma um estado reduzido estável. Como conseqüência, evita-se um longo estado reduzido de flavina, que pode reagir de maneira não específica com o O_2. Desta forma, os dois processos impedem a produção de ERO (espécies reactivas de oxigénio) in vivo.

O estudo dos NDH-2s foi explorado a nível celular através da construção de NDH-2s marcados com proteínas verde fluorescente, a mNeonGreen, e estirpes knockout. Os primeiros indicaram que NDH-2A-mNeonGreen localiza na membrana e o NDH-2B-mNeonGreen parece localizar principalmente no citoplasma, refletindo as fracas interações que estes enzimas podem ter com a membrana. A microscopia de fluorescência das estirpes Δ*ndh-2a* e Δ*ndh-2b*

revelou um aumento do volume celular em ambos os mutantes, quando comparado às células do tipo selvagem, confirmado pelo cálculo do volume de cada célula em cada fase (P1, P2 e P3) do ciclo celular de *S. aureus*. O Δ*ndh-2a* apresentou mais células nas fases P2 e P3, o que significa que a divisão celular pode estar comprometida neste mutante. Os dados de metabolômica baseada em RMN revelaram um forte fenótipo para a estirpe Δ*ndh-2a* com elevados níveis de excreção de lactato, 4 vezes mais quando comparado com as linhagens WT e Δ*ndh-2b*. A nossa hipótese baseia-se em que na ausência de NDH-2A, *S. aureus* pode ter optado pelo metabolismo da fermentação, oxidando glucose a lactato, na qual ocorre a regeneração de NAD^+ através de NADH:piruvato oxidoredutase, com produção de lactato, para manter o fluxo glicolítico.

De um modo geral, o nosso trabalho fornece uma investigação minuciosa dos NDH-2s, em que as duas NAD(P)H:quinona oxidoredutases de *Staphylococcus aureus* estão posicionadas para desempenhar papéis importantes na cadeia respiratória deste patogénio e contribuir para a regeneração de $NAD(P)^+$, um oxidante crítico para inúmeras reações bioquímicas. Além disso, e sabendo que NDH-2s podem ser os únicos enzimas com atividade NAD(P)H:quinona oxidoredutase em muitos organismos patogénicos, incluindo *S. aureus*, este trabalho pode, também contribuir para uma visão mais clara do planeamento racional de novos antibióticos direcionados para estes enzimas.

Contents

Chapter 1

Chapter 2

Chapter 3

Chapter 4

Chapter 5

Chapter 6

Chapter 1

General Introduction

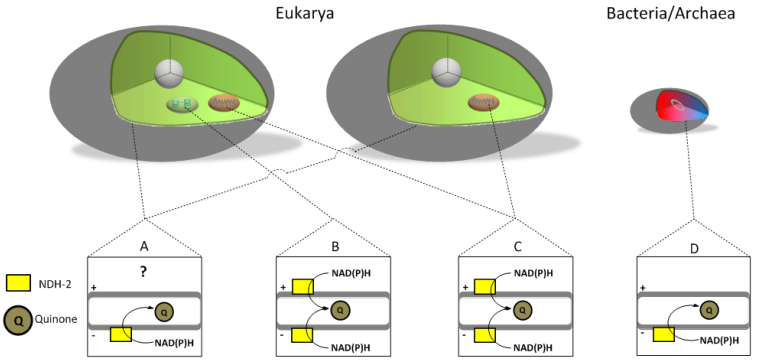

Chapter 1- General Introduction

This section is based on the following publications:

- ✓ Marreiros CM, Calisto F, Castro PJ, Duarte AM, **Sena FV,** Silva AF, Sousa FM, Teixeira M, Refojo PN, Pereira MM. Exploring membrane respiratory chains. *BBA bioenergetics*. (2016). Doi: 10.1016/j.bbabio.2016.03.028.

- ✓ Marreiros BC, **Sena FV**, Sousa FM, Batista AP, Pereira MM. Type II NADH:quinone oxidoreductase family: phylogenetic distribution, structural diversity and evolutionary divergences. *Environ Microbiol*. (2016). Doi: 10.1111/1462-2920.13352.

- ✓ Refojo PN*, **Sena FV***, Calisto F*, Sousa FM*, Pereira MM. The plethora of membrane respiratory chains in the phyla of life. *Adv Microb Physiol.* (2019). Doi: 10.1016/bs.ampbs.2019.03.002.

* Equally contributing authors.

Author Contribution:

Sena FV participated in the design of the studies, performed and analyzed the experiments and critically discussed the data.

1.1 Overview of respiration

Respiration is an important life process that takes place in the cytoplasmic membrane of prokaryotes and in the inner mitochondrial membrane of eukaryotes. In respiration energy is conserved in the form of transmembrane difference of the electrochemical potential ($\Delta\tilde{\mu}$, membrane potential). This membrane potential can directly power ATP synthesis, solute transport across membrane and motility (Figure 1.1). This is the basis of the Chemiosmotic Hypothesis, postulated by Peter Mitchell in 1961[1].

Electrons obtained from the oxidation of intermediates from glucose, lipids and amino acids metabolisms or from some inorganic compounds, like H_2S, may enter the respiratory chain by the action of quinone reductases, which promote the link between several catabolic pathways and the respiratory chains. In aerobic respiration, these electrons are transferred in the electron transport chain (ETC), and the final electron acceptor is Oxygen (O_2). In anaerobic respiration, other electron acceptors such as nitrate, fumarate, sulphate, or elemental sulfur are reduced. The energy released from the oxidation of an electron donor using O_2 as electron acceptor is greater than if the same compound is oxidized with most alternative electron acceptors (with a known exception being Fe^{3+}/Fe^{2+})[2]. Nevertheless, because O_2 is often limiting or absent in many microbial habitats, anaerobic respiration can be very important means of energy conversion. Other electron acceptors for which the reduction potential is close to the one of O_2 are manganic ion, ferric iron, nitrate, and nitrite. Examples of more electronegative acceptors are sulfate, elemental sulfur, and carbon dioxide, and organisms that use these acceptors are typically restricted into an anaerobic lifestyle.

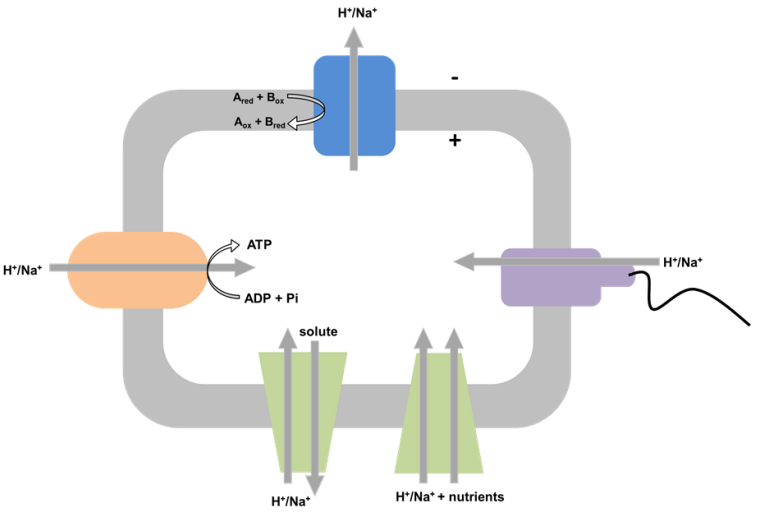

Figure 1.1 Schematic representation of a cell with a membrane potential generating system, transport systems, ATP synthase and flagella.

1.2 Respiratory chains

Most of energy conversion is performed by respiratory chains, composed of protein complexes that use the free energy released from oxidoreduction reactions to translocate charges (electrons or ions, H^+ or Na^+) across the membrane conserving energy in the form of $\Delta\tilde{\mu}$.

Most studied respiratory chains, as the mitochondrial one, are composed of several membrane proteins, which perform a stepwise oxidation of metabolites towards the reduction of terminal electron acceptors, which in the case of the mitochondrial respiratory chain, is O_2. Some of these membrane proteins, isolated do not contribute to the establishment of membrane potential, but by reducing or oxidizing metabolites of the respiratory chain, as quinone or quinol (see below), may allow the buildup of membrane potential by other proteins of the respiratory chain. Many other proteins may couple

oxidoreduction reactions to the translocation of charges across the membrane, being considered as energy conserving enzymes.

Isoprenoid quinones (commonly referred as quinones) are chemical entities that are composed of a highly aliphatic isoprenyl chain and an aromatic ring system. They can be found in the membrane systems of cells, working as lipid soluble electron carriers playing a vital role in electron transport, oxidative stress control and gene regulation[3]. Isoprenoid quinones can be structurally divided according to their aromatic ring composition, into four main classes: benzoquinones, naphthoquinones, benzothiophenequinones and phenazines. Despite the structural variability, all quinones have in common the ability to be reduced giving rise to their quinol forms (or hydroquinones) in a reaction that involves two electrons and two protons.

One way to investigate the composition of an organism's respiratory chain is through a bioinformatic approach, by searching genes coding for proteins or protein complexes belonging to different taxonomic clades, and also based on the state of the art in protein biochemical studies. To study the composition of a respiratory chain of a given organism it is necessary to have in mind that the identification of a gene coding for a membrane bound respiratory protein only indicates that an organism may express that protein but does not elucidate which proteins are expressed at the same time under a certain growth or cellular condition. We need to consider that the regulation of the expression of a given gene is dependent on several conditions including environmental ones. However, we cannot exclude the fact that the great diversity of organisms on Earth is reflected on the composition of their respiratory chains, which provide metabolic versatility and allow their survival in very dynamic and diverse environments. And in fact, prokaryotes may express different respiratory chains with alternative pathways, allowing them to reduce besides

oxygen a large set of other compounds. In the following pages we will describe respiratory chains that we have considered to be representative of different taxonomic clades.

1.2.1 Animals respiratory chains

As all eukaryotes do, mammals have their respiratory chain in the mitochondrial membranes, which is well conserved within the kingdom. When comparing with the plethora of possibilities of all the membrane bound proteins that can compose a respiratory chain, there is not great variability of the respiratory chain among animal phyla. The respiratory chain of mammals consists of four multisubunit protein complexes, I, II, III and IV, located in the inner mitochondrial membrane and of mobile electron carriers ubiquinone and cytochrome *c* (Figure 1.2). Complex I (Type I NADH:ubiquinone oxidoreductase) catalyzes the two electron oxidation of NADH and the reduction of ubiquinone to ubiquinol, coupled to the translocation of possibly four protons from the mitochondrial matrix to the intermembrane space, contributing in this way to the establishment of the transmembrane difference of the electrochemical potential. Mitochondrial Complex I consists of 14 core subunits and 30 accessory subunits[4]. Complex II (succinate:quinone oxidoreductase or succinate dehydrogenase, SDH) catalyzes the two-electron oxidation of succinate to fumarate with the reduction of ubiquinone to ubiquinol[5]. SDH is constituted by four subunits and does not conserve energy.

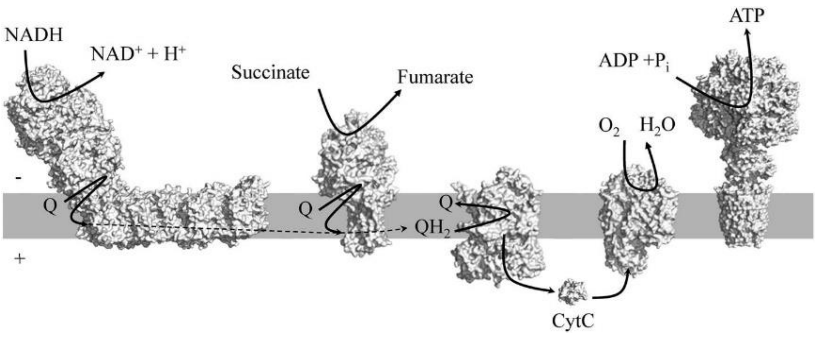

Figure 1.2 Canonical respiratory chain. The electron donors, NADH and Succinate, are oxidized by Complexes I and II, respectively, with concomitant reduction of quinone to quinol. Complex III oxidizes quinol and reduces cytochrome *c*. Complex IV oxidizes cytochrome *c* and reduces oxygen to water. Complexes I, III and IV contribute to the establishment of the transmembrane difference in electrochemical potential by translocating protons across the membrane. This membrane potential is used by Complex V for the synthesis of ATP (+and – indicate the positive and negative sides of the transmembrane difference in electrochemical potential, respectively).

Besides complexes I and II, at least five other single subunit enzymes in mammalian mitochondria reduce quinones without involving proton translocation across the membrane: Type II NADH:quinone oxidoreductase (NDH-2), that catalyzes the transfer of two electrons from NADH to quinone, Sulfide:quinone oxidoreductase (SQR) which reduces quinone by sulfide oxidation, Electron transfer flavoprotein:ubiquinone oxidoreductase (ETF-QO), which oxidizes electron transfer flavoprotein (ETF) and may be considered a promiscuous electron acceptor hub, since it can accept electrons from different soluble flavoprotein dehydrogenases (from the oxidation of fatty acids and some amino acids) and reduce ubiquinone [6], Glycerol 3-phosphate:quinone oxidoreductase (G3PQO), which catalyzes the oxidation of glycerol 3-phosphate, and Dihydroorotate:quinone oxidoreductase (DHOQO), that oxidizes dihydroorotate to orotate and is involved in pyrimidine biosynthesis[7] (Figure 1.3). These enzymes confer the animals' respiratory chain high

versatility through the possibility of receiving electrons from alternative pathways.

In the beginning of this thesis project NDH-2s were considered to be absent in mammals but some studies have emerged reporting NDH-2 from *Homo sapiens* [8,9]. NDH-2 from *H. sapiens* was named AMID (apoptosis-inducing factor-homologous mitochondrion-associated inducer of death), later AIF-M2, and was shown to have NADH:ubiquinone oxidoreductase activity[10]. Moreover, we performed a taxonomic profile and our sequence analyses identified this protein as being part of a large group of NDH-2s[9], which further support the idea that AIF-M2 proteins are NDH-2s[8]. AIF-M2 is membrane attached by its C-terminal domain and inhibited by HQNO, a quinolone derivative[10,11]. This enzyme is ubiquitously expressed, but a relatively small amount is expressed in mitochondria as compared to Complex I. Thus, although NDH-2 from *H. sapiens* exert NADH:ubiquinone oxidoreductase activity under certain conditions, its activity in mammals respiratory chain might be dispensable, as Complex I is more expressed.

In addition, mammals respiratory chain is composed of Complex III (ubiquinol:cytochrome *c* oxidoreductase or cytochrome bc_1 complex) that catalyzes the electron transfer from ubiquinol to a soluble cytochrome *c*, a process coupled to energy conservation [7]. Cytochrome bc_1 complex operates by the so-called Q-cycle mechanism where the electron bifurcation mode for energy conservation, allows direct-coupling to occur by the translocation of one electron across the membrane from the positive to the negative side of the membrane[12]. In mitochondria of mammals, Complex III contains 11 subunits[13]. The final step in the mammal mitochondrial respiratory chain involves the transfer of electrons from reduced cytochrome *c* to O_2, forming 2 molecules of H_2O. This four electrons reaction is catalyzed by Complex IV

(cytochrome *c* oxidase)[14]. The mechanism of energy conservation involves the movement of four electrons and four protons, needed for the reaction. Translocation of up to 4 additional charges results from the proton pumping. Thus, a total of 8 protons are translocated across the membrane per O_2. Mitochondrial Complex IV is composed of two catalytic subunits and 11 additional subunits[7] (Figure 1.3).

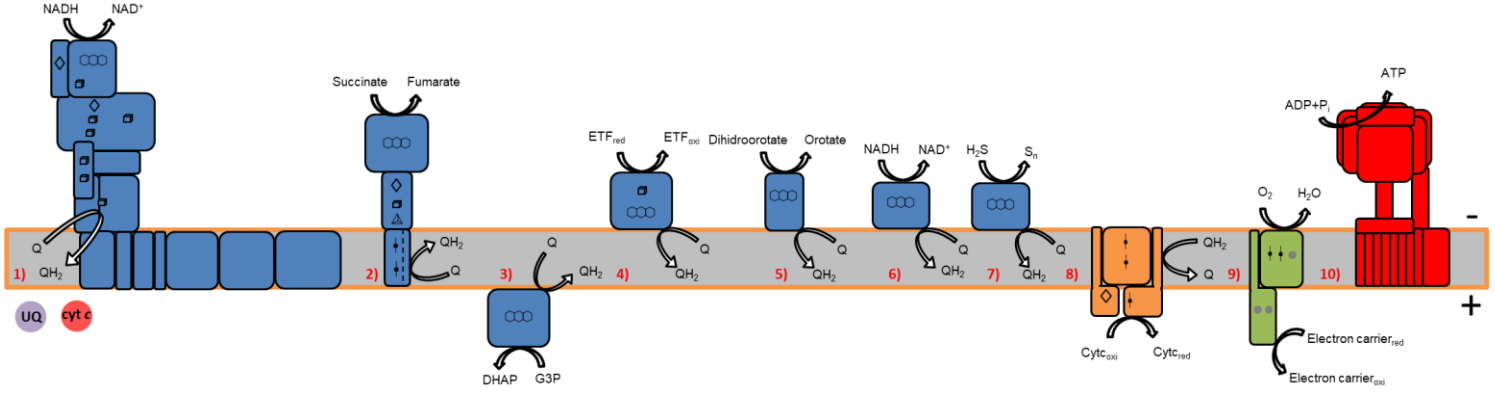

Figure 1.3 Schematic representation of the Animals respiratory chain. Protein representation is proportional to its MM. + and - indicate the positive and negative sides of the transmembrane difference in electrochemical potential, respectively. The blue, orange, and green colors of the protein complexes correspond to Quinone reductases, Quinol oxidases and Non-quinone interacting respiratory proteins, respectively. In red Non-respiratory proteins are represented despite not being part of respiratory chains, when present in the membranes, may contribute to the establishment of membrane potential. UQ - ubiquinone; MQ - menaquinone; PQ - plastoquinone; RQ - rhodoquinone; MP - methanophenazine; CQ – caldariella quinone; cyt *c* - cytochrome *c*; BC - blue cooper protein; Fd - ferredoxin; HP – HIPIP.

1.2.2 Plants respiratory chains

There are over three hundred thousand species of organisms contemplated in the Plantae kingdom from which only, nearly, fifty have their genome fully sequenced. Plants are photosynthetic organisms, meaning that they convert radiant energy from the sun firstly into membrane potential and them into chemical energy. Nonetheless, plants also respire having respiratory proteins localized on the membranes of mitochondria or chloroplasts[15,16]. The classical electron transport chain in plant mitochondria is like that of animal mitochondria: it comprises the four core complexes, I, II, III and IV (Figure 1.4). Complex I is composed of up to 50 subunits, 17 of which are different from the mammalian homologue (32 have similarity with mammalian complex I)[17,18]. Complex I from plants was first purified in 2006 and since then many subunits have been characterized. Complex II is composed of four subunits and four additional proteins of unknown function in plants[17]. Ubiquinol produced by complexes I and II is oxidized by Complex III, the ubiquinone:cytochrome *c* oxidoreductase or bc_1 complex[19]. Plant Complex IV also shows supplementary proteins that may represent plant-specific subunits[17]. Plants electron transfer chain also includes a non-heme diiron alternative oxygen reductase (AOX), which is a quinol:O_2 oxidoreductase that does not conserve energy (Figure 1.4). The expression of AOX is manifested by the ability of plants to respire in the presence of cyanide, a potent inhibitor of Complex IV[18]. Additionally, several dehydrogenases can directly reduce ubiquinone such as NDH-2, G3PQO and ETF-QO[17][18] (Figure 1.4). Interestingly, genes coding for NDH-2s were observed to be present in 100 % of the species which genome is totally sequenced in KEGG's database[9].

In chloroplasts, the presence of respiratory complexes has also been observed[20], which includes a Complex I-like enzyme[21,22] that it is a

ferredoxin-dependent plastoquinone reductase rather than an NAD(P)H dehydrogenase, and NDH-2[23]. Another component of the chloroplastidial respiratory chain is a plastid terminal oxidase (PTOX), which belongs to the same family of AOX and mediates electron flow from plastoquinol to O_2[24].

The second energy conserving respiratory complex found in plant chloroplasts is cytochrome b_6f complex. This complex has plastoquinol:plastocyanin/cytochrome c_6 oxidoreductase activity, analogous to the reaction catalyzed by cytochrome bc_1 complex, and is part of the electron transfer chain between the two photosynthetic reaction center complexes, photosystems II and I[25,26] (Figure 1.4). Although the structures of cytochrome b_6f and cytochrome bc_1 complexes are not the same, cytochrome b_6f also contribute to the formation of the $\Delta\tilde{\mu}$ by the Q-cycle mechanism[26].

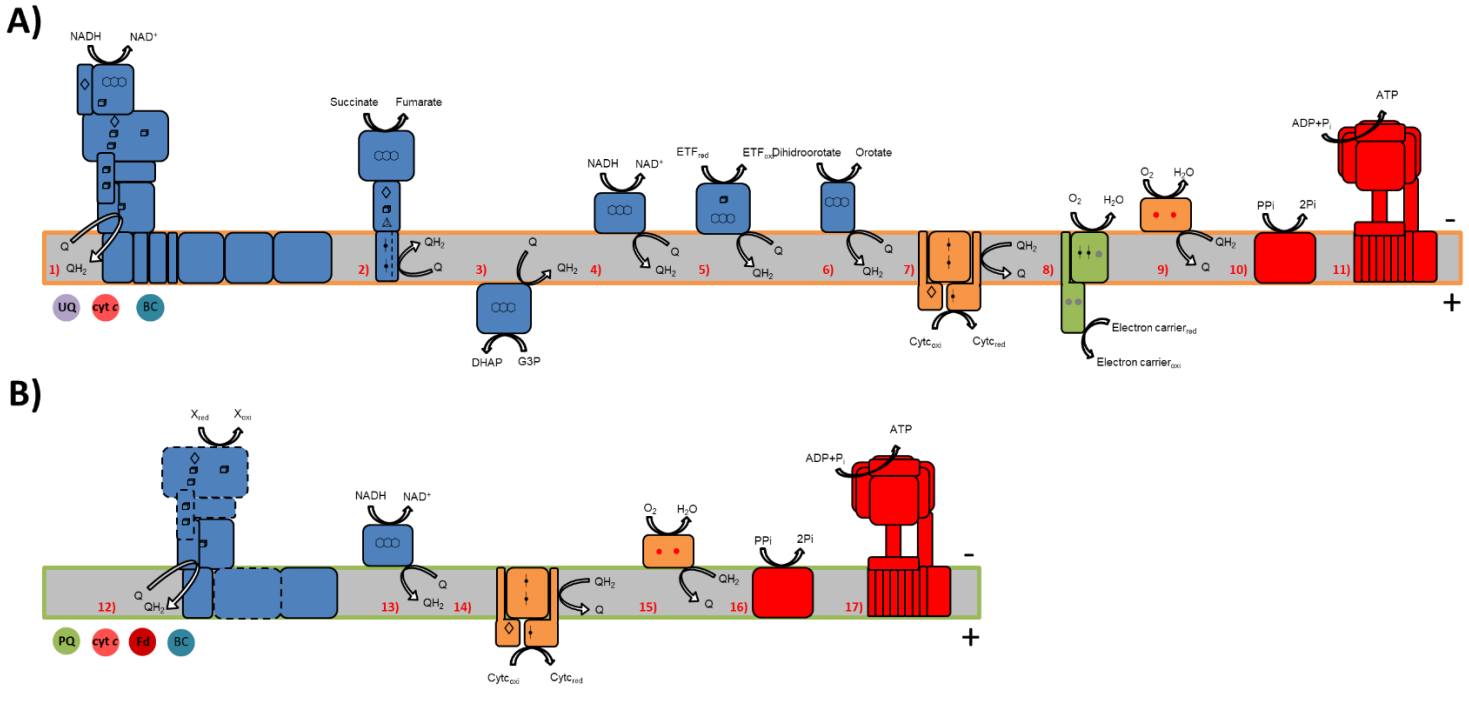

Figure 1.4 Schematic representation of the Plants respiratory chain, mitochondrial (A) and chloroplastidial (B). Protein representation is proportional to its MM. + and - indicate the positive and negative sides of the transmembrane difference in electrochemical potential, respectively. Color code and abbreviations are the same as described in the legend of Figure 1.3.

1.2.3 Fungi and Protista respiratory chains

Mitochondrial electron transport chains of Fungi and Protista also contain protein complexes similar to their homologues of the classic mammalian mitochondrial chain, complexes I, II, III and IV[27–29]. Most fungal mitochondria have the canonical respiratory chain, but some fungi, such as *Saccharomyces cerevisiae*, lack Complex I[30]. *S. cerevisiae* have four genes encoding NDH-2s[11]. These enzymes can be present on both sides of the mitochondrial membrane, allowing the oxidation of cytosolic and mitochondrial NADH[31]. Also usually, fungi have additional components, such as the AOX[32,33] (Figure 1.5). Fungal parasites, like obligate intracellular Microsporidians, lack genes for energy metabolism and are strictly dependent on the host for energy, they uptake ATP from their host cells via ADP/ATP translocases located in their plasma membranes[34]. Several filamentous fungi are able to survive in anoxic conditions, being competent to produce ATP using nitrogen or sulfur as final electron acceptors[35,36]. *Fusarium oxysporum*, from the Ascomycetes phylum has the ability to reduce nitrate to nitrous oxide, in a process coupled to ATP synthesis in the mitochondria, which is catalyzed by nitrate reductase, nitrite reductase and nitric oxide reductase[35,37]. *F. oxysporum* is also able to reduce inorganic sulfur to hydrogen sulfide by a NADH-dependent sulfur reductase[36].

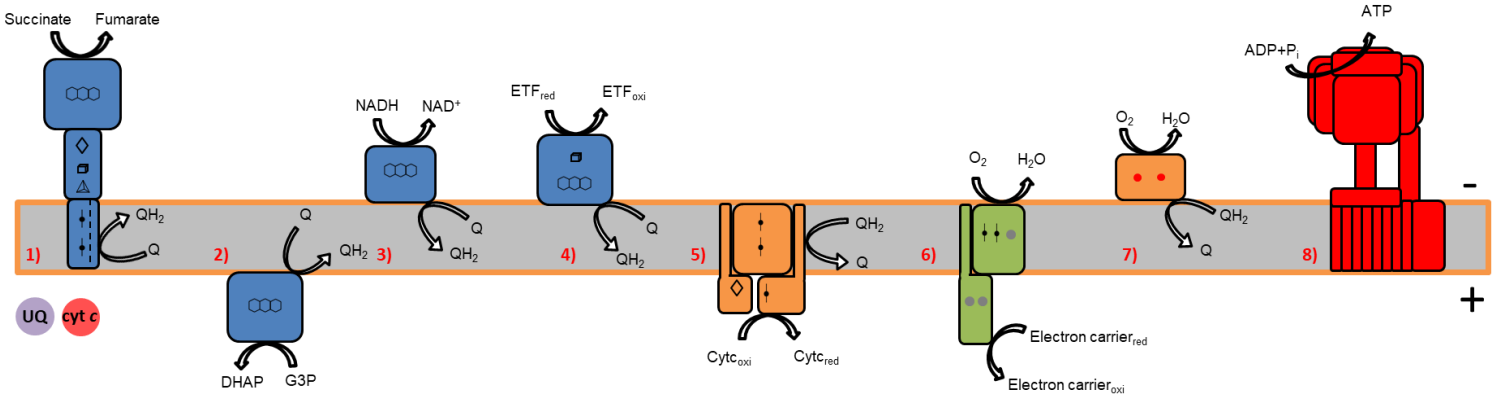

Figure 1.5 Schematic representation of the Fungi respiratory chain. Protein representation is proportional to its MM. + and - indicate the positive and negative sides of the transmembrane difference in electrochemical potential, respectively. Color code and abbreviations are the same as described in the legend of Figure 1.3.

Protists may live in different environments and are able to live as free-living organisms, parasites, or symbionts of multicellular eukaryotes, having different enzyme complexes on their respiratory chain depending on their needs. For example, the free living aerobic amoeboflagellate *Naegleria gruberi* possesses the canonical mitochondrial respiratory enzymes and in addition it has NDH-2 and AOX[38] (Figure 1.6). Also *Euglena gracilis*, a single-celled flagellate protist, has a typical eukaryotic mitochondria but includes lactate:quinone oxidoreductase (LQO) and AOX[39,40]. In the case of *Pygsuia biforma*, an amoeba-like organism, an ETF-QO, a G3PQO and an AOX are components of its respiratory chain[41] (Figure 1.6). Life cycles of protozoan parasites include development in the vector and in the host, and the mitochondrial metabolism change depending on the life cycle stage, switching between an active and a fully repressed state[42,43]. A number of protist pathogenic species from low oxygen habitats, including *Trichomonas vaginalis*, *Giardia intestinalis* and *Entamoeba histolytica*, lack typical mitochondria[44–47]. The Apicomplexa, a group of obligate intracellular parasites, include the protists *Plasmodium*, *Toxoplasma* and *Cryptosporidium*, the causative agents for malaria, toxoplasmosis, and cryptosporidiosis, respectively. *Cryptosporidium* species have lost the respective mtDNA and most mitochondrial enzymes, with the exception of AOX, malate:quinone oxidoreductase (MQO) and NDH-2[48]. *Plasmodium falciparum* is an example of a protozoan parasite that carries out oxidative phosphorylation in the insect vector stages. *P. falciparum* genome lacks Complex I, and possesses a gene encoding NDH-2, being in this way able to oxidize NADH[49].

The general pattern of the mitochondria related organelles, in both Protista and Fungi, of the free-living organisms differs from those of parasites. These organisms often rely on the host to fulfill their needs and lost the

bioenergetics complexity and versatility which is in fact a frequent feature of intracellular organisms. It is possible that since free living organisms tend to occupy dynamic environments compared with parasites, several enzymes could provide metabolic versatility allowing their survival.

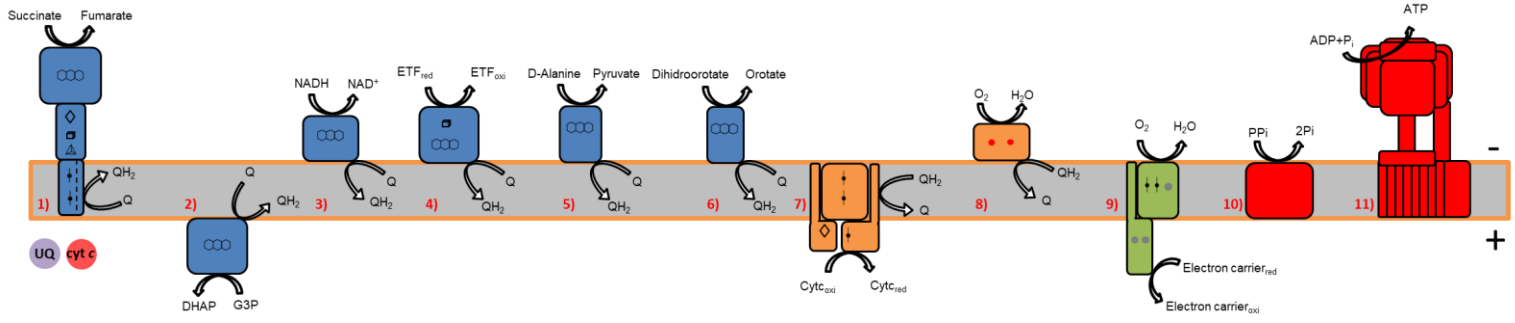

Figure 1.6 Schematic representation of the Protista respiratory chains. Protein representation is proportional to its MM. + and - indicate the positive and negative sides of the transmembrane difference in electrochemical potential, respectively. Color code and abbreviations are the same as described in the legend of Figure 1.3.

1.2.4 Bacterial respiratory chains

Prokaryotes show a remarkable diversity, flexibility, and robustness of their energetic metabolism, which allow them to live or survive under the most diverse conditions. They may acquire energy by photosynthesis, fermentation or respiration and can use different organic or inorganic compounds as electron donors or electron acceptors. Bacteria have proteins on their respiratory chain that carry out the same reaction but are structurally different, like the different types of NADH dehydrogenases, or carry out the same reaction but are expressed in different conditions. For example, bo_3 oxidase and *bd* oxidase from *E. coli* are expressed under high oxygen conditions and low oxygen conditions respectively[50,51]. This shows how the bacterial respiratory chains can be flexible and diverse. Furthermore, the presence of alternative complexes such as NDH-2, the Alternative Complex III, AOX and others, in the bacterial respiratory chain, makes bacteria more resilient and adaptable to changes in environmental conditions.

From the plethora of different complexes that compose the respiratory chains of bacteria, we are going to focus on microorganisms of the order Bacillales because *Staphylococcus aureus* belongs to this order and is the working model in this thesis. The Bacillales is an order of Gram-positive bacteria, placed within the Firmicutes with the representative genera *Staphylococcus, Bacillus* and *Listeria.* Most of these microorganisms must adapt rapidly to overcome unique challenges, relying in a very dynamic metabolism having for example the ability to form biofilms. Their respiratory chain is characterized by the absence of Complex I in the majority of the species and the presence of NDH-2s in all species, being the only proteins with NADH dehydrogenase activity[11] (Figure 1.7). Besides NDH-2, G3PQO, MQO, PQO, DHOQO, SQR and SDH are present and can also reduce quinone to quinol. In

addition, *S. aureus* genome also codifies to a quinone reductase named formate dehydrogenase (Fdn-N) catalyzing the oxidation of formate. Analysis of the genome indicates there is no cytochrome bc_1 complex in *S. aureus* (Figure 1.7). However, most of the species of the Bacillales order do have this complex, including *B. subtilis.* In fact, *B. subtilis* respiratory chain is composed of a menaquinol:cytochrome reductase or a b_6c complex in which one of the subunits has a b_6 cytochrome with high similarity to the photosynthetic b_6[52]. Bacillales species can also conserve energy through *bd* oxidase where electrons can be directly transferred to O_2[52]. In addition, other types of respiratory oxygen reductases coupled to proton translocation are found in Bacillales order, mainly HCO aa_3-type menaquinol oxidase which is present in *S. aureus* [53] (Figure 1.7). *B. subtillis* respiratory contains a second HCO, the caa_3 cytochrome oxidase which forms a supercomplex with the cytochrome b_6c and the membrane bound c_{550}. ATP synthase was also suggested to include this supercomplex[52]. Some of the species that belong to Bacillales order can use nitrate as final electron acceptor, having a periplasmic nitrate reductase (NapABC) which allows energy conservation and its presence is proposed to be determinant to microbial survival during host colonization[54]. In addition, *S. aureus* respiratory chain also contains a particulate methane monooxygenase (pMMO) allowing the aerobic hydroxylation of methane to methanol using O_2.

By the analysis of the previously described respiratory chains we observe the presence of NDH-2s in most of them, giving emphasis to the importance of these enzymes in the metabolism of several organisms. NDH-2s are present in species belonging to the three domains of life and many organisms have multiple NDH-2 copies in their genomes and lack Complex I or Na^+-NQR. Since NDH-2 promotes regeneration of NAD^+ without directly coupling NADH:quinone oxidoreduction to charge translocation, which is

different from what is observed for Complex I or Na^+-NQR, we can speculate that in some organisms, NAD^+ regeneration is preferred over energy transduction.

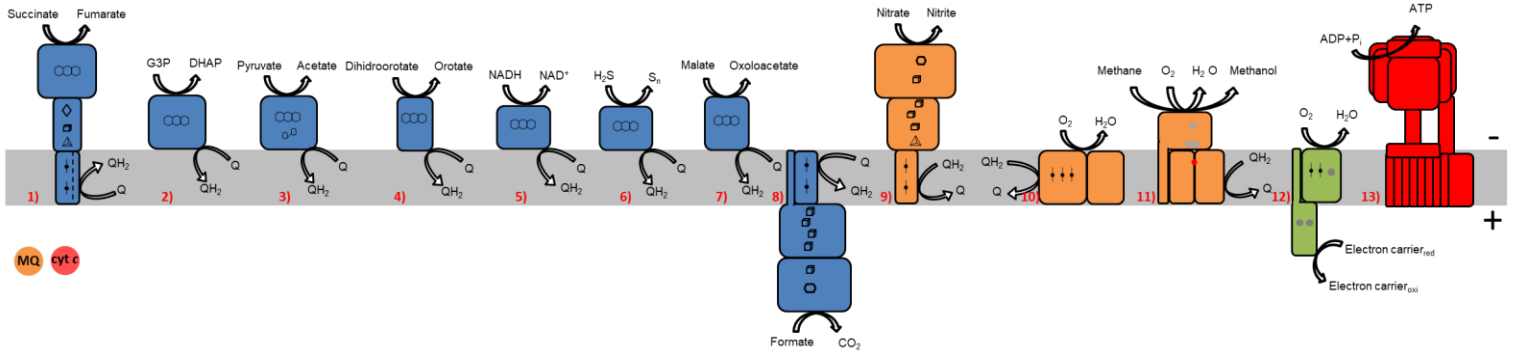

Figure 1.7 Schematic representation of the *Staphylococcus aureus* respiratory chain. Protein representation is proportional to its MM. + and - indicate the positive and negative sides of the transmembrane difference in electrochemical potential, respectively. Color code and abbreviations are the same as described in the legend of Figure 1.3.

1.3 Biology, pathogenicity, and metabolism of *S. aureus*

Staphylococcus aureus is a Gram-positive coccus both commensal and pathogen organism responsible for nosocomial and community-acquired infections. It colonizes persistently about 30 % of human population, preferentially in the skin and nasopharynx, and it is intermittently carried by a further 60 % of individuals[55]. Colonization is often asymptomatic but if the skin barrier or the mucous membranes are breached, *S. aureus* may enter the soft tissues and establish an invasive infection. Therefore *S. aureus* can cause from relatively minor skin lesions to more serious and life threatening diseases, such as bacteremia, endocarditis or hemolytic pneumonia[56]. *S. aureus* is a very versatile and virulent pathogen due to the ability to express various virulent factors. In addition, it is also a serious health-care problem due to its remarkable potential to develop antimicrobial resistance[57]. β-lactam penicillin was the first drug effective against *S. aureus*, but soon penicillin resistance strains were encountered in hospital settings[58]. The resistant strains carried plasmid-encoded β-lactamases that catalyzed the hydrolysis of the penicillin β-lactam ring, thus rendering the antibiotic inactive. The first β-lactamase-insensitive penicillin derivative, methicillin, for the treatment of infections caused by penicillin-resistant *S. aureus* strains, was introduced in the late 1950s. However, soon after, the first methicillin resistant *S. aureus* (MRSA) strains were identified in the UK[59]. By the 1980s, infections caused by *S. aureus* MRSA strains reached global proportions and, nowadays, MRSAs are one of the leading causes of nosocomial infections worldwide[60,61]. In the past decade, MRSA strains have also been emerging in community settings, affecting even healthy individuals lacking predisposing risk factors[62,63].

S. aureus is a facultative anaerobic bacterium that under aerobic conditions uses oxygen as final electron acceptor, otherwise under anaerobic

environments can grow by fermentation or nitrate respiration[64]. *S. aureus* uses the pentose phosphate and glycolytic pathways to catabolize glucose. According to the annotated genome sequence, this pathogen lacks the enzymes involved in β-oxidation pathway, not being able to metabolize fatty acids[65]. Therefore, other carbon sources that are usable include lactate, as well as peptides and free amino acids. *S. aureus* can utilize both D- and L-lactate with NAD-dependent, D-lactate dehydrogenase or L-lactate dehydrogenase and in addition, *S. aureus* encodes an NAD-independent lactate dehydrogenase, lactate:quinone oxidoreductase (LQO). Lactate generation or utilization is critical to *S. aureus* virulence because strains with mutations affecting these enzymes exhibit attenuated phenotypes in a variety of murine infection models[66]. *S. aureus* also encodes several transporters predicted to import single free amino acids, some of which have been implicated in virulence[67]. Some amino acids can be directly catabolized as carbon sources, including alanine, arginine, aspartate, cysteine, glutamate, glycine, proline, serine, and histidine. Others are consumed much more slowly because are used primarily for protein synthesis rather than as energy sources, like isoleucine, leucine, lysine, methionine, phenylalanine, tyrosine, and valine[68].

S. aureus must rapidly adapt to a diversity of carbon sources during invasion of a host. The fast-metabolic adaptation of this opportunistic pathogen provides it greater pathogenicity when compared to other innocuous staphylococci in humans. This versatile capability to adapt to different conditions is associated with its bioenergetics metabolism. However, even being a prominent human pathogen, its respiratory enzymes have been escaping attention. The intensive knowledge of this organism through the study of enzymes, as NDH-2s, involved in its energetic metabolism will open new

approaches for the design of new antimicrobial drugs against *S. aureus* infections.

1.4 Type II NADH:quinone oxidoreductases (NDH-2s)

Type II NADH:quinone oxidoreductases (NDH-2s, EC 1.6.99.3) are monotopic proteins, meaning they are attached to the membrane from one side but do not cross the lipid bilayer completely, with approximately 45 kDa. They catalyze the two-electron oxidation of NADH and the reduction of quinone but do not contribute to the establishment of a membrane potential. NDH-2s are recognized as suitable targets for novel antimicrobial therapies since they are the only enzymes with NADH:quinone oxidoreductase activity expressed in many pathogenic organisms, both bacteria and protozoa[69].

According to Marreiros *et al* that performed a taxonomic profile of NDH-2s evaluating the presence of their coding genes in all species deposited in the KEGG database, NDH-2s are present in the three domains of life, Eukarya, Bacteria and Archaea (Figure 1 .8).

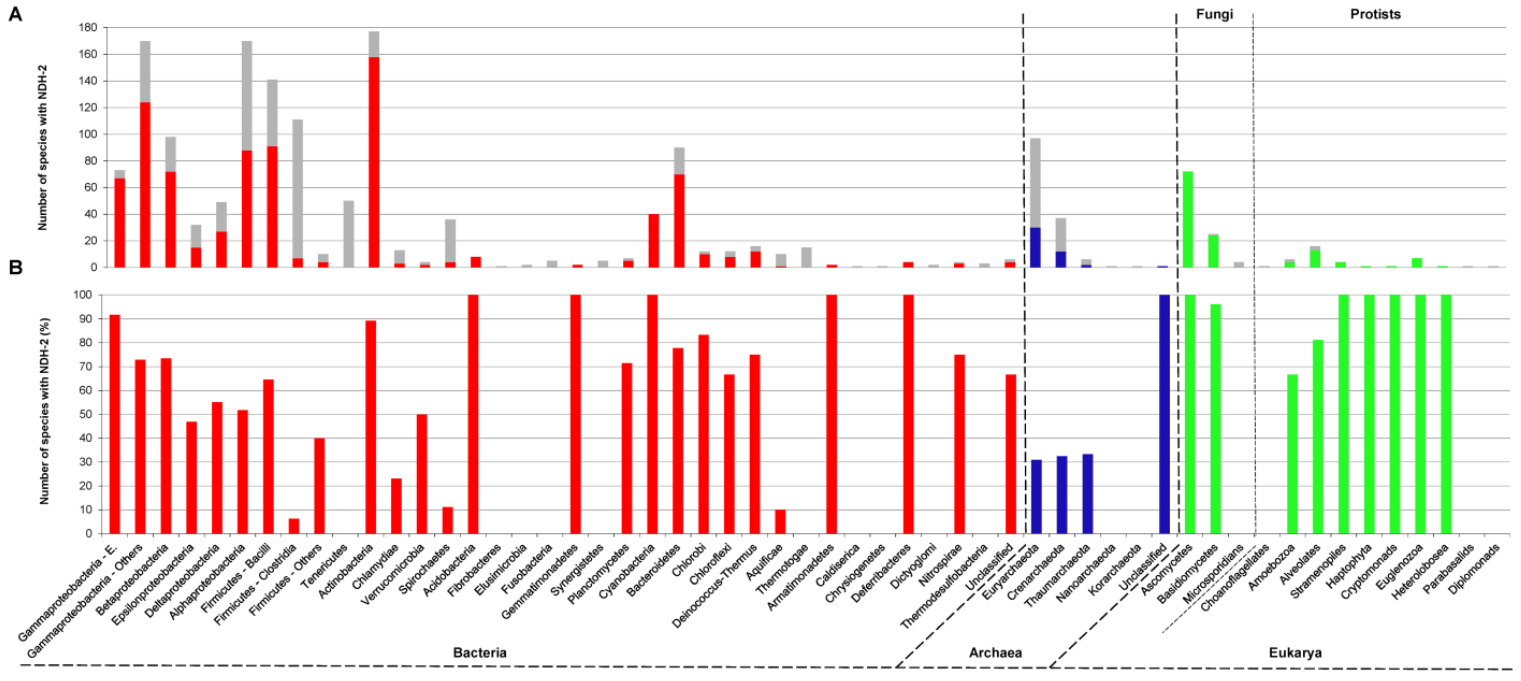

Figure 1.8 Distribution of NDH-2s in the three domains of life. The diagram indicates the number and fraction of species per phylum that encode at least one NDH-2. **A)** The bars in gray indicate the total number of species present in each phylum. These are superimposed by colored bars indicating the number of species per phylum with at least one gene encoding a NDH-2. **B)** Percentage of the species within each phylum containing at least one gene encoding a NDH-2. The color code is: Eukarya, green; Bacteria, red and Archaea, blue.

In Bacteria, genes coding for NDH-2 (Figure 1.8) are observed in 26 of the 36 phyla and in 60 % of the species. Hundred percent of the species from Cyanobacteria (40 species), 89 % from Actinobacteria (177 species), 66 % from Proteobacteria superphylum (592 species) and 39 % from Firmicutes (262 species) contain at least one gene encoding NDH-2. In Archaea, we noticed 71 NDH-2s that are present in 32 % of the 143 species, mainly belonging to the Halobacteriales (Euryarchaeota) and Sulfolobales (Crenarchaeota) orders. In Fungi, the Ascomycetes and Basidiomycetes phyla have 100 % (72 species) and 96 % (25 species) of the species with genes encoding NDH-2, respectively, whereas these genes are not observed in the four species of the Microsporidia phylum (Figure 1.8). 80 % of the 39 protist species have at least one gene encoding NDH-2.

Several organisms may express multiple NDH-2s, like in fungi these enzymes are present on both sides of the mitochondrial membrane, allowing the oxidation of both the cytosolic and mitochondrial NAD(P)H. For example, one of the NDH-2s (NDI1) of *Neurospora crassa* [70–72] was suggested to be essential for the initial steps of germination of both sexual and asexual spores of this fungus[72]. *Saccharomyces cerevisiae* contains two external NDH-2s (NDE1 and NDE2), one internal (Ndi1), and another one of unknown localization (Aif1p)[31,73–76]. Ndi1 was observed to be essential for the yeast survival[77] and was also reported to induce apoptosis[78]. The phytopathogenic fungus *Ustilago maydis* have two NDH-2s on both sides of the inner mitochondrial membrane and in addition an external NADPH:quinone oxidoreductase, being the three enzymes essential for the continuous operations of glycolysis and other metabolic routes dependent on the availability of NAD^+[79]. NDH-2s from protists *P. falciparum*, *Toxoplasma gondii*, *Trypanosoma brucei* and *Chlamydomonas reinhardtii* have been also investigated[69,80,81]. These

organisms have developed different strategies to succeed in hypoxic and anoxic environments and depending on the energy metabolism demands, some rely exclusively on NDH-2 for their NADH:quinone oxidoreductase activity as the case of *P. falciparum*[69]. The reason for the presence of multiple NDH-2s in the same organism is not clear, but it could be related to their role in different metabolic pathways, for example in respiration or photosynthesis, or/and different organelle localization. Some NDH-2s sequences contain mitochondrial or chloroplast signal peptides and proteins have been detected facing both sides of plastid membranes.

NDH-2s are members of the two-dinucleotide binding domains flavoproteins (tDBDF) superfamily[82]. tDBDF members are characterized by having NAD(P)H and flavin binding domains, with identical structural Rossmann folds[83] (Figure 1.9). All the members of the family contain flavin adenine dinucleotide, FAD, as prosthetic group and interact with NAD(P)H/NAD(P)$^+$, with the exception of sulfide:quinone oxidoreductase (SQR) and sulfide:flavocytochrome *c* oxidoreductase (also called flavocytochrome *c* sulfide dehydrogenase, FCSD).

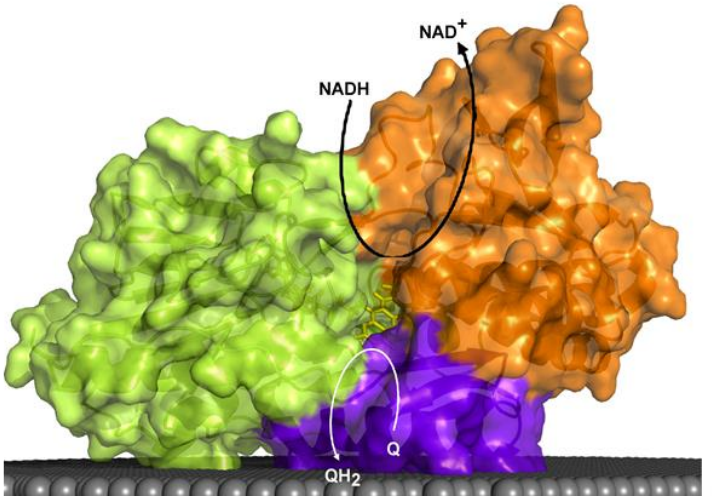

Figure 1.9 Schematic representation of the crystal structural of NDH-2. NDH-2 contains three domains: first dinucleotide binding domain, or FAD binding (green); second dinucleotide binding domain or NADH binding (orange); and membrane interacting domain, amphipathic helices at the C-terminal (purple).

SQRs and FCSDs also have the two dinucleotide binding domains but the NADH binding site is structurally inaccessible owing to the presence of a loop[84–87]. Some members of the tDBDF superfamily have additional redox centres, a disulfide bridge, as for example glutathione reductases or dihydrolipoamide dehydrogenases. In fact, the superfamily has also been named the flavin-disulfide reductases family. Several members of the superfamily have C-terminal extensions, which in the case of NDH-2 constitutes the membrane interacting domain composed of two amphipathic helices[77,88,89]. The crystal structures of yeast Ndi1, obtained by two different groups (PDB:4G6H and PDB:4G9K), stimulated discussions on the number and location of the substrate binding sites[77,88]. The structures from bacterial enzymes, those of the thermoalkaliphilic bacterium *Caldalkalibacillus thermarum* (PDB: 4NWZ) and of *S. aureus* (PDB: 5NA1) were also obtained but

in the absence of the substrates, the latter was solved by our group and will be presented and discussed in chapter 3[89,90]. Several structural features are conserved among NDH-2 family, in *C. thermarum* NDH-2 the amino acid sequence motif AQxAxQ was proposed to characterize the quinone binding site[89], which is also present in the NDH-2 from *C. cerevisiae*[77,88]. In NDH-2s from *N. crassa* and *Arabidopsis thaliana* an additional sequence insertion corresponding to an EF-hand structural motif is present. This motif is able to bind calcium, suggesting in this way different possibilities of protein regulation[91,92].

The origin and evolution of NDH-2s are unclear and difficult to track because it may not always be possible to distinguish them from the other members of the tDBDF superfamily. Marreiros *et al*[9] showed through the study of the phylogenetic distribution of NDH-2s, these enzymes form several groups of sequences, and when analyzing a generated Neighbour-joining (NJ) dendrogram, their distribution is not congruent with the taxonomic tree, suggesting different origins for the eukaryotic sequences and possible lateral gene transfer among prokaryotes (Figure 1.10). It was already mentioned that genes coding for NDH-2s were observed in all 40 cyanobacteria species with known complete genomes (the only prokaryotic phylum in which this situation occurs), as well as in 100 % of plant species. This observation raised the prospect that NDH-2s appeared with the origin of photosynthesis. Photosynthesis would already contribute extensively to the transmembrane difference of the electrochemical potential and could generate an oversupply of NADH if biosynthetic processes were less needed. This would lead to a scenario with excess of NADH and high membrane potential.

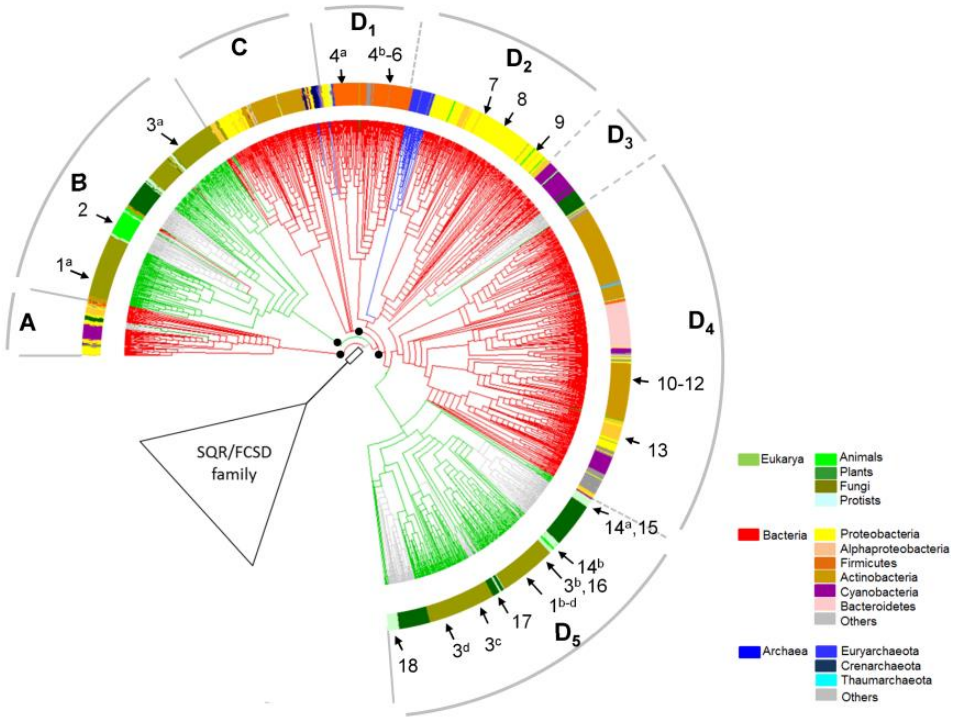

Figure 1.10 Neighbor-joining dendrogram of NDH-2s. The dendrogram was obtained using 2567 sequences of NDH-2s and sequences from SQRs/ FCSDs to define the outer group, midpoint root, 1000 replicates of bootstrap, 999 generated seeds. Branches are colored according to the three domains of life from which the organism containing the respective NDH-2 originates: green corresponds to microorganisms from Eukarya (plant and animal sequences are represented in grey), red to Bacteria and blue to Archaea. The external ring of the dendrogram, in the region of NDH-2s, indicates the phyla containing the organisms with the respective NDH-2 sequences according to the color code indicated in the figure. Sequences of biochemically characterized NDH-2s are indicated as: 1a-d) *S. cerevisiae*, 2) *H. sapiens*, 3a-d) *N. crassa*, 4a-b) *S. aureus*, 5) *C. thermarum*, 6) *B. pseudofirmus*, 7) *M. capsulatus*, 8) *E. coli*, 9) *G. oxydans*, 10) *M. tuberculosis*, 11) *M. smegmatis*, 12) *C. glutamicum*, 13) *A. tumefaciens*, 14a-b) *T. gondii*, 15) *P. falciparum*, 16) *Y. lipolytica*, 17) *C. reinhardtii*, 18) *T. brucei*.

In such case, NDH-2 could appear as the solution to regenerate NAD^+ without contributing to the membrane potential, that is, the way to reoxidize NADH independently of the membrane potential. This idea is totally speculative, although it can stimulate further discussion on the existence and

evolution of alternative metabolic pathways and enzymes, bringing robustness and versatility to biological systems.

An exhaustive biochemical, structural, and cellular approaches was applied to this work and the results will be presented and discussed in the following chapters.

1.5 References

[1] P. Mitchell, Coupling of phosphorylation to electron and hydrogen transfer by a chemi-osmotic type of mechanism, Nature. (1961). https://doi.org/10.1038/191144a0.

[2] M.T. Madigan, J.M. Martinko, D.A. Stahl, D.P. Clark, Brock Biology of Microorganisms 13th Edition, 2009. https://doi.org/10.1017/CBO9781107415324.004.

[3] B. Søballe, R.K. Poole, Microbial ubiquinones: Multiple roles in respiration, gene regulation and oxidative stress management, Microbiology. (1999) 1817–1830. https://doi.org/10.1099/13500872-145-8-1817.

[4] J. Hirst, Mitochondrial Complex I, Annu. Rev. Biochem. 82 (2013) 551–575. https://doi.org/10.1146/annurev-biochem-070511-103700.

[5] C.R.D. Lancaster, A. Kröger, Succinate: Quinone oxidoreductases: new insights from X-ray crystal structures, Biochim. Biophys. Acta - Bioenerg. 1459 (2000) 422–31. https://doi.org/10.1016/S0005-2728(00)00180-8.

[6] N.J. Watmough, F.E. Frerman, The electron transfer flavoprotein: Ubiquinone oxidoreductases, Biochim. Biophys. Acta - Bioenerg. (2010) 1910–1916. https://doi.org/10.1016/j.bbabio.2010.10.007.

[7] D.G. Nicholls, S.J. Ferguson, Respiratory chains, in: Bioenergetics, 2003. https://doi.org/10.1016/b978-012518121-1/50007-5.

[8] M.M. Elguindy, E. Nakamaru-Ogiso, Apoptosis-inducing factor (AIF) and its family member protein, AMID, are rotenone-sensitive NADH:ubiquinone oxidoreductases (NDH-2), J. Biol. Chem. 290 (2015) 20815–26. https://doi.org/10.1074/jbc.M115.641498.

[9] B.C. Marreiros, F. V. Sena, F.M. Sousa, A.P. Batista, M.M. Pereira, Type II NADH:quinone oxidoreductase family: phylogenetic distribution, structural diversity and evolutionary divergences, Environ. Microbiol. 18 (2016) 4697–4709. https://doi.org/10.1111/1462-2920.13352.

[10] K.R. Marshall, M. Gong, L. Wodke, J.H. Lamb, D.J.L. Jones, P.B. Farmer, N.S. Scrutton, A.W. Munro, The human apoptosis-inducing protein AMID is an

oxidoreductase with a modified flavin cofactor and DNA binding activity, J. Biol. Chem. 280 (2005) 30735–40. https://doi.org/10.1074/jbc.M414018200.

[11] B.C. Marreiros, F. Calisto, P.J. Castro, A.M. Duarte, F. V. Sena, A.F. Silva, F.M. Sousa, M. Teixeira, P.N. Refojo, M.M. Pereira, Exploring membrane respiratory chains, Biochim. Biophys. Acta - Bioenerg. 1857 (2016) 1039–1067. https://doi.org/10.1016/j.bbabio.2016.03.028.

[12] P. Mitchell, Protonmotive redox mechanism of the cytochrome b-c1 complex in the respiratory chain: Protonmotive ubiquinone cycle, FEBS Lett. (1975) 1–6. https://doi.org/10.1016/0014-5793(75)80098-6.

[13] S. Iwata, J.W. Lee, K. Okada, J.K. Lee, M. Iwata, B. Rasmussen, T.A. Link, S. Ramaswamy, B.K. Jap, Complete structure of the 11-subunit bovine mitochondrial cytochrome bc1 complex, Science (80-.). 281 (1998) 64–71. https://doi.org/10.1126/science.281.5373.64.

[14] M. Wikström, Identification of the electron transfers in cytochrome oxidase that are coupled to proton-pumping, Nature. 338 (1989) 776–8. https://doi.org/10.1038/338776a0.

[15] H. Eubel, L. Jänsch, H.P. Braun, New insights into the respiratory chain of plant mitochondria. Supercomplexes and a unique composition of complex II, Plant Physiol. 133 (2003) 274–86. https://doi.org/10.1104/pp.103.024620.

[16] P. Bennoun, Evidence for a respiratory chain in the chloroplast, Proc. Natl. Acad. Sci. 79 (1982) 4352–6. https://doi.org/10.1073/pnas.79.14.4352.

[17] A.H. Millar, J. Whelan, K.L. Soole, D.A. Day, Organization and Regulation of Mitochondrial Respiration in Plants, Annu. Rev. Plant Biol. 62 (2011) 79–104. https://doi.org/10.1146/annurev-arplant-042110-103857.

[18] P. Schertl, H.P. Braun, Respiratory electron transfer pathways in plant mitochondria, Front. Plant Sci. (2014). https://doi.org/10.3389/fpls.2014.00163.

[19] D.C. Logan, Plant Mitochondria, 2007. https://doi.org/10.1002/9780470986592.

[20] J.D. Rochaix, Regulation of photosynthetic electron transport, Biochim.

Biophys. Acta - Bioenerg. (2011) 375–83. https://doi.org/10.1016/j.bbabio.2011.05.009.

[21] K. Ifuku, T. Endo, T. Shikanai, E.M. Aro, Structure of the chloroplast NADH dehydrogenase-like complex: Nomenclature for nuclear-encoded subunits, Plant Cell Physiol. (2011) 1560–8. https://doi.org/10.1093/pcp/pcr098.

[22] L. Peng, H. Shimizu, T. Shikanai, The chloroplast NAD(P)H dehydrogenase complex interacts with photosystem I in Arabidopsis, J. Biol. Chem. 283 (2008) 34873–9. https://doi.org/10.1074/jbc.M803207200.

[23] G. Peltier, E.-M. Aro, T. Shikanai, NDH-1 and NDH-2 Plastoquinone Reductases in Oxygenic Photosynthesis, Annu. Rev. Plant Biol. 67 (2016) 55–80. https://doi.org/10.1146/annurev-arplant-043014-114752.

[24] A. Krieger-Liszkay, K. Feilke, The dual role of the plastid terminal oxidase PTOX: Between a protective and a pro-oxidant function, Front. Plant Sci. 6 (2016). https://doi.org/10.3389/fpls.2015.01147.

[25] A.S. Bhagwat, A. Blokesch, K.D. Irrgang, J. Salnikow, J. Vater, Crosslinking of Components of the Cytochrome b6f Complex from Spinach Thylakoids by o-Phthalaldehyde, Arch. Biochem. Biophys. 304 (1993) 38–44. https://doi.org/10.1006/abbi.1993.1318.

[26] G. Kurisu, H. Zhang, J.L. Smith, W.A. Cramer, Structure of the Cytochrome b6f Complex of Oxygenic Photosynthesis: Tuning the Cavity, Science (80-.). 302 (2003) 1009–14. https://doi.org/10.1126/science.1090165.

[27] A. Abdrakhmanova, V. Zickermann, M. Bostina, M. Radermacher, H. Schägger, S. Kerscher, U. Brandt, Subunit composition of mitochondrial complex I from the yeast Yarrowia lipolytica, Biochim. Biophys. Acta - Bioenerg. (2004) 148–56. https://doi.org/10.1016/j.bbabio.2004.04.019.

[28] A. Maréchal, B. Meunier, D. Lee, C. Orengo, P.R. Rich, Yeast cytochrome c oxidase: A model system to study mitochondrial forms of the haem-copper oxidase superfamily, Biochim. Biophys. Acta - Bioenerg. (2012) 620–8. https://doi.org/10.1016/j.bbabio.2011.08.011.

[29] T. Gabaldón, D. Rainey, M.A. Huynen, Tracing the evolution of a large protein

complex in the eukaryotes, NADH:ubiquinone oxidoreductase (Complex I), J. Mol. Biol. 348 (2005) 857–70. https://doi.org/10.1016/j.jmb.2005.02.067.

[30] J. Nosek, H. Fukuhara, NADH dehydrogenase subunit genes in the mitochondrial DNA of yeasts, J. Bacteriol. 176 (1994) 5622–30. https://doi.org/10.1128/jb.176.18.5622-5630.1994.

[31] M.A.H. Luttik, K.M. Overkamp, P. Kötter, S. De Vries, J.P. Van Dijken, J.T. Pronk, The *Saccharomyces cerevisiae* NDE1 and NDE2 genes encode separate mitochondrial NADH dehydrogenases catalyzing the oxidation of cytosolic NADH, J. Biol. Chem. 273 (1998) 24529–34. https://doi.org/10.1074/jbc.273.38.24529.

[32] D. Uribe, G.G. Khachatourians, Identification and characterization of an alternative oxidase in the entomopathogenic fungus *Metarhizium anisopliae*, Can. J. Microbiol. 54 (2008) 119–27. https://doi.org/10.1139/W07-127.

[33] T. Joseph-Horne, D.W. Hollomon, P.M. Wood, Fungal respiration: A fusion of standard and alternative components, Biochim. Biophys. Acta - Bioenerg. (2001) 179–95. https://doi.org/10.1016/S0005-2728(00)00251-6.

[34] A.D. Tsaousis, E.R.S. Kunji, A. V. Goldberg, J.M. Lucocq, R.P. Hirt, T.M. Embley, A novel route for ATP acquisition by the remnant mitochondria of *Encephalitozoon cuniculi,* Nature. 453 (2008) 553–6. https://doi.org/10.1038/nature06903.

[35] N. Takaya, S. Kuwazaki, Y. Adachi, S. Suzuki, T. Kikuchi, H. Nakamura, Y. Shiro, H. Shoun, Hybrid respiration in the denitrifying mitochondria of *Fusarium oxysporum*, J. Biochem. 133 (2003) 461–5. https://doi.org/10.1093/jb/mvg060.

[36] T. Abe, T. Hoshino, A. Nakamura, N. Takaya, Anaerobic elemental sulfur reduction by fungus *Fusarium oxysporum*, Biosci. Biotechnol. Biochem. 71 (2007) 2402–7. https://doi.org/10.1271/bbb.70083.

[37] M. Kobayashi, Y. Matsuo, A. Takimoto, S. Suzuki, F. Maruo, H. Shoun, Denitrification, a novel type of respiratory metabolism in fungal mitochondrion, J. Biol. Chem. 271 (1996) 16263–7. https://doi.org/10.1074/jbc.271.27.16263.

[38] L.K. Fritz-Laylin, S.E. Prochnik, M.L. Ginger, J.B. Dacks, M.L. Carpenter, M.C.

Field, A. Kuo, A. Paredez, J. Chapman, J. Pham, S. Shu, R. Neupane, M. Cipriano, J. Mancuso, H. Tu, A. Salamov, E. Lindquist, H. Shapiro, S. Lucas, I. V. Grigoriev, W.Z. Cande, C. Fulton, D.S. Rokhsar, S.C. Dawson, The Genome of *Naegleria gruberi* Illuminates Early Eukaryotic Versatility, Cell. 140 (2010) 631–42. https://doi.org/10.1016/j.cell.2010.01.032.

[39] N.A. Castro-Guerrero, K. Krab, R. Moreno-Sánchez, The alternative respiratory pathway of Euglena mitochondria, J. Bioenerg. Biomembr. 36 (2004) 459–69. https://doi.org/10.1023/B:JOBB.0000047328.82733.ef.

[40] R. Moreno-Sánchez, R. Covián, R. Jasso-Chávez, S. Rodríguez-Enríquez, F. Pacheco-Moisés, M.E. Torres-Márquez, Oxidative phosphorylation supported by an alternative respiratory pathway in mitochondria from Euglena, Biochim. Biophys. Acta - Bioenerg. 1457 (2000) 200–10. https://doi.org/10.1016/S0005-2728(00)00102-X.

[41] C.W. Stairs, L. Eme, M.W. Brown, C. Mutsaers, E. Susko, G. Dellaire, D.M. Soanes, M. Van Der Giezen, A.J. Roger, A SUF Fe-S cluster biogenesis system in the mitochondrion-related organelles of the anaerobic protist Pygsuia, Curr. Biol. 24 (2014) 1176–86. https://doi.org/10.1016/j.cub.2014.04.033.

[42] S. Surve, M. Heestand, B. Panicucci, A. Schnaufer, M. Parsons, Enigmatic presence of mitochondrial complex I in *Trypanosoma brucei* bloodstream forms, Eukaryot. Cell. 11 (2012) 183–93. https://doi.org/10.1128/EC.05282-11.

[43] F. Bringaud, L. Rivière, V. Coustou, Energy metabolism of trypanosomatids: Adaptation to available carbon sources, Mol. Biochem. Parasitol. (2006) 1–9. https://doi.org/10.1016/j.molbiopara.2006.03.017.

[44] A.J. Roger, C.G. Clark, W.F. Doolittle, A possible mitochondrial gene in the early-branching amitochondriate protist *Trichomonas vaginalis*, Proc. Natl. Acad. Sci. U. S. A. 93 (1996) 14618–14622. https://doi.org/10.1073/pnas.93.25.14618.

[45] A.J. Roger, S.G. Svärd, J. Tovar, C.G. Clark, M.W. Smith, F.D. Gillin, M.L. Sogin, A mitochondrial-like chaperonin 60 gene in *Giardia lamblia:* Evidence that diplomonads once harbored an endosymbiont related to the progenitor of mitochondria, Proc. Natl. Acad. Sci. U. S. A. 95 (1998) 229–234.

https://doi.org/10.1073/pnas.95.1.229.

[46] C.G. Clark, A.J. Roger, Direct evidence for secondary loss of mitochondria in *Entamoeba histolytica*, Proc. Natl. Acad. Sci. U. S. A. 92 (1995) 6518–21. https://doi.org/10.1073/pnas.92.14.6518.

[47] C.W. Stairs, M.M. Leger, A.J. Roger, Diversity and origins of anaerobic metabolism in mitochondria and related organelles, Philos. Trans. R. Soc. B Biol. Sci. (2015). https://doi.org/10.1098/rstb.2014.0326.

[48] T. Mogi, K. Kita, Diversity in mitochondrial metabolic pathways in parasitic protists Plasmodium and Cryptosporidium, Parasitol. Int. (2010) 305–12. https://doi.org/10.1016/j.parint.2010.04.005.

[49] Y. Yang, Y. Yu, X. Li, J. Li, Y. Wu, J. Yu, J. Ge, Z. Huang, L. Jiang, Y. Rao, M. Yang, Target Elucidation by Cocrystal Structures of NADH-Ubiquinone Oxidoreductase of *Plasmodium falciparum* (PfNDH2) with Small Molecule To Eliminate Drug-Resistant Malaria, J. Med. Chem. 60 (2017) 1994–2005. https://doi.org/10.1021/acs.jmedchem.6b01733.

[50] S. Kerscher, S. Dröse, V. Zickermann, U. Brandt, The three families of respiratory NADH dehydrogenases, Results Probl. Cell Differ. (2008) 185–222. https://doi.org/10.1007/400_2007_028.

[51] P.M.F. Sousa, M.A.M. Videira, A. Bohn, B.L. Hood, T.P. Conrads, L.F. Goulao, A.M.P. Melo, The aerobic respiratory chain of *Escherichia coli*: From genes to supercomplexes, Microbiol. (United Kingdom). 158 (2012) 2408–2418. https://doi.org/10.1099/mic.0.056531-0.

[52] L.Y.J.G. Montes De Oca, A. Chagolla-López, L.G. De La Vara, T. Cabellos-Avelar, C. Gómez-Lojero, E.B.G. Cirlos, The composition of the *bacillus subtilis* aerobic respiratory chain supercomplexes, J. Bioenerg. Biomembr. 44 (2012) 473–486. https://doi.org/10.1007/s10863-012-9454-z.

[53] N.D. Hammer, L.A. Schurig-Briccio, S.Y. Gerdes, R.B. Gennis, E.P. Skaar, CtaM is required for menaquinol oxidase aa3function in *Staphylococcus aureus*, MBio. 7 (2016) e00823-16. https://doi.org/10.1128/mBio.00823-16.

[54] C. Sparacino-Watkins, J.F. Stolz, P. Basu, Nitrate and periplasmic nitrate

reductases, Chem. Soc. Rev. 43 (2014) 676–706. https://doi.org/10.1039/c3cs60249d.

[55] A.M. Edwards, R.C. Massey, S.R. Clarke, Molecular mechanisms of *Staphylococcus aureus* nasopharyngeal colonization, Mol. Oral Microbiol. (2012) 1–10. https://doi.org/10.1111/j.2041-1014.2011.00628.x.

[56] S.Y.C. Tong, J.S. Davis, E. Eichenberger, T.L. Holland, V.G. Fowler, *Staphylococcus aureus* infections: Epidemiology, pathophysiology, clinical manifestations, and management, Clin. Microbiol. Rev. 28 (2015) 603–61. https://doi.org/10.1128/CMR.00134-14.

[57] H.W. Boucher, G.R. Corey, Community-associated methicillin-resistant *Staphylococcus aureus*: diagnosis and treatment., Compr. Ther. 34 (2008) 143–146. https://doi.org/10.1086/533590.

[58] M. Barber, M. Rozwadowska-Dowzenko, Infection by penicillin-resistant staphylococci, Lancet. 2 (1948) 641–4. https://doi.org/10.1016/S0140-6736(48)92166-7.

[59] M.P. Jevons, A.W. Coe, M.T. Parker, Methicillin resistance in staphylococci, Lancet. 281 (1963) P904-907. https://doi.org/10.1016/S0140-6736(63)91687-8.

[60] H.F. Chambers, F.R. DeLeo, Waves of resistance: *Staphylococcus aureus* in the antibiotic era, Nat. Rev. Microbiol. (2009) 629–41. https://doi.org/10.1038/nrmicro2200.

[61] R.M. Klevens, M.A. Morrison, J. Nadle, S. Petit, K. Gershman, S. Ray, L.H. Harrison, R. Lynfield, G. Dumyati, J.M. Townes, A.S. Craig, E.R. Zell, G.E. Fosheim, L.K. McDougal, R.B. Carey, S.K. Fridkin, Invasive Methicillin-Resistant *Staphylococcus aureus* Infections in the United States, J. Am. Med. Assoc. 298 (2007) 1763–1771. https://doi.org/10.1001/jama.298.15.1763.

[62] J.M. Conly, B.L. Johnston, The emergence of methicillin-resistant *Staphylococcus aureus* as a community-acquired pathogen in Canada, Can. J. Infect. Dis. (2003) 249–251. https://doi.org/10.1155/2003/197126.

[63] A.D. Kennedy, M. Otto, K.R. Braughton, A.R. Whitney, L. Chen, B. Mathema, J.R.

Mediavilla, K.A. Byrne, L.D. Parkins, F.C. Tenover, B.N. Kreiswirth, J.M. Musser, F.R. DeLeo, Epidemic community-associated methicillin-resistant *Staphylococcus aureus*: Recent clonal expansion and diversification, Proc. Natl. Acad. Sci. U. S. A. 105 (2008) 1327–1332. https://doi.org/10.1073/pnas.0710217105.

[64] S. Fuchs, J. Pané-Farré, C. Kohler, M. Hecker, S. Engelmann, Anaerobic gene expression in *Staphylococcus aureus*, J. Bacteriol. 189 (2007) 4275–4289. https://doi.org/10.1128/JB.00081-07.

[65] G.A. Somerville, M.S. Chaussee, C.I. Morgan, J.R. Fitzgerald, D.W. Dorward, L.J. Reitzer, J.M. Musser, *Staphylococcus aureus* aconitase inactivation unexpectedly inhibits post-exponential-phase growth and enhances stationary-phase survival, Infect. Immun. 70 (2002) 6373–82. https://doi.org/10.1128/IAI.70.11.6373-6382.2002.

[66] N.A. Spahich, N.P. Vitko, L.R. Thurlow, B. Temple, A.R. Richardson, *Staphylococcus aureus* lactate- and malate-quinone oxidoreductases contribute to nitric oxide resistance and virulence, Mol. Microbiol. 100 (2016) 759–73. https://doi.org/10.1111/mmi.13347.

[67] J.C. Kaiser, S. Omer, J.R. Sheldon, I. Welch, D.E. Heinrichs, Role of BrnQ1 and BrnQ2 in branched-chain amino acid transport and virulence in *Staphylococcus aureus*, Infect. Immun. 83 (2015) 1019–29. https://doi.org/10.1128/IAI.02542-14.

[68] C.R. Halsey, S. Lei, J.K. Wax, M.K. Lehman, A.S. Nuxoll, L. Steinke, M. Sadykov, R. Powers, P.D. Fey, Amino acid catabolism in *Staphylococcus aureus* and the function of carbon catabolite repression, MBio. 8 (2017). https://doi.org/10.1128/mBio.01434-16.

[69] G.A. Biagini, P. Viriyavejakul, P.M. O'Neill, P.G. Bray, S.A. Ward, Functional characterization and target validation of alternative complex I of *Plasmodium falciparum* mitochondria, Antimicrob. Agents Chemother. 50 (2006) 1841–51. https://doi.org/10.1128/AAC.50.5.1841-1851.2006.

[70] H. Weiss, G. von Jagow, M. Klingenberg, T. Bücher, Characterization of

Neurospora crassa Mitochondria Prepared with a Grind-Mill, Eur. J. Biochem. 14 (1970) 75–82. https://doi.org/10.1111/j.1432-1033.1970.tb00263.x.

[71] P. Carneiro, M. Duarte, A. Videira, Characterization of apoptosis-related oxidoreductases from *neurospora crassa*, PLoS One. 7 (2012) e34270. https://doi.org/10.1371/journal.pone.0034270.

[72] P. Carneiro, M. Duarte, A. Videira, The main external alternative NAD(P)H dehydrogenase of *Neurospora crassa* mitochondria, Biochim. Biophys. Acta - Bioenerg. 1608 (2004) 45–52. https://doi.org/10.1016/j.bbabio.2003.10.004.

[73] K.M. Overkamp, B.M. Bakker, P. Kötter, A. Van Tuijl, S. De Vries, J.P. Van Dijken, J.T. Pronk, In vivo analysis of the mechanisms for oxidation of cytosolic NADH by *Saccharomyces cerevisiae* mitochondria, J. Bacteriol. 182 (2000) 2823–30. https://doi.org/10.1128/JB.182.10.2823-2830.2000.

[74] I. Velázquez, J.P. Pardo, Kinetic characterization of the rotenone-insensitive internal NADH: Ubiquinone oxidoreductase of mitochondria from *Saccharomyces cerevisiae,* Arch. Biochem. Biophys. 389 (2001) 7–14. https://doi.org/10.1006/abbi.2001.2293.

[75] S. Wissing, P. Ludovico, E. Herker, S. Büttner, S.M. Engelhardt, T. Decker, A. Link, A. Proksch, F. Rodrigues, M. Corte-Real, K.U. Fröhlich, J. Manns, C. Candé, S.J. Sigrist, G. Kroemer, F. Madeo, An AIF orthologue regulates apoptosis in yeast, J. Cell Biol. 166 (2004) 969–974. https://doi.org/10.1083/jcb.200404138.

[76] T. Yamashita, E. Nakamaru-Ogiso, H. Miyoshi, A. Matsuno-Yagi, T. Yagi, Roles of bound quinone in the single subunit NADH-quinone oxidoreductase (Ndi1) from *Saccharomyces cerevisiae*, J. Biol. Chem. 282 (2007) 6012–20. https://doi.org/10.1074/jbc.M610646200.

[77] Y. Feng, W. Li, J. Li, J. Wang, J. Ge, D. Xu, Y. Liu, K. Wu, Q. Zeng, J.W. Wu, C. Tian, B. Zhou, M. Yang, Structural insight into the type-II mitochondrial NADH dehydrogenases, Nature. 491 (2012) 478–82. https://doi.org/10.1038/nature11541.

[78] Y. Cui, S. Zhao, Z. Wu, P. Dai, B. Zhou, Mitochondrial release of the NADH dehydrogenase Ndi1 induces apoptosis in yeast, Mol. Biol. Cell. 23 (2012) 4373–

4382. https://doi.org/10.1091/mbc.E12-04-0281.

[79] D. Matuz-Mares, G. Matus-Ortega, C. Cárdenas-Monroy, L. Romero-Aguilar, J.C. Villalobos-Rocha, H. Vázquez-Meza, G. Guerra-Sánchez, A. Peña-Díaz, J.P. Pardo, Expression of alternative NADH dehydrogenases (NDH-2) in the phytopathogenic fungus *Ustilago maydis*, FEBS Open Bio. 8 (2018) 1267–1279. https://doi.org/10.1002/2211-5463.12475.

[80] J. Fang, D.S. Beattie, Novel FMN-containing rotenone-insensitive NADH dehydrogenase from *Trypanosoma brucei* mitochondria: Isolation and characterization, Biochemistry. 41 (2002) 3065–72. https://doi.org/10.1021/bi015989w.

[81] S.S. Lin, S. Kerscher, A. Saleh, U. Brandt, U. Groß, W. Bohne, The *Toxoplasma gondii* type-II NADH dehydrogenase TgNDH2-I is inhibited by 1-hydroxy-2-alkyl-4(1H)quinolones, Biochim. Biophys. Acta - Bioenerg. 1777 (2008) 1455–62. https://doi.org/10.1016/j.bbabio.2008.08.006.

[82] S. Ojha, E.C. Meng, P.C. Babbitt, Evolution of function in the "two dinucleotide binding domains" flavoproteins, PLoS Comput. Biol. 3 (2007) e121. https://doi.org/10.1371/journal.pcbi.0030121.

[83] S.T. Rao, M.G. Rossmann, Comparison of super-secondary structures in proteins, J. Mol. Biol. 76 (1973) 241–56. https://doi.org/10.1016/0022-2836(73)90388-4.

[84] Z.W. Chen, M. Koh, G. Van Driessche, J.J. Van Beeumen, R.G. Bartsch, T.E. Meyer, M.A. Cusanovich, F.S. Mathews, The structure of flavocytochrome c sulfide dehydrogenase from a purple phototrophic bacterium, Science (80-.). 266 (1994) 430–2. https://doi.org/10.1126/science.7939681.

[85] J.A. Brito, F.L. Sousa, M. Stelter, T.M. Bandeiras, C. Vonrhein, M. Teixeira, M.M. Pereira, M. Archer, Structural and functional insights into sulfide:quinone oxidoreductase, Biochemistry. 48 (2009) 5613–22. https://doi.org/10.1021/bi9003827.

[86] M. Marcia, U. Ermler, G. Peng, H. Michel, The structure of *Aquifex aeolicus* sulfide:quinone oxidoreductase, a basis to understand sulfide detoxification

and respiration, Proc. Natl. Acad. Sci. U. S. A. 106 (2009) 9625–30. https://doi.org/10.1073/pnas.0904165106.

[87] M.M. Cherney, Y. Zhang, M. Solomonson, J.H. Weiner, M.N.G. James, Crystal structure of sulfide:Quinone oxidoreductase from *acidithiobacillus ferrooxidans*: Insights into sulfidotrophic respiration and detoxification, J. Mol. Biol. 398 (2010) 292–305. https://doi.org/10.1016/j.jmb.2010.03.018.

[88] M. Iwata, Y. Lee, T. Yamashita, T. Yagi, S. Iwata, A.D. Cameron, M.J. Maher, The structure of the yeast NADH dehydrogenase (Ndi1) reveals overlapping binding sites for water- and lipid-soluble substrates, Proc. Natl. Acad. Sci. U. S. A. 109 (2012) 15247–52. https://doi.org/10.1073/pnas.1210059109.

[89] A. Heikal, Y. Nakatani, E. Dunn, M.R. Weimar, C.L. Day, E.N. Baker, J.S. Lott, L.A. Sazanov, G.M. Cook, Structure of the bacterial type II NADH dehydrogenase: A monotopic membrane protein with an essential role in energy generation, Mol. Microbiol. 91 (2014) 950–64. https://doi.org/10.1111/mmi.12507.

[90] F. V. Sena, A.P. Batista, T. Catarino, J.A. Brito, M. Archer, M. Viertler, T. Madl, E.J. Cabrita, M.M. Pereira, Type-II NADH: Quinone oxidoreductase from *Staphylococcus aureus* has two distinct binding sites and is rate limited by quinone reduction, Mol. Microbiol. 98 (2015) 272–288. https://doi.org/10.1111/mmi.13120.

[91] A.M.P. Melo, M. Duarte, I.M. Møller, H. Prokisch, P.L. Dolan, L. Pinto, M.A. Nelson, A. Videira, The External Calcium-dependent NADPH Dehydrogenase from *Neurospora crassa* Mitochondria, J. Biol. Chem. 276 (2001) 3947–51. https://doi.org/10.1074/jbc.M008199200.

[92] A.M. Michalecka, Å.S. Svensson, F.I. Johansson, S.C. Agius, U. Johanson, A. Brennicke, S. Binder, A.G. Rasmusson, Arabidopsis Genes Encoding Mitochondrial Type II NAD(P)H Dehydrogenases Have Different Evolutionary Origin and Show Distinct Responses to Light, Plant Physiol. 133 (2003) 642–652. https://doi.org/10.1104/pp.103.024208.

Chapter 2

Expression, purification and biochemical characterization of the two Alternative NAD(P)H:quinone oxidoreductases from *Staphylococcus aureus*

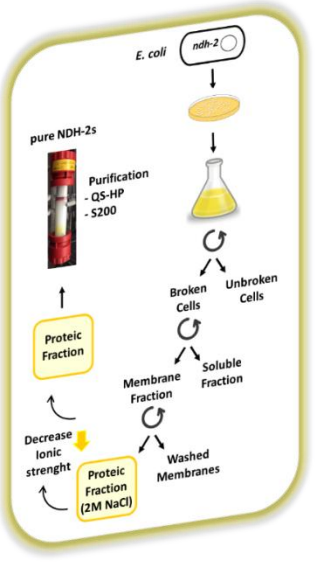

Chapter 2- Expression, purification and biochemical characterization of the two Alternative NAD(P)H:quinone oxidoreductases from *Staphylococcus aureus*

This section is based on the following publications:

- ✓ Rosário AL*, **Sena FV***, Batista AP, Athayde D, Oliveira TF, Pereira MM, Brito JA, Archer M. Expression, purification, crystallization and preliminary X-ray diffraction analysis on a type-II NADH:quinone oxidoreductase from the human pathogen *Staphylococcus aureus*. *Acta Crystallogr F Struct Biol Commun.* (2015) Apr; 71(Pt 4):477-82. Doi: 10.1107/S2053230X15005178.

- ✓ **Sena FV**, Batista AP, Catarino T, Brito JA, Archer M, Viertler M, Madl T, Cabrita EJ, Pereira, MM. Type-II NADH:quinone oxidoreductase from *Staphylococcus aureus* has two distinct binding sites and is rate limited by quinone reduction. *Mol Microbiol.* 98 (2015) 272–288. Doi: 10.1111/mmi.13120.

- ✓ Marreiros BC, **Sena FV**, Sousa FM, Batista AP, Pereira MM. Type II NADH:quinone oxidoreductase family: phylogenetic distribution, structural diversity and evolutionary divergences. *Environ Microbiol*. (2016). Doi: 10.1111/1462-2920.13352.

* Equally contributing authors.

Author Contribution:

Sena FV performed all the experiments and critically discussed the data, except for the HPLC analysis performed by Paula Chicau, and CV measurements performed with the help of Célia Silveira. **Sena FV** also participated in the design of the taxonomic profile of NDH-2s, analyzed and discussed the data.

2.1 Summary

Type II NADH:quinone oxidoreductases (NDH-2s) are monotopic enzymes involved in respiratory chains. *Staphylococcus aureus* has two genes encoding NDH-2s, *ndh-2a* and *ndh-2b*. In this work, the two NDH-2s enzymes from *S. aureus* were recombinantly expressed in *Escherichia coli*, successfully purified in two chromatography steps without using any detergents and the biochemical properties of both proteins were studied and compared. The flavin prosthetic group was shown to be FAD by reverse phase HPLC for both enzymes. Sequence analysis showed the two sequences share 23 % of identity and 42 % of similarity. We observed by UV visible absorption spectroscopy the presence of a band in the 650-800 nm region, typical of a Charge-Transfer (CT) complex formed between NAD^+ and the reduced flavin, in NDH-2A enzyme. Such CT complex is not observed in the case of NDH-2B enzyme. NDH-2B showed to be a NADPH:quinone oxidoreductase enzyme with maximal activity at pH 5.5 in contrast to NDH-2A, that oxidizes preferentially NADH. The biochemical characterization of the two NDH-2s from *S. aureus* settled the basis for the structural and functional understanding of these proteins.

2.2 Introduction

Type II NADH:quinone oxidoreductases (NDH-2s) are monotopic enzymes composed of a single subunit of approximately 50 kDa with non-covalently bound FAD as prosthetic group. The enzymes catalyze the transfer of two electrons from NAD(P)H to menaquinone, the Staphylococci's physiological quinone.

As previously described in Chapter 1, *Staphylococcus aureus* has no genes coding for the multisubunits Complex I or Na^+-NQR, but its genome contains two genes encoding NDH-2s. These proteins named as NDH-2A and NDH-2B are the object of study of this PhD work. *S. aureus* is not the only organism expressing more than one *ndh-2* gene, most of the species from bacterial and archaeal phyla contain on average one or two copies of NDH-2s, the exceptions being the species from Actinobacteria and Cyanobacteria phyla with averages of 2.7 and 3.5, respectively[1]. Eukaryotic species, as plants or fungi, may have two or more NDH-2 enzymes that can be facing either the mitochondrial matrix (internal enzymes), or the cytoplasm (external enzymes)[2,3]. The reason for the presence of multiple NDH-2s in the same organism is not clear, but it can be related to their role in different metabolic pathways, for example in respiration or photosynthesis, or/and different organelle localization[1].

NDH-2 enzymes that were already biochemically characterized are listed in Table 2.1. Different strategies of expression and purification of these proteins were addressed; some of the NDH-2s were recombinantly expressed in *E. coli*, and others the native protein was studied as the ones from *Neurospora crassa*, *Trypanosoma brucei* or *Mycobacterium tuberculosis.* NDH-2 from the thermoalkaliphilic bacterium *Caldalkalibacillus thermarum*, was expressed in *E. coli* and purified to homogeneity in the detergent octylglucoside

(OG) and was the first bacterial protein to be structurally characterized[4]. NDH-2 from *Bacillus pseudofirmus* was characterized and observed to be able to complement NADH dehydrogenase activity in a deficient *E. coli* strain[5]. As shown in table 2.1, the enzymes from *Gluconobacter oxydans*, *Methylococcus capsulatus* and *E. coli*, were also biochemically characterized[6–8]. NDH-2 from *E.coli* was expressed as a His-tagged protein, solubilized from the membranes using the detergent n-Decyl-β-D-Maltopyranoside (DM), purified by metal-chelating chromatography and eluted by an imidazole gradient in the presence of high ionic strength buffer[6]. NDH-2 from the proteobacterium *G. oxydans* was never fully purified but activities studies using membrane vesicles were performed and a screening of 304 antimicrobial compounds for new NDH-2 inhibitors was done[8]. NDH-2s from *M. tuberculosis*, *Mycobacterium smegmatis*, *Corynebacterium glutamicum* and *Agrobacterium tumefaciens* were also biochemically characterized (Table 2.1)[9–13]. *A. tumefaciens* NDH-2 (AtuNDH-2) was expressed and purified as NDH-2 from *E. coli*, and the purified enzyme was able to oxidize preferentially NADH towards NADPH[14]. NDH-2 from *Chlamydomonas reinhardtii* was produced as a recombinant protein in *E. coli* and the flavin cofactor was shown to be FMN by reverse phase HPLC[15]. One of the two sequences of NDH-2s from the parasite *T. brucei* was investigated and again FMN was suggested to be the flavin prosthetic group[16].

Table 2.1 List of biochemically characterized NDH-2s. Adapted from Marreiros *et al*[1].

Species	Name	KEGG ID	UniProt ID	Locus tag	Size (aa)	PDB	References
Agrobacterium tumefaciens	AtuNDH-2	atf:Ach5_19080	UPI000618764E	Ach5_19080	421	-	Bernard *et al,* 2006
Bacillus pseudofirmus	NDH-2A	bpf:BpOF4_04810	A7LKG4	BpOF4_04810	405	-	Liu *et al,* 2008
Bacillus subtilis	NDH-2	168:BSU12290	P80861	BSU12290	392	-	Krishna *et al* , 2019
Caldalkalibacillus thermarum	NDH-2	-	F5L3B8	-	399	5WED; 6BDO	Heikal *et al,* 2014; Nakatani *et al* , 2018; Petri *et al* , 2018
Chlamydomonas reinhardtii	Nda2	cre:CHLREDRAFT_133334	A8JI60	CHLREDRAFT_133334	615	-	Desplats *et al,* 2009
Corynebacterium glutamicum	NDH-2	cgl:NCgl1409	Q79VG1	NCgl1409	467	-	Nantapong *et al,* 2005; Matsushita *et al,* 2001
Escherichia coli	NDH-2	eco:b1109	P00393	b1109	434	-	Bjorklof *et al,* 2000; Villegas *et al,* 2011
Gluconobacter oxydans	NDH-II	gox:GOX1675	Q5FQD1	GOX1675	409	-	Mogi *et al,* 2009
Homo sapiens	AIF-M2	hsa:84883	Q9BRQ8	-	373	-	Marshall *et al,* 2005; Elguindy *et al,* 2015
Methylococcus capsulatus	NDH-2	mca:MCA1918	Q606U6	MCA1918	440	-	Cook *et al,* 2002
Mycobacterium smegmatis	NdhII	msm:MSMEG_3621	O52473	MSMEG_3621	457	-	Vilcheze *et al,* 2005
Mycobacterium tuberculosis	Mtb NDH-2	mtu:Rv1854c	P95160	Rv1854c	463	-	Yano *et al,* 2006; 2014
Neurospora crassa	NDE3	ncr:NCU09447	Q7S1W8	NCU09447	485	-	Carneiro *et al,* 2007
	NDE2	ncr:NCU08980	Q7S2Y9	NCU08980	577	-	Carneiro *et al,* 2004
	NDE1	ncr:NCU05225	Q7RVX4	NCU05225	673	-	Melo *et al,* 2001
	NDI1	ncr:NCU00153	Q7RXQ5	NCU00153	550		Duarte *et al,* 2003
Plasmodium falciparum	PfNDH2	pfa:PF3D7_0915000	Q8I302	PFI0735c	533	5JWA; 5JWB; 5JWC	Biagini *et al,* 2006; Yiqing Yang *et al, 2017*
Saccharomyces cerevisiae	Aif1p	sce:YNR074C	P52923	YNR074C	378	-	Wissing *et al,* 2004
	Ndi1	sce:YML120C	P32340	YML120C	513	4G6H; 4G9K; 5YJW; 5YJY; 5YJX	Vellazquez *et al,* 2001; Yamashita *et al,* 2007; Iwata *et al,* 2012; Feng *et al,* 2012; Yamashita *et al* , 2018
	NDE2	sce:YDL085W	Q07500	YDL085W	545	-	Luttik *et al,* 1998
	NDE1	sce:YMR145C	P40215	YMR145C	560	-	Luttik *et al,* 1998
Staphylococcus aureus	NDH-2B	sau:SA0799	W8TN11	SA0799	354	-	Schurig-Briccio *et al,* 2014
	NDH-2A	sau:SA0802	Q2FZV7	SA0802	402	5NA1; 5NA4	Schurig-Briccio *et al,* 2014; Sena *et al,* 2015
Toxoplasma gondii	TgNDH2-I	tgo:TGME49_009150	Q3HLX0	TGME49_009150	618	-	Lin *et al,* 2008
	TgNDH2-II	tgo:TGME49_088830	S8EWS1	TGME49_088830	657	-	Lin *et al,* 2008
Trypanosoma brucei	NDH-2	tbr:Tb10.6k15.0960	Q38A31	Tb10.6k15.0960	491	-	Fang and Beattie, 2002
Yarrowia lipolytica	NDH2	yli:YALI0F25135g	F2Z699	YALI0F25135g	582	-	Kerscher *et al,* 1999; Eschemann *et al,* 2005

2.3 Experimental procedures

2.3.1 Sequence alignment

Sequences encoding NDH-2s were retrieved from KEGG (the Kyoto Encyclopedia of Genes and Genomes). The sequences were aligned using BLAST (Basic local alignment search tool)[17].

2.3.2 Molecular cloning

The gene SAOUHSC_00878 coding for the *S. aureus* NCTC8325-4 NDH-2A and the gene SAOUHSC_00875 coding for the *S. aureus* NCTC8325-4 NDH-2B were cloned separately into pET-28a(+) between NdeI and XhoI restriction sites at the 5' and 3' ends, respectively, engineering the addition of a six histidine residue tag at the N-terminus (Table 2.2). The product of gene *ndh-2a* corresponds to a 408 amino acid residues protein with a theoretical molecular mass of ~45.6 kDa and the product of *ndh-2b* corresponds to a 360 amino acid residues protein with a theoretical molecular mass of ~40 kDa.

Table 2.2 Protein information related to NDH-2A and NDH-2B cloning.

Source organism	*Staphylococcus aureus* NCTC8325
DNA source	Genomic
Forward primer	CGTCATATGATGGCTCAAGATC
Reverse primer	CGGCTCGAGCTAGAATTTACCT
Cloning vector	pET-28a(+)
Expression vector	pET-28a(+)
Expression host	*E. coli* Rosetta 2 (DE3)pLysS
Complete amino acid sequence *ndh-2a*	HHHHHHMAQDRKKVLVLGAGYAGLQTVTKLQKAI STEEAEITLINKNEYHYEATWLHEASAGTLNYEDVLY PVESVLKKDKVNFVQAEVTKIDRDAKKVETNQGIY DFDILVVALGFVSETFGIEGMKDHAFQIENVITARE LSRHIEDKFANYAASKEKDDNDLSILVGGAGFTGVE FLGELTDRIPELCSKYGVDQNKVKITCVEAAPKMLP MFSEELVNHAVSYLEDRGVEFKIATPIVACNEKGFV VEVDGEKQQLNAGTSVWAAGVRGSKLMEESFEG VKRGRIVTKQDLTINGYDNIFVIGDCSAFIPAGEERP LPTTAQIAMQQGESVAKNIKRILNGESTEEFEYVDR GTVCSLGSHDGVGMVFGKPIAGKKAAFMKKVIDT RAVFKIGGIGLAFKKGK
Complete amino acid sequence *ndh-2b*	HHHHHHMKNLVLLGGGYGNMRIMSRILTTSLPQD YTVTLVDRMPFHGLKPEFYALAAGTKSDKDVRMKF PNHPQVNTVYGEINDIDLDAQIVSVGNSKIDYDELI IGLGCEDKYHNVPGAEEYTHSIQTLSKARDTFHSISE LPEGAKVGIVGAGLSGIELASELRESRSDLEIYLYDRG PRILRNFPEKLSKYVAKWFAKNNVTVVPNSNINKV EPGKIYNCDEPKDIDLVVWTAGIQPVEVVRNLPIDI NSNGRVIVNQYHQVPTYRNVYVVGDCADLPHAPS AQLAEVQGDQIADVLKKQWLNEPLPDKMPELKVQ GIVGSLGDKQGFAYIMDRTVTGRLASILKSGVLWLY KYHNG

2.3.3 Gene expression and protein purification

The following procedures are the same for the two NDH-2s under study. In both cases, *Escherichia coli* Rosetta 2 (DE3) pLysS cells were transformed using the heat shock method with the respective vector ndh-*S. aureus* and the cells were grown in 2 x YT-rich medium supplemented with 100 μg mL^{-1} kanamycin and 34 μg mL^{-1} chloramphenicol at 37 °C and 180 rpm min^{-1}. Gene expression was induced by the addition of 1 mM IPTG (isopropyl-β-D-thiogalactopyranoside) when the cells reached an OD_{600} of 0.6. The cells were harvested 4 h after induction by centrifugation at 11,305 g, for 10 min. The pellets were then resuspended in 100 mM K_2HPO_4/KH_2PO_4 pH 7.0, 250 mM NaCl

containing one tablet of protease inhibitors cocktail (Roche) and disrupted in a French press at 41.4 MPa. Cellular debris and undisrupted cells were separated by centrifugation at 4,100 g, for 10 min. The resulting suspension was ultracentrifuged at 204,709 g for 2 h. The membrane pellet was resuspended with a Potter-Elvehjem homogenizer in 100 mM K_2HPO_4/KH_2PO_4 pH 7.0, 2 M NaCl and incubated overnight at 4 °C. No detergents were used during the solubilization and purification of the enzyme (see below). The membrane fraction was again ultracentrifuged at 204,709 g for 1 h. The NaCl concentration of the supernatant containing NDH-2 was decreased to approximately 50 mM NaCl at 4 °C by successive additions of 100 mM K_2HPO_4/KH_2PO_4 pH 7.0 and concentrated in an Amicon system (30 000 MWCO).

Protein chromatography was performed on an AKTA Prime Plus system (GE Healthcare). The sample was injected in an ion-exchange Q-Sepharose High Performance column (GE Healthcare) and eluted with a gradient from 0 to 1 M NaCl in 100 mM K_2HPO_4/KH_2PO_4 pH 7.0. The fraction containing NDH-2 was then applied onto a gel-filtration Superdex 200 XK 26/60 column (GE Healthcare) and eluted with 100 mM K_2HPO_4/KH_2PO_4 pH 7.0, 250 mM NaCl containing one protease inhibitor cocktail tablet (Roche). The pure protein was stored at -80 °C.

2.3.4 Biochemical analyses

2.3.4.1 Protein purity

Protein purity of NDH-2A and NDH-2B was analyzed by sodium dodecyl sulphate – polyacrylamide gel electrophoresis (SDS-PAGE) using a Mini-PROTEAN® Electrophoresis System from BIORAD. Samples were diluted in loading buffer (Tris-HCl 50 mM, pH 8; SDS; bromophenol blue; glycerol; β-mercaptoethanol and urea) and were subsequently injected in a 15 %

acrylamide stacking and resolving gel. Low molecular weight (LMW) standards (GE Healthcare) were used ranging from 14 to 97 kDa. Electrophoresis was carried out at 180 V, 400 mA, 200 W for 1 h. Protein bands were revealed using Blue Coomassie Stainer (0.1 %).

2.3.4.2 Protein and FAD content

Protein concentration was determined by the BCA (bicinchoninic acid assay) Protein Assay Reagent (Pierce) using BSA (bovine serum albumin) as standard (Thermo Fisher Scientific). The protein was identified by mass spectrometry at the Unit MS, ITQB/IBET. The data was acquired in positive reflector MS and MS/MS modes in a 4800 plus MALDI-TOF/TOF (AB Sciex) mass spectrometer, using 4000 Series Explorer Software v.3.5.3 (Applied Biosystems). External calibration was performed using Pepmix1 (Laser BioLabs).

The flavin prosthetic group was identified by reverse phase chromatography. The protein was denatured by incubation at 100 °C for 10 min and removed by centrifugation. The supernatant was injected in a Waters, Nova Pack C18 60 Å 4 µm (3.9 × 150 mm) column operated in a Waters-Alliance HPLC system. The column was equilibrated with 100 mM ammonium acetate at pH 6 and 5 % methanol (V/V) and the sample was eluted in the same buffer with a linear gradient from 5 to 15 % methanol (V/V) at 1 mL min^{-1}. Commercial FAD (Merck) and FMN (Sigma Aldrich) were used as standards.

Flavin content of the pure protein was determined spectroscopically with a Shimadzu UV-1603 spectrophotometer, using the extinction coefficient of 11.3 mM^{-1} cm^{-1} at 450 nm for the free oxidized flavin.

2.3.4.3 Protein oligomerization state

To investigate the oligomerization state of NDH-2s size exclusion chromatography was performed using a Superdex 200 10/300 GL column (GE Healthcare) pre-equilibrated with 100 mM K_2HPO_4/KH_2PO_4, pH 7.0, 250 mM NaCl buffer and operated in an AKTA Prime Plus system (GE Healthcare). Standards: Blue dextran, ferritin, aldolase, conalbumin, BSA and cytochrome *c* were used to obtain a calibration curve.

To further confirm the oligomeric state of the two NDH-2s, a Native-PAGE was performed. The protein samples, containing 0.5 µg of NDH-2 with sample buffer and Coomassie G250 were loaded into 4-16 % acrylamide gel and submitted to 160 V, for 1 hour and 20 minutes in an Amersham ECL Gel BOX (Amersham). High molecular mass markers (GE Healthcare) were used ranging from 66 to 669 kDa.

2.3.4.4 Protein stability

Thermal denaturation assays (25–90 °C) were performed using a Peltier temperature controller with a rate of 0.5 °C min^{-1}, and the data were recorded in intervals of 0.5 °C with an acquisition time of 0.1 min. Denaturation was monitored by fluorescence spectroscopy using excitation at 450 nm and emission at 530 nm to monitor flavin fluorescence. The assays were performed using 2 µM of protein in 100 mM K_2HPO_4/KH_2PO_4 pH 7.0, 250 mM NaCl buffer. The melting temperature was calculated using the OriginPro8 software, fitting a Boltzman function to the data.

2.3.4.5 Protein reduction potential

NDH-2 reduction potential was determined by cyclic voltammetry using a silver chloride (Ag/AgCl) electrode as reference, graphite (Pg) as working

electrode and platinum (Pt), as counter electrode controlled by a potentiostat. The electrolyte solution used was 100 mM K_2HPO_4/KH_2PO_4, pH 7.0 to ensure sufficient conductivity. Measurements were done with scan rates of 20 mV s^{-1}, 50 mV s^{-1}, 100 mV s^{-1}, 200 mV s^{-1} or 500 mV s^{-1} and data were then plotted as current (i) vs potential (E) to give the cyclic voltammogram trace. To ensure anaerobic conditions during the assays, a constant influx of argon was maintained into the voltammetry cell. Reduction potentials were calculated by averaging the Epc and Epa values of each scan rate, and then re-averaging the values obtained from the five tested scan rates. Final reduction potential was converted to have the reduction potential of the Standard Hydrogen Electrode (SHE) as reference.

2.3.4.6 Protein secondary structure analysis

Far-UV CD spectroscopy experiments were performed in a Spectropolarimeter J-815 at 25 °C with 8 sequential acquisitions at 100 nm/sec. Measurements were taken from 260 to 200 nm. NDH-2s were studied at 5 µM concentration using for NDH-2A 100 mM K_2HPO_4/KH_2PO_4 250 mM NaCl pH 7.0 buffer and for NDH-2B 50 mM MES Bis Tris Propane 250 mM NaCl pH 5.5 buffer.

2.3.4.7 UV-visible absorption spectroscopic characterization

NDH-2 (0.44 mg of each) was reduced by the addition of NADH or NADPH or sodium dithionite in an anaerobic chamber. Oxidation of NDH-2 by 2,3-Dimethyl-1,4-naphtoquinone (DMN) (synthesized from menadione from Sigma Aldrich) was achieved in a 1:1 ratio. When needed, a mixture of 5 mM glucose, 4 U mL^{-1} glucose oxidase and 130 U mL^{-1} catalase was used, to ensure total O_2-free conditions. Spectra were collected at wavelengths ranging from

250 to 850 nm, at 35 °C and using 100 mM K_2HPO_4/KH_2PO_4 250 mM NaCl pH 7.0 buffer or 50 mM MES Bis Tris Propane 250 mM NaCl pH 5.5 buffer.

2.3.4.8 Steady-state kinetics

To investigate if the purified proteins were catalytically active, preliminary activity assays were performed in an anaerobic chamber on a Shimadzu UV-1800 spectrophotometer equipped with a Peltier temperature controlling and a stirring system. The reaction was started with the addition of 100 µM NADH or 100 µM NADPH (depending on the NDH-2), followed by the addition of 150 µM of quinone and NDH-2, 20 nM NDH-2A or 200nM NDH-2B. The buffers were 100 mM K_2HPO_4/KH_2PO_4 250 mM NaCl pH 7.0 or 50 mM MES Bis Tris Propane pH 5.5, 250 mM NaCl, depending on the enzyme. The reaction was monitored by the decrease in absorption of NAD(P)H at 340 nm. The extinction coefficient of 6.22 cm^{-1} mM^{-1} at 340 nm was used for the absorption of NAD(P)H to calculate NDH-2-specific activity (µmol min^{-1} mg^{-1}).

For NDH-2A an activity temperature profile study was performed using different quinones as electron acceptors (DMN, 2,3-Dimethoxy-5,6dimethyl-benzoquinone (DDB) and 2,3,5,6-Tetramethyl-1,4-benzoquinone (Duroquinone)) at pH 7.0 and between 20 and 55 °C. For NDH-2B an activity pH profile study was performed at 35 °C and between pH 5.5 and 8, using DMN as substrate.

2.4 Results and Discussion

2.4.1 Sequence analysis reveals NDH-2A and NDH-2B share 23 % identity and similarity 42 %

Sequence alignment (Figure 2.1) shows both NDH-2s, NDH-2A (SAOUHSC_00878) and NDH-2B (SAOUHSC_00875) share ~23 % identity and a high sequence similarity of ~42 %, being these values calculated by using four different matrices (Blosum62, Blosum90, PAM30 or PAM250) from protein-protein BLAST program. Bioinformatics analysis reveals similar sequence identity values of NDH-2A from *S. aureus* with other NDH-2s, including NDH-2 enzymes from the bacterial pathogen *M. tuberculosis* (~30 %) and the yeast Ndi1 (27 %), showing a higher identity with the NDH-2 from *C. thermarum* (~46 %). Given that NDH-2s belong to the two-Dinucleotide Binding Domains Flavoprotein (tDBDF) superfamily, they are expected to present two domains for the binding of the dinucleotides (NADH and FAD) that are structurally similar between each other and each one adopts a Rossmann fold, known to stabilize the adenine rings of dinucleotides. The NDH-2A amino acid sequence contains two conserved GxGxxG motifs, each one present in the two domains mentioned above. Curiously, NDH-2B amino acid sequence presents instead of a GxGxxG, a GxGxG motif in the first dinucleotide binding domain. It is important to mention that the presence of such motifs is shared with members from the tDBDF superfamily and as a result it is difficult to predict the function of NDH-2A and NDH-2B simply based on the presence of these motifs. In addition, the amino acid sequence of both NDH-2s present one (NDH-2B) or two (NDH-2A) predicted amphipathic helices at the C-terminus (Figure 2.1). This last information was obtained using the PSIPRED (v3.0) software.

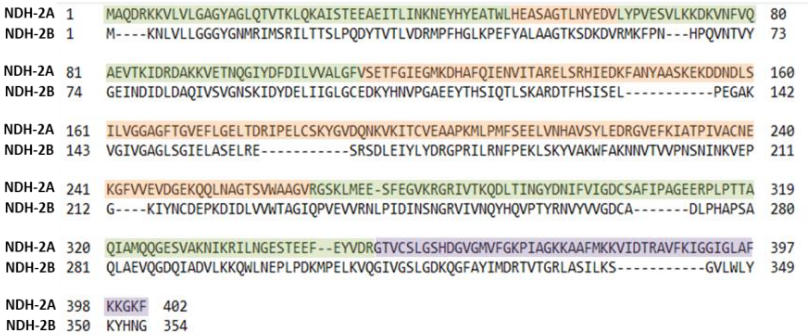

Figure 2.1 Alignment of the amino acid sequences of NDH-2A and NDH-2B from *S. aureus* using BLAST. First dinucleotide binding domain, or FAD binding domain (green); second dinucleotide binding domain or NADH binding domain (orange); and membrane interacting domain at the C-terminal (purple).

2.4.2 NDH-2s were successfully expressed and purified from *E. coli* membranes

The genes encoding the two NDH-2s from *S. aureus*, NDH-2A and NDH-2B, were expressed in the same conditions as well as the two proteins were purified following the same procedure. The membrane protein (NDH-2A and/or NDH-2B) was heterologous expressed in *E. coli* and purified by two chromatographic steps: anion exchange followed by size exclusion. No detergents were used during the solubilization and purification of NDH-2. Since NDH-2 is a monotonic membrane protein (and hence has no transmembrane regions), washing the membranes with 2 M NaCl was sufficient to solubilize this membrane-attached protein. This step revealed to be crucial for two reasons: firstly, it had the advantage of immediately separating all the soluble and integral membrane proteins and, secondly, the obtained preparation was stable and we could observe the presence of the prosthetic group, FAD, meaning no flavin was lost during this purification step. Notably, this allowed the functional characterization of an NDH-2 for the first time without possible interference caused by the presence of detergent. Although the protein was

produced with a His6 tag at the N-terminus, no affinity chromatography step was used, due to the increased probability of losing the FAD, obtaining a preparation with an NDH-2:FAD ratio of 1:1. We observed that this type of chromatography quite often leads to loss of the prosthetic group as previously reported [18,19]. To summarize both proteins were detected in the membranes and successfully purified in two chromatographic steps with a yield of 1 mg of protein/L of growth medium. Figure 2.2 shows the chromatograms of the gel-filtration column of NDH-2A and NDH-2B purifications. The proteins identified by mass spectrometry were pure as judged by SDS–PAGE analysis (Figure 2.2, inset).

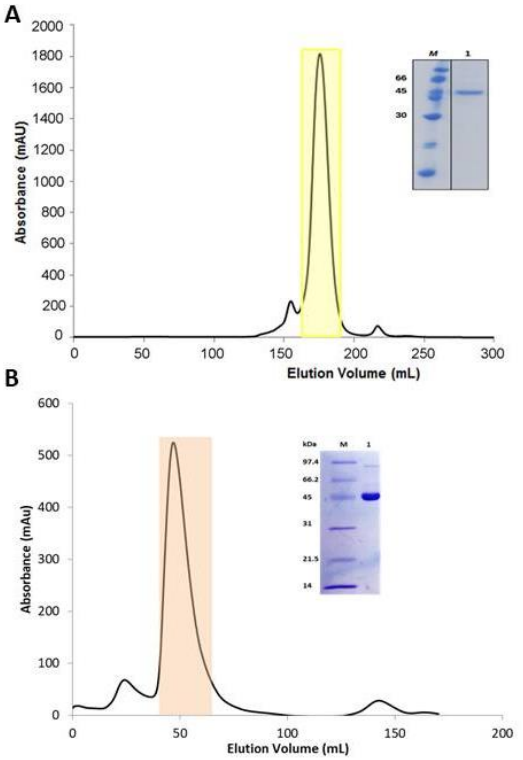

Figure 2.2 Chromatograms of the Size-exclusion chromatography and SDS–PAGE analysis (inset) of purified *S. aureus* NDH-2A (A) and NDH-2B (B). Lane M contains molecular-weight markers and lane 1 contains the peak depicted in yellow or orange in the chromatogram.

2.4.3 NDH-2s biochemical characterization

2.4.3.1 Flavin cofactor identification and reduction potential

The flavin cofactor was identified as flavin adenine dinucleotide (FAD) for both NDH-2s by HPLC analysis and is noncovalently bound as it could be removed by acidic precipitation or thermal denaturation. One molecule of FAD was present per molecule of protein, and the presence of other compounds, such as quinones, was not observed.

The reduction potential of FAD, determined by cyclic voltammetry, was −222 ± 20 mV and - 202 ± 20 mV vs SHE for NDH-A and NDH-2B, respectively. These values are in the same range of typical flavin cofactors[20](Figure 2.3).

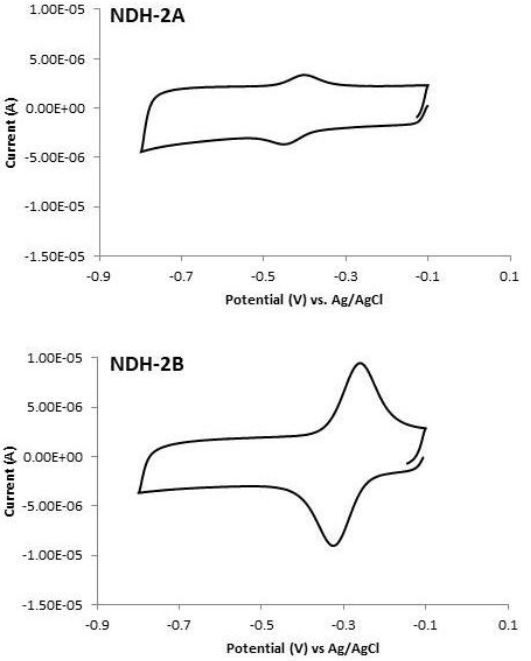

Figure 2.3 Cyclic voltammogrames recorded for NDH-2A and for NDH-2B. Experiments were done using a silver/silver chloride electrode (Ag/AgCl) as the reference electrode, graphite as the working electrode and platinum as the counter electrode electrodes.

The experience itself has been described as having a margin of error of approximately 20 mV. Analyzing the obtained results, we observe that between both copies of NDH-2, the reduction potential varies indeed 20 mV which is within the error, concluding that FAD's reduction potential of these two proteins is similar.

2.4.3.2 Oligomerization state

The oligomerization state of the proteins was investigated by analytical size exclusion chromatography, which is considered to be a good approach since NDH-2 has an approximate globular structure. In Figure 2.4, the superimposition of the chromatograms of the individually injected standards (blue dextran, ferritin, aldolase, conalbumin, BSA and cytochrome *c*) and NDH-2A is represented. NDH-2A is a dimer in solution. By blue native-PAGE, the presence of the dimer was confirmed although it was also possible to observe a band correspondent to the monomer (Figure S2.1). The quaternary structure of NDH-2B was also investigated by a blue native-PAGE that revealed only one band below the 66 kDa marker. Considering that the gel itself has an inherent error, it is possible to conclude that this protein is predominantly a monomer (Figure S2.2).

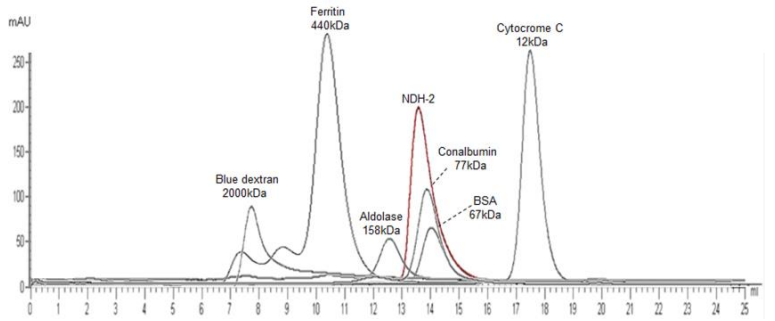

Figure 2.4 Size exclusion chromatography of NDH-2A from *S. aureus*. Superimposition of the chromatograms obtained for independent elutions of each standard protein and NDH-2A. The elution volumes of the standards allowed obtaining a Ve/Vo vs log [MM] plot and calculating the molecular mass of NDH-2A in solution.

2.4.3.3 Protein stability/integrity

Protein stability/integrity was analyzed, by measuring the fluorescence emission intensity at 530 nm (excitation at 450 nm), which corresponds to the FAD emission peak. An increase in the fluorescence emission can be interpreted as an increase in the exposure of the flavin cofactor to the environment, which is probably caused by exposure to the buffer as the protein loses its conformation.

The thermal denaturation profile of NDH-2A and NDH-2B monitored by the change in fluorescence of FAD shows a transition at approximately 55 °C, indicating that both NDH-2s maintain their FAD up to 50 °C (Figure 2.5).

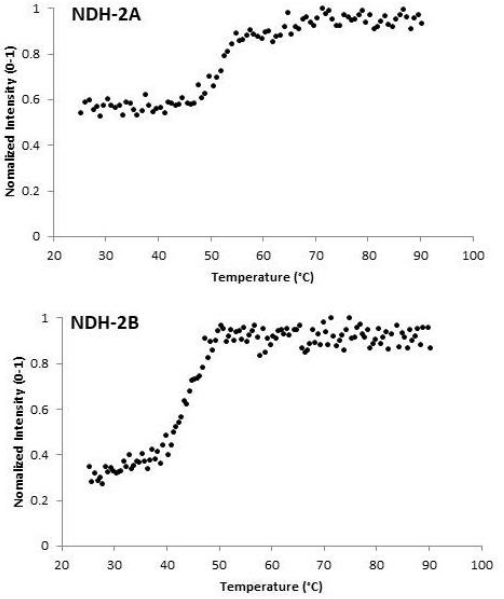

Figure 2.5 Thermal denaturation profiles of NDH-2A and NDH-2B from *S. aureus*. Thermal denaturation assays (25-90 °C) were performed using a Peltier temperature controller with a rate of 0.5 °C/min and the data was recorded in intervals of 0.5 °C with acquisition time of 0.1 min. Protein denaturation was monitored by fluorescence spectroscopy using excitation at 450 nm and emission at 530 nm to monitor flavin fluorescence.

Circular dichroism (CD) is a very useful method to rapidly study the folded state of a purified protein. Far UV CD spectroscopy (180–260 nm region) allows to study a protein's secondary structure content (% α-helix, β-sheet and random coil), so it was considered a good approach to assess if the secondary structure was maintained in the studied NDH-2s. CD spectra were measured between 200 and 260 nm. Far UV CD signals at 208 and 222 nm can give us information about the α-helix content as described by Greenfield & Fasman[21]. The obtained CD spectra for the studied NDH-2s are shown below in Figure 2.6.

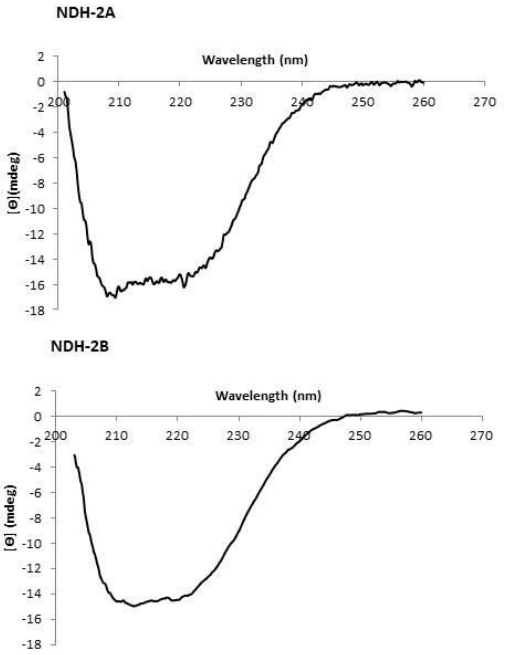

Figure 2.6 Far UV CD spectra of NDH-2A and NDH-2B from *S. aureus*. CD spectra were acquired at 25 °C using 5 µM NDH-2. Proteins show a similar CD spectrum.

Figure 2.6 shows that spectra are similar in terms of shape, with similar intensities at 200 and 208 nm, indicating that both proteins have the correct secondary structure, which is critical to assure biological function. A

quantitative analysis was performed analyzing the CD signal intensities at 208 and 222 nm and the ratio between them. NDH-2A has a $R^{208}/_{222}$ of 1.10 and NDH-2B of 0.94, meaning the two proteins differ between each other, in helices, sheets and loop content, in 15 %.

2.4.3.4 UV-visible absorption spectroscopic studies

NDH-2A presents an absorption spectrum typical of a flavoprotein, exhibiting bands with maxima at 375 and 450 nm and a shoulder close to 475 nm.

The fully reduced state of NDH-2A was achieved under anaerobic conditions by incubation with NADH. NDH-2A reduction is characterized by the loss of absorption in the 375–450 nm region and appearance of a broad absorption band with maximum at 650–800 nm (Figure 2.7). Further incubation with 2,3-Dimethyl-1,4-naphthoquinone (DMN) reoxidized the protein, leading to the reappearance of absorption in the 375–450 nm region and disappearance of that in the 650–800 nm region. A fully reduced state of NDH-2A was also obtained using sodium dithionite, and a loss of absorption in the 375–450 nm region was also observed, but the absorption in the 650–800 nm region was not detected (Figure 2.7). The absorption in the latter region could be restored by adding NAD^+ to the dithionite reduced NDH-2A (Figure 2.7). This result shows that the absorption in the 650–800 nm region indicates the presence of NAD^+ bound to the reduced protein. This broad absorption band was already observed and reported for many flavoproteins as a charge-transfer (CT) complex[22]. In flavoproteins, the CT complex is usually formed as a result of π–π interaction between the parallel stacked isoalloxazine ring of the reduced flavin and the nicotinamide ring of NAD^+ and has a broad absorption band in the long wavelength region.

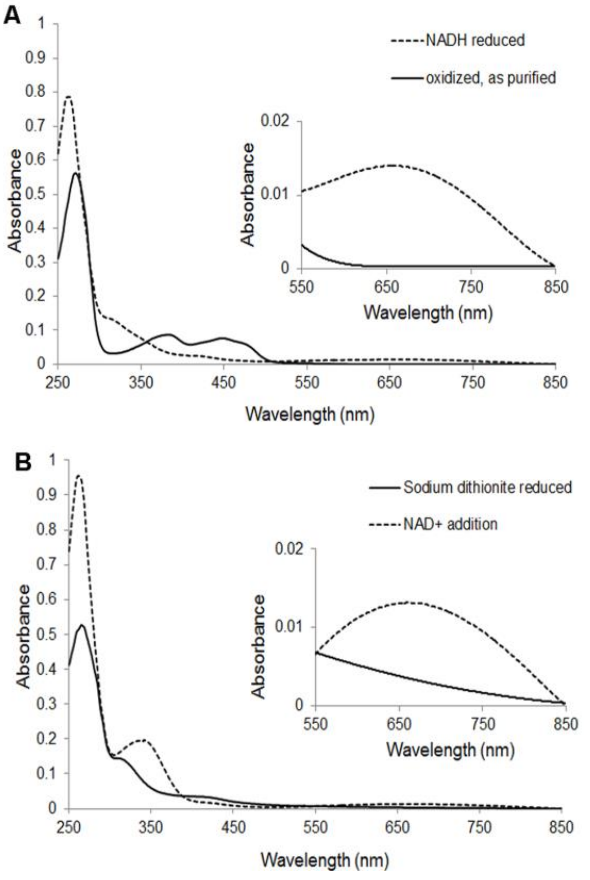

Figure 2.7 UV-visible absorption spectra of NDH-2A from *S. aureus*. A. NDH-2A as purified (solid line) and reduced with NADH (dashed line). The inserted figure expands absorption spectrum in the 600–800 nm region. **B.** NDH-2A reduced with dithionite (solid line) and incubated with NAD^+ (dashed line). The inserted figure expands absorption spectrum in the 600–800 nm region.

NDH-2B was also studied by UV-visible absorption spectroscopy and its oxidized state showed the presence of FAD, with a peak with maximum at 450 nm. The spectrum also presented a peak at 375 nm and an additional broad absorption band at 550 nm (Figure 2.8). This additional band that was not observed in NDH-2A may be responsible for the brownish color of the solution of NDH-2B, compared to the typical yellow color of NDH-2A.

The reduced state of NDH-2B was achieved under anaerobic conditions by the addition of NADPH (instead of NADH, discussed below) in 1:1 stoichiometry. This reduced state is characterized by the loss of absorbance in the 325-500 nm regions of the UV-visible spectrum. This spectrum did not show the presence of any absorbance band in the visible region, namely the one around 650-800 nm, that was noticed for the NADH reduced NDH-2A. As it was mentioned before such a band is typical of the presence of a charge-transfer complex between NAD^+ and the reduced flavin. Thus, in the case of NDH-2B there is no evidence for the presence of such complex.

Further incubation with stoichiometric amount of the acceptor DMN leaded to reoxidation of NDH-2B as observed by the reappearance of the typical absorbance band of the flavin (Figure 2.8).

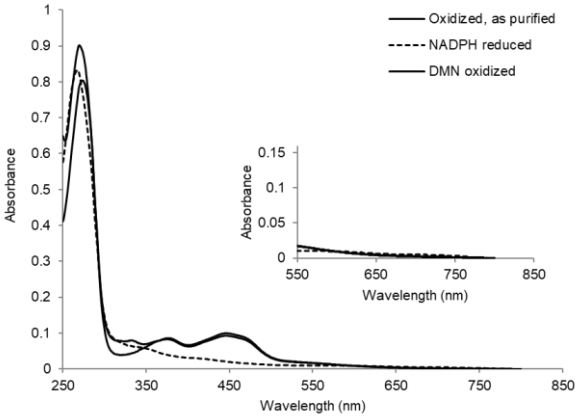

Figure 2.8 UV-visible absorption spectra of NDH-2B from *S. aureus.* NDH-2B as purified (solid line), reduced with NADPH in a 1:1 ratio (dotted line) and oxidized by DMN (1:1) (thin solid line). The inserted figure expands absorption spectrum in 550-850 region.

2.4.3.5 Kinetic studies

We tested the activity of NDH-2A using three different quinones, differing in their ring systems. DMN is a naphthoquinone characterized by its bicyclic ring system. DDB and DQ are benzoquinones thus presenting only one ring, which in the case of DDB contains two methoxy groups (Figure S2.3). Besides their chemical differences, the three quinones also present distinct reduction potentials, −70 mV for DMN, 0 mV for DQ and 120 mV for DDB. Enzymatic activities of NDH-2A were determined using NADH as the electron donor. The highest activity for the three tested quinones was obtained at 35 °C (Figure 2.9) which is consistent with the optimum temperature of growth of *S. aureus*, which is 37 °C. The specific activity for NDH-2A was 131.1 ± 2.7 µmol min^{-1} mg^{-1}, 125.3 ± 0.2 µmol min^{-1} mg^{-1} and 111.9 ± 1.6 µmol min^{-1} mg^{-1} using as electron acceptors DMN, DDB and DQ, respectively. The highest activity was observed when DMN, the menaquinone analogue, was used as substrate and this result was expected since menaquinone is the physiological quinone of *S. aureus* microorganism[23].

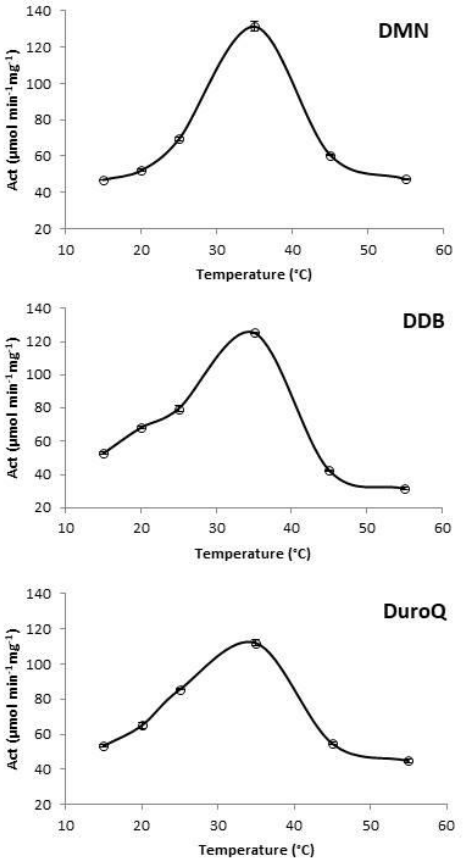

Figure 2.9 Temperature profiles of the activity of NDH-2A from *S. aureus*. Temperature profiles of NADH:quinone oxidoreductase activity (20-55 °C) using independently three different quinones, DMN, DDB and DQ.

NDH-2B activity was tested in the same conditions as NDH-2A, using the same substrates (NADH and DMN) and buffer. However, the specific activity was very low when comparing with the one of NDH-2A, 34.03 ± 0.86 µmol min^{-1} mg^{-1}. Towards this result we decided to test NDH-2B activity using NADPH instead of NADH, and NDH-2B specific activity was 49.24 ± 3.56 µmol min^{-1} mg^{-1} at pH 7. With the aim of determining the ideal pH for the maximum activity of NDH-2B, we performed a pH-dependent enzyme activity assay using NADH or NADPH and the results that are shown in Figure 2.10, indicate that the maximal

activity for NDH-2B occurs at pH 5.5 with NADPH as electron donor, having a specific activity of 80 µmol min^{-1} mg^{-1}. The activity of NDH-2B enzyme using NADH as substrate was almost constant for all the tested pH values and much lower than when using NADPH as substrate.

We also observed that NDH-2A has nearly no activity when NADPH is the substrate.

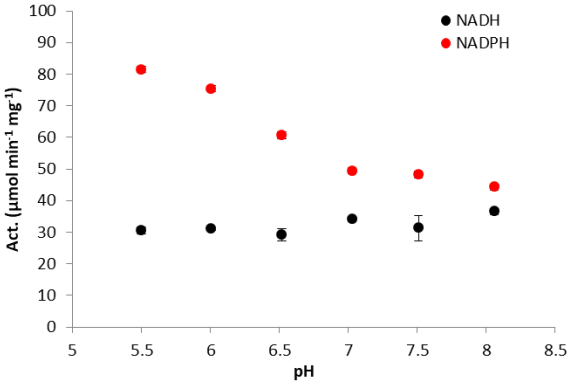

Figure 2.10 pH-dependent enzyme profile activity of NDH-2B from *S. aureus*. 200 µM NADH (black) and/or 200 µM NADPH (red) as the electron donors were measured in an anaerobic chamber at 35 °C with 150 µM DMN, 0.2 µM NDH-2B and different pH buffer solutions of 50 mM MES Bis Tris Propane.

2.5 Conclusion

The two NDH-2s from *S. aureus* were successfully expressed in *E. coli* and purified similarly from the membranes by two chromatographic steps without using any detergents since washing the membranes with 2 M NaCl was sufficient to solubilize these membrane-attached proteins. Both enzymes possess a FAD as prosthetic group, having similar reduction potentials, approximately 200 mV vs SHE. The oligomerization state of the proteins was analyzed by size exclusion chromatography and blue Native-PAGE and we conclude that NDH-2A is a dimer in solution and NDH-2B is in a monomer conformation. Investigation of the quaternary structure of NDH-2s by CD revealed the two proteins differ between each other in 15 % of α-helix, β-sheet, and random coil content.

We observed the appearance of a broad absorption band in the 650–800 nm region, upon addition of NADH under anaerobic conditions and in the absence of quinone with NDH-2A enzyme. This absorption band is due to the establishment of a Charge Transfer (CT) complex between the reduced flavin and NAD^+: upon reduction with dithionite the band in the 650–800 nm region did not appear, but was observed when NAD^+ was added. These observations were not detected for NDH-2B enzyme. The CT complex was observed in Ndi1 from yeast but in this case the quinone was required as an electron acceptor for the formation of the CT complex[22]. In the yeast's case the CT band increased in intensity in the presence of the electron acceptors, quinone or O_2 and this was not observed with NDH-2A. Preliminary kinetic assays were performed and both enzymes showed to have NAD(P)H:quinone oxidoreductase activities. NDH-2A catalyzes preferentially the oxidation of NADH and NDH-2B uses NADPH at optimal pH 5.5. Together these results demonstrate that the two NDH-2s from *S. aureus* have different preferences for

the electron donor (NADH or NADPH) and settled the basis for the following studies regarding the catalytic mechanism of the enzymes under investigation.

2.6 Acknowledgements

We acknowledge João Carita for cell growth, Isabel Pacheco for helping in protein purification, and Smilja Todorovic Lab for CV measurements. F.V.S. is recipient of fellowship by Fundação para a Ciência e a Tecnologia PD/BD/113985/2015, within the scope of the PhD program Molecular Biosciences PD/00133/2012. The work was supported by Fundação para a Ciência e a Tecnologia through Grant # PEst-OE/EQB/LA0004/2011.

2.7 References

[1] B.C. Marreiros, F. V. Sena, F.M. Sousa, A.P. Batista, M.M. Pereira, Type II NADH:quinone oxidoreductase family: phylogenetic distribution, structural diversity and evolutionary divergences, Environ. Microbiol. 18 (2016) 4697–4709. https://doi.org/10.1111/1462-2920.13352.

[2] P. Carneiro, M. Duarte, A. Videira, Characterization of apoptosis-related oxidoreductases from *neurospora crassa*, PLoS One. 7 (2012) e34270. https://doi.org/10.1371/journal.pone.0034270.

[3] H. Weiss, G. von Jagow, M. Klingenberg, T. Bücher, Characterization of *Neurospora crassa* Mitochondria Prepared with a Grind-Mill, Eur. J. Biochem. (1970). https://doi.org/10.1111/j.1432-1033.1970.tb00263.x.

[4] A. Heikal, Y. Nakatani, E. Dunn, M.R. Weimar, C.L. Day, E.N. Baker, J.S. Lott, L.A. Sazanov, G.M. Cook, Structure of the bacterial type II NADH dehydrogenase: A monotopic membrane protein with an essential role in energy generation, Mol. Microbiol. 91 (2014) 950–64. https://doi.org/10.1111/mmi.12507.

[5] J. Liu, T.A. Krulwich, D.B. Hicks, Purification of two putative type II NADH dehydrogenases with different substrate specificities from alkaliphilic *Bacillus pseudofirmus* OF4, Biochim. Biophys. Acta - Bioenerg. 1777 (2008) 453–61. https://doi.org/10.1016/j.bbabio.2008.02.004.

[6] K. Björklöf, V. Zickermann, M. Finel, Purification of the 45 kDa, membrane bound NADH dehydrogenase of *Escherichia coli* (NDH-2) and analysis of its interaction with ubiquinone analogues, FEBS Lett. 467 (2000) 105–10. https://doi.org/10.1016/S0014-5793(00)01130-3.

[7] S.A. Cook, A.K. Shiemke, Evidence that a type-2 NADH:quinone oxidoreductase mediates electron transfer to particulate methane monooxygenase in *Methylococcus capsulatus*, Arch. Biochem. Biophys. 398 (2002) 32–40. https://doi.org/10.1006/abbi.2001.2628.

[8] T. Mogi, K. Matsushita, Y. Murase, K. Kawahara, H. Miyoshi, H. Ui, K. Shiomi, S. Omura, K. Kita, Identification of new inhibitors for alternative NADH

dehydrogenase (NDH-II), FEMS Microbiol. Lett. 291 (2009) 157–61. https://doi.org/10.1111/j.1574-6968.2008.01451.x.

[9] T. Yano, L. Lin-Sheng, E. Weinstein, J.S. Teh, H. Rubin, Steady-state kinetics and inhibitory action of antitubercular phenothiazines on *Mycobacterium tuberculosis* Type-II NADH-menaquinone oxidoreductase (NDH-2), J. Biol. Chem. 281 (2006) 11456–63. https://doi.org/10.1074/jbc.M508844200.

[10] T. Yano, M. Rahimian, K.K. Aneja, N.M. Schechter, H. Rubin, C.P. Scott, *Mycobacterium tuberculosis* type II NADH-menaquinone oxidoreductase catalyzes electron transfer through a two-site ping-pong mechanism and has two quinone-binding sites, Biochemistry. 53 (2014) 1179–90. https://doi.org/10.1021/bi4013897.

[11] C. Vilchèze, T.R. Weisbrod, B. Chen, L. Kremer, M.H. Hazbón, F. Wang, D. Alland, J.C. Sacchettini, W.R. Jacobs, Altered NADH/NAD+ ratio mediates coresistance to isoniazid and ethionamide in mycobacteria, Antimicrob. Agents Chemother. 49 (2005) 708–20. https://doi.org/10.1128/AAC.49.2.708-720.2005.

[12] N. Nantapong, A. Otofuji, C.T. Migita, O. Adachi, H. Toyama, K. Matsushita, Electron transfer ability from NADH to menaquinone and from NADPH to oxygen of type II NADH dehydrogenase of *Corynebacterium glutamicum*, Biosci. Biotechnol. Biochem. 69 (2005) 149–59. https://doi.org/10.1271/bbb.69.149.

[13] L. Bernard, C. Desplats, F. Mus, S. Cuiné, L. Cournac, G. Peltier, Agrobacterium tumefaciens type II NADH dehydrogenase: Characterization and interactions with bacterial and thylakoid membranes, FEBS J. 273 (2006) 3625–37. https://doi.org/10.1111/j.1742-4658.2006.05370.x.

[14] C. Desplats, A. Beyly, S. Cuiné, L. Bernard, L. Cournac, G. Peltier, Modification of substrate specificity in single point mutants of *Agrobacterium tumefaciens* type II NADH dehydrogenase, FEBS Lett. 581 (2007) 4017–22. https://doi.org/10.1016/j.febslet.2007.07.035.

[15] C. Desplats, F. Mus, S. Cuiné, E. Billon, L. Cournac, G. Peltier, Characterization

of Nda2, a plastoquinone-reducing type II NAD (P) H dehydrogenase in chlamydomonas chloroplasts, J. Biol. Chem. 284 (2009) 4148–57. https://doi.org/10.1074/jbc.M804546200.

[16] J. Fang, D.S. Beattie, Novel FMN-containing rotenone-insensitive NADH dehydrogenase from *Trypanosoma brucei* mitochondria: Isolation and characterization, Biochemistry. 41 (2002) 3065–72. https://doi.org/10.1021/bi015989w.

[17] S.F. Altschul, W. Gish, W. Miller, E.W. Myers, D.J. Lipman, Basic local alignment search tool, J. Mol. Biol. 215 (1990) 403–10. https://doi.org/10.1016/S0022-2836(05)80360-2.

[18] M. Husain, V. Massey, Reversible Resolution of Flavoproteins into Apoproteins and Free Flavins, Methods Enzymol. 53 (1978) 429–37. https://doi.org/10.1016/S0076-6879(78)53047-4.

[19] F. Müller, Chemistry and biochemistry of flavoenzymes, 2018. https://doi.org/10.1201/9781351070584.

[20] S. Weber, E. Schleicher, Flavins and flavoproteins methods and protocols, 2014. https://doi.org/10.1007/978-1-4939-0452-5.

[21] N. Greenfield, G.D. Fasman, Computed Circular Dichroism Spectra for the Evaluation of Protein Conformation, Biochemistry. 8 (1969) 4108–4116. https://doi.org/10.1021/bi00838a031.

[22] Y. Yang, T. Yamashita, E. Nakamaru-Ogiso, T. Hashimoto, M. Murai, J. Igarashi, H. Miyoshi, N. Mori, A. Matsuno-Yagi, T. Yagi, H. Kosaka, Reaction mechanism of single subunit NADH-ubiquinone oxidoreductase (Ndi1) from *Saccharomyces cerevisiae*: Evidence for a ternary complex mechanism, J. Biol. Chem. 286 (2011) 9287–9297. https://doi.org/10.1074/jbc.M110.175547.

[23] R. Bentley, R. Meganathan, Biosynthesis of vitamin K (menaquinone) in bacteria, Microbiol. Rev. (1982) 241–280. https://doi.org/10.1128/mmbr.46.3.241-280.1982.

2.8 Supplementary Information

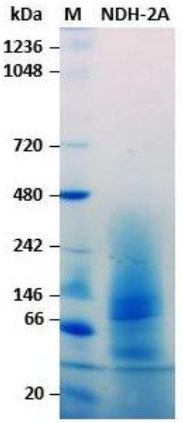

Figure S2.1 Blue Native-PAGE gel of NDH-2A. Native Mark Unstained Protein Standards was used to estimate the molecular mass of NDH-2A.

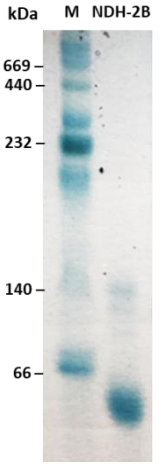

Figure S2.2 Blue Native-PAGE gel of NDH-2B. HMW calibration proteins from the calibration Kit for native electrophoresis was used to estimate the molecular mass of NDH-2B.

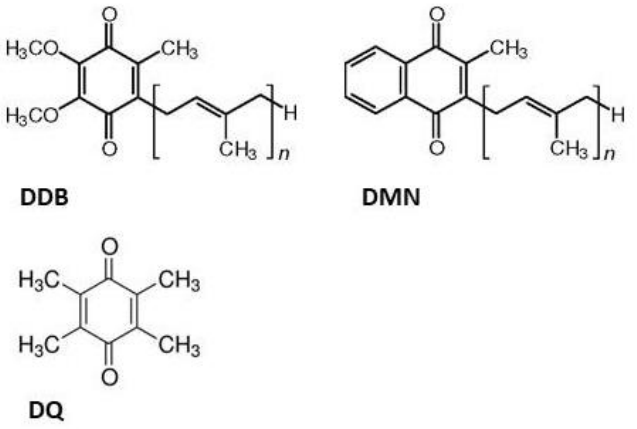

Figure S2.3 Quinone structures. Schematic representation of the three quinones, DMN, DDB and DQ, used in NDH-2A activity assays.

Chapter 3

Structural insights into Type II NAD(P)H:quinone oxidoreductases of *Staphylococcus aureus*

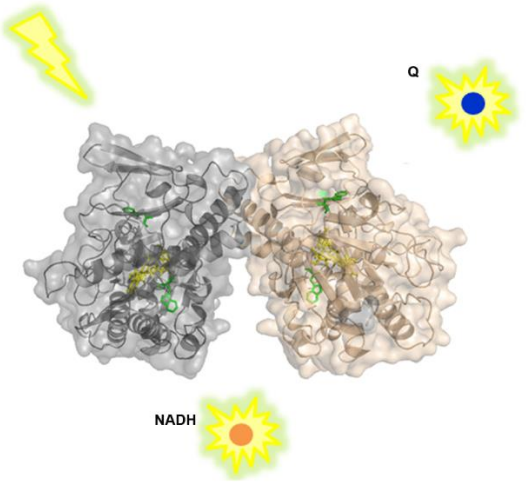

Chapter 3- Structural insights into Type II NAD(P)H:quinone oxidoreductases of *Staphylococcus aureus*

This section is based on the following publications:

- ✓ Rosário AL*, **Sena FV***, Batista AP, Athayde D, Oliveira TF, Pereira MM, Brito JA, Archer M. Expression, purification, crystallization and preliminary X-ray diffraction analysis on a type-II NADH:quinone oxidoreductase from the human pathogen *Staphylococcus aureus*. *Acta Crystallogr F Struct Biol Commun.* 2015 Apr; 71(Pt 4) (2015) 477-82. Doi: 10.1107/S2053230X15005178.

- ✓ **Sena FV**, Batista AP, Catarino T, Brito JA, Archer M, Viertler M, Madl T, Cabrita EJ, Pereira, MM. Type-II NADH:quinone oxidoreductase from *Staphylococcus aureus* has two distinct binding sites and is rate limited by quinone reduction. *Mol Microbiol.* 98 (2015) 272–288. Doi: 10.1111/mmi.13120.

- ✓ Marreiros BC, **Sena FV**, Sousa FM, Oliveira AS, Soares CM, Batista AP, Pereira MM. Structural and Functional insights into the catalytic mechanism of the Type II NADH:quinone oxidoreductase family. *Sci Rep.* 7 (2017) 42303. Doi: 10.1038/srep42303.

- ✓

* Equally contributing authors.

Author Contribution:

Sena FV performed most of the experiments at ITQB, analyzed and critically discussed the data. The crystallization and structure determination of NDH-2A were performed by Margarida Archer Lab at ITQB and at ESRF Grenoble; SAXS studies were done by Tobias Madl Lab at University of Graz. STD-NMR experiments were done by **Sena FV** at FCT (REQUIMTE, UCIBIO) at Eurico J Cabrita Lab. NDH-2B model was done with the help of Filipe Sousa and Sequence analysis and Amino acid residue conservation were done by Bruno Marreiros.

3.1 Summary

Type II NADH dehydrogenases (NDH-2s) belong to the two-Dinucleotide Binding Domains Flavoprotein (tDBDF) superfamily, presenting two structural domains for the binding of dinucleotides. These domains are structurally similar to each other and each one adopts a Rossmann fold, known to stabilize the adenine rings of dinucleotides. In this work, NDH-2A from the Gram-positive human pathogen *Staphylococcus aureus* was crystallized and the crystallographic data set was collected at a wavelength of 0.873 Å. The crystals contained four monomers per asymmetric unit and diffracted to a resolution of 3.32 Å. A molecular-replacement solution was obtained and model building and refinement were determined. NDH-2A crystallographic structure showed to be typical of the proteins of the tDBDF superfamily containing NADH and FAD binding domains and in addition a membrane binding domain. SAXS measurements analysis showed that NDH-2A from *S. aureus* is a dimer in solution. Model of NDH-2B is similar to NDH-2A enzyme structure having the two domains for the binding of NAD(P)H and FAD and in addition the membrane interacting domain is composed of one amphipathic helix instead of two as it was observed in NDH-2A structure.

Additionally, we concluded that the two proteins present different binding sites for the substrates, NAD(P)H and quinone. This was based on our data on protein-substrate interactions monitored by fluorescence and STD-NMR spectroscopies in the absence and in the presence of HQNO, a quinolone analogue, which only interfered with the binding of the quinone.

3.2 Introduction

All NDH-2s share the same domain organization containing two typical dinucleotide binding domains, both harbors a conserved GxGxxG motif. One of these motifs interacts with FAD, the only prosthetic group, whereas the other interacts with NAD(P)H[1].

The function of NDH-2s has been intensively studied, in biochemical and structural terms, with an increasing number of crystal structures being solved by different groups, raising a lot of discussion among the scientific community.

The study of NDH-2 gained a new impetus after the publication of two different crystal structures of the same NDH-2 from *Saccharomyces cerevisiae* (Ndi1), by two distinct groups[2,3] (Figure 3.1). These studies prompted further discussions including the number and location of the substrate binding sites. Both studies reported the yeast NDH-2 structure complexed with ubiquinone and NADH or NAD^+. The work by Iwata *et al*[2] discussed overlapping binding sites for NADH and quinone, whereas Feng *et al*[3] proposed separated binding sites at opposite sides of the isoalloxazine ring of FAD.

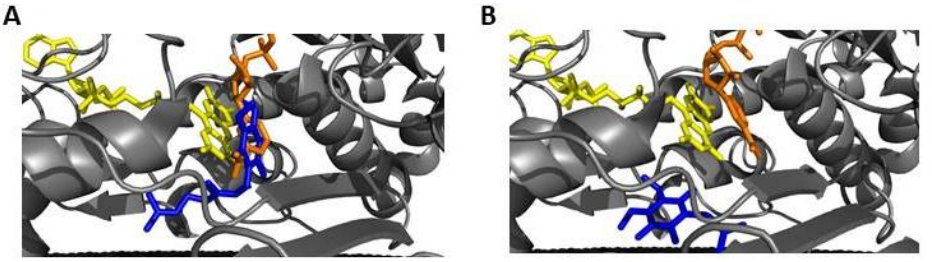

Figure 3.1 X-ray crystal structures of NDH-2 from *S. cerevisiae* (Ndi1) showing the binding sites for the two substrates, ubiquinone and NADH. Cartoon representation of a zoomed view of the FAD region and co-crystallized ubiquinone and NADH of the NDH-2 from *S. cerevisiae* (Ndi1) solved by **(A)** Iwata *et al* (PDB: 4G9K) and **(B)** Feng *et al* (PDB: 4G73). The atoms of the FAD group are shown in yellow sticks, NADH in orange and ubiquinone in blue.

Yamashita *et al* determined the crystal structure of the same enzyme in complex with three different inhibitors stigmatellin, AC0-12 and myxothiazol and found two separated binding sites of stigmatellin, STG-1 and STG-2[4]. Moreover the inherent binding site of ubiquinone was suggested to overlap with that of STG-1 that is distinct from the binding site of NADH[4]. In addition the structure of NDH-2 from the malaria parasite *Plasmodium falciparum* was solved by Yang *et al*[5], with NADH and with RYL-552, a new inhibitor. Beyond the two canonical Rossmann fold domains the authors found an additional domain, Domain C, in the middle of the sequence, but its function is still unknown[5]. All the reported structures have a homodimeric composition, but the functional significance of it remains unknown. The first crystal structure of a bacterial NDH-2 was from *Caldalkalibacillus thermarum* and was reported by Heikal *et al*[6], that suggested the existence of distinct binding sites for the two substrates in spite of the absence of substrates, NADH and quinone in the solved structure. Later, Petri *et al* determined the crystal structure of NDH-2 from *C. thermarum* complexed with a quinolone inhibitor 2-heptyl-4-hydroxyquinoline-N-oxide (HQNO)[7]. Here the authors found HQNO bound in the hydrophobic Q-site localizing in the C-terminal membrane-anchoring domain of bacterial *C. thermarum* NDH-2. Inhibition activity experiments against NDH-2 using menadione as electron acceptor, also shown HQNO targets the Q-site with high specificity and affinity of the inhibitor.

Quinones are two-electron acceptors and flavin-dependent quinone reductases, including NDH-2, afford the two-electron reduction of the quinone to its hydroquinone form and avoid the generation of the semiquinone anion, which is prone to react with molecular oxygen, leading to the generation of ROS[8]. However, it is not yet clear how NDH-2 interacts with its hydrophobic substrate, quinone.

In this chapter both solution and crystal NDH-2A structure will be described and the later compared with NDH-2B model. Based on structure information and combining it with protein-substrate interaction studies we aim to investigate the structural and functional relationship in NDH-2s.

3.3 Experimental procedures

3.3.1 Crystallization, data collection, structure determination and refinement of NDH-2A

NDH-2A enzyme was crystallized as described in Rosario *et al*[9]. Briefly, the first NDH-2A crystals were grown in 25 % (w/V) PEG 3350 and 0.2 M sodium acetate pH 7.2, at 20 °C, using 7 mg mL^{-1} of protein. As these crystals diffract poorly, streak seeding was successfully carried out yielding better quality crystals suitable for X-ray diffraction measurements. Crystals were cryo-protected by transferring to a drop of solution 7 from the CryoProtX screen (Molecular Dimensions) and flash-frozen by quick plunging in liquid nitrogen. A crystallographic dataset was collected at a wavelength of 0.873 Å to about 3 Å resolution on beamline ID23-2 of the European Synchrotron Radiation Facility (ESRF – Grenoble, France), from a single crystal. Crystals belong to the orthorhombic space group $P2_12_12_1$, with unit cell parameters a = 81.78, b = 86.03 and c = 269.95 Å, with α=β=γ=90°. Data were indexed and integrated using XDS[10] space group assignment was performed with POINTLESS[11] and scaling with SCALA/AIMLESS[12]. All of these programs were used within the autoPROC[13] data processing pipeline. A R_{free} flag was created at this stage corresponding to 5 % of the measured reflections for this dataset. A summary of the diffraction protocol and data-collection statistics is given in Table 3.1.

Table 3.1 Data collection and refinement statistics for the structure of NDH-2A from *S. aureus.*

Data colection	
Wavelength (Å)	0.873
Resolution (Å)*	60.5 – 3.32 (3.33 – 3.32)
Space group	$P2_12_12_1$
a, b, c (Å)	81.78, 86.03, 269.95
α, β, γ (°)	90, 90, 90
R_{pim}	0.09 (0.36)
R_{merge}	0.15 (0.49)
$CC_{1/2}$	0.98 (0.72)
$<I/\sigma(I)>$	8.3 (2.0)
Completeness (%)	99.5 (90.4)
Redundancy	3.6 (2.3)
No. reflections	104532 (617)
No. of unique reflections	28851 (264)
Wilson B factor (Å^2)	60.46
Refinement	
R_{cryst} (%)	20.4 (26.3)
R_{free} (%)	24.9 (31.3)
RMSD bond lengths (Å)	0.003
RMSD bond angles (°)	0.724
No. of protein atoms	12298
No. of ligand/ion atoms	218
No. of water atoms	77
Average protein *B*-factor (Å^2)	55.89
Average ligand/ion *B*-factor (Å^2)	44.64
Average water *B*-factor (Å^2)	39.27
Ramachandran plot statistics (%)	
Favoured regions	95.0
Allowed regions	4.2
Outliers	0.8
PDB entry	4XDB

The NDH-2A structure was solved by molecular replacement with PHASER [14] using the bacterial *Caldalkalibacillus thermarum* (4NWZ), as search model and searching for four monomers in the asymmetric unit (corresponding to a Matthews coefficient [15] of 2.64 Å3Da^{-1} and a solvent content of ~ 53 %). The resulting PDB and MTZ files were loaded into the AutoBuild wizard [16] in PHENIX [17] for automated model building. The program built and docked to

sequence 1483 residues belonging to four molecules in the asymmetric unit (a dimer of dimers, Fig. S3.1), with Rcrystof 20.5 %, R_{free} of 24.6 % and a map-model-correlation coefficient of 75 % (Table 3.1). After an initial refinement carried out with BUSTER-TNT [18], clear electron density was observed for the FAD prosthetic group. Iterative manual model building and refinement were carried out in a cyclic manner with COOT [19] and phenix.refine [20], until a complete model was built and refinement convergence achieved. The stereochemistry of the refined model and the Ramachandran plot were assessed with MolProbity[21]. The model comprises 95.1 %, 4.1 % and 0.8 % of the residues in the favored, allowed, and disallowed regions of the Ramachandran plot respectively. Structure representations were rendered with PyMOL (The PyMOL Molecular Graphics System, Version 1.5.0.4 Schrödinger, LLC). Electrostatic surface potentials were calculated with APBS [22] after generating PQR input files with the online PDB2PQR server [23]. The coordinates and structure factor amplitudes of *S. aureus* NDH-2A have been deposited in the Protein Data Bank under the accession number 4XDB. Later, the structure of NDH-2A was solved with a better resolution of 2.32 Å by molecular replacement using the former *S. aureus* NDH-2A (PDB ID: 4XDB) and the coordinates were deposited in the Protein Data Bank under the accession number 5NA1.

3.3.2 Small-angle X-ray Scattering measurements and data analysis of NDH-2A

SAXS data for NDH-2A from *S. aureus* in solution were recorded on an in-house SAXS instrument (SAXSess mc2, Anton Paar, Graz, Austria) equipped with a Kratky camera, a sealed X-ray tube source and a two-dimensional Princeton Instruments PI•SCX:4300 (Roper Scientific) CCD detector. The

scattering patterns were measured with a 180 min exposure time (1080 frames, each 10 s) for several protein concentrations in the range from 0.6 to 8.0 mg mL^{-1}. For the measurement of ligand-bound states, 35 µM NDH-2 was mixed with a three times stoichiometric excess of DMN, HQNO, DMN/HQNO, NAD^+, and NADH, respectively. Radiation damage was excluded based on a comparison of individual frames of the 180 min exposures, where no changes were detected. A range of momentum transfer of $0.012 < s < 0.63$ $Å^{-1}$ was covered ($s = 4\pi\sin(\theta)/\lambda$, where 2θ is the scattering angle and λ=1.5 Å is the X-ray wavelength). All SAXS data were analyzed with the package ATSAS (version 2.5 EMBL Hamburg, Hamburg, Germany). The data were processed with the SAXSQuant software (version 3.9 Anton Paar GmbH, Graz, Austria) and desmeared using the programs GNOM [24] and GIFT [25]. The forward scattering, I (0), the radius of gyration, R_g, the maximum dimension, D_{max}, and the inter-atomic distance distribution functions, (P(R)), were computed with the program GNOM. The masses of the protein were evaluated by comparison of the forward scattering intensity with that of a human serum albumin reference solution (molecular mass 69 kDa) and using Porod's law. SAXS data were backcalculated for NDH-2 from *C. thermarum* (4NWZ) and *S. cerevisiae* Ndi1 (4G9K) using the program CRYSOL (EMBL Hamburg, Hamburg, Germany)[24] and taken as input for population analysis. The solution structures of dimeric *S. aureus* were modeled using the program CORAL (EMBL Hamburg, Hamburg, Germany) [26]. Input were the crystal structure of *S. aureus* determined here, SAXS data, and maximal Cα-Cα distance restraints loosely defining the dimer interface based on that of the crystal structure of NDH-2 from *C. thermarum* (4NWZ; Ile132-Ala14915.9 Å, Thr133-Ala15017.2 Å, Arg135-Ala146 15.6 Å, Glu136-Asn147 15.4 Å, Arg139-Glu142 16.4 Å, His140-His140 18.5 Å, His140-Asp143 16.0 Å, Asp143Asp143 16.8 Å; all distances are

the distances of the aligning residues in 4NWZ plus an additional tolerance of 10 Å). Throughout the calculations, the 5 N-terminal residues were defined flexible and randomized. A total of 50 structures were calculated, and the best structures based on the fit to the experimental data selected to prepare the figures.

3.3.3 NDH-2B structural model

NDH-2B structural model was generated using the Protein Homology/analogy Recognition Engine V 2.0 (Phyre^2) web tool[27], using bacterial *S. aureus* NDH-2A structure (PDB ID: 5NA1) as the crystallographic protein template. The generated model was analyzed and used to create NDH-2B figure 3.8, using PyMOL[28].

3.3.4 Sequence analysis

We have previously used the KEGG database to identify and select the members of the NDH-2 family (2567 NDH-2s). We performed the respective taxonomic analysis and observed that NDH-2 family is distributed in four main branches which we called groups A to D[29]. In this work we opted to analyze the enzymes with the typical quinone binding site (AQxAxQ), or its alternatives (AQxAxR and APxAxQ). We aligned the remaining 1779 NDH-2 sequences (~70 % amino acid sequences from the NDH-2 family) using PROMALS3D[30]. We manually refined our data set using Jalview 2.8.118 for which we considered three criteria: (a) existence of two GxGxxG like motifs for interaction with FAD and NAD(P)H and included few variations, namely the GxGxxA motif; (b) presence of a C-terminal amino acid extension for membrane interaction (C-terminal domain), and (c) absence of possible other domains fused at the N- or

C-terminal. Our final data set included, in this way, 1762 amino acid sequences (distributed in the three domains of life, Eukarya, Bacteria and Archaea).

3.3.5 Fluorescence quenching studies on NDH-2s

Fluorescence spectra were obtained on a Varian Cary Eclipse spectrofluorimeter and on a Fluorolog Jobin Yvon, Horiba with a detector power source TBX-PS. The reaction mixture (400 µL) contained 2 µM NDH-2A in 100 mM K_2HPO_4/KH_2PO_4 250 mM NaCl pH 7.0 buffer or 2 µM NDH-2B in 25 mM MES Bis Tris Propane 250 mM NaCl pH 5.5 buffer. The effect of $NADP^+$, NAD^+, DMN, or HQNO was tested. Three independent NDH-2A titrations were performed with each substrate (NADH, NAD^+, DMN, DDB, DQ or HQNO) in the range of 0 to 100 µM. Three independent NDH-2B titrations were also performed but in this case with $NADP^+$ and NAD^+ (0 to 711 µM) and in the range of 0 to 250 µM with DMN and HQNO due to ligand solubility. Aromatic residues as tryptophan, phenylalanine, and tyrosine are all present in NDH-2s and all of them fluoresce. We excited NDH-2 at 280 nm that corresponds to tryptophan wavelength maximum absorption. Flavin fluorescence emission spectrum was recorded at 25 °C with excitation wavelengths at 450 nm. The change in emission at 330 nm (ΔF) was normalized and plotted vs ligand concentration. The equation of Monod-Wyman-Changeux (MWC) model, $\Delta F = \Delta F^{max} \times \frac{\frac{[S]}{K_S}\left(1+\frac{[S]}{K_S}\right)}{L+\left(1+\frac{[S]}{K_S}\right)^2}$, for a dimeric enzyme was used to simulate the data.

3.3.6 Saturation transfer difference (STD) NMR spectroscopy of NDH-2s

NMR spectra were acquired in a Bruker Avance III spectrometer at 15 °C, operating at a proton frequency of 600.13 MHz with a 5 mm triple resonance cryogenic probe head. STD-NMR spectra were acquired with 1024 transients in

a matrix with 32 k data points in t2 in a spectral window of 12019.23 Hz centered at 2814.60 Hz. Excitation sculpting with gradients was employed to suppress the water proton signals. Selective saturation of protein resonances (on resonance spectrum) was performed by irradiating at −300 Hz using a series of 40 Eburp2.1000 shaped 90° pulses (50 ms, 1 ms delay between pulses), for a total saturation time of 2.0 s. For the reference spectrum (off resonance), the samples were irradiated at 20000 Hz. Control experiments were performed with the reference samples in order to optimize the frequency for protein saturation (−0.5 ppm) and off-resonance irradiation to ensure that none of the tested ligands would be saturated at this frequency. STD spectra were obtained by subtraction of the off resonance and the on-resonance spectra. The STD effect was calculated by $(I_0–I_{STD})/I_0$, in which $(I_0–I_{STD})$ is the peak intensity in the STD spectrum and I_0 is the peak intensity in the off-resonance spectrum. STD amplification factors were calculated by multiplying the STD effect by the ligand protein ratio. For epitope mapping the STD intensity of the largest STD effect was set to 100 % as a reference, and the relative intensities were determined. Relative STD-NMR values for the experiments of NDH-2A with DMN, DDB or DQ and for the STD competition experiments were obtained from at least three independent assays. The STD-NMR experiments were performed in 100 mM K_2HPO_4/KH_2PO_4 buffer 250 mM NaCl pH 7.0 (prepared in D_2O). NDH-2A was titrated with the different ligands: NADH, NAD^+, DMN, DDB, DQ or HQNO and NDH-2B with $NADP^+$ or DMN. The final concentrations of protein and ligands were 10 μM and 0.5 mM, respectively.

3.4 Results and Discussion

3.4.1 Structural studies on NDH-2A

3.4.1.1 X-ray structure

NDH-2A crystallized in several conditions, most of which involved polyethylene glycol of different molecular weight as the precipitant, over the course of one week. Streak seeding was successfully carried out yielding small rhomboid quality crystals within 24 hours (Figure 3.2).

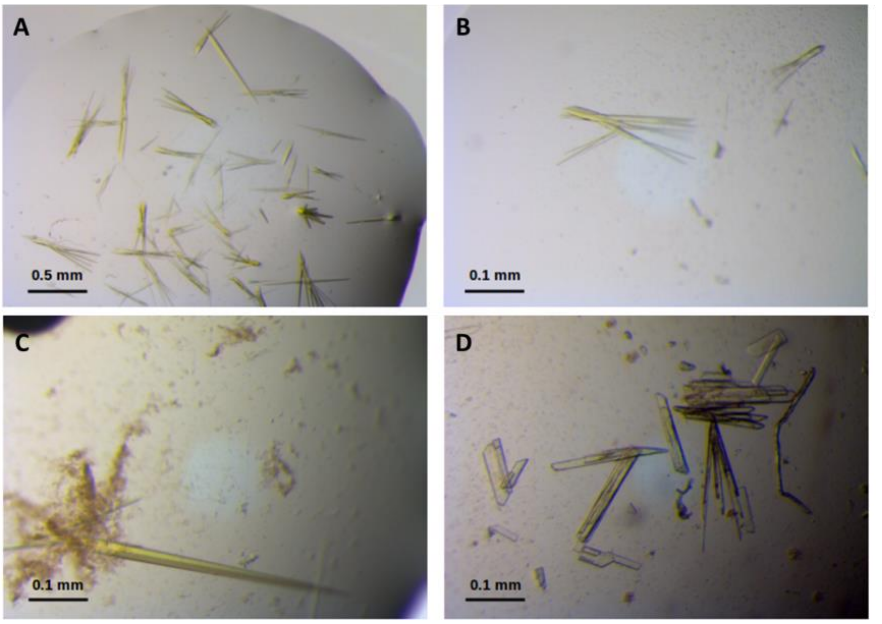

Figure 3.2 NDH-2A crystals grown **A)**, **(B)** during initial crystallization trials using the robot, **(C)** on scaling-up using the hand-made crystallization solution [20 % (w/v) PEG 3350, 0.2 M sodium acetate] and **(D)** on scaling-up using solution C3 [20 % (w/v) PEG 3350, 0.2 M ammonium nitrate] from the JCSG+ crystallization screen (Molecular Dimensions) and streak-seeding from the crystals in **(C)**. The crystals in **(D)** diffracted to 3.32 Å resolution using a synchrotron-radiation source. The crystals are yellow owing to the presence of the FAD prosthetic group.

These crystals were cryoprotected and a complete crystallographic data set was collected on beamline ID23-2 at the ESRF, Grenoble, France and the X-ray diffraction pattern is showed in figure 3.3.

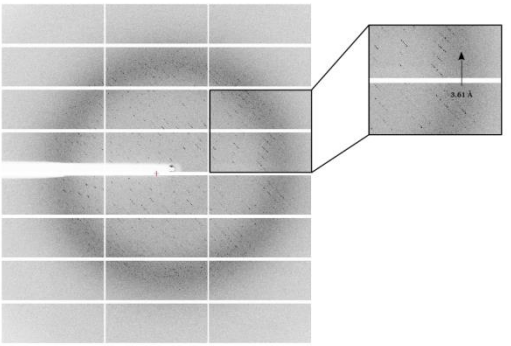

Figure 3.3 X-ray diffraction image of a single crystal of NDH-2A. An X-ray diffraction pattern collected from a single crystal of NDH-2A on the ID23-2 beamline at the ESRF. The image was prepared by merging ten consecutive diffraction images (corresponding to 1.5° rotation) with the MERGE2CBF program from the XDS package. The arrow points to the last visible reflections, although the maximum resolution observed was 3.32 Å (Pilatus 2M detector).

The crystal structure of NDH-2A from *S. aureus* (PDB entry 4XDB) was solved by molecular replacement using the coordinates of the homologue from *C. thermarum* (PDB 4NWZ)[6]. *S. aureus* NDH-2A and *C. thermarum* NDH-2 share 46 % sequence identity and 66.7 % sequence similarity for 185 and 268 aligned amino-acid residues, respectively.

The structure was refined to 3.32 Å with R_{cryst} of 20.4 % and R_{free} of 24.9 %, data collection and refinement statistics are depicted in Table 3.1. The final crystallographic model comprises four monomers (amino acid residues Gln3 or Lys6 to Phe402, depending on the monomer), four FAD molecules, six chloride ions and 77 water molecules. The NDH-2A overall fold is composed of two Rossmann fold containing domains and a C-terminal domain (Figure 3.4A and B). The first domain, or FAD binding domain, comprises residues 3–114 and 265–349 and binds non-covalently the FAD group that is present in an extended

conformation. The second domain is the NADH-binding domain and includes residues 115–264. These two domains compose the canonical fold for the glutathione-reductase family of flavin-containing enzymes. The C-terminal, or membrane attachment domain, comprising residues 350–402, is constituted by an anti-parallel three-stranded β-sheet followed by two helices arranged in a helix-turn-helix motif. The most similar structures to *S. aureus* NDH-2 are those of *C. thermarum* NDH-2 (PDB 4NWZ)[6] and *S. cerevisiae* Ndi (PDB entries 4G6G and 4G9K[2,3]) showing RMSDs of 1.2 Å and 2.4 Å for the aligned Cα atoms and sharing 46 % and 27 % of sequence identity respectively (Figure 3.5).

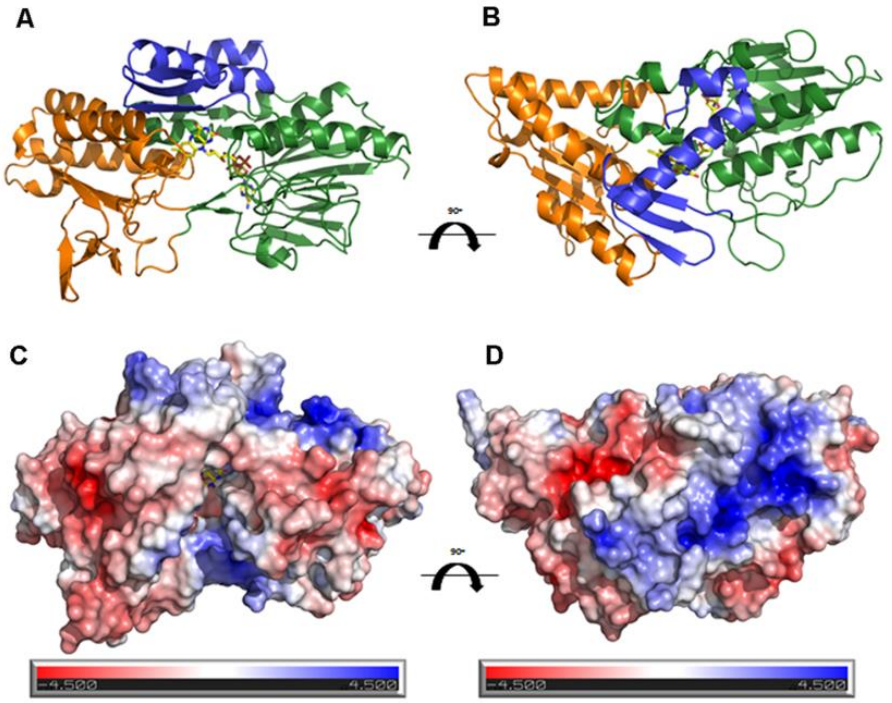

Figure 3.4 Crystal structure of *S. aureus* NDH-2A. (A) Cartoon representation of NDH-2A monomer from *S. aureus*; NADH-binding domain is colored in orange, FAD-binding domain in green and membrane attachment (C-terminal) domain in blue; FAD cofactor is shown in sticks with carbon atoms colored in yellow, oxygen in red and nitrogen in blue. **(B)** NDH-2 as viewed from the membrane (90° rotation relative to A); color code as in A. **(C)** and **(D)** Electrostatic surface potential of NDH-2 in the same orientations as in (A) and (B) (± 4.5 kT/e).

Sulfide:quinone oxidoreductases [e.g. SQRs from *Acidithiobacillus ferroxidans* (PDB 3T2Y;[31]), *Aquifex aeolicus* (PDB 3HYW;[32]) and *Acidianus ambivalens* (PDB 3H8L;[33]] show the same overall fold with RMSDs of ~ 2.4 Å for 360 aligned Cα atoms. The electrostatic surface potential (Figure 3.4C and D) displays a hydrophobic surface surrounded by two patches of positively charged residues at the C-terminus, as previously reported for *C. thermarum* NDH-2 and *S. cerevisiae* Ndi1[2,3,6].

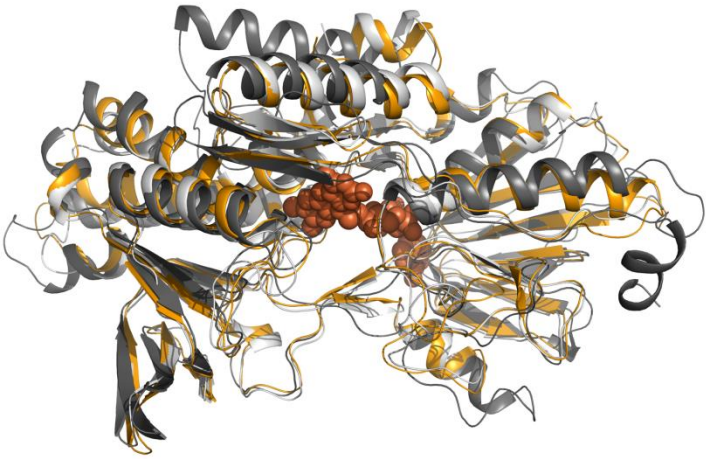

Figure 3.5 Structural superposition of NDH-2s. X-ray structures from NDH-2 from *S. aureus* (in yellow), *C. thermarum* (in lighter gray, PDB 4NWZ) and Ndi1 from *S. cerevisiae* (in darker gray, PDB 4G9K) with FAD in CPK mode.

These patches are important to establish interactions with the negatively charged head of the phospholipids, whereas the adjacent hydrophobic surface comprised mainly by phenylalanine residues within the helix-turn-helix motif, is buried within the membrane. Similar to the aforementioned structures, *S. aureus* NDH-2A also presents a cleft formed by residues Phe116, Ile118, Thr233-Ile235, Trp261-Gly263, Pro317 and Thr318 that leads to the re-side of FAD, which is suggested to be the NADH-binding site (Figure 3.6A). These amino acid residues are highly conserved among the reported 3D-structures of NDH-2[2,3,6]. Moreover, the turn Val163-Gly170 is

also suggested to be involved in NADH binding by Heikal *et al*[6]. Here the bulkier side-chain of phenylalanine in *S. aureus* NDH-2 (Phe168 in contrast to Pro238 in *S. cerevisiae*) causes some steric constraints in the pocket where the NADH nicotinamide moiety stacks against the FAD isoalloxazine ring. This implies a slight structural rearrangement of Phe168 upon NADH binding.

S. aureus NDH-2A contains a tunnel that gives access to the si-side of FAD and is lined mostly by hydrophobic residues, namely Tyr15, Ala319, Met323, Ile382 and Ala386, also including the 319-AQxAxQ-324 motif proposed to constitute the quinone binding site[6]. The hydrophobic feature of this cavity as well as the AQxAxQ motif is maintained in the other NDH-2 structures (Figure 3.6B). Interestingly, a quinone was observed to bind in this cavity in the *S. cerevisiae* Ndi1 reported by Feng *et al* [3], in contrast to the one reported by Iwata *et al.* [2], where the quinone and NADH binding sites overlap on the re-side of FAD. Upon superposition with the *S. cerevisiae* Ndi1 structure with the two substrates present (PDB code 4G73, [3]), it is clear that *S. aureus* NDH-2A can accommodate a quinone in the cavity described above (Figure 3.6B). This cavity is delineated by Val353, Val365, Phe366, Ile370 and Met378, similarly to *C. thermarum* structure[6]. Conformational rearrangements would be necessary for the quinone to surpass the FAD moiety in order to bind at the same site as the NADH, as proposed by Iwata *et al*[2], which do not seem likely (Figure 3.6C). Two arginine residues, Arg350 and Arg385, are located at the tunnel entrance showing high thermal displacement parameters (B-factor around 80 Å2), which suggest flexibility on their side-chains.

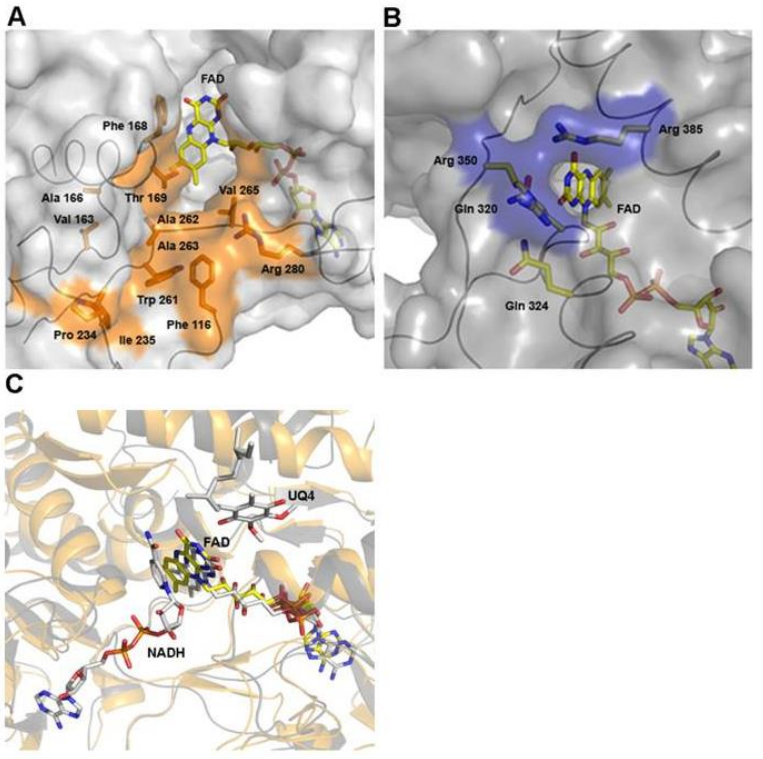

Figure 3.6 Ligand binding sites around FAD. **(A)** NADH-binding cleft; surface representation with relevant residues for NADH-binding in orange. **(B)** Putative quinone binding site; surface with important residues in blue; Arg350 and Arg385 at the pocket entrance and Gln320 and Gln324 from AQxAxQ motif. **(C)** Superposing (with FAD cofactors) of NDH-2 from *S. aureus* (in yellow) and Ndi1 from *S. cerevisiae* (in gray, PDB 4G73) structures, showing the NADH and ubiquinone-4 (UQ4) in sticks bound to it (PDB 4G73).

The crystal asymmetric unit of *S. aureus* NDH-2A contains 4 polypeptide chains packed as two nearly identical homodimers (Figure S3.1). The dimeric interface is mainly hydrophilic and has a buried area around 1.076 $Å^2$ per monomer, corresponding to ca. 6 % of the total solvent accessible area as assessed by PISA[34]. Most of the polar and charged residues (Arg, Lys and Glu) present at the interface are located in a long stretch just before the C-terminal membrane attachment domain. This arrangement is not physiologically relevant as the C-terminal membrane domains of both monomers face each

other and shield some hydrophobic residues from the solvent; this architecture of dimerization makes the membrane domains to package against their counter part from the neighboring monomer and hence inaccessible for membrane attachment (Figure S3.1). We have posteriorly re-determined the crystal structure of NDH-2A enzyme to 2.32 Å resolution (PDB: 5NA1). The new NDH-2A structure contains 1 FAD molecule, 1 phosphate ion, 2 malonate ions and 112 waters. Superposition of 2.32 Å NDH-2A structure with the previously reported *S. aureus* NDH-2A structure (PDB ID: 4XDB) shows a RMSD of 0.65 Å for 398 aligned Cα atoms. This improvement in resolution (1 Å resolution better than the first one reported) did not lead to any significant change in the interpretation of the structure but gave us more confidence in the data including side chain orientation.

3.4.1.2 SAXS structure

Given that the dimer interfaces for previously reported homologous structures differ significantly[2,6], we set off to characterize the conformation of *S. aureus* NDH-2A in solution using small angle X-ray scattering (SAXS). We found that, in agreement with size exclusion chromatography (showed in figure 2.2 of Chapter 2), NDH-2A is a dimer in solution (maximal dimension (D_{max}): 110 Å, radius of gyration (R_g): 34 ± 1, molecular mass 93 kDa) (Figure 3.7). To evaluate whether any of the reported dimer orientations match the SAXS data of *S. aureus* NDH-2A, we compared SAXS data back-calculated from crystal structures of the homologous proteins from *C. thermarum* (4NWZ) and *S. cerevisiae* (4G9K). Clearly, neither of the dimer orientations of these two crystal structures was in good agreement with the data obtained for *S. aureus* (Figure 3.7A). In *S. cerevisiae* Ndi1, the dimer interface includes a long C-terminal helix, which is not present in the bacterial homologues. Furthermore, due to the lack of solution studies of the homologous proteins, we cannot exclude that the

different dimer orientation observed in the crystal structures might be due to crystal packing forces.

Thus, the observed difference may reflect different orientations of the monomers, or equilibrium between different conformations. Indeed, a superposition of SAXS data back-calculated for the two homologous proteins and assuming a population ratio of 40:60 % (*C. thermarum: S. cerevisiae*) resulted in good agreement with the dimer interface according to the *C. thermarum* NDH-2 dimer. The rationale for selecting this interface is based on the sequence alignment and the lack of the *S. cerevisiae* C-terminal dimerization helix in *S. aureus* NDH-2A (Figure S3.2). Our SAXS-based structural model shows that a slightly twisted orientation of the monomers compared with the *C. thermarum* NDH-2 dimer results in an excellent agreement of the experimental and back-calculated SAXS data (Figure 3.7C). Close inspection of the interface shows that the dimer is mainly stabilized by salt bridges (Figure 3.7B). In the twisted dimeric structure, and in agreement with the homologous NDH-2 structures, the membrane attachment region is located at the same side of the dimer. Both helices including the conserved hydrophobic residues (F388, I393, and F397) are oriented parallel to the membrane and well-available for membrane binding (Figure S3.2).

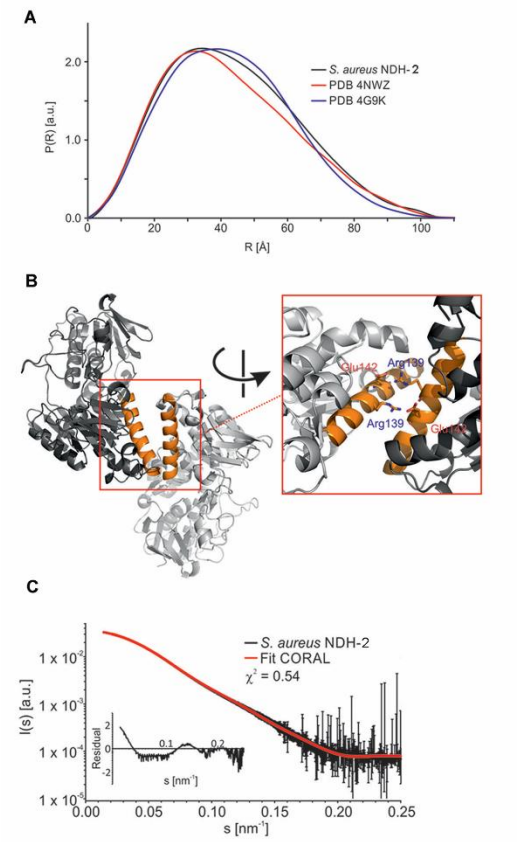

Figure 3.7 SAXS Measurements. (A) Comparison of SAXS radial density distributions of NDH-2A from *S. aureus* (experimental data), *C. thermarum* NDH-2 (back-calculated from PDB 4NWZ) and *S. cerevisiae* (back-calculated from PDB 4G9K). The P(R) of the physiologically relevant dimer orientations is shown. Neither of the other dimer interfaces observed in the crystal structures yielded an acceptable agreement (χ2 between 3.1 and 12.0). **(B)** SAXS rigid body model of NDH-2A from *S. aureus*. Residues in the dimerization interface forming salt bridges are labeled. **(C)** Comparison of experimental NDH-2A from *S. aureus* SAXS data with SAXS data back-calculated from the CORAL model of the dimer of NDH-2A from *S. aureus*. I(s) axis is shown in a logarithmic representation. The angular ranges from 0.0012–0.25 nm^{-1} are compared.

Furthermore, to evaluate whether the conformation of the NDH-2A dimer could be different depending on the oxidation state of the enzyme, we performed SAXS analyses upon NADH reduction or quinone oxidation. We also tested if the conformation of the enzyme was also the same in the presence of

2-n-Heptyl-4-hydroxyquinoline-N-oxide (HQNO) or quinone alone (Table S3.1). Based on only minor differences in the SAXS data, we conclude that the oxidation state has only a minor or no effect on the dimerization and dimer orientation. Given the lack of the *S. cerevisiae* Ndi1 C-terminal dimerization region in *S. aureus* NDH-2A and the observation that the dimer interface does not change in the presence of substrates we conclude that in solution NDH-2A adopts a conformation, which is slightly different to that of *C. thermarum* NDH-2 dimer structure, rather than a conformational equilibrium between different conformations of the monomers.

3.4.2 Structural considerations on NDH-2B

The structural model of NDH-2B is represented in figure 3.8. NDH-2B model is similar to NDH-2A enzyme X-ray structure, having the domain for the binding of NAD(P)H with the GxGxxG motif and the other motif, present in the domain where FAD binds, differs in one amino acid residue, GxGxG. In addition, NDH-2B model reveals only one amphipathic helix at the C-terminus for membrane-anchor. An interesting feature observed in NDH-2B sequence is the presence of two cysteines residues, Cys104 and Cys271, (Figure 3.8 in orange) which we can predict to establish a disulfide bond despite being still relatively far to the isoalloxazine ring of FAD. If these Cys were close to the flavin ring we could justify the red color of NDH-2B pure protein, characterized by an additional absorption band at 550 nm, possibly due to a charge transfer interaction between the FAD and a cysteine. This absorbance at 550 nm has been reported for flavoprotein disulfide reductases and has been ascribed, in the AhpF protein, to a thiolate-FAD charge transfer band arising from the interaction with a cysteine far the C4a position of the flavin ring[35,36]. The presence of these two cysteines could influence the activity of the enzyme

through conformational changes or these could act as a regulating site for divalent ions. In fact, we performed some enzymatic assays in the presence of divalent ions to test their influence on NDH-2B activity but the enzymatic activity was not significantly affected by their presence and so further studies should be done to search for the possible role of these two cysteine residues.

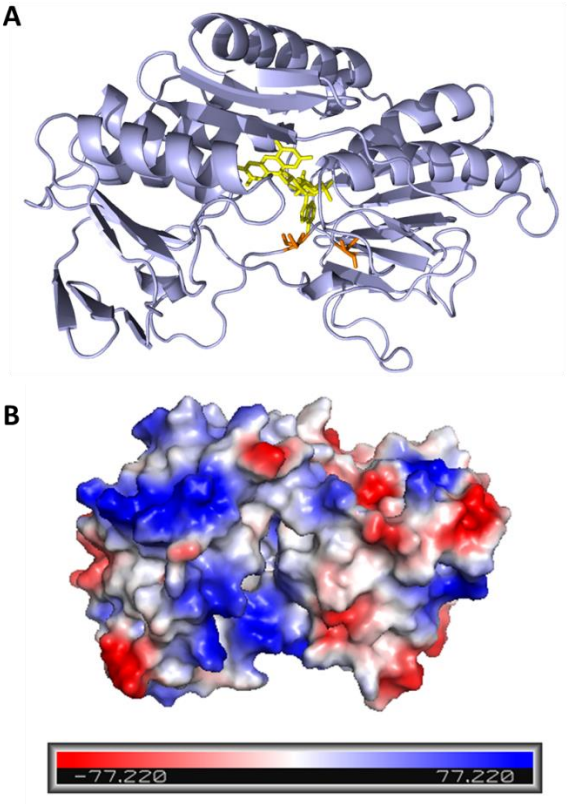

Figure 3.8 Cartoon representation of the homology structural model of NDH-2B. (A) The FAD cofactor and two cysteine residues are shown in sticks with carbon atoms colored in yellow and in orange, respectively. **(B)** Electrostatic surface potential of NDH-2 in the same orientations as in **(A).**

3.4.3 Amino acid residue conservation analysis

Sequence and structural analyses are very informative when we are investigating the catalytic mechanism of an enzyme, based on the rationale that

conservation of some elements reflects their structural/functional importance. We identified relevant amino acid residues, sequence motifs and structural elements and the integrated data allowed us to identify common denominators of 1762 NDH-2 sequences and establish the basis to discuss and propose a catalytic mechanism for NDH-2A[37]. In general, NDH-2s have on average 430 amino acid residues, 30 of which we observed to have conservation equal to or higher than 80 %, i.e. these 30 amino acid residues are present at the same position in at least 80 % of the analyzed sequences (Table 3.2). Eighteen conserved amino acid residues are present in the first dinucleotide binding domain, arranged in four motifs and seven isolated residues (Figure 3.9A and Table 3.2). The first conserved motif observed is GxGxxG ($G_{12}xG_{14}xxG_{17}$, *S. aureus* NDH-2A numbering). This glycine rich motif is placed in a loop located close to the pyrophosphate moiety of the FAD and should stabilize it (Figure 3.10)[6,38,39]. The second conserved motif, located at the surface of the protein, is composed of the residue pair YD ($F_{102}D_{103}$ in *S. aureus*), the Y and D residues being present in 92 % and 96 % of the NDH-2s, respectively (Figure 3.9A). We observed that the tyrosine residue is replaced by a phenylalanine residue in 7 % of the NDH-2s, as in the case of NDH-2 from *S. aureus* (F_{102}). The conservation of the YD pair is intriguing because it is located far from the active centre and binding sites of the two substrates so we hypothesize that YD may constitute a site for regulation of the enzymatic activity. A third strictly conserved pair, $G_{301}D_{302}$, forming the third conserved motif, is observed close to O3* of FAD (Figures 3.9 and 3.10). The backbone of G_{301} establishes a hydrogen bond (2.7 Å) with the side chain of a residue located after the proposed quinone binding site motif ($A_{319}Q_{320}xA_{322}xQ_{324}$) in α -helix 7[6]. This residue is a glutamine in 57 % of the NDH-2s, such as Q_{325} in *S. aureus*[40]. D_{302} was previously suggested to make hydrogen bonds with FAD, both through its

backbone to the PO_4 group and its side chain to O3* (Figure 3.10) [2,6,41,42]. The high conservation of this aspartate residue (D_{302}) is extended to several families of the tDBDF superfamily, even to those whose members do not interact with quinones, suggesting that it could be important in the oxidation/reduction processes of the FAD (Table 3.2 shaded in blue). The role of D_{302} will be discussed further on chapter 4. We also observed that three out of the four first residues from the quinone binding site motif, AQxAxQ, are more than 80 % conserved (Figure 3.9A), and that the last glutamine residue is still present in 78 % of NDH-2s[6,29].

The second dinucleotide binding domain harbors the NADH binding site. In this domain, we identified nine conserved residues forming two different motifs plus three isolated residues (Figure 3.9B and Table 3.2). The first conserved motif, GxGxxGxE, is located at the beginning of α -helix 4 ($G_{165}xG_{167}xxG_{170}xE_{172}$). As in the case of the similar motif observed for the first dinucleotide binding domain, the glycine residues were proposed to stabilize the pyrophosphate moiety of the dinucleotide, now NADH[3,6,43]. The glutamate residue E_{172} (Table 3.2 shaded in blue) is at hydrogen bond distance from the co-crystallized NADH nicotinamide ring in the structure of NDH-2 from *S. cerevisiae* (Figure 3.9B)[3].

This residue is conserved in 97 % of the 1762 NDH-2s, while a glutamine residue is present in the remaining sequences (3 %, mainly Archaea). We performed site-directed mutagenesis to E_{172} and its role on NDH-2A mechanism will be described on the next chapter. The motif WxxG ($W_{261}xxG_{264}$) is also highly conserved, 99 % and 100 % for W_{261} and G_{264}, respectively (Figure 3.9B). As W_{261} is close to the adenine base of NADH we hypothesize that it is of importance in the orientation and/or stabilization of NAD(P)H.

Table 3.2 Amino acid residue conservation in the three domains of NDH-2. List of the 30 amino acid residues present in the 1st dinucleotide (FAD) binding domain, 2nd dinucleotide binding domain and in the C-terminal domain that are conserved in at least 80 % of the NDH-2s. Shaded in blue are the amino acid residues that are studied in detail in the next chapter (4) of this thesis.

	S. aureus NDH-2 sequence		Alignment of 1762 sequences from NDH-2 family		Proposed Function
	Amino acid number	Amino acid type	Conservation (%)	Consensus	
1st dinucleotide binding domain	12	G	100	G	FAD stabilization
	14	G	100	G	FAD stabilization
	17	G	83	G	FAD stabilization
	48	T	87	P	Structural / H-bond with Y15
	50	L	91	L	-
	87	D	88	D	-
	102	F	92	Y	Structural / Regulation
	103	D	96	D	Structural / Regulation
	105	L	98	L	Structural
	110	G	100	G	FAD stabilization
	289	L	82	L	-
	301	G	100	G	H-bond with Q325
	302	D	100	D	H-bond with O3* (FAD)
	316	P	83	P	H-bond with N1 and O2 (FAD)
	319	A	96	A	Quinone binding site motif
	320	Q	84	Q	Quinone binding site motif
	322	A	98	A	Quinone binding site motif
	347	Y	82	Y	H-bond with Q320
2nd dinucleotide binding domain	56	G	81	G	-
	134	A	90	A	-
	165	G	100	G	NAD(P)H stabilization
	167	G	99	G	NAD(P)H stabilization
	170	G	99	G	NAD(P)H stabilization
	172	E	97	E	NAD(P)H stabilization / Part of a proton pathway
	207	L	92	L	-
	261	W	99	W	NAD(P)H stabilization
C-terminal domain	351	G	99	G	Structural
	357	G	80	G	Structural
	372	G	99	G	Structural / Orientation of α9

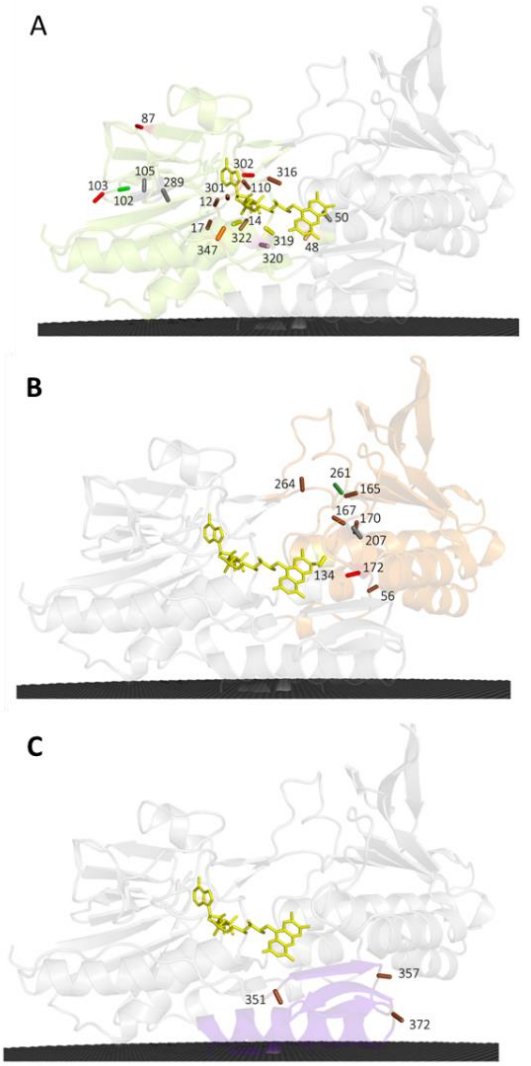

Figure 3.9 Amino acid residue conservation. Cartoon representation of the X-ray crystal structure of NDH-2 from *S. aureus* (PDB:4XDB) highlighting the location of the 18**(A)**, 9**(B)** and 3**(C)** conserved amino acid residues present in the different domains. Membrane is represented in black.

The C-terminal domain allows protein interaction with the membrane through two amphipathic α -helices[9–11,25]. We found three conserved glycine residues (G_{351}, G_{357} and G_{372}), with G_{372} conserved in 99 % of NDH-2s (Figure 3.9C and Table 3.2) and we hypothesize that its presence is important

to define the position of the first amphipathic α-helix in relation to the catalytic centre. By comparing the crystallographic structures of the members of the two families of quinone reducing proteins of the tDBDF superfamily (NDH-2[9–11,25] and SQR[31,32] we observed, in both cases, that the first amphipathic α-helix occupies the same position in relation to the isoalloxazine ring of the FAD. The localization of this α-helix allows the side chains of its amino acid residues to interact with FAD and substrates (NAD(P)H or sulfide and quinone).

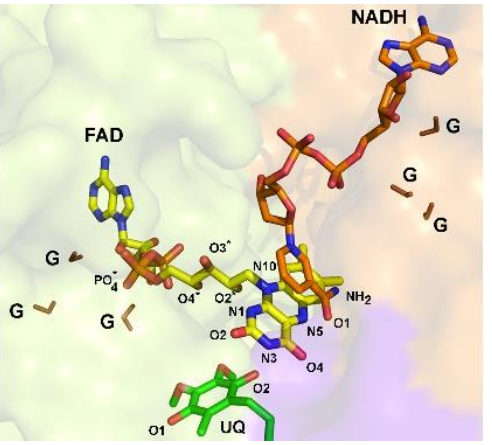

Figure 3.10 Cartoon representation of a zoomed view of the FAD region and co-crystallized ubiquinone and NADH of the NDH-2 from *S. cerevisiae* (PDB:4G73). The atoms of the FAD group are ordered and colored in: blue – Nitrogen atom (N); red – Oxygen atom (O); orange – Phosphorus atom (P) and yellow – Carbon atom. The glycine residues composing the GxGxxG motif present each of dinucleotide binding domain are colored in brown and indicated by "G".

3.4.4 Protein-substrate interaction studies on NDH-2s

3.4.4.1 Fluorescence spectroscopy studies

NDH-2A from *S. aureus* has two tryptophan residues (W49 and W261). W261 is located at the re-side of FAD and may interact with NADH[6], whereas W49 is situated at the si-side of FAD (Figure S3.3). The fluorescence emission spectra of NDH-2s with excitation at 280 nm exhibited the characteristics of a

typical tryptophan fluorescence spectrum with a broad maximum at around 320–330 nm, whereas the fluorescence emission spectrum with excitation at 450 nm was typical of a flavoprotein, presenting a band with a maximum intensity at 530 nm (Figure S3.4). Only slight changes were observed in the region of the flavin fluorescence emission spectra in the presence of some ligands (DMN, DDB, Duroquinone, NADH, NAD^+ and HQNO) (Figure S3.4). By contrast the intensity in the region of the tryptophan fluorescence emission spectra changed significantly and differently upon addition of each ligand. We tested the NDH-2A–substrate interaction using three different quinones, differing in their ring systems (Figure S3.5). In the case of NDH-2A, when titrated independently with each quinone, DMN, DDB or DQ, a maximum decrease in tryptophan fluorescence between 80 and 90 % was obtained (Figures 3.11A and S3.4), while for NADH or NAD^+ this maximum was approximately 45 % (Figures 3.11B and S3.4), showing that the environment of the tryptophan residues is perturbed differently by the quinones and by NADH/NAD^+. The titration curve could be simulated using the equation of Monod-Wyman-Changeux (MWC) model for a dimeric enzyme, obtaining microscopic dissociation constants (K_s) of 11.4 ± 0.5 μM for NADH and 20.3 ± 0.3 μM for NAD^+ and 16.3 ± 0.2, 19.1 ± 1.2 and 25.8 ± 2.8 μM for DMN, DDB and DQ respectively. The maximum change in tryptophan fluorescence observed upon titration with HQNO, a quinone inhibitor, was 20 % (Figure 3.11C), which suggests yet another mode of perturbation. NDH-2A was also titrated with NAD^+ or DMN in the presence of HQNO. The titration profile of NDH-2A with NAD^+ and HQNO is similar to that observed in the absence of HQNO (Figure 3.11B); however, the titration profile with DMN in the presence of HQNO is different from that without HQNO (Figure 3.11A). In fact, in the presence of HQNO, the titration profile with DMN could be fitted with a sigmoidal curve also using the equation of MWC model. Despite

this sigmoidal behavior, the curve obtained in the presence of HQNO gave the same microscopic dissociation constant value (K_S) of the one obtained in the absence of HQNO for DMN (K_S =16.3 ± 0.2 µM).

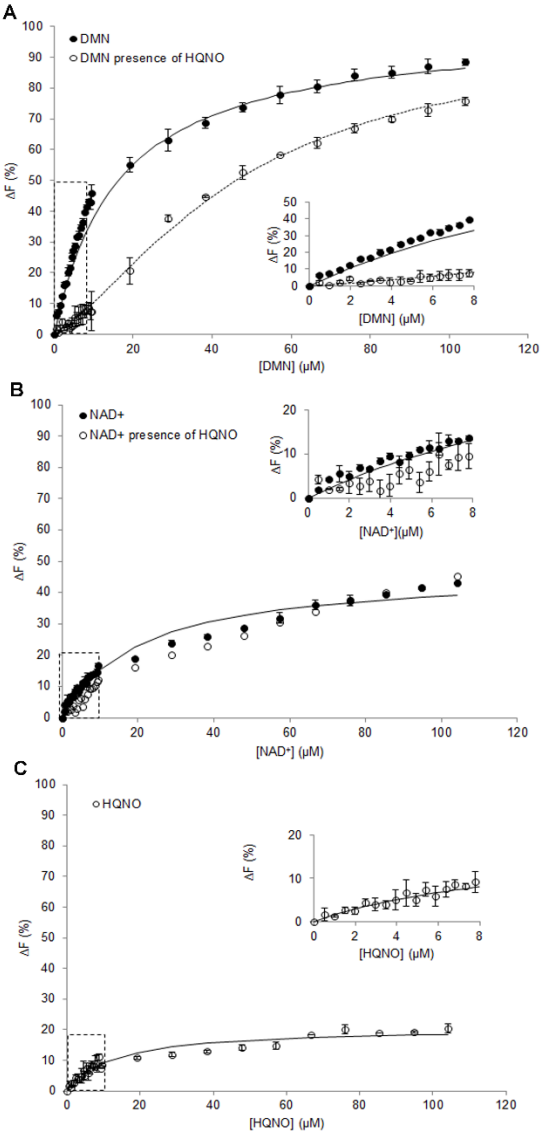

Figure 3.11 Fluorescence spectroscopy studies on NDH-2A. (A) Change in the fluorescence emission at 330 nm with excitation at 280 nm of NDH-2A by sequential addition of DMN or **(B)** NAD^+ in the absence (closed circles) or in the presence of HQNO (open circles). **(C)** Change in the fluorescence emission at 330 nm with excitation at 280

nm of NDH-2A by sequential addition of HQNO. The curves were simulated with Monod-Wyman-Changeux (MWC) model equation, $\Delta F = \Delta F^{max} \times \frac{\frac{[S]}{K_S}\left(1+\frac{[S]}{K_S}\right)}{L+\left(1+\frac{[S]}{K_S}\right)^2}$, for a dimeric enzyme to the data using L=0 (no cooperativity), solid lines and L = 7 for the sigmoidal behavior, dashed line. The inserted figures expand the first measuring points at low concentration of DMN, NAD^+ or HQNO.

NDH-2B from *S. aureus* has four tryptophan residues (W192, W228, W298 and W347) and in this case the maximum change in tryptophan fluorescence observed upon titration with $NADP^+$ and with NAD^+ was approximately 96 % for both ligands (Figure 3.12A). The microscopic dissociation constants (K_s) obtained for $NADP^+$ and for NAD^+ were very similar. We obtained a K_s value of 182 ± 29 µM for $NADP^+$ and for NAD^+ a value of 170 ± 7.6 µM (Figure 3.12A). When titrated independently with the quinone, DMN (Figure 3.12B), a maximum decrease in tryptophan fluorescence of approximately 75 % and a K_s of 160 ± 35 µM was obtained. This result showed that the environment of the tryptophan residues is perturbed differently by the quinone and by $NADP^+$. In addition, NDH-2B was titrated with HQNO and the maximum change in tryptophan fluorescence was 20 % which suggests, as in NDH-2A, a different interaction of the inhibitor with the enzyme (Figure 3.12C). Moreover, titrations of NDH-2B with $NADP^+$ and DMN in the presence of HQNO were made. The titration profile of NDH-2B with $NADP^+$ in the presence of the inhibitor was similar to that observed in its absence, showing that HQNO binds to a site that is distant from $NADP^+$ pocket. However, when titrated with the quinone, in the presence of HQNO, a sigmoidal profile was observed indicating, as it was already observed for NDH-2A, that HQNO is affecting the binding of the quinone (Figure 3.12A and 3.12B).

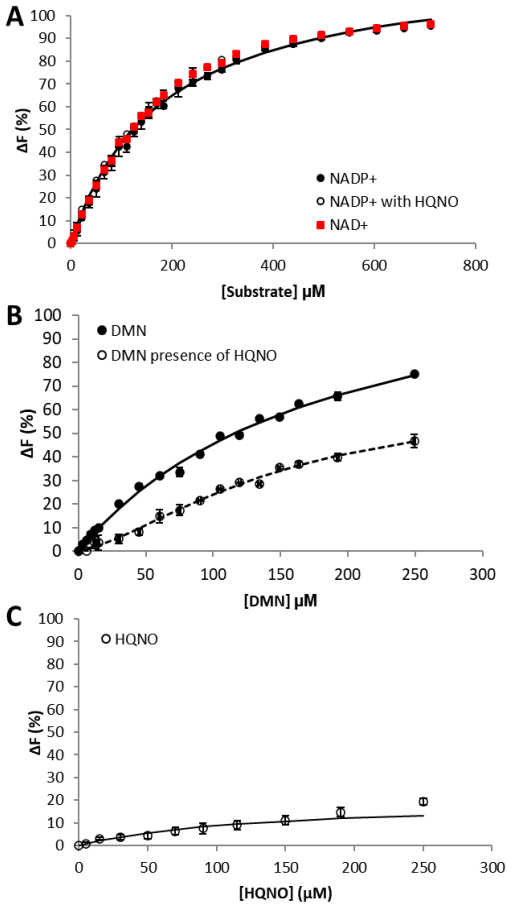

Figure 3.12 Fluorescence spectroscopy of NDH-2B. (A) Change in the fluorescence emission at 350 nm with excitation at 280 nm of NDH-2B by sequential addition of $NADP^+$ in the absence (closed circles) or in presence of HQNO (open circles); of NAD^+ (squares). **(B)** Change in the fluorescence emission at 350 nm with excitation at 295 nm of NDH-2B by sequential addition of DMN in the absence (closed circles) or in presence of HQNO (open circles). **(C)** Change in the fluorescence emission at 350 nm with excitation at 295 nm of NDH-2B by sequential addition of HQNO.

3.4.4.2 STD-NMR measurements

Protein ligand interactions were also investigated by saturation transfer difference (STD) NMR spectroscopy[44,45]. In this case, the study of the interaction of different ligands with NDH-2 is monitored via the ligand by measuring the level of saturation transfer from the protein to the ligand when

the protein is selectively saturated by magnetization. Initially the quinones, DMN, DDB and DQ were screened individually in the presence and in the absence of NDH-2A, and clear STD-NMR signals were detected for the three quinones only in the presence of the protein (Figure S3.5). STD competition experiments revealed that DMN, DDB and DQ compete for the same binding site, indicating that their binding is specific (Table S3.2). Moreover, not all protons of DMN and DDB receive the same percentage of saturation (Table S3.2). For DMN, the STD spectrum (Figure S3.5A) shows higher relative saturation percentages for the aromatic hydrogens (H2 and H3, close to 100 %) than for the methyl groups (H1, 87 %) (Figure S3.5A and Table S3.2). Also, in the case of DDB the relative STD percentages determined for the protons of the methyl (H1, 87 %) and methoxy groups (H2, 100 %) are different (Figure S3.5B and Table S3.2). These observations indicate a preferred orientation of DMN and DDB, with the contact with the protein occurring through the side of the aromatic ring in DMN and through the side of the methoxy groups in DDB. To address the question of whether the two substrates, NADH and quinone, have the same binding site, the protein was titrated with NAD^+ in the presence of DMN and vice-versa. STD-NMR spectra were recorded for each condition and the STD amplification factor of DMN and NAD^+ were determined (Figure 3.13A and B). NAD^+ was chosen instead of NADH to avoid the oxidoreduction reaction and the consequent disappearance of the NADH resonances and appearance of resonances assigned to NAD^+. Such situation would make the interpretation of the spectra much more complex. The STD amplification factors of DMN recorded in the absence or presence of a fixed concentration of NAD^+ were almost identical (Figure 3.13A). Also, in the presence of both compounds (DMN and NAD^+) the increase of DMN concentration had no effect on the STD amplification factor of NAD^+ (Figure 3.13A). These results indicate that NAD^+

does not affect the binding of DMN to NDH-2A. A similar behavior was observed on the reverse addition experiment upon increasing of NAD^+ concentration in the absence or presence of a fixed concentration of DMN; the STD amplification factor of NAD^+ increased with the increasing of NAD^+ in solution while the STD amplification factor of DMN did not change (Figure 3.13B). These results clearly indicate the existence of different binding sites for NADH and quinone. No STD effect was observed upon saturation of the protein in the presence of HQNO. This result can be interpreted as an absence of interaction between HQNO and the protein or as the occurrence of a strong interaction. Taking into account that the presence of HQNO affects the NADH:quinone oxidoreductase activity, a strong interaction between the protein and HQNO can be inferred. To check whether the HQNO effect is due to a possible binding to the quinone or to the NAD^+ site the variation of the STD amplification factor of DMN and NAD^+ were monitored as before, but in the presence of HQNO (Figure S3.6). For DMN a substantial reduction of the STD amplification factor was observed when compared to the experiment in the absence of HQNO (Figure 3.13A), but for NAD^+ the presence of HQNO had no significant effect on the profile of the STD amplification (Figure 3.13B). These results also indicate that HQNO does not interfere with the NAD^+ binding and suggest a possible interaction with the quinone binding site. To check if the STD response of DMN could be completely suppressed by HQNO a STD experiment using a 15-fold excess of HQNO to DMN was performed. Even under these conditions the STD amplification factor was still similar to the one obtained with a 1:1 mixture of DMN and HQNO. Since the interaction of HQNO with the protein is stronger than that of DMN, this result is an indication that HQNO binds at a site which is close to that of DMN but not coincident with it.

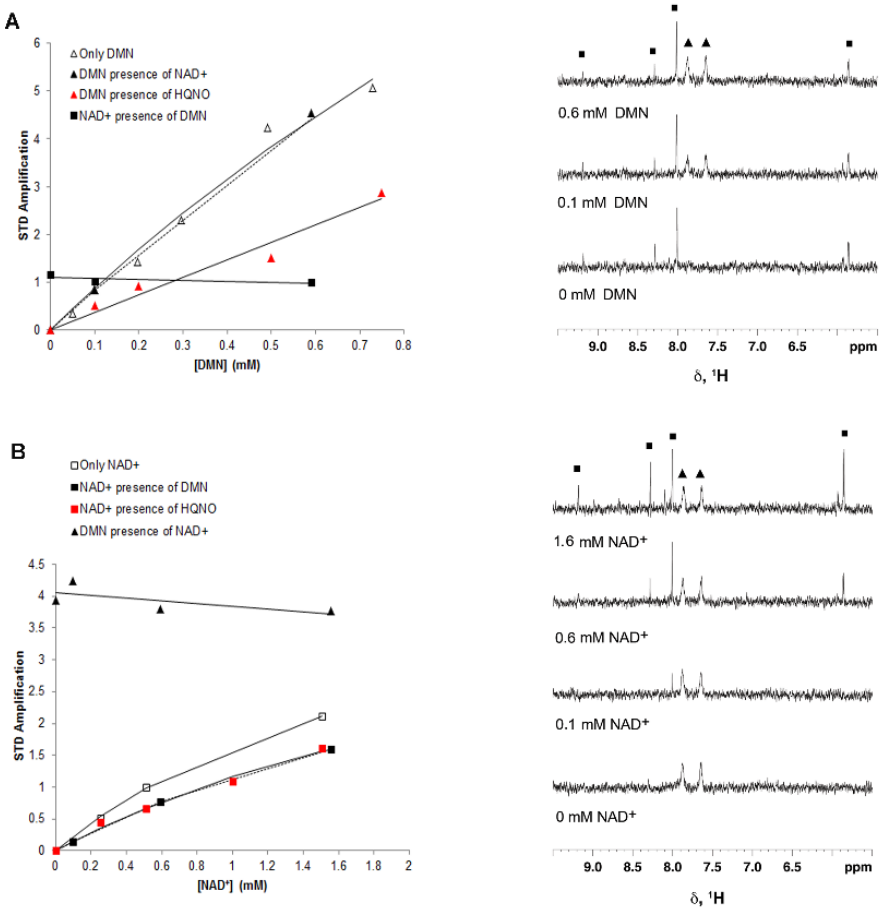

Figure 3.13 STD-NMR Measurements. (A) Right – Plot of the STD amplification factor of DMN (from signal at 7.88 ppm) vs [DMN] measured in NDH-2 solutions titrated with DMN or in the presence of different compounds: only DMN (△, open triangle); DMN (▲, black closed triangle) in the presence of NAD^+, for which the NAD^+ amplification factor (from signal at 8 ppm) in the same sample was also measured (■, black closed square) and DMN (▲, red closed triangle) in the presence of HQNO. The curves are meant to be visual guidelines. Left – Illustrative STD-NMR spectra of NDH-2 titrated with DMN in the presence of NAD^+. **(B)** Right – Plot of the STD amplification factor of NAD^+ vs [NAD^+] measured in NDH-2 solutions titrated with NAD^+ in the presence of different compounds: only NAD^+ (□, open square); NAD^+ (■, black closed square) in the presence of DMN, for which the DMN amplification factor in the same sample was also measured (▲, black closed triangle), and NAD^+ in the presence of HQNO (■, red closed square). The curves are meant to be visual guidelines. Left – Illustrative STD-NMR spectra of NDH-2 titrated with NAD^+ in the presence of DMN.

Concerning the STD-NMR studies of NDH-2B, the substrates DMN and $NADP^+$ were tested. $NADP^+$ was chosen instead of NADPH to avoid the catalytic reaction to occur and the consequent changes in NADPH and $NADP^+$ due to substrate consumption. Two STD-NMR signals (7.88 ppm and at 7.65 ppm) were detected corresponding to the hydrogens of the aromatic rings of the quinone (Figure S3.7A). These two signals showed relative saturation percentages of 92 % and 96 %, revealing that probably the contact with the protein is occurring through these groups. It was possible to observe that with the increase of DMN concentration the integral of the signals corresponding to the DMN peaks also increased (Figure 3.14A). The same was performed for $NADP^+$ and in this case five signals were detected (9.2, 9.0, 8.671, 8.28 and 6.0 ppm). The signals, correspondent to the aromatic ring of the nicotinamide (signal 1, 2 and 3, see Figure S3.7B), have relative saturation percentages in the range of 27 to 46 %. The 8.2 and 6.0 ppm signals correspond to the adenine and ribose of the adenosine molecule of $NADP^+$ (signals 4 and 5 see Figure S3.7B) and have a relative saturation percentage around 35 %. (Figure S3.7B).

We choose two signals correspondent to $NADP^+$ (8.671 and 8.28 ppm) and the increase of the peaks integrals with the increasing of $NADP^+$ concentration was also observed (Figure 3.14B). In addition, NDH-2B was titrated with $NADP^+$ in the presence of DMN and vice-versa, to know whether the two substrates were competing for the same binding site. The STD-NMR spectra of the titration of NDH-2B with DMN in the presence of $NADP^+$ originated seven peaks, two from DMN and five from $NADP^+$. The increase of DMN concentration had no effect on the STD amplification factor of $NADP^+$ indicating that DMN does not affect the binding of $NADP^+$ to NDH-2B (Figure 3.14C). In the case of the titration of NDH-2B with $NADP^+$ in the presence of DMN we observed that the STD amplification factor of $NADP^+$ increased with

the increasing of $NADP^+$ in solution while the STD amplification factor of DMN did not change (Figure 3.14D). These results indicate that the binding of one substrate does not influence the binding of the other one, suggesting that the two substrates, NADPH and quinone, have different binding sites.

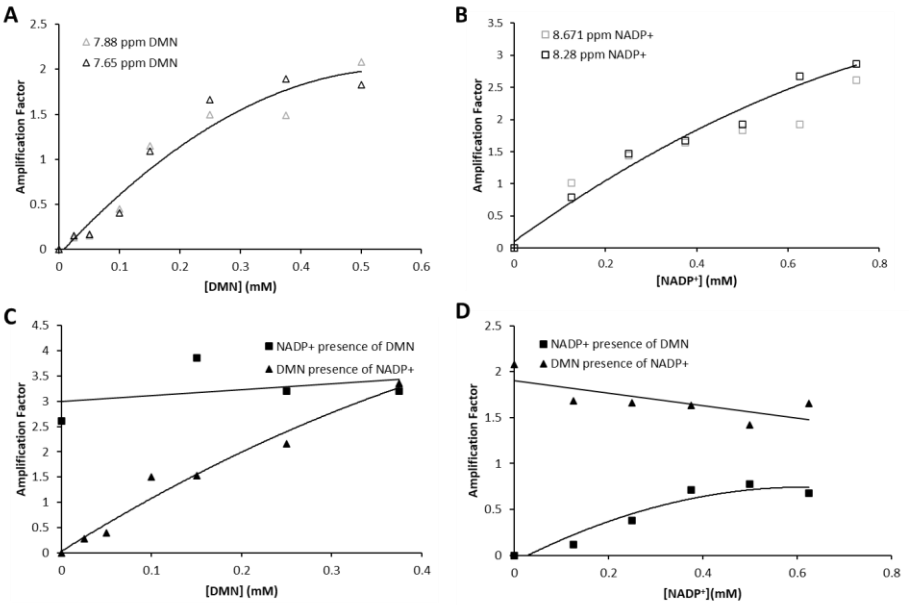

Figure 3.14 STD-NMR measurements with NDH-2B and substrates (DMN and $NADP^+$). **(A)** Plot of the STD amplification factor of DMN (from signals at 7.88 ppm and at 7.65 ppm) vs [DMN] measured in NDH-2B solutions titrated with DMN. **(B)** Plot of the STD amplification factor of $NADP^+$ (from signals at 8.671 and at 8.28 ppm) vs [$NADP^+$] measured in NDH-2B solutions titrated with $NADP^+$.**(C)** Plot of the STD amplification factor of DMN (from signals at 7.88 ppm and at 7.65 ppm) vs [DMN] measured in NDH-2B solutions titrated with DMN in the presence of $NADP^+$ for which the $NADP^+$ amplification factor in the same sample was also measured. **(D)** Plot of the STD amplification factor of $NADP^+$ (from signals at 8.671, and 8.28 ppm) vs [$NADP^+$] measured in NDH-2B solutions titrated with $NADP^+$ in the presence of DMN for which the DMN amplification factor in the same sample was also measured. The curves are meant to be visual guidelines.

3.5 Conclusion

We obtained crystal and solution structures of NDH-2A from *S. aureus*, showing that it is a dimer in solution. A long discussion has taken place about whether NADH and the quinone bind to the same or to different sites[2,3]. The crystal structures of the *S. cerevisiae* Ndi1 protein further stimulated this discussion, since that obtained by Iwata *et al* [2] suggests the same binding site for the two substrates, at the re side of the isoalloxazine ring system of FAD, whereas Feng *et al* report different binding sites for NADH and quinone, at the re and si side of FAD respectively[3]. Our crystal structure also suggests that NADH and the quinone bind to different sites. As already pointed out by Heikal *et al*[6], in order to the quinone to go around the isoalloxazine ring of FAD and interact with it from the re side, as suggested by Iwata *et al*[2], a considerable conformational change involving the membrane anchoring domain has to occur. Additionally, we identified conserved amino acid residues, between them a series of conserved amino acids that can form a proton pathway in each dinucleotide binding domain. The latter may conduct protons from the bulk to the quinone binding pocket necessary for its protonation. These conserved common elements of NDH-2 also suggest that NDH-2 have independent substrates binding sites in agreement with the structure obtained.

Our fluorescence and STD data showed, for both NDH-2s, that indeed NAD(P)H and quinone bind to different sites. Furthermore, fluorescence and STD-NMR spectroscopic indicated that HQNO only interfered with the binding of the quinone. HQNO seemed not to affect the binding of NAD(P)H. If the two substrates would bind to the same site, HQNO should affect both protein–substrate interactions for the two substrates similarly. These differences indicate that NADH and quinone interact with the protein in distinct binding sites. Fluorescence and STD-NMR spectroscopic data also reveal that HQNO

interacts with the protein in a different way from those of NAD(P)H or DMN. The titration profile of HQNO and its maximum effect on tryptophan quenching or STD amplification factor are different from either NAD(P)H/NAD(P)$^+$ or DMN. These observations, in addition to the result showing that the fluorescence titration profile of DMN is sigmoidal in the presence of HQNO, suggest that the inhibitor binds to a distinct site, stabilizing a conformation with less affinity for quinone, which is possibly also located at the si-side of the isoalloxazine ring of FAD as that of the quinone. In fact the existence of another quinone binding site has been already proposed, which would allow quinol to function as an allosteric activator[3,46].

In this work, we explored the interaction of NDH-2s from *S. aureus* with substrates and present its structural and characterization. This investigation will provide a framework for structure-based drug design, mainly if we will manage to obtain the structure with its substrates and with strong inhibitors candidates.

3.6 Acknowledgements

We acknowledge Tatiana Pires for performing the STD experiments of NDH-2B. F.V.S. and F.M.S. are recipients of fellowships by Fundação para a Ciência e a Tecnologia (PD/BD/113985/2015, PD/BD/128213/2016, respectively (within the scope of the PhD program Molecular Biosciences PD/00133/2012)). We are grateful to the beamline staff for helping and for the technical support during diffraction data experiments. This project was funded by Fundação para a Ciência e a Tecnologia through grants PTDC/BIA-PRO/118535/2010 to M.A., PTDC/BBB-BQB/2294/2012 to MMP and #PEst-OE/EQB/LA0004/2011. M.A. acknowledges funding from Bio-Struct-X (proposal 1493). The NMR spectrometers are part of The Portuguese National NMR Facility, supported by Fundação para a Ciência e a Tecnologia (RECI/BBB-BQB/0230/2012). A.P.B. and J.A.B are recipients of grants SFRH/BPD/80741/2011 and SFRH/BPD/79224/2011, respectively, from Fundação para a Ciência e a Tecnologia. T.M. was supported by the Bavarian Ministry of Sciences, Research and the Arts (Bavarian Molecular Biosystems Research Network, to T.M.), the German Research Foundation (Emmy Noether program MA 5703/1-1, to T.M.), the Centre for Integrated Protein Science Munich (CIPSM), the President's International Fellowship Initiative of CAS (No:2015VBB045, to T.M.) and the National Natural Science Foundation of China (No. 31450110423, to T.M.). The authors acknowledge the Leibniz Supercomputing Centre (LRZ, http://www.lrz.de) for providing computing time on the Linux Cluster. M.M.P. and E.J.C. acknowledge networking support by the COSTAction CM1306 – Understanding Movement and Mechanism in Molecular Machines. The project was funded by Fundação para a Ciência e a Tecnologia (PTDC/BBB-BQB/2294/2012 to M.M.P.). The work was supported by Fundação para a Ciência e a Tecnologia through Grant # PEst-OE/EQB/LA0004/2011.

3.7 References

[1] S.J. Kerscher, Diversity and origin of alternative NADH:ubiquinone oxidoreductases, Biochim. Biophys. Acta - Bioenerg. 1459 (2000) 274–83. https://doi.org/10.1016/S0005-2728(00)00162-6.

[2] M. Iwata, Y. Lee, T. Yamashita, T. Yagi, S. Iwata, A.D. Cameron, M.J. Maher, The structure of the yeast NADH dehydrogenase (Ndi1) reveals overlapping binding sites for water- and lipid-soluble substrates, Proc. Natl. Acad. Sci. U. S. A. 109 (2012) 15247–52. https://doi.org/10.1073/pnas.1210059109.

[3] Y. Feng, W. Li, J. Li, J. Wang, J. Ge, D. Xu, Y. Liu, K. Wu, Q. Zeng, J.W. Wu, C. Tian, B. Zhou, M. Yang, Structural insight into the type-II mitochondrial NADH dehydrogenases, Nature. 491 (2012) 478–82. https://doi.org/10.1038/nature11541.

[4] T. Yamashita, D.K. Inaoka, T. Shiba, T. Oohashi, S. Iwata, T. Yagi, H. Kosaka, H. Miyoshi, S. Harada, K. Kita, K. Hirano, Ubiquinone binding site of yeast NADH dehydrogenase revealed by structures binding novel competitive- and mixed-type inhibitors, Sci. Rep. 8 (2018) 2427. https://doi.org/10.1038/s41598-018-20775-6.

[5] Y. Yang, Y. Yu, X. Li, J. Li, Y. Wu, J. Yu, J. Ge, Z. Huang, L. Jiang, Y. Rao, M. Yang, Target Elucidation by Cocrystal Structures of NADH-Ubiquinone Oxidoreductase of *Plasmodium falciparum (*PfNDH2) with Small Molecule To Eliminate Drug-Resistant Malaria, J. Med. Chem. 60 (2017) 1994–2005. https://doi.org/10.1021/acs.jmedchem.6b01733.

[6] A. Heikal, Y. Nakatani, E. Dunn, M.R. Weimar, C.L. Day, E.N. Baker, J.S. Lott, L.A. Sazanov, G.M. Cook, Structure of the bacterial type II NADH dehydrogenase: A monotopic membrane protein with an essential role in energy generation, Mol. Microbiol. 91 (2014) 950–64. https://doi.org/10.1111/mmi.12507.

[7] J. Petri, Y. Shimaki, W. Jiao, H.R. Bridges, E.R. Russell, E.J. Parker, D. Aragão, G.M. Cook, Y. Nakatani, Structure of the NDH-2 – HQNO inhibited complex provides molecular insight into quinone-binding site inhibitors, Biochim. Biophys. Acta - Bioenerg. 1859 (2018) 482–490.

https://doi.org/10.1016/j.bbabio.2018.03.014.

[8] A. V. Kozlov, H. Nohl, L. Gille, Are reduced ubiquinones oxygen radical generators?, Bioorg. Chem. 26 (1998) 334–344. https://doi.org/10.1006/bioo.1998.1109.

[9] A.L. Rosário, F.V. Sena, A.P. Batista, T.F. Oliveira, D. Athayde, M.M. Pereira, J.A. Brito, M. Archer, Expression, purification, crystallization and preliminary X-ray diffraction analysis of a type II NADH:quinone oxidoreductase from the human pathogen *Staphylococcus aureus*, Acta Crystallogr. Sect. FStructural Biol. Commun. 71 (2015). https://doi.org/10.1107/S2053230X15005178.

[10] W. Kabsch, XDS, Acta Crystallogr. Sect. D Biol. Crystallogr. 66 (2010) 125–132. https://doi.org/10.1107/S0907444909047337.

[11] P.R. Evans, An introduction to data reduction: Space-group determination, scaling and intensity statistics, Acta Crystallogr. Sect. D Biol. Crystallogr. 67 (2011) 282–92. https://doi.org/10.1107/S090744491003982X.

[12] P. Evans, Scaling and assessment of data quality, in: Acta Crystallogr. Sect. D Biol. Crystallogr., 2006: pp. 72–82. https://doi.org/10.1107/S0907444905036693.

[13] C. Vonrhein, C. Flensburg, P. Keller, A. Sharff, O. Smart, W. Paciorek, T. Womack, G. Bricogne, Data processing and analysis with the autoPROC toolbox, Acta Crystallogr. Sect. D Biol. Crystallogr. D67 (2011) 293–302. https://doi.org/10.1107/S0907444911007773.

[14] A.J. McCoy, R.W. Grosse-Kunstleve, P.D. Adams, M.D. Winn, L.C. Storoni, R.J. Read, Phaser crystallographic software, J. Appl. Crystallogr. 40 (2007) 658–674. https://doi.org/10.1107/S0021889807021206.

[15] B.W. Matthews, Solvent content of protein crystals, J. Mol. Biol. 33 (1968) 491–497. https://doi.org/10.1016/0022-2836(68)90205-2.

[16] T.C. Terwilliger, R.W. Grosse-Kunstleve, P. V. Afonine, N.W. Moriarty, P.H. Zwart, L.W. Hung, R.J. Read, P.D. Adams, Iterative model building, structure refinement and density modification with the PHENIX AutoBuild wizard, in: Acta Crystallogr. Sect. D Biol. Crystallogr., 2007: pp. 61–9.

https://doi.org/10.1107/S090744490705024X.

[17] P.D. Adams, R.W. Grosse-Kunstleve, L.W. Hung, T.R. Ioerger, A.J. McCoy, N.W. Moriarty, R.J. Read, J.C. Sacchettini, N.K. Sauter, T.C. Terwilliger, PHENIX: Building new software for automated crystallographic structure determination, in: Acta Crystallogr. Sect. D Biol. Crystallogr., 2002: pp. 1948–54. https://doi.org/10.1107/S0907444902016657.

[18] G. Bricogne, E. Blanc, M. Brandl, C. Flensbueg, P. Keller, W. Paciorek, P. Roversi, A. Sharff, O.S. Smart, C. Vonrhein, T.O. Womack, BUSTER version 2.10.3, Cambridge, United Kingdom Glob. Phasing Ltd. (2011).

[19] P. Emsley, B. Lohkamp, W.G. Scott, K. Cowtan, Features and development of Coot, Acta Crystallogr. Sect. D Biol. Crystallogr. 66 (2010) 486–501. https://doi.org/10.1107/S0907444910007493.

[20] P. V. Afonine, R.W. Grosse-Kunstleve, N. Echols, J.J. Headd, N.W. Moriarty, M. Mustyakimov, T.C. Terwilliger, A. Urzhumtsev, P.H. Zwart, P.D. Adams, Towards automated crystallographic structure refinement with phenix.refine, Acta Crystallogr. Sect. D Biol. Crystallogr. 68 (2012) 352–67. https://doi.org/10.1107/S0907444912001308.

[21] V.B. Chen, W.B. Arendall, J.J. Headd, D.A. Keedy, R.M. Immormino, G.J. Kapral, L.W. Murray, J.S. Richardson, D.C. Richardson, MolProbity: All-atom structure validation for macromolecular crystallography, Acta Crystallogr. Sect. D Biol. Crystallogr. 66 (2010) 12–21. https://doi.org/10.1107/S0907444909042073.

[22] N.A. Baker, D. Sept, S. Joseph, M.J. Holst, J.A. McCammon, Electrostatics of nanosystems: Application to microtubules and the ribosome, Proc. Natl. Acad. Sci. U. S. A. 98 (2001) 10037–10041. https://doi.org/10.1073/pnas.181342398.

[23] T.J. Dolinsky, J.E. Nielsen, J.A. McCammon, N.A. Baker, PDB2PQR: An automated pipeline for the setup of Poisson-Boltzmann electrostatics calculations, Nucleic Acids Res. 32 (2004) W665-7. https://doi.org/10.1093/nar/gkh381.

[24] D.I. Svergun, Determination of the regularization parameter in indirect-transform methods using perceptual criteria, J. Appl. Crystallogr. 25 (1992)

495–503. https://doi.org/10.1107/S0021889892001663.

[25] A. Bergmann, G. Fritz, O. Glatter, Solving the generalized indirect Fourier transformation (GIFT) by Boltzmann simplex simulated annealing (BSSA), J. Appl. Crystallogr. 33 (2000) 1212–1216. https://doi.org/10.1107/S0021889800008372.

[26] M. V. Petoukhov, D. Franke, A. V. Shkumatov, G. Tria, A.G. Kikhney, M. Gajda, C. Gorba, H.D.T. Mertens, P. V. Konarev, D.I. Svergun, New developments in the ATSAS program package for small-angle scattering data analysis, J. Appl. Crystallogr. 45 (2012) 342–350. https://doi.org/10.1107/S0021889812007662.

[27] L.A. Kelley, M.J.E. Sternberg, Protein structure prediction on the web: A case study using the phyre server, Nat. Protoc. 4 (2009) 363–371. https://doi.org/10.1038/nprot.2009.2.

[28] W.L. DeLano, The PyMOL Molecular Graphics System, Version 1.1, Schr{ö}dinger LLC. (2002). https://doi.org/10.1038/hr.2014.17.

[29] B.C. Marreiros, F. V. Sena, F.M. Sousa, A.P. Batista, M.M. Pereira, Type II NADH:quinone oxidoreductase family: phylogenetic distribution, structural diversity and evolutionary divergences, Environ. Microbiol. 18 (2016) 4697–4709. https://doi.org/10.1111/1462-2920.13352.

[30] J. Pei, B.H. Kim, N. V. Grishin, PROMALS3D: A tool for multiple protein sequence and structure alignments, Nucleic Acids Res. 36 (2008) 2295–300. https://doi.org/10.1093/nar/gkn072.

[31] M.M. Cherney, Y. Zhang, M. Solomonson, J.H. Weiner, M.N.G. James, Crystal structure of sulfide:Quinone oxidoreductase from *acidithiobacillus ferrooxidans*: Insights into sulfidotrophic respiration and detoxification, J. Mol. Biol. 398 (2010) 292–305. https://doi.org/10.1016/j.jmb.2010.03.018.

[32] M. Marcia, U. Ermler, G. Peng, H. Michel, The structure of *Aquifex aeolicus* sulfide:quinone oxidoreductase, a basis to understand sulfide detoxification and respiration, Proc. Natl. Acad. Sci. U. S. A. 106 (2009) 9625–30. https://doi.org/10.1073/pnas.0904165106.

[33] J.A. Brito, F.L. Sousa, M. Stelter, T.M. Bandeiras, C. Vonrhein, M. Teixeira, M.M.

Pereira, M. Archer, Structural and functional insights into sulfide:quinone oxidoreductase, Biochemistry. 48 (2009) 5613–22. https://doi.org/10.1021/bi9003827.

[34] E. Krissinel, K. Henrick, Inference of Macromolecular Assemblies from Crystalline State, J. Mol. Biol. 372 (2007) 774–97. https://doi.org/10.1016/j.jmb.2007.05.022.

[35] A.J. Prongay, C.H. Williams, Oxidation-reduction properties of *Escherichia coli* thioredoxin reductase altered at each active site cysteine residue, J. Biol. Chem. 267 (1992) 25181–8.

[36] T.J. Jönsson, H.R. Ellis, L.B. Poole, Cysteine reactivity and thiol-disulfide interchange pathways in AhpF and AhpC of the bacterial alkyl hydroperoxide reductase system, Biochemistry. 46 (2007) 5709–21. https://doi.org/10.1021/bi7001218.

[37] B.C. Marreiros, F. V. Sena, F.M. Sousa, A.S.F. Oliveira, C.M. Soares, A.P. Batista, M.M. Pereira, Structural and Functional insights into the catalytic mechanism of the Type II NADH:quinone oxidoreductase family, Sci. Rep. 7 (2017) 42303. https://doi.org/10.1038/srep42303.

[38] R.K. Wierenga, P. Terpstra, W.G.J. Hol, Prediction of the occurrence of the ADP-binding βαβ-fold in proteins, using an amino acid sequence fingerprint, J. Mol. Biol. 187 (1986) 101–7. https://doi.org/10.1016/0022-2836(86)90409-2.

[39] R.K. Wierenga, J. Drenth, G.E. Schulz, R. Huber, Comparison of the three-dimensional protein and nucleotide structure of the FAD-binding domain of p-hydroxybenzoate hydroxylase with the FAD- as well as NADPH-binding domains of glutathione reductase, J. Mol. Biol. 167 (1983) 725–39. https://doi.org/10.1016/S0022-2836(83)80106-5.

[40] F. V. Sena, A.P. Batista, T. Catarino, J.A. Brito, M. Archer, M. Viertler, T. Madl, E.J. Cabrita, M.M. Pereira, Type-II NADH: Quinone oxidoreductase from *Staphylococcus aureus* has two distinct binding sites and is rate limited by quinone reduction, Mol. Microbiol. 98 (2015) 272–288. https://doi.org/10.1111/mmi.13120.

[41] B.W. Lennon, C.H. Williams, M.L. Ludwig, Crystal structure of reduced thioredoxin reductase from *Escherichia coli:* Structural flexibility in the isoalloxazine ring of the flavin adenine dinucleotide cofactor, Protein Sci. 8 (1999) 2366–79. https://doi.org/10.1110/ps.8.11.2366.

[42] M. Senda, S. Kishigami, S. Kimura, M. Fukuda, T. Ishida, T. Senda, Molecular Mechanism of the Redox-dependent Interaction between NADH-dependent Ferredoxin Reductase and Rieske-type [2Fe-2S] Ferredoxin, J. Mol. Biol. 373 (2007) 382–400. https://doi.org/10.1016/j.jmb.2007.08.002.

[43] Y. Yang, T. Yamashita, E. Nakamaru-Ogiso, T. Hashimoto, M. Murai, J. Igarashi, H. Miyoshi, N. Mori, A. Matsuno-Yagi, T. Yagi, H. Kosaka, Reaction mechanism of single subunit NADH-ubiquinone oxidoreductase (Ndi1) from *Saccharomyces cerevisiae*: Evidence for a ternary complex mechanism, J. Biol. Chem. 286 (2011) 9287–9297. https://doi.org/10.1074/jbc.M110.175547.

[44] M. Mayer, B. Meyer, Group epitope mapping by saturation transfer difference NMR to identify segments of a ligand in direct contact with a protein receptor, J. Am. Chem. Soc. 123 (2001) 6108–17. https://doi.org/10.1021/ja0100120.

[45] J. Angulo, P.M. Enríquez-Navas, P.M. Nieto, Ligand-Receptor Binding Affinities from Saturation Transfer Difference (STD) NMR Spectroscopy: The Binding Isotherm of STD Initial Growth Rates, Chem. - A Eur. J. 16 (2010) 7803–7812. https://doi.org/10.1002/chem.200903528.

[46] T. Yano, M. Rahimian, K.K. Aneja, N.M. Schechter, H. Rubin, C.P. Scott, *Mycobacterium tuberculosis* type II NADH-menaquinone oxidoreductase catalyzes electron transfer through a two-site ping-pong mechanism and has two quinone-binding sites, Biochemistry. 53 (2014) 1179–90. https://doi.org/10.1021/bi4013897.

3.8 Supplementary Information

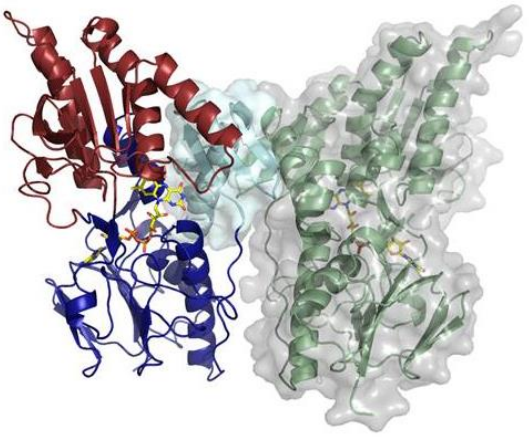

Figure S3.1 Homodimer of NDH-2A from *S. aureus* as observed in the asymmetric crystallographic unit. In monomer A (left), NADH-binding domain is colored in red, FAD-binding domain in blue and membrane attachment (C-terminal) domain in pale cyan with surface representation; FAD cofactor is shown in sticks with carbon atoms colored in yellow, oxygen in red and nitrogen in blue; in monomer B (right), cartoon representation is colored in green and solvent accessible area is represented as surface colored in grey.

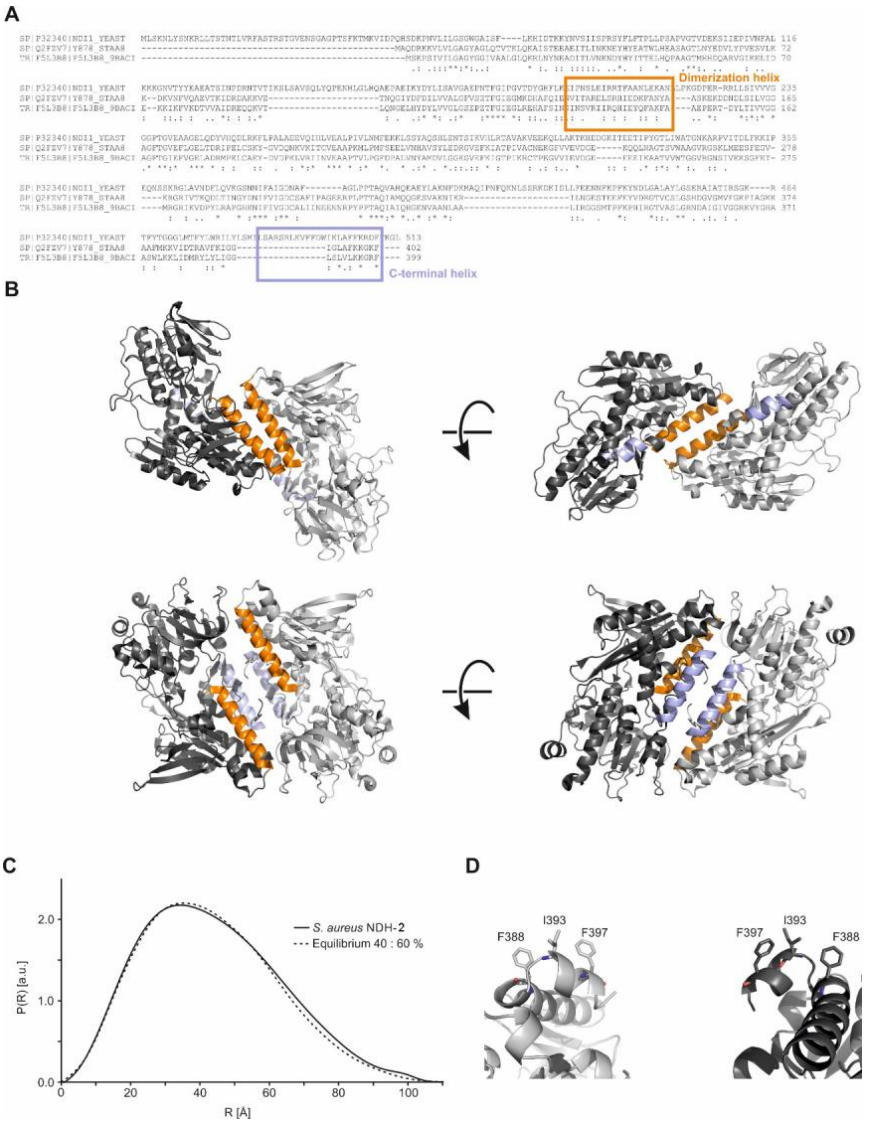

Figure S3.2 SAXS analyses. (A) Sequence alignment of *S. cerevisiae* (Uniprot-ID P32340), *C. thermarum* (Uniprot-ID F5L3B8), and *S. aureus* (Uniprot-ID Q2FZV7) NDH-2. The dimerization and C-terminal helices are labeled. Multiple sequence alignment was carried out using the CLUSTAL O (1.2.1) tool on the Uniprot webpage (http://www.uniprot.org); SAXS data of NDH-2A from *S. aureus* were compared to SAXS data back-calculated from crystal structures of the homologous proteins from *C. thermarum* (4NWZ) and *S. cerevisiae* (4G9K) (Figure 3.6). Clearly, neither of these two crystal structures was in good agreement with the data obtained for *S. aureus* (Figure 3.6). This result may reflect different possible orientations of the monomers, or an equilibrium between different conformations. In the crystal structures of the

homologous proteins, the orientation of the NDH-2 monomers in the dimer is different. In NDH-2 from *C. thermarum* dimerization involves a long α-helix (Ser128-Ala147 in 4NWZ), whereas these residues are not in contact with each other in the structure of NDH-2 from *S. cerevisiae*, instead the dimer is stabilized by a network of contacts involving a C-terminal α-helix (Ala489-Lys506 in 4G9K) and a loop region (Ser145-Ala165; **(B)** A shorter version of this C-terminal helix is conserved in NDH-2s from *S. aureus* and *C. thermarum* (Leu393-Gly397 in 4NWZ), which may raise the hypothesis that NDH-2A from *S. aureus*, could establish a dimer interaction through this short helix, under certain conditions. In this case NDH-2 from *S. aureus* could adopt two different conformations in solution. Thus, to test whether our results could be explained by a conformational equilibrium based on the two previous published structures, we estimated the ratio between the two different conformations, using the SAXS data back-calculated for the two homologous proteins. Provided that the scattering intensities of the end-point structures are known (form factors), SAXS data are a measure of the populations in the different conformations (in the form of volume fractions of each component). Indeed, a superposition of SAXS data back-calculated for the two homologous proteins and assuming a population ratio of 40:60 % (*C. thermarum: S. cerevisiae*) resulted in good agreement with the experimental data **(C)**. In the twisted dimeric structure the membrane attachment region is located at the same side of the dimer. Both helices including the conserved hydrophobic residues (F388, I393, and F397) are oriented parallel to the membrane and well-available for membrane binding **(D)**.

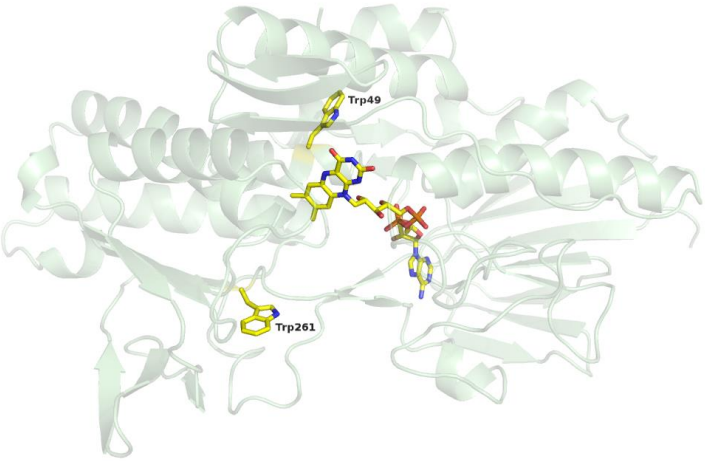

Figure S3.3 Cartoon representation of the NDH-2A from *S. aureus*. The positions of the two tryptophan residues are highlighted. FAD cofactor is shown in sticks with carbons atoms colored in yellow, oxygen in red and nitrogen in blue. W261 is located at the *re* side of FAD while W49 is situated at the *si* side of FAD.

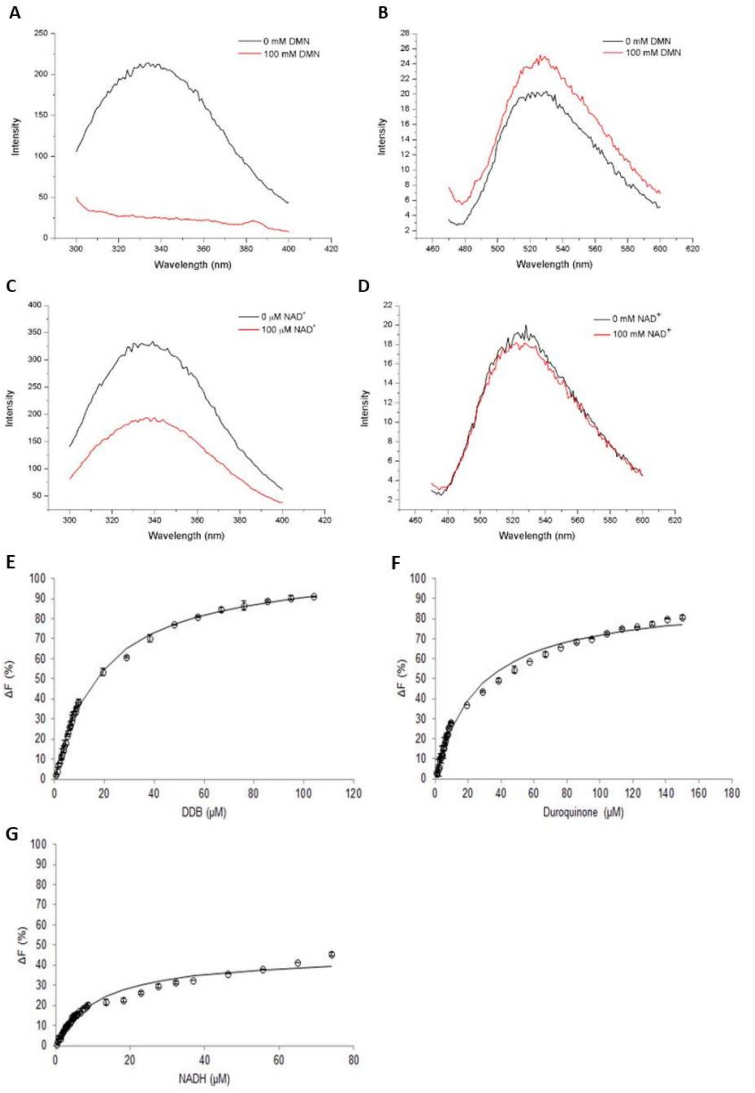

Figure S3.4 Fluorescence spectroscopy of NDH-2A. The fluorescence emission spectrum of NDH-2A with excitation at 280 nm exhibited the characteristics of a typical tryptophan fluorescence spectrum, while the fluorescence emission spectrum with excitation at 450 nm was typical of a flavoprotein. Only slight changes were observed in the region of the flavin fluorescence emission spectra in the presence of some ligands. By contrast, the intensity in the region of the tryptophan fluorescence emission spectra changed significantly and differently upon addition of each ligand. Fluorescence emission spectra of NDH-2A with excitation at 280 nm, in the absence and in the presence of 100 μM DMN **(A)** or 100 μM NAD^+ **(C).** Fluorescence emission spectra of NDH-2A with excitation at 450 nm, in the absence and in the presence of 100 μM DMN

(B) or 100 µM NAD^+**(D)**. Change in the fluorescence emission at 330 nm with excitation at 280 nm of NDH-2A by sequential addition of DDB **(E)** or Duroquinone **(F)** or NADH **(G)**. The solid lines were obtained by fitting the Monod-Wyman-Changeux (MWC) model equation, $\Delta F = \Delta F^{max} \times \frac{\frac{[S]}{K_S}\left(1+\frac{[S]}{K_S}\right)}{L+\left(1+\frac{[S]}{K_S}\right)^2}$ for a dimeric enzyme to the data using L=0.

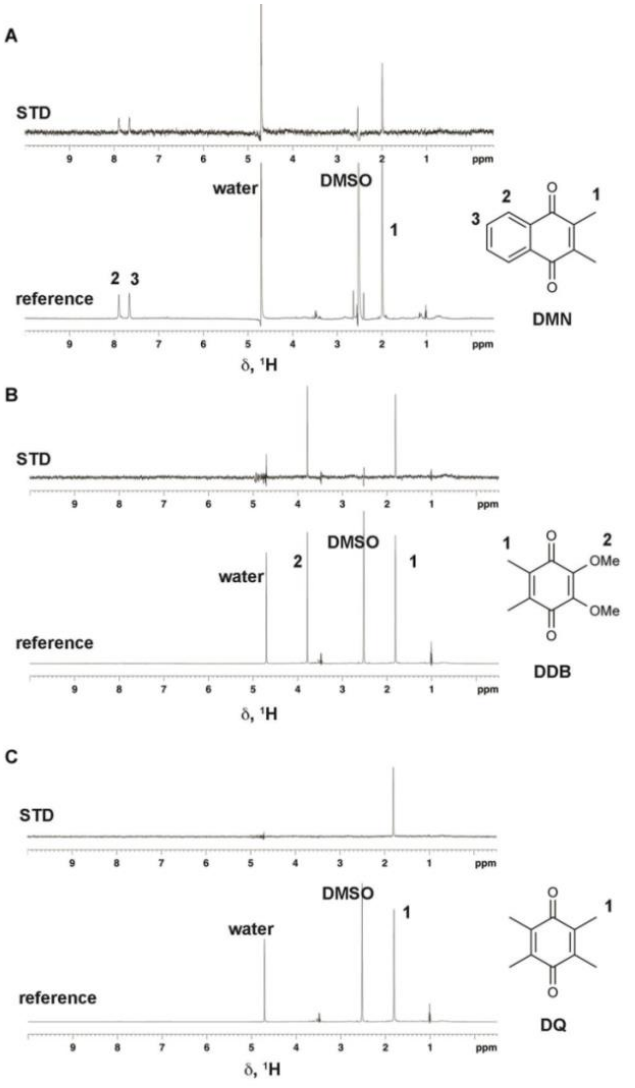

Figure S3.5 STD-NMR Measurements. Reference spectrum (off resonance) and STD-NMR spectrum of NDH-2A from *S. aureus* in the presence of **(A)** DMN **(B)** DDB and **(C)** DQ.

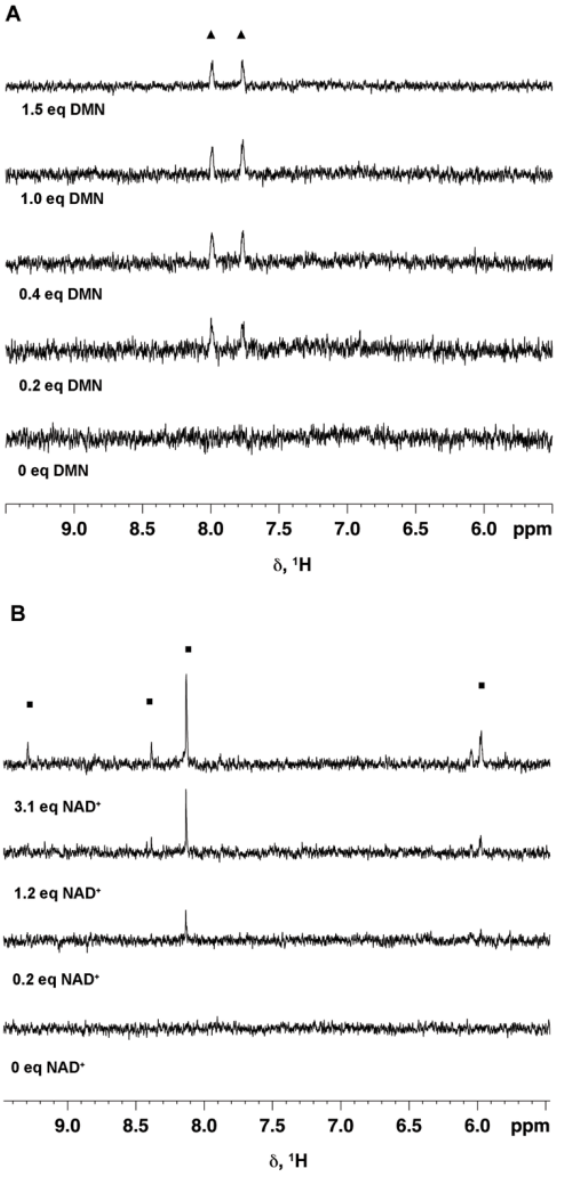

Figure S3.6 STD-NMR spectra obtained in the presence of HQNO. (A) STD-NMR spectra of NDH-2A titrated with DMN in the presence of HQNO (▲, black closed triangle). **(B)** STD-NMR spectra of NDH-2 titrated with NAD^+ in the presence of HQNO (■, black closed square).

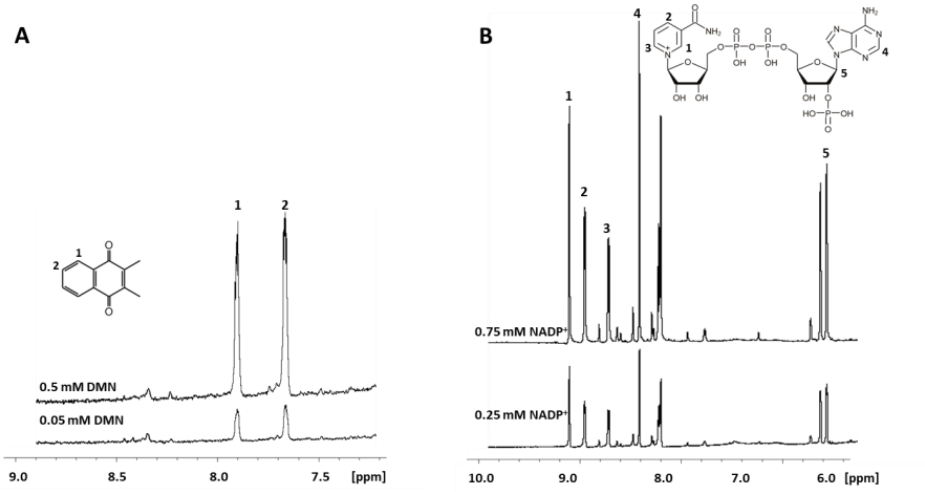

Figure S3.7 STD-NMR measurements of NDH-2B and substrates (DMN and NADP$^+$). Illustrative STD-NMR spectra of NDH-2B titrated with DMN **(A)** and with NADP$^+$**(B)**.

Table S3.1 SAXS data and analysis.

Sample	R_g [Å]	Molecular mass [kDa]*
Staphylococcus aureus NDH-2A	34 ± 1	93
+ DMN	35 ± 1	109
+ HQNO	38 ± 4	90
+ DMN/HQNO	39 ± 4	88
+ NAD	36 ± 1	110
+ NADH	35 ± 1	107

*The molecular mass was determined using Porod's law.

Table S3.2 Relative STD NMR values for the experiments of NDH-2A with DMN, DDB or DQ and for the STD competition experiments where the order of quinone addition was varied.

Quinone	Peak number	Relative STD*				
		Individual quinone	DMN+DDB	DDB+DMN	DMN+DQ	DQ+DMN
DMN	1	87%	85%	82%	70%	79%
	2	99%	100%	100%	100%	94%
	3	100%	98%	97%	89%	100%
DDB	1	87%	16%	16%	-	-
	2	100%	16%	16%	-	-
DQ	1	100%	-	-	27%	34%

* STD competition experiments were also performed with DQ and DDB but the peak overlaps between the peak 1 of DQ and the peak 1 of DDB not allowing determining individual relative STD responses.

Chapter 4

The catalytic mechanism of Type II NAD(P)H:quinone oxidoreductases of *Staphylococcus aureus*

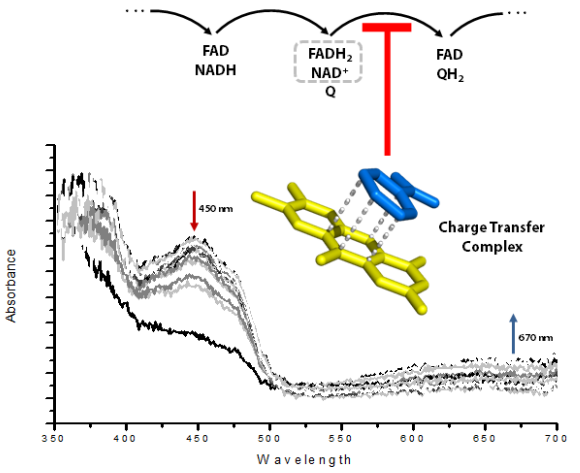

Chapter 4- The catalytic mechanism of Type II NAD(P)H:quinone oxidoreductases of *Staphylococcus aureus*

This section is based on the following publications:

- ✓ **Sena FV**, Batista AP, Catarino T, Brito JA, Archer M, Viertler M, Madl T, Cabrita EJ, Pereira MM. Type-II NADH:quinone oxidoreductase from *Staphylococcus aureus* has two distinct binding sites and is rate limited by quinone reduction. *Mol Microbiol.* 98 (2015) 272–288. Doi: 10.1111/mmi.13120.

- ✓ Marreiros BC, **Sena FV**, Sousa FM, Oliveira AS, Soares CM, Batista AP, Pereira MM. Structural and Functional insights into the catalytic mechanism of the Type II NADH:quinone oxidoreductase family. *Sci Rep.* 7 (2017) 42303. Doi: 10.1038/srep42303.

- ✓ Sousa FM, **Sena FV**, Batista AP, Athayde D, Brito JA, Archer M, Oliveira ASF, Soares CM, Catarino T, Pereira MM. The key role of glutamate 172 in the mechanism of type II NADH:quinone oxidoreductase of *Staphylococcus aureus*. *Biochim. Biophys. Acta - Bioenerg*. 1858 (2017) 823–832. Doi: 10.1016/j.bbabio.2017.08.002.

- ✓ **Sena FV**, Sousa FM, Oliveira ASF, Soares CM, Catarino T, Pereira MM. Regulation of the mechanism of Type-II NADH: Quinone oxidoreductase from *S. aureus*. *Redox Biol*. (2018) 16:209-214. Doi: 10.1016/j.redox.2018.02.004.

Author Contribution:

Sena FV performed all the steady-state and fast kinetics experiments at ITQB, critically discussed all the data and drafted the manuscript. The assays with E_{172} variants were done with the help of Filipe Sousa and the simulation studies on D_{302} protonation were made by Sofia Oliveira, at Cláudio M. Soares Lab, at ITQB. Bruno Marreiros performed and analyzed the experiments of sequence analysis and amino acid conservation.

4.1 Summary

NDH-2 is a single-subunit monotopic membrane protein with flavin as the only prosthetic group, present in organisms belonging to the three domains of life. In this work we used steady-state and pre-steady-state kinetics combined with mutagenesis and structural studies to investigate the mechanism of NDH-2A and NDH-2B from *Staphylococcus aureus.*

We report pre steady-state kinetic analyses of NDH-2A enzyme, in which we detected a charge-transfer (CT) complex formed between NAD^+ and the reduced flavin. This CT complex is dissociated by the presence of the quinone, leading to the conclusion that NDH-2A establishes a ternary complex during catalysis. Additionally, the rate-limiting step in NDH-2A is the reduction of the quinone. Our hypothesis is that the CT complex is important to avoid reactivity with O_2, since NAD^+ remains bound in the vicinity of $FADH_2$ upon reduction. In contrast, after the reduction of NDH-2B with NADPH, we did not observe a charge-transfer complex, but in this case, the limiting step is the oxidation of NADPH, which imply that the enzyme under turnover condition does not remain in its reduced state.

According to these results, we conclude both enzymes from *S. aureus* organism resort to two different strategies/processes, the formation of the CT complex or the limiting step being NAD(P)H oxidation, to obtain the same effect, the protein does not form a stable and free (accessible) reduced state and, therefore, it avoids the reduced flavin to react unspecifically with O_2, preventing the production of ROS in vivo. Additionally, we investigated the common elements of all NDH-2s, based on the rationale that conservation of such elements reflects their structural and/or functional importance. Among the conserved amino acid residues, we selected glutamate 172 in NDH-2A which is conserved in 97 % of 1762 analyzed NDH-2s to perform site-directed

mutagenesis. We also performed protonation equilibrium simulations for aspartate 302 (in NDH-2A) present in the vicinity of FAD and totally conserved (100 %), even among other members of the tDBDF superfamily. The integrated data allowed us to establish the basis to discuss and propose a universal catalytic mechanism for NDH-2s.

4.2 Introduction

Type II NADH:quinone oxidoreductases (NDH-2s) are membrane proteins involved in respiratory chains responsible for the regeneration of NAD^+. NDH-2s catalyze the oxidation of NAD(P)H and the reduction of quinones having FAD as prosthetic group. In the previous chapter we investigated the number of binding sites of *S. aureus* NDH-2s, solving the long controversy on the number of the substrate binding sites. This is a crucial information for the discussion of the reaction mechanism of the enzyme that will be presented in this chapter. Under two substrate steady-state conditions, two types of kinetic mechanisms can take place, the so-called ping-pong mechanism, and the ternary complex mechanism. In a ping-pong mechanism the second substrate only binds after the release of the first product. In this situation the two substrates, in the case of NDH-2, NAD(P)H and quinone, are never observed to be bound to the enzyme at the same time (Figure 4.1). Furthermore, the reaction can occur via a one-site or two-site ping-pong mechanism, depending on whether the two substrates bind to the same site or to two different sites. In a ternary complex mechanism, the two substrates simultaneously bind to the enzyme before the release of the products, which implies the existence of two distinct binding sites for each of the substrates (Figure 4.1). A number of studies analyzing the kinetic properties of the NDH-2s from *Yarrowia lipolytica*[1], *Mycobacterium tuberculosis*[2] and *S. cerevisiae*[3,4] indicated that these enzymes operate by a ping-pong mechanism and suggested the existence of only one binding site (Figure 4.1A). Another study of NDH-2 from *M. tuberculosis* proposed a two-site ping-pong mechanism where quinone binds to a different site from that of NADH [2] (Figure 4.1B).

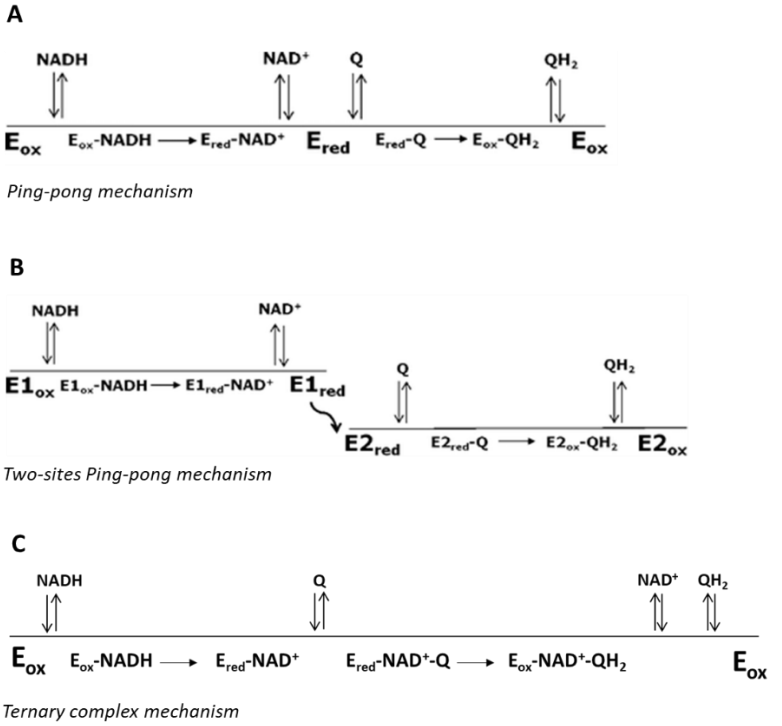

Figure 4.1 Two types of reaction mechanisms. (A and B) One and two-sites Ping-pong mechanism and **(C)** Ternary complex mechanism. E_{ox} represents the oxidized form of NDH-2 and E_{red} represents the reduced form of NDH-2.

In contrast, Yang *et al* concluded that the reaction proceeds through the establishment of a ternary complex[5] (Figure 4.1C). This study revealed that the enzyme from *S. cerevisiae*, Ndi1, forms a CT complex with NADH and then the bound ubiquinone (UQ) accepts two electrons from the NADH-reduced FAD. The UQ-bound form prevents oxygen from accessing the FAD site in Ndi1. The authors observed the bound UQ facilitated the formation of a ternary complex with NADH because it accepts two electrons directly from the NADH-reduced FAD and after that the resulting ubiquinol leaves Ndi1. The UQ binding site is then occupied with UQ from the quinone pool. The whole reaction mechanism contributes to the suppression of ROS generation from

Ndi1[5]. A study on *Caldalkalibacillus thermarum* NDH-2 reported this enzyme follows either a two-site ping-pong mechanism or a ternary complex mechanism, depending on the concentrations of substrate/ products and the dissociation constants, i.e. is determined stochastically[6]. According to this study, NADPH favors a two-site ping-pong mechanism, while NADH favors a ternary complex mechanism. These results, are in agreement with ours in the sense that these two reaction mechanisms require separate binding sites for NADH and quinone[6].

In this chapter we present an exhaustive analysis of the reaction mechanism of the two NDH-2s from *S. aureus* using steady-state and pre-steady-state kinetic methods. We found both proteins use distinct processes to avoid unspecific reaction with molecular oxygen and propose a universal catalytic mechanism for all NDH-2s.

4.3 Experimental procedures

4.3.1 Steady-state kinetics

Activity assays were performed on a Shimadzu UV-1800 spectrophotometer monitoring the change in absorbance of NAD(P)H, at 340 nm. The reaction mixture (1000 µL) contained 20 nM NDH-2A or 200nM NDH-2B in 100 mM K_2HPO_4/KH_2PO_4 250 mM NaCl pH 7.0 or 50 mM MES Bis Tris Propane pH 5.5, 250 mM NaCl, depending on the enzyme. The activity assays were made inside an anaerobic chamber at 35 °C, using as electron acceptors 2,3-Dimethyl-1,4-naphthoquinone (DMN) a menaquinone analogue, 2,3-Dimethoxy-5,6-dimethyl-benzoquinone (DDB) a ubiquinone analogue, or 2,3,5,6-Tetramethyl-1,4-benzoquinone (Duroquinone, DQ) a plastoquinone analogue. The quinone concentrations used in the assays were in the range from 5 to 200 µM (at 100 µM NAD(P)H) and the NAD(P)H concentrations were in the range from 5 to 150 µM (at 150 µM DMN). 2-n-Heptyl-4-hydroxyquinoline N-oxide (HQNO) was added in the range from 1 to 100 µM. The NAD(P)H extinction coefficient of 6.22 mM^{-1} cm^{-1} was used to calculate NDH-2 specific activity (µmol min^{-1} mg^{-1} protein). Data were fitted by the Michaelis-Menten equation, $v_0 = \frac{v_{max}[S]}{K_m+[S]}$ using a non-linear least-squares regression to determine K_M and V_{MAX} values for the reactions with NAD(P)H and with DMN, DDB or DQ. All the values were obtained from three independent assays. The equilibrium dissociation constant for the inhibitor was obtained using the equation $v_0^i = v_0^{max} \frac{\left(1+\beta\frac{[I]}{K_i{}^{app}}\right)}{\left(1+\frac{[I]}{K_i{}^{app}}\right)}$.

4.3.2 Pre-steady-state kinetics

The transient kinetics of reduction of NDH-2s by NAD(P)H and oxidation of reduced NDH-2s by quinone were studied by stopped-flow methodology using a TGK Scientific SF-61 DX2 apparatus placed inside an anaerobic chamber MBraun 130. The temperature of the drive syringes and mixing chamber was maintained at 15 °C, and the pH was controlled with 100 mM K_2HPO_4/KH_2PO_4 pH 7.0, 250 mM NaCl or 50 mM MES Bis Tris Propane pH 5.5, 250 mM NaCl (depending on the enzyme). All solutions were prepared inside the anaerobic chamber with degassed water and a mixture of 5 mM glucose, 4 U ml^{-1} glucose oxidase and 130 U ml^{-1} catalase were used, to ensure total O_2-free conditions. The time course of the reactions was monitored with a photodiode array (350–700 nm). The reductive reaction was monitored after mixing oxidized NDH-2s with NAD(P)H or sodium dithionite, $Na_2S_2O_4$ (1:1 ratio). Reduced NDH-2 was mixed with quinone or O_2 (1:2 ratio) to study the oxidative reaction.

For the study of the reductive half-reaction of NDH-2A, 10 µM oxidized protein was mixed with 10 µM NADH (1:1 ratio). For the study of the reductive half-reaction of NDH-2B 10 µM oxidized protein was mixed with 20 µM NADPH (1:2 ratio). To follow the time evolution of the reduction of the protein 100 spectra were acquired in 150 ms. The rate constant was obtained from the fitting of the kinetic traces recorded at the wavelengths at which spectral changes were most evident (in this case at 450 nm and 670 nm). As a significant part of the signal is lost in the dead time of the apparatus (even at 15 °C), the absorbance at time zero was taken from a control experiment where NDH-2 was mixed with buffer. The time scale was corrected for the dead time of the apparatus (3 ms), and the fit of an exponential curve to the data was performed with the tool *solver* from Microsoft Office Excel program. For the study of the oxidative half-reaction of NDH-2A, 10 µM protein was reduced with a

stoichiometric amount of NADH and the reduced state of the enzyme checked in a control experiment against buffer. Reduced NDH-2A was then mixed with 10 µM DMN in a 1:1 ratio. For the study of the oxidative half-reaction of NDH-2B 10 µM protein was reduced with 30 µM NADPH and the reduced state of the enzyme checked in a control experiment against buffer. Reduced NDH-2 was then mixed with 30 µM DMN in a 1:3 ratio. Another experiment was performed mixing 10 µM of NDH-2B reduced with 50 µM NADPH with 30 µM of DMN (1:5:3 ratio) to allow complete turnover. The software Kinetic Studio from TGK was used to fit exponential curves to the kinetic traces acquired at 450 nm and 670 nm. The values of the rate constants presented are the median of at least three independent experiments.

The effect of the inhibitor HQNO was tested with NDH-2A in experiments in which the enzyme could complete two turnovers. Control experiments were performed with 10 µM NDH-2A plus 30 µM DMN mixed with 20 µM NADH. In the experiments with inhibitor, 50 µM HQNO was added to the syringe containing the enzyme and DMN, before mixing it with NADH in the stopped-flow apparatus.

4.3.3 Simulation of equilibrium protonation states

pH titration curves were calculated for all ionizable amino acid residues, including D_{302}, of NDH-2A from *S. aureus* (PDB: 5NA1), based on the thermodynamics of proton binding as described before in detail[7,8]. These methodologies use a combination of Poisson-Boltzmann (PB) calculations, performed with the program MEAD (version 2.2.9)[9–11], and Metropolis Monte Carlo (MC) simulations, using the program PETIT (version 1.5)[12]. Here, two systems were simulated: the fully reduced protein like that obtained with dithionite, $FADH_2$, and the fully reduced protein with NAD^+ forming the charge-

transfer complex in the catalytic site, $FADH_2$-NAD^+. The position of the NAD^+ was inferred upon fitting to the structure of the *S. cerevisiae* enzyme (PDB entry: 4G73).

4.4 Results and Discussion

4.4.1 NDH-2A and NDH-2B showed a Michaelis-Menten behavior towards their substrates

Enzymatic activities of NDH-2A were determined using DMN, DDB, or DQ as electron acceptors with NADH as the electron donor. k_{cat} values, obtained monitoring the consumption of NADH were 67.9 ± 2.4 s^{-1} for DMN, 69.4 ± 2.3 s^{-1} for DDB and 68.2 ± 0.06 s^{-1} for DQ. The enzyme showed a Michaelis-Menten behavior toward NADH (using DMN as the electron acceptor), DMN, DDB and DQ (Figure 4.2). V_{MAX} of 132.7 ± 6.6, 129.3 ± 4.6 and 119.1 ± 0.9 µmol NADH oxidized min^{-1} mg^{-1} of protein were obtained when using DMN, DDB or DQ as electron acceptors, respectively. K_M values obtained for the three quinones were also similar to each other, 69.9 ± 6.4 µM for DMN, 63.7 ± 4.1 µM for DDB and 55.4 ± 0.5 µM for DQ. The K_M value for NADH was 20.5 ± 0.3 µM and V_{MAX} 175.9 ± 0.6 µmol NADH oxidized min^{-1} mg^{-1} of protein. Similar activity values when using different quinones were also observed for NDH-2 from *M. tuberculosis*[13]. The similar activity and K_M values for the three quinones, seem to reflect an absence of protein selectivity for different quinones. The presence of HQNO, a quinone derivative, already identified as a potent inhibitor of *S. cerevisiae* Ndi1[4], was shown to decrease enzyme activity, regardless of the type of quinone used as substrate.

A K_i app value of 6.8 ± 0.4 µM for HQNO was obtained when using DMN as electron acceptor (Figure 4.4A).

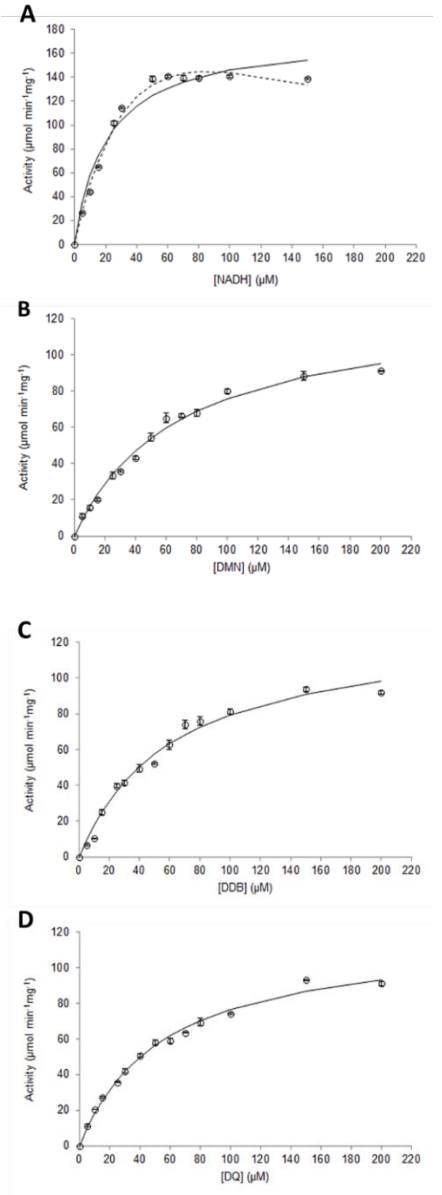

Figure 4.2 Steady-state analyses of the activity of NDH-2A from *S. aureus*. NADH:quinone oxidoreductase activity as function of the concentration of NADH **(A)**, DMN **(B)**, DDB **(C)** or Duroquinone **(D)**. The data points were fitted with a Michaelis-Menten equation (full line), $v_0 = \frac{v_{max}[S]}{K_m+[S]}$. NADH:Quinone oxidoreductase activity as function of the concentration of NADH (A) could also be fitted with an equation that describes substrate inhibition, $v_0 = \frac{v_{max}[S]}{K_m+[S]+\frac{[S]^2}{K_I}}$ (dotted line).

We previously showed (see chapter 2) that NDH-2A has nearly no activity when NADPH is the substrate compared to NADH and that NDH-2B presents a higher activity value using NADPH instead of NADH. We determined the kinetic constants for NDH-2B in the presence of DMN varying the concentration of NADPH from 5 to 200 µM. The maximal velocity (V_{MAX}) obtained was 102.8 ± 2.5 µmol min^{-1} mg^{-1} and the Michaelis-Menten constant (K_M) obtained was 80.4 ± 7.7 µM (Figure 4.3A). The kinetic constants for NDH-2B in the presence of NADPH varying the concentration of DMN from 0 to 200 µM were 38.1 ± 4.1 µM, K_M, and were 88.0 ± 3.8 µmol min^{-1} mg^{-1}, V_{MAX} (Figure 4.3B). These results showed similar V_{MAX} values towards NADPH and DMN and additionally, DMN showed a lower K_M value, indicating that the enzyme has higher catalytic efficiency for DMN compared to NADPH, requiring less quinone to reach the maximum velocity. This result contrasts with what was observed for NDH-2A since it presented a lower K_M value towards NADH than DMN, meaning the enzyme requires less NADH to reach the maximum velocity. A K_i app value of 6.4 ± 1.25 µM for HQNO, was obtained when using NADPH as electron donor and DMN as electron acceptor (Figure 4.4B). A summary of NDH-2A and NDH-2B data is presented in table 4.1.

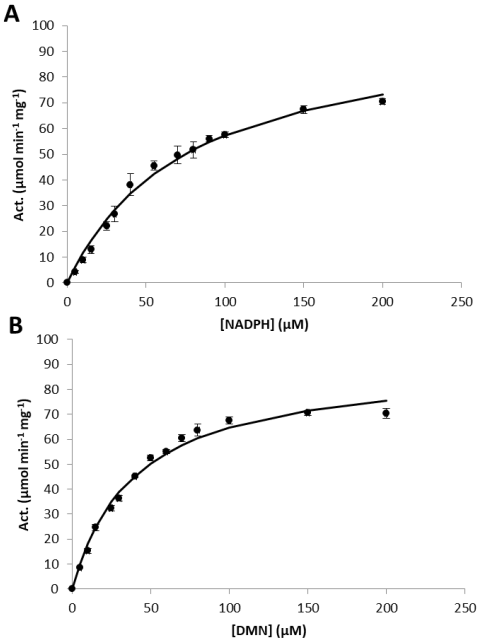

Figure 4.3 Steady-state analyses of the activity of NDH-2B from *S. aureus*. NAD(P)H:quinone oxidoreductase activity is represented as function of the concentration of NADPH (A) and of DMN (B). The experimental data (black dots) were fitted with a Michaelis-Menten equation (solid line).

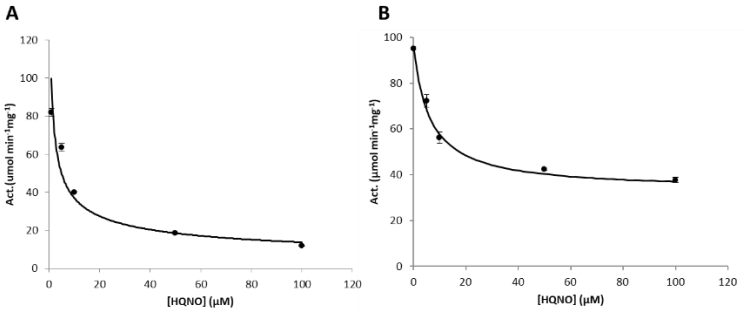

Figure 4.4 Steady-state analyses of the activity of NDH-2A (A) and NDH-2B (B) from *S. aureus* in the presence of HQNO. NAD(P)H:quinone oxidoreductase activity as function of the concentration of the inhibitor HQNO (2-n-Heptyl-4-hydroxyquinoline N-oxide, $C_{16}H_{21}NO_2$) using as electron acceptor DMN. The data points were fitted using equation $v_0^i = v_0^{max} \frac{1+\beta\frac{[I]}{K_i}}{1+\frac{[I]}{K_i}}$.

Table 4.1 Summary of data of NDH-2A and NDH-2B obtained with steady-state and pre steady-state kinetics assays (*- pH 7 and #- pH 5.5).

Steady State Kinetics	**NDH-2A**	**NDH-2B**
V_{max} µmol NADH oxidized min^{-1} mg^{-1} pH 7	175.9 ± 0.6	34.03 ± 0.86
V_{max} µmol NADH oxidized min^{-1} mg^{-1} pH 5.5	122.1 ± 18.3	30.37 ± 1.05
V_{max} µmol NADPH oxidized min^{-1} mg^{-1} pH 7	2.81 ± 1.44	49.24 ± 3.56
V_{max} µmol NADPH oxidized min^{-1} mg^{-1} pH 5.5	19.65 ± 2.06	102.8 ± 2.5
k_{cat} s^{-1}	128.96*	67.51#
K_M NAD(P)H µM	20.5 ± 0.3*	80.4 ± 7.7#
K_M DMN µM	69.9 ± 6.4*	38.1 ± 4.1#
Pre- Steady State Kinetics	**NDH-2A**	**NDH-2B**
k_{red} s^{-1}	NADH (1:1) 180 ± 30*	NADPH (1:2) 0.86 ± 0.018#
k_{oxi} s^{-1}	DMN (1:1) 5 ± 0.5*	DMN (1:3) 6.7 ± 0.3#

4.4.2 The presence of a Charge-Transfer (CT) complex in NDH-2A

In the oxidized form, NDH-2A presents an absorption spectrum with maxima at 375 and 450 nm and a shoulder close to 475 nm, typical of flavoproteins (Figure 4.5). Upon reduction with NADH, the absorption at 375–450 nm decreases and a broad absorption band in the 650–800 nm region appears. This band is originated by the establishment of a CT complex resulting from a π-π interaction between the parallel stacked isoalloxazine and nicotinamide rings of reduced FAD and NAD^+, respectively. The enzyme was also reduced with sodium dithionite and in this case the decrease in absorption at

375–450 nm was also observed, but the band resulting from the establishment of the CT complex was not detected (Figure 4.5). A CT complex could also be observed by adding NAD^+ to the dithionite-reduced NDH-2 (Figure 2.7, chapter 2), indicating the charge-transfer complex was only formed in the presence of the $NAD^+/FADH_2$, independently of the reducing agent.

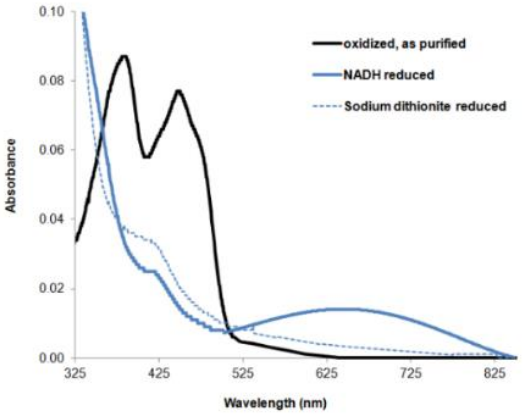

Figure 4.5 UV–visible absorption spectra of NDH-2A. As purified (black solid line), reduced with NADH (blue solid line) or reduced with sodium dithionite (blue dashed line).

4.4.3 Quinone reduction is the slowest half-reaction in NDH-2A and is affected by the presence of HQNO

Upon addition of NADH to the oxidized NDH-2A (in a 1:1 ratio) spectral changes showed a very fast reduction of the enzyme, such that a significant part of the reaction is lost in the 3 ms dead time of the stopped flow apparatus. The absorbance of the peak at 450 nm decreased and a broad band in the region 650–700 nm appeared (longer wavelength detection is limited by the diode array detector). Identical observed rate constants, 180 ± 30 s^{-1}, were obtained by fitting the kinetic traces acquired at 450 nm and at 670 nm using an exponential curve (Figure 4.6A). The spectral changes observed during the reduction of the enzyme were completely reversed when the NADH-reduced

enzyme was mixed with DMN (1:1) (Figure S4.1): the absorbance at 450 nm increased and the broad peak in the region 650–700 nm disappeared. The observed rate constants obtained by exponential fitting of the kinetic curves at 450 and 670 nm, were again identical and equal to 5.0 ± 0.5 s^{-1} (Figure 4.6B). DDB and DQ were also tested, and the rate constants for the oxidation of the enzyme were of the same order of magnitude (Figure S4.2).

Experiments allowing the enzyme to perform two turnovers were used to assess the effect of the inhibitor HQNO in the two half-reactions. NDH-2A plus DMN mixed with NADH was rapidly reduced, as observed by the decrease in absorbance at 450 nm, and remained reduced while NADH was being oxidized, which was monitored by the decrease in absorbance at 350 nm (Figure 4.6C–E). Upon NADH exhaustion the enzyme was reoxidized by DMN (Figure S4.3). The turnover rate determined from the decrease in absorbance at 350 nm was comparable with the rate at which the enzyme was reoxidized.

In the presence of HQNO the two half reactions were affected in a totally different manner: the rate of reduction of NDH-2A by NADH (1:2, protein:NADH), 364 ± 88 s^{-1}, was not significantly affected (considering that in this case the concentration of NADH present is the double than NDH-2A) (Figure 4.6C), the traces with and without inhibitor being superimposable in the 50 ms time scale. In the 0.75 s time scale, the reoxidation of the enzyme by DMN was only observed in the absence of the inhibitor, showing that the reoxidation of NDH-2A by DMN is strongly impaired in the presence of HQNO (Figure 4.6D). To observe the reoxidation of NDH-2A by DMN in the presence of the inhibitor, it was necessary to acquire the signal in an even-longer time scale (75 s) (Figure 4.6E). The rate of reoxidation of the enzyme by DMN slowed down by two orders of magnitude: 0.08 ± 0.02 s^{-1} vs 8 ± 2 s^{-1}, in the presence and absence of HQNO, respectively.

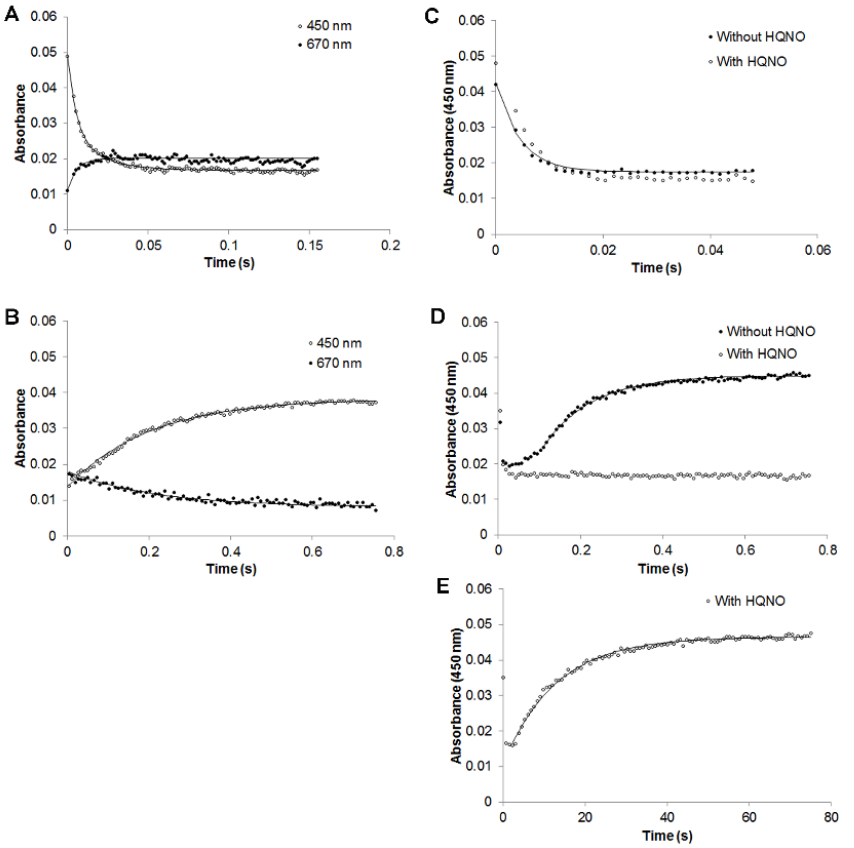

Figure 4.6 Pre steady-state kinetics experiments. (A) Time-resolved reduction of NDH-2A from *S. aureus* by NADH (1:1, protein: NADH ratio). The absorbance of the peak at 450 nm decreases and a broad band appears in the region 650–700 nm. Identical rate constants, 180 ± 30 s^{-1}, were obtained by fitting the kinetic traces acquired at 450 nm and at 670 nm to an exponential curve. **(B)** Time-resolved oxidation of NDH-2 by DMN (1:1, protein: DMN ratio). The absorbance at 450 nm increased and the broad peak in the region 650–700 nm disappeared. The observed rate constants of the two processes, acquired at 450 nm and at 670 nm, obtained by exponential fitting of the kinetic curves at 450 and 670 nm, were identical and equal to 5 ± 0.5 s^{-1}. **(C)** Time-resolved reduction of NDH-2 by NADH in the presence and absence of the inhibitor, HQNO. The traces with and without inhibitor are superimposable in the 50 ms time scale. **(D)** In the 0.75 s time scale, the reoxidation of the enzyme by DMN is only observed in the absence of the inhibitor. **(E)** The reoxidation of NDH-2 by DMN in the presence of the inhibitor is observed when the signal is acquired in a longer time scale (75 s). The values of the rate constants are the median of at least three independent experiments.

Our pre steady-state kinetics data are consistent with the fluorescence and STD-NMR spectroscopic results presented in the previous chapter (chapter 3) which indicated that HQNO only interfered with the binding and reduction of the quinone. These measurements allowed the deconvolution of the two half-reactions in NDH-2A. NADH oxidation occurs very fast, ~ 200 s^{-1} (for a stoichiometric reaction at 15 °C), whereas quinone reduction is approximately 40 times slower. This is reinforced by the observation that the enzyme is reduced during turnover (Figure 4.6D, Figure S4.3). Hence the rate limiting step of the reaction is the flavin oxidation reaction. Yano and co-workers suggested NADH oxidation was the reaction rate limiting step based on the fact that activity values were similar for quinones with high and low reduction potentials, i.e. that k_{cat} values were not simply a function of the midpoint reduction potential of each quinone[13]. We have now observed that this is not the case for *S. aureus* NDH-2. Upon addition of the quinone to the NADH reduced NDH-2A (1:1), FAD is immediately oxidized as indicated by the appearance of absorption in the 370–450 region. Typical spectra indicating the presence of possible semiquinone forms of FAD were never observed, which suggests that FAD oxidation by the quinone is a two-electron process. The enzymatic reaction mechanism of NDH-2A will be discussed below, but the absence of semiquinone radicals is consistent with the hypothesis of a hydride transfer from NADH to $FADH_2$ or quinol. Our pre steady-state kinetics measurements revealed that the reduction of the flavin is concomitant with the formation of the CT complex (Figure 4.6 and Figure S4.3). Furthermore, addition of quinone did not increase the intensity of the absorption band of the CT complex, as it was observed by Yang *et al*[5]. Contrariwise, pre steady-state kinetic experiments showed that characteristic absorption bands of the flavin at 370–450 nm reappears, and the CT band disappears upon addition of quinone, the oxidation of the flavin being

simultaneous with the release of the CT complex. Although the reduction of FAD is independent on the presence of the quinone, the dissociation of the charge-transfer complex, which indicates the release of NAD^+ (i.e. the release of the first product), is not. In a ping-pong mechanism NAD^+ would have to be released before quinone binding and this is not observed. The release of NAD^+ upon flavin oxidation by the quinone suggests the establishment of a ternary complex.

4.4.4 The CT complex is a limiting factor in NDH-2A oxidation

In order to investigate the role of the charge-transfer complex on the catalytic mechanism of NDH-2A, we compared the oxidation of NDH-2A when reduced by NADH, which establishes a CT complex, to that of the enzyme reduced by dithionite, which does not establish a CT complex. As it was showed above, upon addition of quinone (in a 1:1 ratio) to NDH-2A previously reduced with NADH, spectral changes showed an increase in the absorbance peak at 450 nm and the disappearance of the broad band at 650–800 nm. The rate constant obtained for this second half-reaction was equal to 5.0 ± 0.5 s^{-1} (Figure 4.6B). The dithionite-reduced NDH-2 was mixed with DMN in a 1:1 ratio (Figure 4.7A) and a rate constant equal to 196 ± 15 s^{-1} was measured. This reaction was approximately 40 times faster than the oxidation of the NADH-reduced NDH-2 (Figure 4.6B) and interestingly related to the rate constant obtained for the reduction of the protein by NADH. To confirm whether the difference observed in the oxidation reaction of FAD was due to the presence of the CT complex, we incubated the dithionite-reduced enzyme with NAD^+ and monitored its reaction with DMN (all the components were in a 1:1 ratio) (Figure 4.7B). The rate constant obtained was 11.4 ± 2.2 s^{-1}, which is comparable to that observed for the oxidation of the NADH-reduced enzyme by the quinone. These data

demonstrate the presence of the charge-transfer complex is a limiting factor in protein oxidation.

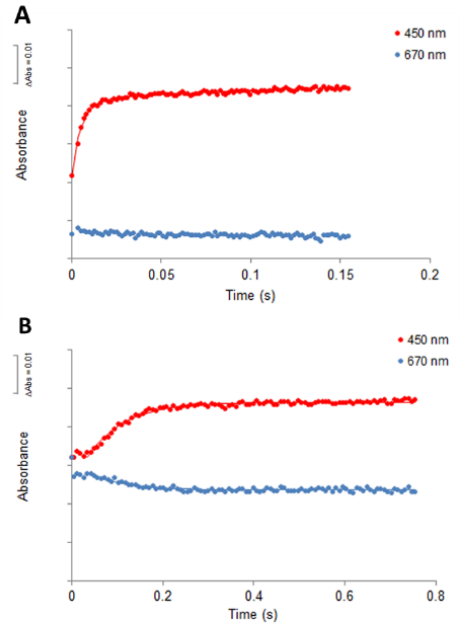

Figure 4.7 Pre steady-state kinetics experiments. Time-resolved oxidation by DMN of **(A)** sodium dithionite-reduced NDH-2 (1:1, protein:DMN ratio) and **(B)** sodium dithionite-reduced NDH-2 in the presence of NAD^+ (1:1:1, protein: DMN: NAD^+ ratio), monitored at 450 nm (red dots) and at 670 nm (blue dots).

4.4.5 The CT complex decreases the oxidation rate of NDH-2A independently of the oxidant

We also considered whether the observed effect of the CT complex on the oxidation reaction was dependent on the quinone, i.e., of the oxidant. For this we used oxygen, O_2, as the electron acceptor. In the first experiment 10 µM NDH-2A was reduced with a stoichiometric amount of NADH and then the reduced NDH-2A was mixed with buffer containing 24 µM O_2 in approximately 1:2 protein:O_2 ratio (Figure 4.8A). The oxidation of the protein by oxygen was very slow, with a rate constant of 0.0044 ± 0.0007 s^{-1}. In this assay we could also observe a decrease in absorbance at 650–800 nm due to the dissociation

of the CT complex (Figure 4.8A). In a second experiment, we reduced the protein with sodium dithionite (1:1 ratio) and monitored its reaction with O_2 (1:2 ratio). The rate constant obtained was 0.76 ± 0.2 s^{-1} higher than that measured for the oxidation of the NADH-reduced NDH-2A (Figure 4.8B). Also, as expected, the absorbance in the 650–800 nm region did not change, as a CT complex was not present in the reduced enzyme to begin with. These results strengthened the hypothesis the presence of the CT complex determines the oxidation rate of the protein.

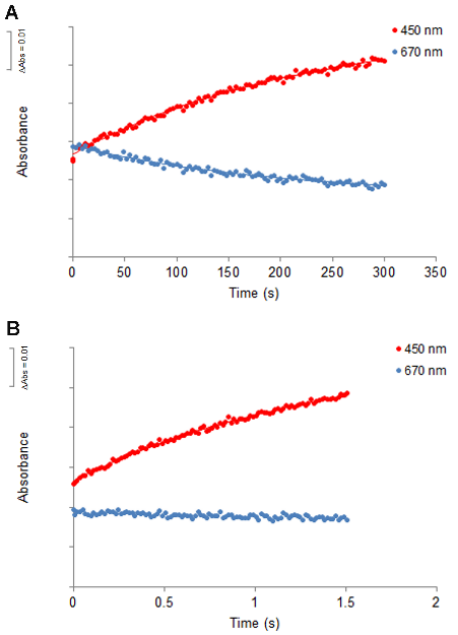

Figure 4.8 Pre steady-state kinetics experiments. Time-resolved oxidation by O_2 of **(A)** NADH-reduced NDH-2 (1:2, NDH-2: O_2 ratio) and **(B)** dithionite-reduced NDH-2 (1:2, NDH-2: O_2 ratio) monitored at 450 nm (red dots) and at 670 nm (blue dots)**.**

4.4.6 The presence of the CT complex determines the inhibitory effect of HQNO in NDH-2A

We already showed that HQNO, a quinone analogue, acts as an inhibitor of *S. aureus´* NDH-2 activity with an apparent K_i value of 6.8 ± 0.4 μM. It was also demonstrated that the oxidation of the enzyme by DMN is strongly impaired in the presence of HQNO (unlike the first half reaction which is not affected) and that the binding sites for HQNO and the quinone are superimposed or very close (showed in chapter 3). Here we tested whether the presence of the CT complex, which also influences the second half reaction, would alter the effect of the inhibitor. For this we compared the effect of HQNO (10 μM) on the rate of protein oxidation by DMN (10 μM), in the case of NADH or dithionite reduced protein (10 μM). The rate of oxidation of dithionite-reduced protein by DMN in the presence of HQNO was 179 ± 12 s^{-1}, a value similar to that obtained in the absence of the inhibitor, which suggests that in the absence of CT complex the HQNO has no effect (Figure 4.9A). This is completely different from the result obtained previously, where the oxidation of NDH-2 by DMN, after its reduction by NADH, was slowed-down by a factor of 50 (to 0.08 ± 0.02 s^{-1}) in the presence of HQNO (Figure 4.6E). Again, to verify whether the difference observed in the effect of HQNO was due to the presence of the CT complex, we incubated the dithionite-reduced enzyme with NAD^+ and monitored its reaction with DMN, in the presence of the inhibitor. In this situation, we observed the protein oxidation was also very slow, with a rate constant of 0.1 ± 0.0006 s^{-1}, a value that is comparable to that obtained when the enzyme was reduced with NADH and then oxidized by DMN in the presence of HQNO (Figure 4.9B). Table S4.1 shows a summary of the of kinetic rate constant values for the second half-reaction (flavin oxidation) in NDH-2A

enzyme, in the presence and absence of the inhibitor with the quinone, DMN, or O_2.

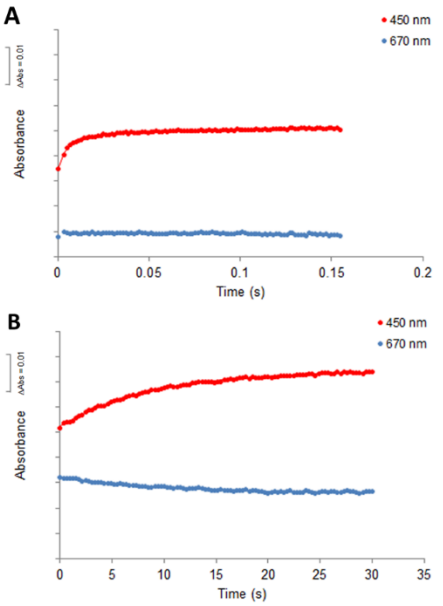

Figure 4.9 Pre steady-state kinetics experiments. Time-resolved oxidation by DMN of **(A)** dithionite- reduced NDH-2 in the presence of HQNO (1:1:5, NDH-2: DMN: HQNO ratio) and **(B)** dithionite- reduced NDH-2 in the presence of HQNO and NAD^+ (1:1:5:1, NDH-2: DMN: HQNO: NAD^+ ratio).

4.4.7 The presence of the CT complex influences the protonation probability of D_{302} in NDH-2A

We performed protonation equilibrium simulations for all the ionizable amino acid residues of NDH-2A from *S. aureus*. Two different systems were simulated: the fully reduced state ($FADH_2$), like that obtained with dithionite, and the fully reduced protein with NAD^+ ($FADH_2$-NAD^+) in which the CT complex is present. Our protonation equilibrium simulations for NDH-2A from *S. aureus* demonstrate that the proton occupancy probability of the majority of the ionizable amino acid residues was not significantly altered by the presence of

the charge-transfer complex. D_{302} was the exception, for which our simulations clearly showed that its proton occupancy probability in the reduced enzyme is influenced by the presence of the CT complex (Figure 4.10).

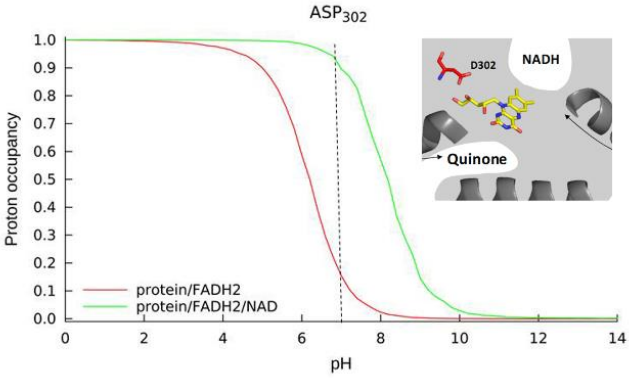

Figure 4.10 Proton equilibrium occupancy probability curves for D_{302} in two reduced conditions: $FADH_2$ (in red) and $FADH_2$-NAD^+ (in green).

We observed that the proton occupancy probability curve of D_{302} in the case of $FADH_2$ (in the absence of CT complex) is different from that obtained in the case of $FADH_2$-NAD^+ (in the presence of the CT complex). The curve (Figure 4.10) in the presence of the CT complex is shifted to higher pH values comparing to that obtained in its absence. This means that at pH 7 it is more difficult to oxidize $FADH_2$-NAD^+, because in this state D_{302} is almost 100 % protonated and therefore unable to receive protons (Figure 4.10). In the absence of NAD^+ at pH 7, D_{302} is expected to have a much lower proton occupancy, allowing proton transfer from the active site and faster oxidation of the $FADH_2$. Therefore, the difference observed for the proton occupancy probability of D_{302} of the reduced protein, in the presence and absence of the CT complex, may contribute to explain the different oxidation rates observed by pre-steady state kinetics. Subsequently, we tried to biochemically characterize four variants of the NDH-2A from *S. aureus* in which D_{302} was replaced either by alanine ($D_{302}A$), serine

($D_{302}S$), asparagine ($D_{302}N$) or tryptophan ($D_{302}W$), but we were not successful in the expression in some of the mutants or in the purification steps of others.

4.4.8 Kinetic parameters of the E_{172} variants of NDH-2A were affected

We addressed the role of the conserved glutamate 172 (E172) residue in the enzymatic mechanism of NDH-2A from *Staphylococcus aureus*. For that, we characterized both structurally and functionally four variants of NDH-2A from *S. aureus* in which E_{172} was replaced either by alanine ($E_{172}A$), serine ($E_{172}S$), glutamine ($E_{172}Q$) or aspartate ($E_{172}D$)[14].

UV–Visible absorbance spectra of the four variants were similar to that of the wild-type (WT), presenting the typical flavin maxima at 375 and 450 nm. Full reduction of $E_{172}A$, $E_{172}Q$ and $E_{172}S$ proteins was only achieved with a 1:2 protein:NADH stoichiometry. In these three cases the broad band centered around 670 nm (corresponding to the CT complex) was also observed, although with less intensity (Figure S4.4). Addition of DMN led to flavin reoxidation and consequent return to the initial state showing complete redox reversibility of the system. Reduction of the same variants with sodium dithionite, in the presence and absence of NAD^+ showed a similar behavior to the WT protein, at the mentioned 450 and 670 nm regions (see above Figure 4.5). The $E_{172}D$ variant showed different characteristics, as no charge-transfer complex band was observed upon addition of NADH, and near complete reduction and reoxidation was only achieved with a 1:5 protein: substrate stoichiometry (Figure S4.4). Knowing that the absorbance of the CT complex is dependent on both of the orientation and distance between isoalloxazine and nicotinamide rings[15,16], the data suggest that the variants provide a less favorable environment for the interaction between NAD^+ and $FADH_2$ than the WT, which indicates the

presence of the E_{172} influences the orientation and stabilization of NADH and, as a consequence, the establishment of the CT complex.

The NADH:quinone oxidoreductase activity was measured for all the purified NDH-2A variants. The $E_{172}D$ variant showed no detectable NADH:quinone oxidoreductase activity, during the acquisition time (under 1 min). The k_{cat} of the variants for DMN, monitoring the NADH consumption, were 20.6 ± 2.7 ($E_{172}A$), 5.7 ± 1.1 ($E_{172}Q$) and 11.3 ± 1.2 ($E_{172}S$) s^{-1}; and were significantly lower compared to that for the WT (67.9 ± 2.4 s^{-1}).

The variants were also analyzed by pre steady-state kinetics where the enzymes were reduced with NADH in a 1:1 ratio and reoxidized with DMN in a 1:2:3, protein:NADH:quinone proportion. For the WT NDH-2A, the reduction half reaction is approximately 40 times faster than the oxidation half reaction. $E_{172}A$, $E_{172}Q$ and $E_{172}S$ variants also presented the reduction half reaction faster than the oxidation half reaction, but in these cases the ratio between the rates of the two-half reactions were much higher (Figure 4.11). The reduction half reaction is approximately 100, 400 and 300 times faster than the oxidation step for $E_{172}A$, $E_{172}Q$ and $E_{172}S$ variants, respectively. The fitted rates for the first and second half reactions were, respectively, 115 ± 16 and 0.98 ± 0.21 s^{-1} ($E_{172}A$); 108 ± 12 and 0.27 ± 0.03 s^{-1} ($E_{172}Q$); 104 ± 3 and 0.32 ± 0.01 s^{-1} ($E_{172}S$). These values correspond to approximately 64, 60 and 57 % of the FAD reduction reaction rate of the WT ($E_{172}A$, $E_{172}Q$ and $E_{172}S$ respectively), while the FAD oxidation rates decreased to approximately 20, 5 and 6 % ($E_{172}A$, $E_{172}Q$ and $E_{172}S$, respectively) (Figure 4.11). Mutation of E_{172} affected, to different extents, both the reductive and oxidative half reactions, having a higher impact on the latter. The three mutations ($E_{172}A$, $E_{172}Q$ and $E_{172}S$) similarly affected the rate of FAD reduction by NADH (approximately 60 %). The effect on FAD oxidation by DMN is more noticeable, but, in addition, it is not the same for the three mutants: in

$E_{172}A$ mutant the rate constant decreases 20 % while in $E_{172}Q$ and $E_{172}S$ it decreases approximately 5 %. This difference in effect is likely to have more to do with structural issues due to the difference in size of the amino acids side chains, than the nature of the side chains. While alanine is small and totally neutral, serine and glutamine are polar.

All the kinetic parameters obtained for the four variants of E_{172} are summarized in Table S4.2, and additionally the values for the wild-type protein (NDH-2A) are also included to be easier to compare.

The mutation in glutamate 172 of NDH-2A enzyme affected the oxidation of FAD more than its reduction. This observation strongly supports our hypothesis, that will be presented hereafter, that E_{172} is part of the proton pathway which delivers protons for quinone reduction to quinol, i.e. supplies the other substrate, the H^+. The study of such common element is likely to have a broad significance in understanding the molecular mechanism of these enzymes.

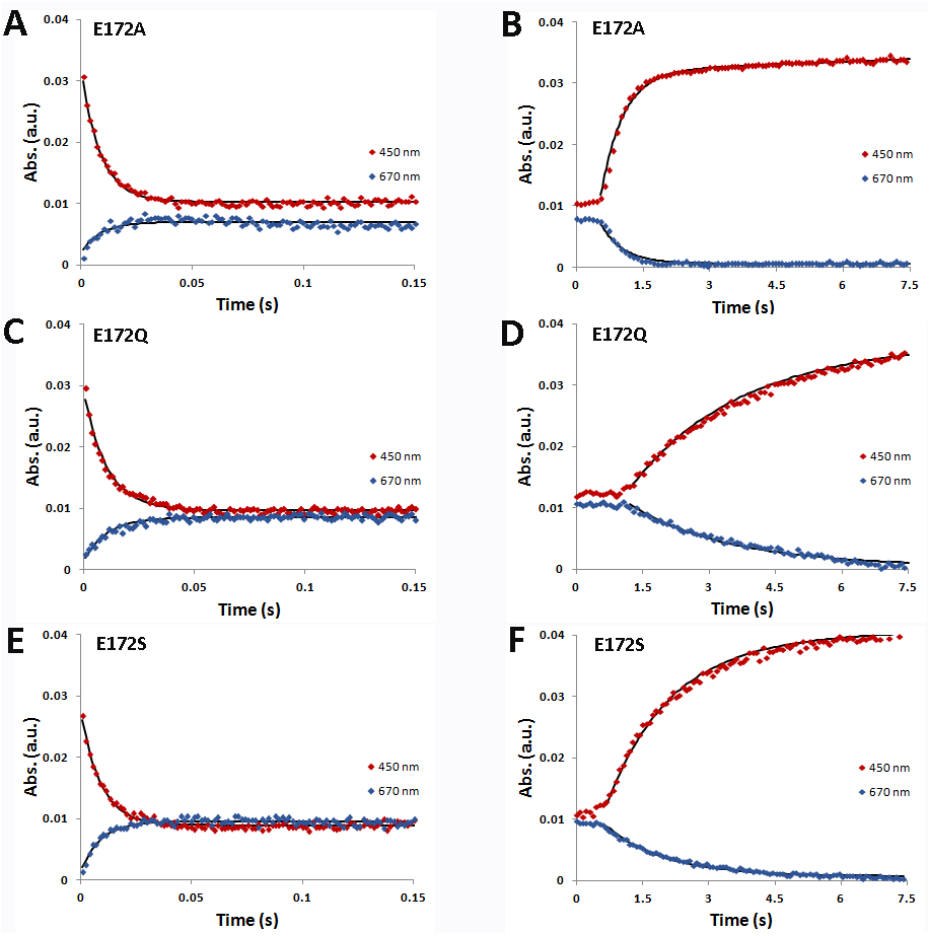

Figure 4.11 Pre-steady state kinetics of NDH-2A variants. Left panels, Time-resolved reduction of NDH-2A variants (1vs1; oxidized NDH-2A vs NADH). The absorbance of the peak at 450 nm decreases and a broad band appears in the region 650 – 700 nm. Identical rate constants were obtained by fitting the kinetic traces acquired at 450 nm and at 670 nm to an exponential curve. **A)** $E_{172}A$, rate constant 115 ± 16 s^{-1} **C)** $E_{172}Q$, rate constant 108 ± 12 s^{-1} **E)** $E_{172}S$ rate constant 104 ± 0.3 s^{-1}. Right panels, Time-resolved oxidation of NDH-2A variants by DMN (1:2vs3, NADH reduced NDH-2A vs DMN). The absorbance at 450 nm increased and the broad peak in the region 650-700 nm disappeared. The observed rate constants of the two processes, acquired at 450 nm and at 670 nm, were obtained by exponential fitting of the kinetic curves at 450 and 670 nm. **B)** $E_{172}A$, rate constant 0.98 ± 0.21 s^{-1} **D)** $E_{172}Q$, rate constant 0.27 ± 0.03 s^{-1} **F)** $E_{172}S$, rate constant 0.32 ± 0.01 s^{-1}. In red dots is represented the 450 nm absorbance and in blue dots the corresponding 670 nm absorbance intensity.

4.4.9 NDH-2B do not form a Charge-Transfer complex and the rate limiting step is the reductive half-reaction

Pre steady-state kinetics assays with NDH-2B of *S. aureus* were also performed inside an anaerobic chamber, in the presence of a scavenging system to assure oxygen levels as low as possible. The temperature was maintained at 18 ˚C. For the study of the reductive half-reaction, 10 μM of NDH-2B was mixed with 20 μM of NADPH (1:2 ratio) at pH 5.5. The oxidized fraction was calculated from the spectra corresponding to the reduction of NDH-2B and then plotted against time. The reduction rate constant obtained for NDH-2B with NADPH in a 1:2 ratio was 0.86 ± 0.018 s^{-1} (Figure 4.12A). The second half reaction was monitored by the addition of DMN (in a 1:3 ratio) to the NADPH-reduced NDH-2B. The rate constant obtained for the oxidation of NDH-2B, by fitting the kinetic traces acquired at 450 nm by an exponential curve, was 6.7 ± 0.3 s^{-1} (Figure 4.12B). Another experiment was performed mixing 10 μM of NDH-2B reduced with 50 μM NADPH with 30 μM of DMN (1:5:3 ratio). The reduction rate constant obtained for NDH-2B in the presence of NADPH and DMN, in a 1:5:3 ratio respectively, was 0.723 ± 0.011 s^{-1} (Figure S4.5). The reduction could only be observed when NADPH was in excess and after all DMN was consumed. We found that the rate constant of the oxidative half reaction is higher than the rate constant of the reductive half reaction, concluding that the rate limiting step is NADPH oxidation. This result, the NADPH oxidation being the rate limiting step, contrasts with that observed for NDH-2A, in which the limiting step is quinone reduction. Besides the differences observed in the kinetic parameters gathered from the steady state assays, we have observed that NDH-2B does not establish a CT complex. Since the CT complex slowed down the reduction of the quinone, this agrees with the fact that in the case of NDH-2B the quinone reducing step is faster than NADPH oxidation. These

results once again strengthened the hypothesis that the presence of the CT complex determines the oxidation rate of the protein. We hypothesize the two enzymes have distinct enzymatic strategies to achieve the same purpose, which is to avoid unspecific reaction with molecular oxygen, by preventing the protein to remain in a stable, free or accessible reduced state.

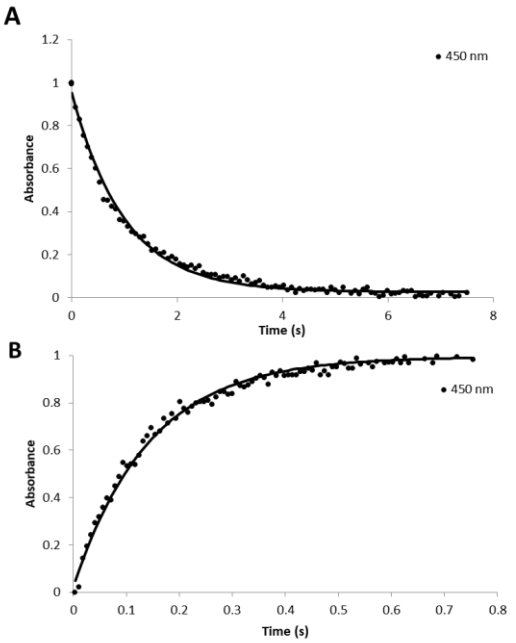

Figure 4.12 Reductive and oxidative half-reactions of NDH-2B from *S. aureus* in the presence of (A) NADPH (1:2 ratio) and of (B) DMN (1:3 ratio) monitored at 450 nm. The concentrations before mixing were 10 µM of NDH-2B, 20 µM of NADPH for the reduction **(A)**; 30 µM of NADPH to reduce NDH-2B before oxidize it with 30 µM of DMN **(B)** in a 50 mM MES Bis Tris Propane 250 mM NaCl buffer pH 5.5. The black dots represent the experimental data and the line represents the fit with an exponential curve.

4.4.10 Hypothesis for the catalytic mechanism of NDH-2s

The catalytic mechanism of NDH-2s is still unclear, even considering the available structural and functional data. Nevertheless, the gathered information showed that the two substrates bind to different sites. Based on

the sequence analysis shown in the previous chapter (chapter 3), here we propose a universal catalytic mechanism for NDH-2s.

Oxidation of NAD(P)H involves the release of two electrons and deprotonation of its nicotinamide ring. The two electrons are transferred to FAD, in a process usually accompanied by FAD protonation at positions N1 and N5 of its isoalloxazine ring (Figure 4.13). The subsequent reduction of quinone comprises the transfer of two electrons from FAD to quinone, deprotonation of FAD and protonation of the two reactive oxygen atoms present in the quinone ($O1_q$ and $O2_q$,) (Figure 4.13). Here, we discuss the possible roles of the conserved elements in the catalytic process of NDH-2 (Figure 4.14), including proton transfer and substrate interaction. We divided the discussion in two parts: FAD reduction (by NAD(P)H) and FAD oxidation (by quinone).

FAD reduction (first half reaction)

The way in which FAD is reduced in NDH-2 is unknown, but, based on what is observed for several flavoproteins, we consider that FAD is reduced by hydride transfer from NAD(P)H at its *re*-side[17]. Therefore, N5 of the FAD isoalloxazine can accept the hydride from C4 of the nicotinamide ring of NAD(P)H (Figure 4.14B). The origin of the second proton needed for the full protonation of FAD is uncertain, nevertheless it can be assumed to occur at the N1 atom of FAD (Figure 4.13). Inspecting the vicinity of N1 we noticed the presence of the conserved aspartate, D_{302} (in NDH-2A) or D_{270} (in NDH-2B), although not at proton binding distance to it (~7–8 Å in NDH-2A, Figure 4.14A). The fact that this amino acid residue (D_{302}/D_{270}) is totally conserved, even among other members of the tDBDF superfamily, and present in the vicinity of FAD suggests its involvement in the second protonation of the flavin.

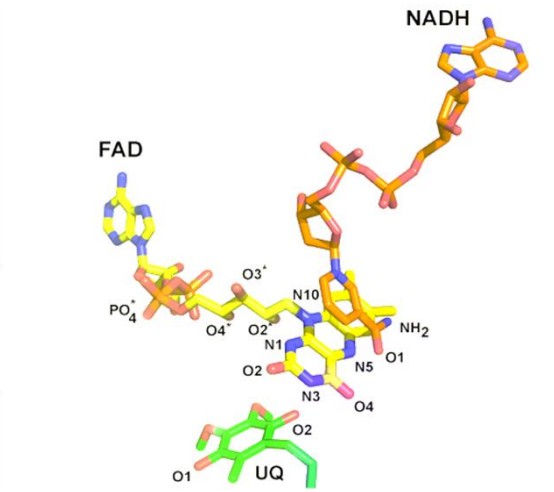

Figure 4.13 Cartoon representation of a zoomed view of the FAD, ubiquinone and NADH of the NDH-2 from *S. cerevisiae* (PDB:4G734). The atoms of the FAD group are ordered and colored in: blue – Nitrogen atom (N); red – Oxygen atom (O); orange – Phosphorus atom (P) and yellow – Carbon atom.

Considering that the members of the tDBDF superfamily are structurally similar, they are likely to share the same protonation mechanism. In the cases of NADH:ferredoxin oxidoreductase and thioredoxin reductase, the isoalloxazine ring of the reduced FAD adopts a bent conformation (the so-called boat conformation) upon reduction, which contrasts with the planar conformation observed in the oxidized form[18,19]. The bent conformation causes the rotation of C2* which indirectly allows O2* to reorient in between D_{302} or D_{270} (NDH-2A or NDH-2B) and N1 from FAD (Figure 4.13), establishing a new hydrogen bond network (Figure 4.14C). This proton network may lead to protonation of N1 by D_{302}/D_{270}.

In summary, NAD(P)H binds to NDH-2 and reduces FAD through hydride transfer to N5. The fully protonated state of the flavin is achieved by rearrangement of the hydrogen bond network around N1 induced by the adoption of a bent conformation by the isoalloxazine ring. We propose that this

proton network rearrangement may involve the strictly conserved D_{302}/D_{270} (NDH-2A/NDH-2B), which has direct access to the bulk (Figure 4.14A, B and C).

FAD oxidation (second half reaction)

The second half-reaction involves electron transfer from $FADH_2$ to the quinone, deprotonation of $FADH_2$ and quinone protonation. Two possibilities for the whole process may be considered: (1) The quinone can be reduced directly by hydride transfer from $FADH_2$, in this way needing only a second proton; (2) or the quinone reduction and protonation events occur separately. The first hypothesis cannot be discarded in the light of the current experimental knowledge, but considering that what is conserved is important to the function of an enzyme family, including the presence of two proton conductive channels leading to the quinone pocket, we propose the second half-reaction of NDH-2s is best described by the hypothesis involving the transfer of two protons to the quinone. We propose that protonation of the quinone upon reduction is performed by protons brought to the quinone binding pocket through two different pathways, one located at the first dinucleotide binding domain, close to FAD, and the other present at the second dinucleotide binding domain where NAD(P)H binds. The latter proton pathway is constituted by E_{172}/E_{154} (NDH-2A/NDH-2B) in addition to H_{51}/Y_{47} (NDH-2A/NDH-2B), E_{176}/E_{158} (NDH-2A/NDH-2B), D_{179}/E_{161} (NDH-2A/NDH-2B) and E_{183} (NDH-2A), already at the protein surface. The proton wire just described connects the surface of the protein and the NAD(P)H binding pocket. However, we hypothesize that this wire may be extended to the quinone binding pocket due to the presence of a lysine, K_{379} in NDH-2A and K_{342} in NDH-2B. This lysine residue provides the connection between E_{172}/E_{154} (NDH-2A/NDH-2B) and the quinone. The other possible

proton wire involves E_{327}/D_{288} (NDH-2A/NDH-2B), K_{23}/R_{19} (NDH-2A/NDH-2B) and K_{331}/D_{292} (NDH-2A/NDH-2B).

So $FADH_2$ is oxidized by the quinone (interacting at the *si*-side) and the two protons are also released from the flavin. The deprotonation of N1 proceeds by rearrangement of the hydrogen bond network due to a conformational change of FAD from the bent back to the planar conformation upon reoxidation. The loss of the bent conformation and consequently of the hydrogen bond network involving D_{302}/D_{270}, O2* and N1 of FAD, results in deprotonation of N1, in a reverse process to that described for the protonation of FAD (Figure 4.14D). The release of the second proton may occur concomitantly with the release of $NAD(P)^+$ which leaves FAD directly connected to the bulk (Figure 4.14D).

Simultaneously with the quinone reduction, the protonation of both its oxygen atoms ($O1_q$ and $O2_q$) occurs, involving the two proposed proton conducting pathways (Figure 4.14D). $O1_q$ is oriented to the proton conductive pathway present in the first dinucleotide binding domain (Figure 4.13), hence its protonation is likely performed by this pathway. $O2_q$ is oriented to the proton conductive pathway at the second dinucleotide binding domain which is responsible for taking up protons from the bulk to E_{172} (in NDH-2A) or E_{154} (in NDH-2B) and then to position K_{379} (in NDH-2A) or K_{342} (in NDH-2B), which is occupied by the final proton donors for $O2_q$. As described above for the first half-reaction, upon reduction, FAD adopts a bent conformation that may induce structural changes in α -helix. This idea strongly suggests that FAD reduction may be a requirement for the protein to adopt the necessary conformational state for quinone protonation by the first dinucleotide binding domain proton pathway. In fact, a similar situation may also occur in the second dinucleotide binding domain, where the side chain of E_{172}/E_{154} undergoes a conformational

change, allowing its hydrogen interaction with K_{379}/K_{342} to be disrupted, leading to protonation of $O2_q$ by the protonated K_{379}/K_{342} (Figure 4.14D). In summary, we propose that the reactive quinone oxygens $O1_q$ and $O2_q$ are protonated by the two proton pathways identified and described here. The proton at N5 atom from FAD is released to the bulk (through the NAD(P)H binding pocket) while that from N1 returns to D_{302}/D_{270} through a reverse process to that described for the protonation of FAD.

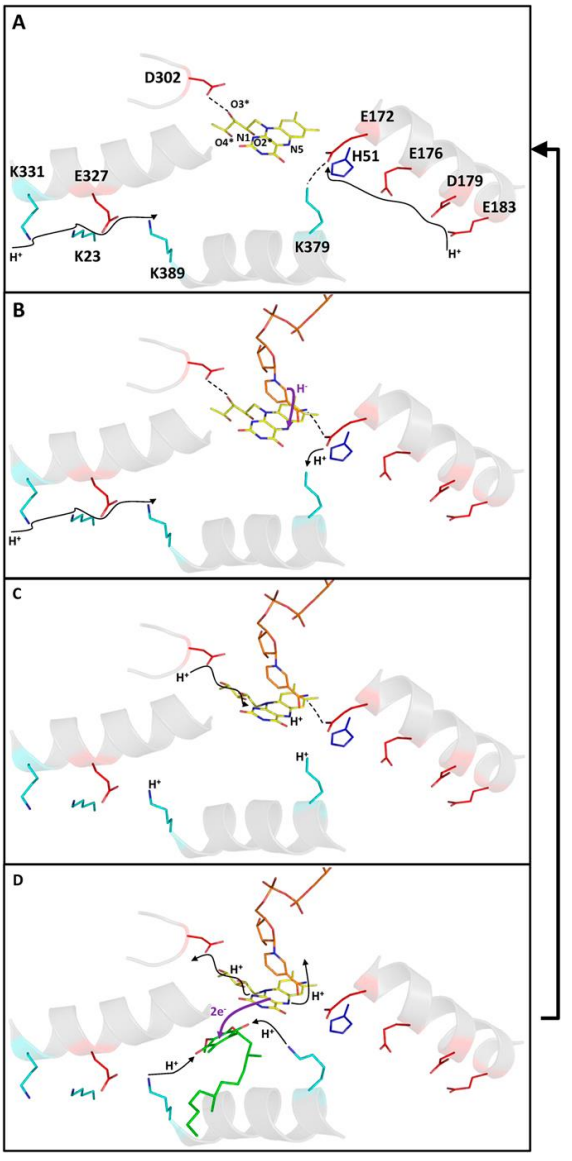

Figure 4.14 NDH-2s enzymatic mechanism. Cartoons are based on the X-ray crystal structure of NDH-2A from *S. aureus* (PDB:5NA1) and are a zoomed view of the FAD and substrate binding sites, including the helices (in gray) which contain the amino acid residues suggested to compose the proposed proton pathways. Substrate positions were predicted by superimposing the substrate free *S. aureus* and NADH/quinone bound *S. cerevisiae* NDH-2s structures (RMSD 1.2 Å). Sticks represent: yellow, the FAD; orange, the NADH/NAD^+; green the quinone/quinol; red, glutamate/aspartate residues; cyan, lysine residues and dark blue, histidine residues. Hydrogen bonding interactions are represented by dashed black lines, proton transfers are schematized by the filled

black arrows and electron/hydride transfers are indicated by purple filled arrows. **(A)** In the absence of substrates FAD is kept oxidized. In this case, D_{302} interacts with O3*. 1st and 2nd dinucleotide binding domain proton pathways allow proton conduction between the bulk and K_{389} or E_{172}, respectively. E_{172} is at hydrogen bonding distance from K_{379}; **(B)** Upon binding, NADH reduces FAD by hydride transfer to N5 and establishes a hydrogen bond with E_{172}, which consequently loses the hydrogen bound to K_{379} (now protonated); **(C)** Concomitantly with its reduction, FAD adopts a bent conformation, leading to the rotation of O2*, O3* and O4*, changing the hydrogen bonding network between D_{302} and N1, allowing their interaction and protonation of N1 by D_{302}. This conformation may also induce additional changes at K_{389} to adopt a protonated form close to the quinone binding pocket; (**D)** Upon quinone binding, $FADH_2$ transfers two electrons to the quinone which also accepts two protons from the final proton conductors of the pathways (K_{379} and K_{389}). After the two electrons transfer ($FADH_2$ oxidation), the flavin returns to its original conformation, leading to the release of the proton at N5 (NADH binding pocket) and the proton at N1 in a reverse process that restores the initial hydrogen bonding network around D_{302}. NAD^+ and quinol are released and the initial positions of K_{379} and K_{389} restored. The protein returns to the state described in **(A)**.

4.5 Conclusion

Our study has revealed how the two enzymes, NDH-2A and NDH-2B from *S. aureus* work in solution at pre-steady-state and steady-state conditions. They both showed a Michaelis-Menten behavior towards their substrates, NADH and NADPH respectively and the quinones and are both inhibited by HQNO.

We describe the formation of a stable charge-transfer (CT) complex upon the reduction of NDH-2A with NADH, which disappears upon oxidation by the quinone. The establishment of a charge-transfer complex between flavoproteins and NADH is well documented, and has been observed for many enzymes catalyzing different reactions[12]. In contrast, we did not observe the formation of a CT complex in NDH-2B when reducing it with NADPH. The study of Yang *et al* showed Ndi1 (NDH-2 from *S. cerevisiae*) formed a charge-transfer complex with NADH, but not with NADPH, under anaerobic conditions[5]. The authors suggest that NADH is specifically required for the CT complex formation[5], which agrees with the absence of charge-transfer complex in NADPH reduced NDH-2B.

Moreover, we describe for NDH-2A that the presence of the CT complex controls the rate of the second half reaction, being quinone reduction the limiting step. We showed that the oxidation reaction is limited by the presence of the CT complex because the dithionite-reduced NDH-2A oxidation rate was 40 times faster than the oxidation rate of the NADH-reduced NDH-2A. The effect of the presence of the CT complex is also observed when oxygen is the electron acceptor, revealing that the presence of CT complex decreases the rate of the second half reaction, independently of the oxidant. In NDH-2B, the CT complex is not formed, we observe the rate limiting step corresponds to NADPH oxidation. In this case it is not fundamental to have $NADP^+$ stablishing a CT

complex with $FADH_2$, since the reduction of the flavin is already slow, avoiding in this way, the overproduction of reactive oxygen species. In addition to the fact NDH-2A forms a CT complex and NDH-2B does not, the enzymes presented differences in the K_M values for their substrates. While NDH-2A showed a higher K_M for DMN, NDH-2B showed a higher K_M for NADPH. When testing HQNO, we noticed it decreases the rate of oxidation of NDH-2A when the CT complex is formed, having no effect when the enzyme is reduced with dithionite. In this case one could hypothesize that DMN could accept electrons from the unoccupied site of NADH. However, we can rule out this hypothesis based on our previous data (see chapter 3) obtained by STD-NMR and fluorescence spectroscopies, which showed that NADH and DMN interact with the protein at two different sites, without interfering with each other. We also observed that HQNO only affects the binding of DMN, discarding the possibility of HQNO binding to the NADH site when the nucleotide is absent. So, we can conclude that the presence of the CT complex slows down the second half reaction of NDH-2A. This is reinforced with the results of NDH-2B, which showed the first half reaction is the slowest one. Still, pre steady-state kinetics data from NDH-2B with HQNO are lacking, as we have only shown that the enzyme is inhibited under steady-state conditions, but we do not know how the inhibitor affects each half-reaction of the enzyme. Nevertheless, it is noteworthy that both processes, the establishment of CT complex by NDH-2A or NADPH oxidation being the limiting step in NDH-2B, may be of physiological importance and should be further explored. We hypothesize that both processes may contribute to keep a low quinol/quinone ratio and thus avoid the production of radical oxygen species by direct reduction of O_2 by the reduced enzymes or unspecific oxidation of quinol with oxygen. NDH-2s are expressed under aerobic conditions and are a component of respiratory chains, thus a mechanism to

prevent their reaction with O_2 would be most beneficial for the electron transfer chain.

We conclude both enzymes have different processes to regulate enzyme reduced state, but it does not imply a different catalytic mechanism. The functional mechanism of NDH-2s here proposed constitute a solid model to foster debate and inspire the design of future experimental approaches aimed at understanding the catalytic mechanism of NDH-2 as well as that of other members of the tDBDF superfamily.

4.6 Acknowledgements

F.V.S. and F.M.S. are recipients of fellowships by Fundação para a Ciência e a Tecnologia (PD/BD/113985/2015, PD/BD/128213/2016, respectively (within the scope of the PhD program Molecular Biosciences PD/00133/2012)). A.S.F.O. is recipient of fellowship from Fundação para a Ciência e a Tecnologia (SFRH/BPD/76621/2011). The stopped flow apparatus was purchased by the grant REEQ/336/BIO/2005 from Fundação para a Ciência e a Tecnologia. The work was funded by Fundação para a Ciência e a Tecnologia (IF/01507/2015 to M.M.P.). This work was also supported by Project LISBOA-01-0145-FEDER-007660 (Microbiologia Molecular, Estrutural e Celular) funded by FEDER funds through COMPETE2020 - Programa Operacional Competitividade e Internacionalização (POCI) and by national funds through FCT - Fundação para a Ciência e a Tecnologia and by national funds through FCT - Fundação para a Ciência e a Tecnologia and by UID/MULTI/ 04046/2013 centre grant from FCT, Portugal (to BioISI).

4.7 References

[1] A. Eschemann, A. Galkin, W. Oettmeier, U. Brandt, S. Kerscher, HDQ (1-hydroxy-2-dodecyl-4(1H)quinolone), a high affinity inhibitor for mitochondrial alternative NADH dehydrogenase: Evidence for a ping-pong mechanism, J. Biol. Chem. 280 (2005) 3138–42. https://doi.org/10.1074/jbc.M411217200.

[2] T. Yano, L. Lin-Sheng, E. Weinstein, J.S. Teh, H. Rubin, Steady-state kinetics and inhibitory action of antitubercular phenothiazines on Mycobacterium tuberculosis Type-II NADH-menaquinone oxidoreductase (NDH-2), J. Biol. Chem. 281 (2006) 11456–63. https://doi.org/10.1074/jbc.M508844200.

[3] I. Velázquez, J.P. Pardo, Kinetic characterization of the rotenone-insensitive internal NADH: Ubiquinone oxidoreductase of mitochondria from Saccharomyces cerevisiae, Arch. Biochem. Biophys. (2001). https://doi.org/10.1006/abbi.2001.2293.

[4] T. Yamashita, E. Nakamaru-Ogiso, H. Miyoshi, A. Matsuno-Yagi, T. Yagi, Roles of bound quinone in the single subunit NADH-quinone oxidoreductase (Ndi1) from Saccharomyces cerevisiae, J. Biol. Chem. 282 (2007) 6012–20. https://doi.org/10.1074/jbc.M610646200.

[5] Y. Yang, T. Yamashita, E. Nakamaru-Ogiso, T. Hashimoto, M. Murai, J. Igarashi, H. Miyoshi, N. Mori, A. Matsuno-Yagi, T. Yagi, H. Kosaka, Reaction mechanism of single subunit NADH-ubiquinone oxidoreductase (Ndi1) from Saccharomyces cerevisiae: Evidence for a ternary complex mechanism, J. Biol. Chem. 286 (2011) 9287–9297. https://doi.org/10.1074/jbc.M110.175547.

[6] J.N. Blaza, H.R. Bridges, D. Aragão, E.A. Dunn, A. Heikal, G.M. Cook, Y. Nakatani, J. Hirst, The mechanism of catalysis by type-II NADH:quinone oxidoreductases, Sci. Rep. 7 (2017). https://doi.org/10.1038/srep40165.

[7] V.H. Teixeira, C.M. Soares, A.M. Baptista, Studies of the reduction and protonation behavior of tetraheme cytochromes using atomic detail, J. Biol. Inorg. Chem. 7 (2002) 200–216. https://doi.org/10.1007/s007750100287.

[8] A.M. Baptista, C.M. Scares, Some theoretical and computational aspects of the inclusion of proton isomerism in the protonation equilibrium of proteins, J.

Phys. Chem. B. 105 (2001) 293–309. https://doi.org/10.1021/jp002763e.

[9] D. Bashford, K. Gerwert, Electrostatic calculations of the pKa values of ionizable groups in bacteriorhodopsin, J. Mol. Biol. 224 (1992) 473–86. https://doi.org/10.1016/0022-2836(92)91009-E.

[10] D. Bashford, M. Karplus, pKa's of Ionizable Groups in Proteins: Atomic Detail from a Continuum Electrostatic Model, Biochemistry. 29 (1990) 10219–25. https://doi.org/10.1021/bi00496a010.

[11] D. Bashford, An object-oriented programming suite for electrostatic effects in biological molecules: An experience report on the MEAD project, in: Lect. Notes Comput. Sci. (Including Subser. Lect. Notes Artif. Intell. Lect. Notes Bioinformatics), 1997: pp. 233–240. https://doi.org/10.1007/3-540-63827-X_66.

[12] T. Sakurai, H. Hosoya, Charge-transfer complexes of nicotinamide-adenine dinucleotide analogues and flavin mononucleotide, BBA - Biophys. Incl. Photosynth. 112 (1966) 459–68. https://doi.org/10.1016/0926-6585(66)90248-2.

[13] T. Yano, M. Rahimian, K.K. Aneja, N.M. Schechter, H. Rubin, C.P. Scott, Mycobacterium tuberculosis type II NADH-menaquinone oxidoreductase catalyzes electron transfer through a two-site ping-pong mechanism and has two quinone-binding sites, Biochemistry. 53 (2014) 1179–90. https://doi.org/10.1021/bi4013897.

[14] F.M. Sousa, F. V. Sena, A.P. Batista, D. Athayde, J.A. Brito, M. Archer, A.S.F. Oliveira, C.M. Soares, T. Catarino, M.M. Pereira, The key role of glutamate 172 in the mechanism of type II NADH:quinone oxidoreductase of Staphylococcus aureus, Biochim. Biophys. Acta - Bioenerg. 1858 (2017) 823–832. https://doi.org/10.1016/j.bbabio.2017.08.002.

[15] S.J.O. Hardman, C.R. Pudney, S. Hay, N.S. Scrutton, Excited state dynamics can be used to probe donor-acceptor distances for H-tunneling reactions catalyzed by flavoproteins, Biophys. J. 105 (2013) 2549–58. https://doi.org/10.1016/j.bpj.2013.10.015.

[16] T.Y. Lin, T. Werther, J.H. Jeoung, H. Dobbek, Suppression of electron transfer to dioxygen by charge transfer and electron transfer complexes in the FAD-dependent reductase componentof toluene dioxygenase, J. Biol. Chem. 287 (2012) 38338–46. https://doi.org/10.1074/jbc.M112.374918.

[17] S. Ojha, E.C. Meng, P.C. Babbitt, Evolution of function in the “two dinucleotide binding domains” flavoproteins, PLoS Comput. Biol. 3 (2007) e121. https://doi.org/10.1371/journal.pcbi.0030121.

[18] B.W. Lennon, C.H. Williams, M.L. Ludwig, Crystal structure of reduced thioredoxin reductase from Escherichia coli: Structural flexibility in the isoalloxazine ring of the flavin adenine dinucleotide cofactor, Protein Sci. 8 (1999) 2366–79. https://doi.org/10.1110/ps.8.11.2366.

[19] M. Senda, S. Kishigami, S. Kimura, M. Fukuda, T. Ishida, T. Senda, Molecular Mechanism of the Redox-dependent Interaction between NADH-dependent Ferredoxin Reductase and Rieske-type [2Fe-2S] Ferredoxin, J. Mol. Biol. 373 (2007) 382–400. https://doi.org/10.1016/j.jmb.2007.08.002.

4.8 Supplementary Information

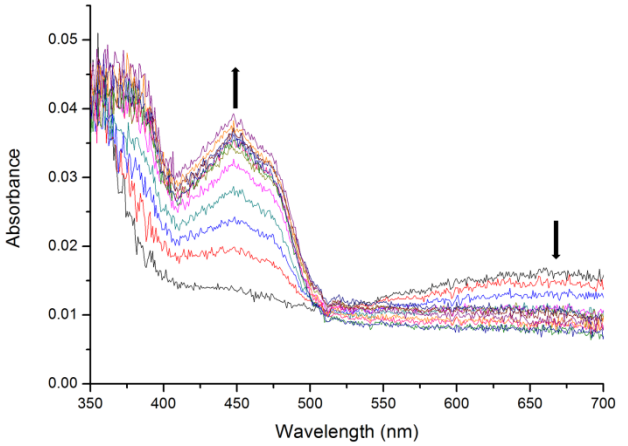

Figure S4.1 Time-resolved oxidation of NADH reduced NDH-2A from *S. aureus* by DMN. The direction of the arrows shows the behavior of the absorbance upon oxidation by quinone, at 450 nm increased and the broad peak in the region 650-700 nm disappeared.

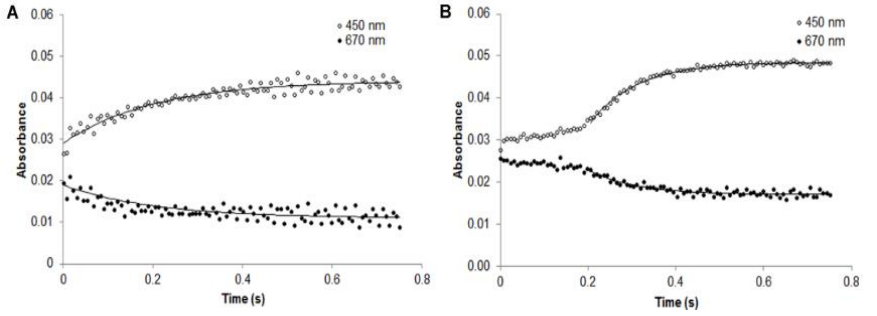

Figure S4.2 Pre steady-state kinetics experiments of NDH-2A. Time-resolved oxidation of NADH reduced NDH-2A by DDB (**A**) (1:1) or Duroquinone(**B**) (1:5). The absorbance at 450 nm increased and the broad peak in the region 650-700 nm disappeared. The observed rate constants of the two processes, acquired at 450 nm and at 670 nm, obtained by exponential fitting of the kinetic curves at 450 nm and 670 nm, were equal to 5 ± 2 s^{-1} for DDB and 2.2 ± 0.4 s^{-1} for Duroquinone. It should be noted that in (**B)** we have an excess of reducer (NADH) and that is why there is a turnover situation up to 0.2 seconds. The adjustment with the exponential was only made from there (0.2 s) and therefore the rate constant is correct, despite the amplitude taken from the fit being much higher than the real one.

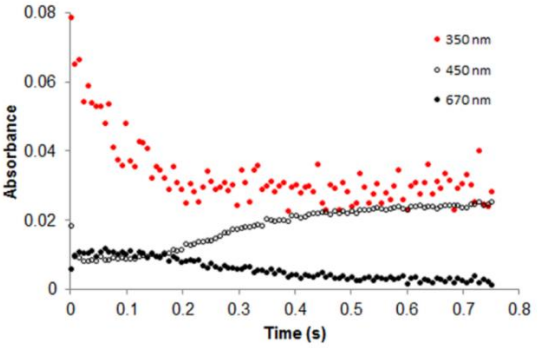

Figure S4.3 Time-resolved reduction of NDH-2A from *S. aureus* at turnover. The decrease in the absorbance of the peak at 350 nm (red dots) corresponds to NADH consumption. The observed ΔAbs at 350 nm (~0.05) corresponds to the oxidation of 8 µM NADH, which agrees with the experiment set up (10 µM of NADH after mixing and 3 ms acquisition dead time). The noise at 350 nm is higher than at other wavelengths due to the smaller intensity of the lamp at this wavelength (equipment limit).

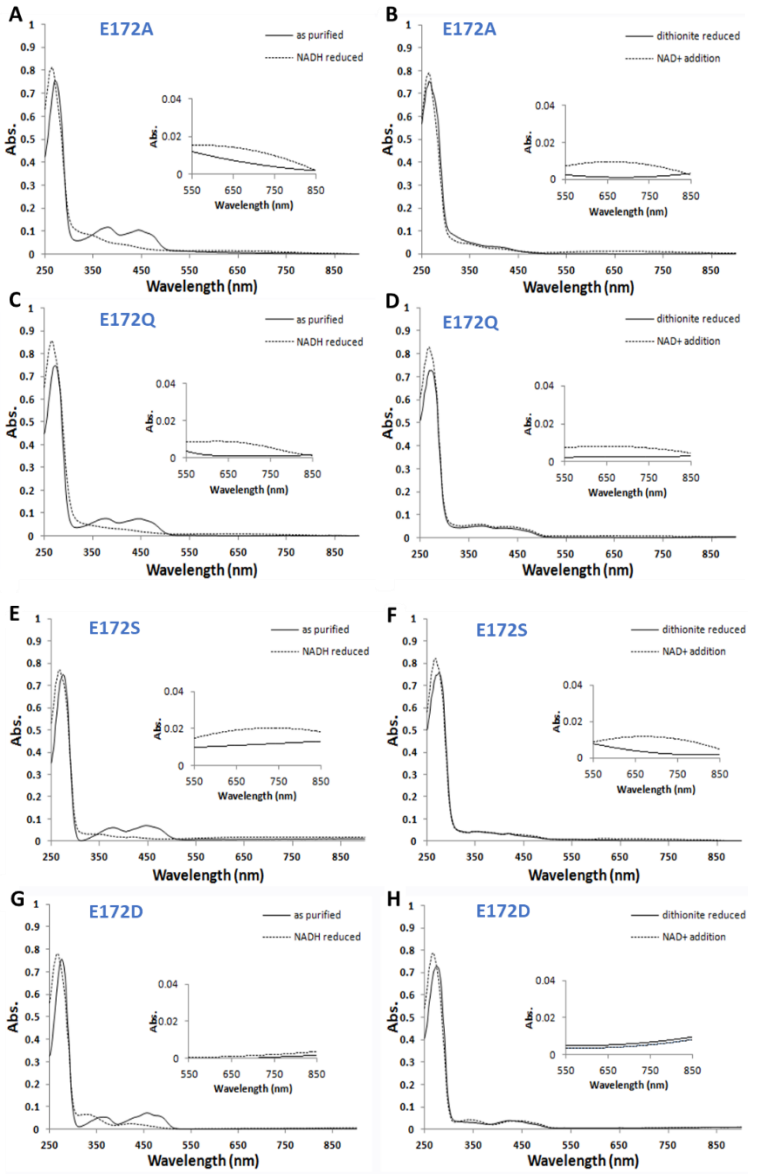

Figure S4.4 UV-Visible absorption spectra of the NDH-2A variants. The UV-Visible absorption spectra of the NDH-2 variants (6 µM) presented maxima in the 350-475 nm region corresponding to FAD absorption and a large band centered at 670 nm (zoomed region) corresponding to the CT complex absorption. **A)** $E_{172}A$ variant as purified (black filled line) and after 12 µM NADH addition (black dashed line). **B)** $E_{172}A$ variant reduced with sodium dithionite (black filled line) and after NAD^+ (12 µM) addition (black dashed line). **C**) $E_{172}Q$ variant as purified (black filled line) and after 12 µM NADH addition (black dashed line). **D)** $E_{172}Q$ variant reduced with sodium dithionite (black filled line) and after

NAD^+ (12 µM) addition (black dashed line). **E)** $E_{172}S$ variant as purified (black filled line) and after 12 µM NADH addition (black dashed line). **F)** $E_{172}S$ variant reduced with sodium dithionite (black filled line) and after NAD^+ (12 µM) addition (black dashed line). **G)** $E_{172}D$ variant as purified (black filled line) and after 18 µM NADH addition (black dashed line). **H)** $E_{172}D$ variant reduced with sodium dithionite (black filled line) and after NAD^+ (18 µM) addition (black dashed line).

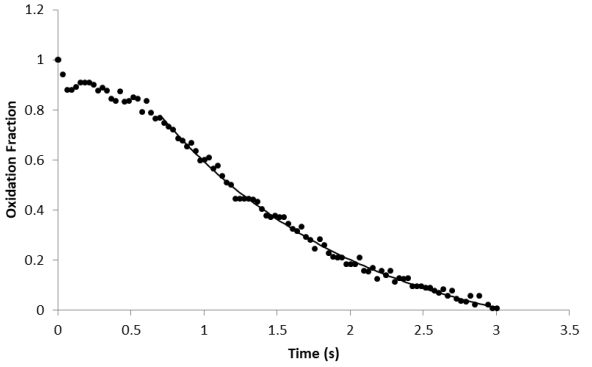

Figure S4.5 Reduction of NDH-2B from *S. aureus* by NADPH in the presence of DMN (1:5:3 ratio) monitored at 450 nm. The concentrations before mixing are 10 µM for NDH-2B, 50 µM for NADPH and 30 µM for DMN in a 50 mM MES Bis Tris Propane 250 mM NaCl buffer pH 5.5. The black dots represent the experimental data and the black line represents the theoretical fit obtained by using an exponential equation.

Table S4.1 Summary of kinetic rate constant values (s^{-1}) for the second half-reaction - flavin oxidation in NDH-2A enzyme.

	Oxidizing substrate / inhibitor		
Reducing substrate	**DMN**	**DMN + HQNO**	**O_2**
NADH	5.0 ± 0.5	0.08 ± 0.02	0.0044 ± 0.0007
Dith + NAD^+	11.4 ± 2.2	0.1 ± 0.0006	-
Dith	196 ± 15	179 ± 12	0.76 ± 0.2

Table S4.2 Summary table of the kinetic parameters determined for NDH-2A and its variants proteins.

NDH-2A	**NADH:quinone oxidoreductase activity**	**Pre steady-state kinetics**	
	k_{cat} (s^{-1})	**Reductive half-reaction (s^{-1})**	**Oxidative half-reaction (s^{-1})**
WT	67.9 ± 2.4	180 ± 30	5 ± 0.5
E172A	20.6 ± 2.7	115 ± 16	0.98 ± 0.21
E172Q	5.7 ± 1.1	108 ± 12	0.27 ± 0.05
E172S	11.3 ± 1.2	104 ± 3	0.32 ± 0.05
E172D	-	-	-

Chapter 5

The cellular role of the two alternative NAD(P)H:quinone oxidoreductases from *Staphylococcus aureus*

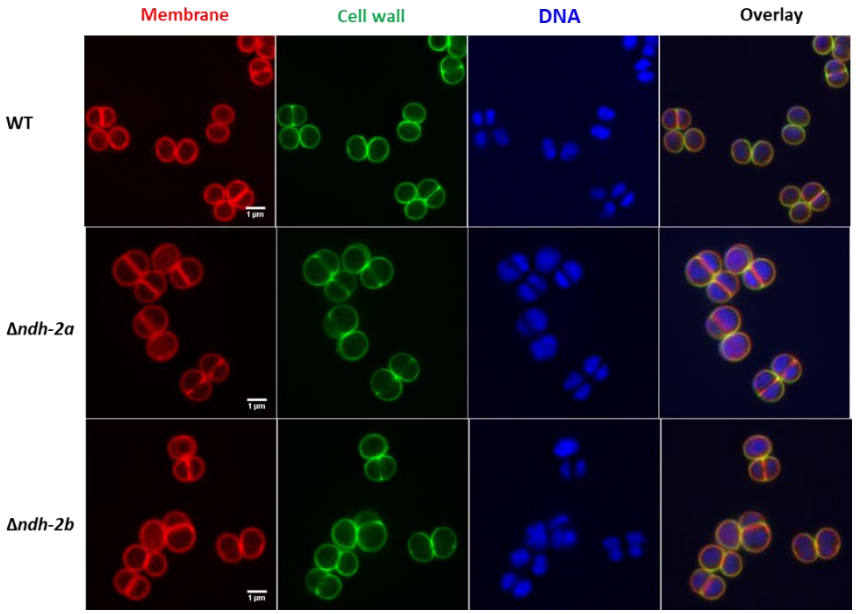

Chapter 5- The cellular role of the two alternative NAD(P)H:quinone oxidoreductases from *Staphylococcus aureus*

This section is based on the following manuscript for publication:

- ✓ **Sena FV**, Sousa FM, Pereira AR, Pires T, Catarino T, Cabrita EJ, Pinho MG, Pereira MM. The two Alternative NADH:quinone oxidoreductases from *Staphylococcus aureus*: two players with different molecular and cellular roles*. To be submitted*.

Author contribution:

Sena FV participated in the design of the study, performed the experiments, analyzed, and discussed the data. Pereira AR designed all the primers and helped with the microscopy experiments. These studies have been performed in collaboration with Mariana Gomes Pinho Lab at ITQB.

5.1 Summary

NDH-2s are membrane flavoproteins involved in respiratory chains, recognized as suitable targets for novel drug therapies. They are the only enzymes with NADH:quinone oxidoreductase activity expressed in many pathogenic organisms, as *Staphylococcus aureus*, a global health problem due to methicillin-resistant strains. *S. aureus* presents two genes encoding NDH-2s and no genes coding for Complex I, the canonical respiratory NADH:quinone oxidoreductase. This genomic information raises many questions regarding the function of NDH-2A and NDH-2B in *S. aureus*. In this study we created knockout mutants for each of the two genes encoding NDH-2s (Δ*ndh-2a* and Δ*ndh-2b*) to investigate their cellular role. In addition, we engineered the wild-type to carry reporter genes, mNeonGreen fluorescent proteins, fused to each *ndh-2* gene (*ndh-2a* and *ndh-2b*) to explore the spatial organization of the enzymes in cell context. Our studies, including cultures growths, NMR-based metabolomics and microscopy revealed the two knockout strains have different phenotypes. Mutant strains grew slower and cells were larger than the wild-type. We observed that Δ*ndh-2a* presents longer phases 2 and 3 of *S. aureus* cell cycle, indicating cell division may be compromised in this mutant strain. Also, Δ*ndh-2a* mutant cells showed to partially adopt a lactate fermentation metabolism. This work strengthened the importance of maintaining a balanced $NAD(P)^+$/NAD(P)H ratio in the cell and how these alternative NAD(P)H:quinone oxidoreductases enzymes contribute to this demand.

5.2 Introduction

Staphylococcus aureus is a facultative anaerobe that may use several carbon sources in aerobic or anaerobic respiration, with oxygen or nitrate as electron acceptors, respectively. In addition, it may also ferment in the absence of external electron acceptors, provided by the presence of a rich carbon source[1–3]. This energetic versatility allows *S. aureus* to survive and proliferate in multiple niches of the host. Despite possessing the Embden-Meyerhof-Parnas (EMP), the pentose phosphate (PPP) and the tricarboxylic acid cycle (TCA) pathways for the catabolism of carbohydrates, reports of this pathogenic organism, from the 1960's, proposed that the activity of the TCA cycle is largely dependent on environmental conditions and nutrient availability, observations that have been fully corroborated by a number of more recent studies[4–6]. Excess of glucose was pinpointed as one of the key conditions antagonistic of TCA cycle activity[7]. Under nutrient-rich conditions, as in the presence of glucose, several bacteria repress the citric acid cycle (TCA), allowing the bacteria to maximize growth rate on its preferred sugar [8]. Genes of the TCA cycle, including aconitate hydratase (*citB*) or succinate dehydrogenase (*sdhB*) that are required for the complete oxidation of glucose, are repressed in response to glucose, via the catabolite control protein A (CcpA)[7]. CcpA is a member of the LacI/GalR repressor family of transcriptional regulators that control carbon metabolism pathways in Gram-positive bacteria, as *S. aureus*. This process, where glucose prevents the use of other carbon sources, is a regulatory mechanism denominated as carbon catabolite repression (CCR)[9]. CCR allows bacteria the assimilation of the higher energetic carbon source, as glucose, when exposed to more than one carbohydrate, thus the genes coding for proteins that enable the use of secondary carbon sources are not expressed when glucose is available[7].

Electrons obtained from the oxidation of intermediates from glucose, lipids, and amino acids metabolisms or from some inorganic compounds, like H_2S, may enter the respiratory chain by the action of quinone reductases, which promote the link between several catabolic pathways and the respiratory chain. Thus, these enzymes have a crucial role in directly connecting the different metabolic pathways with the respiratory chain, ensuring versatility and robustness to the energetic metabolism.

The respiratory chain of *S. aureus*, as most of the ones of organisms belonging to Bacillales order, presents two genes encoding NDH-2s and no genes coding for Complex I (type I NADH:quinone oxidoreductase)[10]. This genomic information raises two simple questions: whether the two proteins perform the same function and if both are important for *S. aureus* metabolism. Besides NDH-2, succinate:quinone oxidoreductase (SDH), glycerol-3 phosphate:quinone oxidoreductase (G3PQO), malate:quinone oxidoreductase (MQO), sulfide:quinone oxidoreductase (SQR), pyruvate:quinone oxidoreductase (PQO) and dihydroorotate:quinone oxidoreductase (DHOQO) are present and can also reduce quinone to quinol[10]. In addition, *S. aureus* genome also codifies to a formate:quinone oxidoreductase (Fdn-N). Analysis of the genome also indicates there is no cytochrome bc_1 complex or alternative complex III (ACIII) in *S. aureus* respiratory chain, and instead quinol may be oxidized by a *bd* oxidase with reduction of O_2 to water [11]. Also, it encodes other type of respiratory oxygen reductase as is the case of an HCO aa_3-type menaquinol oxidase. Additionally, *S. aureus* respiratory chain contains a particulate methane monooxygenase (pMMO) allowing the hydroxylation of methane to methanol using O_2. As it was mentioned before, *S. aureus* can proliferate using nitrate as substrate, in anaerobic conditions, due to the presence of a periplasmic nitrate reductase (NapABC) on its respiratory chain.

Fostered by the gap of knowledge regarding the cellular role of the two NDH-2s from *S. aureus*, we investigated the spatial localization of both proteins and the impact of their absence in the metabolism of this pathogen, through fluorescence microscopy and NMR-based metabolomics analysis. This last approach allowed us to deconvolute the major pathways where these proteins are involved since metabolites can be considered as intermediates of the generality of the metabolic pathways thus representing a reliable fingerprint of the organism status.

5.3 Experimental procedures

5.3.1 Construction of *S. aureus* mutants

The Δ*ndh-2a* and Δ*ndh-2b* mutants were constructed using the pMAD vector35 containing the upstream and downstream regions of each gene of interest, to allow recombination and integration of the plasmids into the chromosome, followed by their excision with the genes to be deleted. Briefly, upstream and downstream regions of ndh-2a and ndh-2b genes were amplified by PCR, using primers P1_ndh-2A/P2_ndh-2A and P3_ndh-2A/P4_ndh-2A, P1_ndh-2B/P2_ndh-2B and P3_ndh-2B/P4_ndh-2B, respectively Table S5.1. The PCR fragments encoding the upstream and downstream regions of each gene were joined by overlap PCR using the pairs of primers P1_ndh-2A/P4_ndh-2A and P1_ndh-2B/P4_ndh-2B. The resulting fragments were digested with NcoI, BamHI, SalI and SmaI (Fermentas) and cloned into the pMAD vector, which was propagated in *E. coli* DC10B and whose inserts were sequenced. The plasmids were then electroporated into *S. aureus* RN4220 strain at 30 °C, using erythromycin and X-gal selection, and transduced into NCTC8325-4 using phage 80α. The recombination and integration of the plasmids into the chromosome was obtained as previously described[12] after a two-step homologous recombination process. In the first step, recombinants were selected at the non-permissive temperature of 43 °C, using erythromycin and light blue colony color. In the second step, cells were incubated at the permissive temperature of 30 °C in the absence of antibiotic selection, and white, erythromycin-sensitive colonies in which the vector had been excised were selected. Gene deletions were confirmed by PCR and sequencing of the amplified fragment.

5.3.2 Construction of mNeonGreen-labelled proteins

Cloning of fluorescent probes in *S. aureus* was done using the following general strategy: plasmids were propagated in *E. coli* strains DC10B and purified from overnight cultures supplemented with the relevant antibiotics. Plasmids were then introduced into electrocompetent *S. aureus* RN4220 cells as previously described and transduced to NCTC8325-4 using phage 80α. Constructs were confirmed by PCR and by sequencing of the amplified fragment. Briefly the strains *ndh-2a*-mNeonGreen and *ndh-2b*-mNeonGreen were constructed by allelic replacement strategies using the pMAD vector. In each case, three DNA fragments (F1, F2 and F3) that contained overhangs that were complementary with adjacent fragments were amplified from NCTC8325-4 DNA, and then joined by overlap PCR to produce F1–F2–F3 fusion constructs. The full constructs were then amplified by PCR using upstream and downstream primers (P1 and P6, respectively, in each case), digested with the corresponding restriction enzymes and cloned into pMAD. Integration and excision of the pMAD derivatives in NCTC8325-4 by a double recombination event that led to allelic exchange was performed as previously described (see Table S5.1).

5.3.3 Bacterial strains and growth conditions

All the strains and plasmids used in this study are listed in Table S5.2 in the supplemental material. The sequences of the primers used are listed in Table S5.1. Overnight cultures of NCTC8325-4 strains that encoded the knockout and fluorescent enzymes were back-diluted to OD_{600nm} = 0.05 in TSB and grown at 37 °C for 11 h with OD_{600nm} measurements taken every one hour and half. *S. aureus* strains were grown on tryptic soy agar (TSA, Difco) or in tryptic soy broth (TSB, Difco) at 37 °C with aeration. For metabolite NMR (nuclear magnetic resonance) analyses, samples were collected at different

time-points during the growth. OD_{600nm} and pH values were measured every 1.5 h and samples (1.5 mL) were collected by centrifugation and the supernatant and pellet solutions were stored at -20 °C. The handling of *S. aureus* strains was always performed inside a laminar flow chamber (NinoLaf Safety Cabinet, Modell ninoSAFE 1200).

5.3.4 Analysis of the expression of fluorescent proteins in *S. aureus*

To compare the expression levels of NDH-2A-mNeonGreen and NDH-2B-mNeonGreen, total protein extracts from each strain were prepared. For that purpose, cells were harvested from mid-exponential phase cultures, re-suspended in 1X Phosphate Buffered Saline (PBS) and disrupted with glass beads in a Fast Prep FP120 (Thermo Electro Corporation). The total protein content of the extracts was quantified by the Biuret method, using bovine serum albumin as a standard and equal amount of protein, from each sample, were loaded onto a 10 % SDS-PAGE gel and separated at 120V. Gel images were acquired on a Fuji FLA 5100 laser scanner (Fuji Photo Film) using 473 nm laser for GFP fusion and 635 nm laser for detection of protein molecular weight marker.

5.3.5 *S. aureus* imaging by fluorescence microscopy

Super-resolution SIM imaging was performed using an Elyra PS.1 microscope (Zeiss) with a Plan-Apochromat 63×/1.4 oil DIC M27 objective. SIM images were acquired using five grid rotations, unless stated otherwise, with a 34-µm grating period for the 561-nm laser (100 mW), a 28-µm period for the 488-nm laser (100 mW) and a 23-µm period for the 405-nm laser (50 mW). Images were captured using a Pco.edge 5.5 camera and reconstructed using ZEN software (black edition, 2012; version 8.1.0.484) on the basis of a

structured illumination algorithm, with synthetic, channel specific optical transfer functions and noise filter settings ranging from −6 to −8.

Wide-field fluorescence microscopy was performed using a Zeiss Axio Observer microscope with a Plan-Apochromat 100×/1.4 oil Ph3 objective. Images were acquired with a Retiga R1 CCD camera (QImaging) using Metamorph 7.5 software (Molecular Devices).

For fluorescence microscopy experiments overnight cultures of *S. aureus* strains were back-diluted to 1:200 in fresh medium with appropriate inducers and allowed to grow until they reached an OD_{600nm} of approximately 0.6 before being collected and washed with phosphate buffered saline (PBS) solution. Cells were then placed on microscope slides covered with a thin layer of agarose (1 % in PBS) and imaged by SIM or wide-field microscopy.

To label *S. aureus* membranes, cells were incubated with Nile Red (Invitrogen), at a final concentration of 10 µg mL^{-1} for 5 min at room temperature, washed with PBS and then mounted on microscope slides. *S. aureus* cell wall labelling with vancomycin was performed by incubating the cells for 2 min at room temperature with a mixture containing equal amounts of vancomycin (Sigma) and a BODIPY FL conjugate of vancomycin (Van-FL, Molecular Probes) to a final concentration of 0.8 µg mL^{-1}. Cells were also stained with the DNA dye Hoechst 33342 (1 µg mL^{-1}).

5.3.6 Calculation of cell dimensions

To calculate the volume of each cell, an ellipse was fitted to the border limits of the cellular membrane of Nile-Red-labelled cells, overlaying the membrane dye signal. Subsequently, the shorter and longer axes were measured, coinciding with the septum and the axis perpendicular to it, respectively. The volume of the cell was obtained by an approximation to the

volume of a prolate spheroid (equation (1)) where *a* and *b* correspond to the longer and shorter semi-axes, respectively.

$$V = \frac{4}{3}\pi ab^2 \qquad (1)$$

5.3.7 NMR-based Metabolomics

Extracellular metabolome ^{1}H-NMR analysis was performed in 5 mm glass tubes. For each collected sample, 400 µL were used and buffered to pH 7.0 by adding 200 µL 200 mM sodium hydrogen phosphate buffer solution, prepared with 100 % D_2O. Additionally, the buffer solution contained a final concentration of 1 mM of TSP (3trimethylsilyl-[2,2,3,3-D4]-1-propionic acid) as an internal standard for subsequent quantification, used for chemical shift referencing and normalization of NMR peak intensities. All ^{1}H-NMR spectra were obtained at 25 °C on a Bruker AVANCE III 500 NMR spectrometer, operating at a central frequency of 500.13 MHz (Bruker Biospin, Rheinstetten, Germany), equipped with 5 mm TCI C/N Prodigy Cryo probe. The equipment was controlled via Topspin version 3.2 software (Bruker Biospin, Rheinstetten, Germany). Spectra were acquired with water presaturation during a delay of 2 s and using a total recycling time of 35 s to allow full relaxation of the signals. Twenty-seven spectra were collected. 16 transients were collected into 64k data points using a spectral width of 16 ppm. Fourier transform was performed with no exponential multiplication. Spectra were automatically phased and baseline-corrected, and the chemical shift scale was set by assigning the value of δ=0.00 ppm to the signal from the added TSP. Compound identification was done by matching the obtained spectra with a ^{1}H-NMR spectra databank using Chenomx Nmr Suite Version 8.12 software (Chenomx Inc.) and comparing with spectra of standard compounds. Quantification was done by integration of designated peaks, regarding the number of protons responsible for each signal

in the defined frequencies (Table S5.3 in Supplemental Material), and comparing with the added standard TSP (integral calibrated as 9 protons, regarding the number of protons and the concentration in which was present, 1 mM). The molar concentration of each compound was estimated also considering the sample dilution (3:2). For each triplicate assay, the median was calculated, and the standard deviations were determined, for all the metabolic peaks studied.

5.4 Results and Discussion

5.4.1 Localization studies of NDH-2s from *S. aureus*

To study NDH-2A and NDH-2B localization in vivo we resort to a fluorescent protein (FP), mNeonGreen, fused to the proteins of interest. We constructed *S. aureus* strains expressing a C-terminal *ndh-2a*-mNeonGreen fusion and an N-terminal *ndh-2b*-mNeonGreen fusion with a linker with 10 amino acid residues in each one of the constructs. By expressing *ndh-2a*- and *ndh-2b*-mNeonGreen from their native locus and under the control of their native promoter, we were able to evaluate the localization of each protein in live cells. The growth curves of the wild-type, *ndh-2a*-mNeonGreen and *ndh-2b*-mNeonGreen strains are shown in figure S5.1 and, as we can observe, *S. aureus* strains with the green fluorescent protein grow similarly to the WT strain. In rich media (TSB), most of the cells had NDH-2A-mNeonGreen distributed uniformly throughout the cytoplasm and appeared as bright fluorescent foci at the cell membrane (Figure 5.1A). Concerning NDH-2B-mNeonGreen, most of the protein localized in the cytoplasm (Figure 5.1B). Additionally, we did a negative control in which we compared *ndh-2b*-mNeonGreen with wild-type (WT strain without mNeonGreen fused) and *ndh-2b*-mNeonGreen showed a higher fluorescence pattern, meaning that the signal that we observe is not autofluorescence of the TSB medium (Figure S5.2). Moreover, we performed fluorescence imaging analysis of NDH2-A-mNeonGreen and NDH-2B-mNeonGreen protein extracts and observed that both proteins were present in soluble and membrane fractions (both bands were present on the SDS-PAGE gel), showing that what we observe in microscopy is indeed the production of the fusion proteins (Figure 5.2). NDH-2A-mNeonGreen showed a more intense band which may mean that this fusion is more abundant in the tested conditions (Figure 5.2). Furthermore, both

constructs demonstrated higher expression in the beginning of the exponential phase (Figure 5.2). The protein extracts result is important, as it validates our microscopy data, which means that the observed pattern is the result of the fusion protein that has the expected size, as observed in the SDS-PAGE gel.

To prove that the *S. aureus* strain with *ndh-2a*-mNeonGreen reporter was functionally active, we performed a growth curve and collected extracellular metabolites. The analysis of the collected extracellular metabolites by ^{1}H-NMR showed that this strain had a similar profile when compared with the *S. aureus* wild-type strain, confirming that the inserted reporter gene did not interfere with the fitness of *S. aureus* (Figure S5.3).

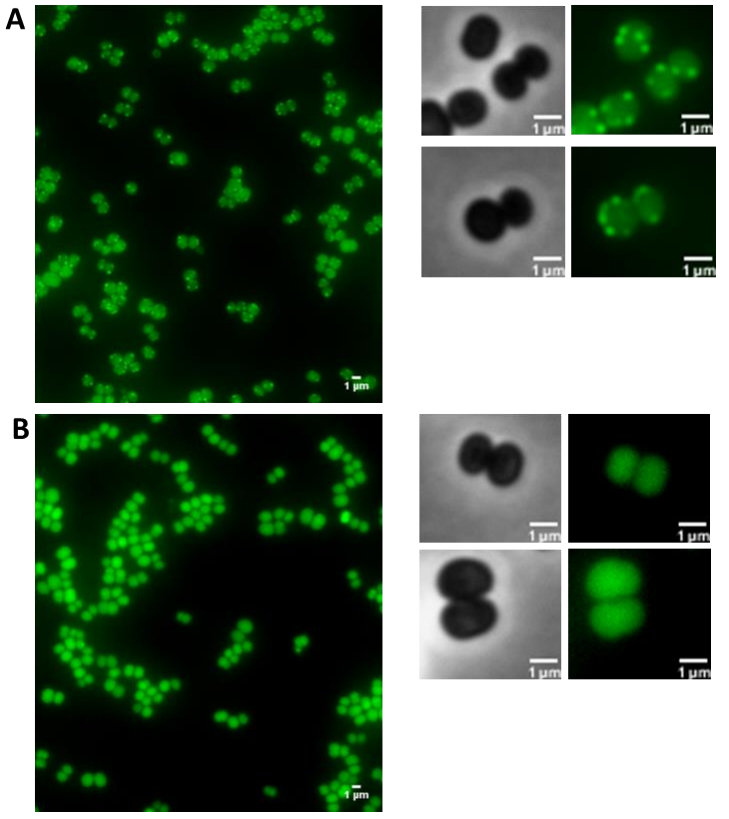

Figure 5.1 Localization of mNeonGreen-labelled NDH-2A (A) and NDH-2B (B) proteins by fluorescence microscopy. Images of *ndh-2a*-mNeonGreen and *ndh-2b*-mNeonGreen fusions location. Scale bar, 1 µm.

Our results show that the two mNeonGreen-NDH-2s localized similarly, in the cytoplasm or/and membrane, and this can be explained by the fact that these are monotopic enzymes that are attached to the membrane, through weak electrostatic interactions, from one side but do not cross the lipid bilayer completely, having no transmembrane domains and can appear temporarily in the cytoplasm.

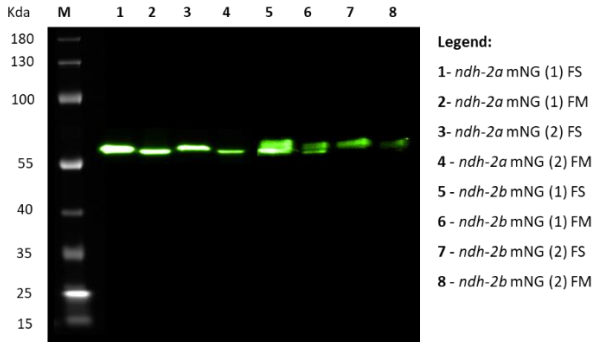

Figure 5.2 Analysis of the expression of mNeonGreen-labelled NDH-2A and NDH-2B proteins. *ndh-2a*-mNeonGreen (71 kDa, lanes 1-4) and *ndh-2b*-mNeonGreen (66 kDa, lanes 5-8) in exponential (1) and stationary (2) phases from the soluble (FS) and membrane fractions (FM).

5.4.2 Growth analysis of the knockout mutants reveals evident delay of the Δ*ndh-2a* strain

To functionally characterize *S. aureus* NDH-2s, we analyzed the phenotypic effects of their absence. For that, *ndh-2a* and *ndh-2b* null mutants were constructed in the background of *S. aureus* strain NCTC8325-4 by removing the entire gene from the chromosome and leaving no resistance marker.

S. aureus growths of the wild-type (NCTC8325-4) and mutant, Δ*ndh-2a* and Δ*ndh-2b*, strains were performed in a rich medium, TSB, containing 14 mM glucose and an ill-defined concentration of peptides and free-amino acids, and were evaluated by monitoring optic density at 600 nm (OD_{600}) and pH changes.

The results presented in figure 5.3A showed a significant difference between the wild-type strain and the Δ*ndh-2a* strain, this last one reaching a maximal OD_{600} approximately of 5. The pH profile is characterized by a continuous decrease from the beginning of growth until ~6 hours, which corresponded to an inflection point, since this decrease was subsequently followed by an increase in pH and was observed in all strains (Figure 5.3B). The other mutant strain (Δ*ndh-2b*) had a similar behavior of the wild-type strain growth curve with a slightly delay in growth (Figure 5.3A).

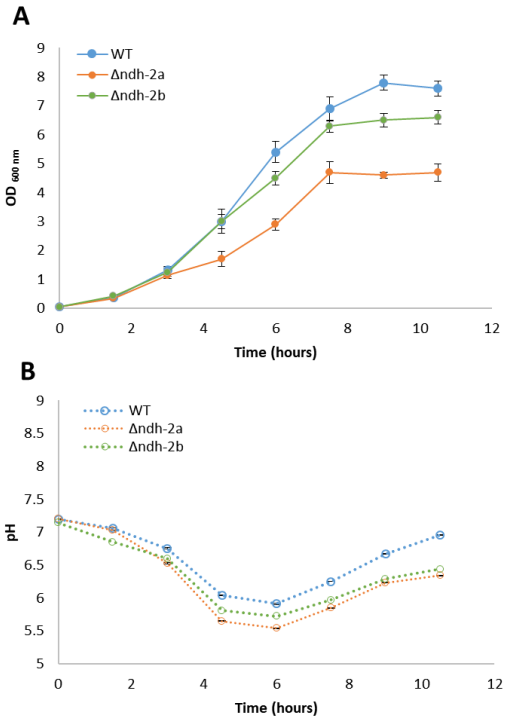

Figure 5.3 Growth of *S. aureus* wild-type strain, Δ*ndh-2a* and Δ*ndh-2b* strains in TSB (initial OD 0.05, in aerobic conditions). The absorbance at 600 nm and the pH values were measured at 1.5 h intervals. The results presented are representative of three independent experiments (respective error bars). Comparison of the growths of *S. aureus* wild-type (blue), Δ*ndh-2a* (orange) and Δ*ndh-2b* (green) strains by optical density **(A)** and pH **(B)**.

These data showed for the three strains studied (WT, Δ*ndh-2a* and Δ*ndh-2b*), although at different time points, a biphasic behavior in the growth and pH profile, which will be discussed below through NMR-based metabolomic analysis.

5.4.3 Cell volume and cell cycle of Δ*ndh-2a* and Δ*ndh-2b* mutant strains is altered compared to the WT strain

To evaluate morphology dynamics during the cell cycle of *S. aureus*, cells were labelled with Nile Red for membrane staining. Fluorescence microscopy analyses of all the strains showed increased cell volumes in both mutants when compared to wild-type cells (Figure 5.4).

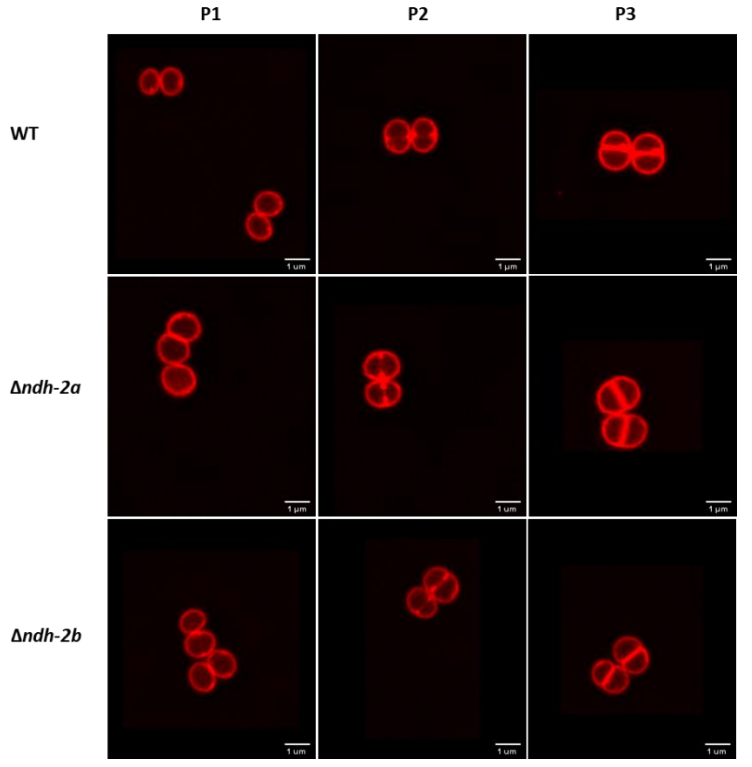

Figure 5.4 Images of *S. aureus* WT and Δ*ndh-2a* and Δ*ndh-2b* cells showing different volumes between each phase (P1, P2 and P3) and between strains. Cells were stained with membrane dye Nile red (red) Scale bars, 1 µm.

This observation was reinforced by calculating the volume of the cells (n = 105 cells for each phase) at different phases of *S. aureus* cell cycle (Table 5.1). According to Monteiro *et al*, in Phase 1 (P1) cells have recently divided and have not initiated synthesis of the septum, in Phase 2 (P2) cells are undergoing septum synthesis and in Phase 3 (P3) cells have a complete septum and are going to split into two daughter cells[13].

Table 5.1 Average ratio of longer/shorter axes of *S. aureus* cells upon the three phases of the cell cycle.

Strain	Volume (μm^3)		
	Phase 1	**Phase 2**	**Phase 3**
WT	0.47 ± 0.1	0.54 ± 0.1	0.64 ± 0.11
Δ*ndh-2a*	0.75 ± 0.14 (****)	0.99 ± 0.14 (***)	1.10 ± 0.15 (***)
Δ*ndh-2b*	0.59 ± 0.13(*)	0.82 ± 0.13(**)	0.94 ± 0.13 (****)

* $p \leq 0.05$, ** $p \leq 0.01$, *** $p \leq 0.001$ mutants vs. parental strain NCTC (n=315 cells for each strain, n=105 cells per phase). Data are presented as mean ± standard deviation. Statistical analysis was performed using the unpaired *t test*.

In this case it was possible to observe that cell volume increases gradually over the entire cell cycle (Figure 5.5). By calculating the volume of each cell in each phase (P1, P2 and P3), the volume of Δ*ndh-2a* and of Δ*ndh-2b* are larger than that of the WT strain (Table 5.1, Figure 5.5). Moreover, our results showed that the wild-type and Δ*ndh-2b* strains spent approximately more than half of the cell cycle in Phase 1 with the other half being spent in septum synthesis (P2), and in the final elongation step (P3), but in contrast Δ*ndh-2a* presented a higher number of cells in P2 and P3 phases which means that cell division may be compromised in this mutant (Figure 5.6).

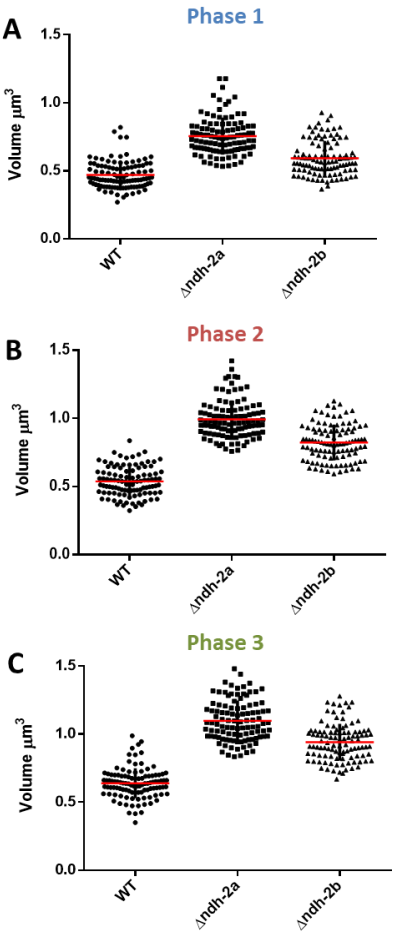

Figure 5.5 Cell volume increases gradually over the entire cell cycle. Cell volume was measured at each phase of the cell cycle of the *S. aureus* WT, Δ*ndh-2a* and Δ*ndh-2b* cells in Phase 1 (A), Phase 2 (B) and Phase 3 (C). Cells increased their volume continuously throughout the cell cycle, from an average volume 0.47 ± 0.1 µm^3 at P1 to an average volume 0.64 ± 0.11 µm^3 at P3 in the case of the WT strain (n = 105 cells for each phase). Scatter plots showing cell size with the median of each distribution indicated by a red line. Scale bars, 1 µm. See table 5.1 for more detail.

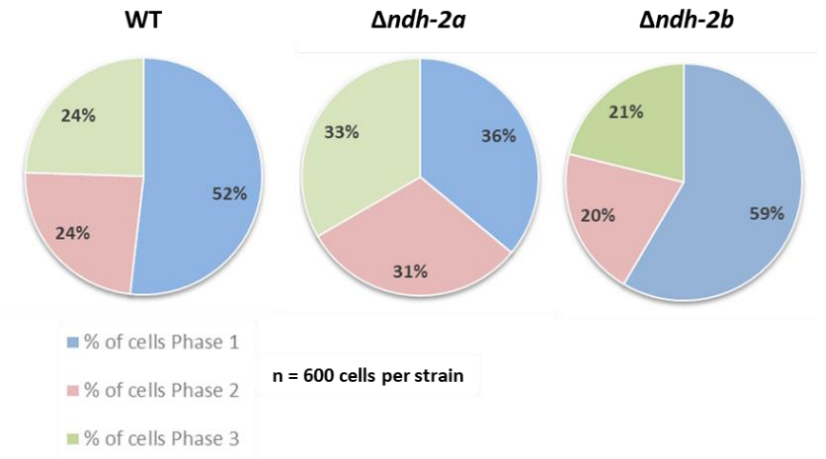

Figure 5.6 Distribution of cell cycle phases of *S. aureus* WT and mutants Δ*ndh-2a* and Δ*ndh-2b* cells. Duration of each phase of the cell cycle was measured in individual cells imaged by SR-SIM. Δ*ndh-2a* strain seems to have longer phases 2 and 3 of cell cycle meaning that cell division may be compromised in this mutant (n= 600 cells per strain).

5.4.4 Δ*ndh-2a* strain excretes high levels of lactate

To investigate the impact of both NDH-2s in the energetic metabolism of *S. aureus*, a thorough NMR-based metabolomics analysis was performed. Figure 5.7 represents the profile of the extracellular metabolites identified and quantified in this study for NCTC8325-4 (wild-type), Δ*ndh-2a* and Δ*ndh-2b* strains, collected from growths in TSB medium under aerobic conditions, shown previously in section 5.4.2. When inspecting the general profile of the excreted metabolites, the trend appears to be similar between the three strains, but a closer inspection shows some differences, for example, in the concentration of lactate, ethanol, and pyruvate (Figure 5.7).

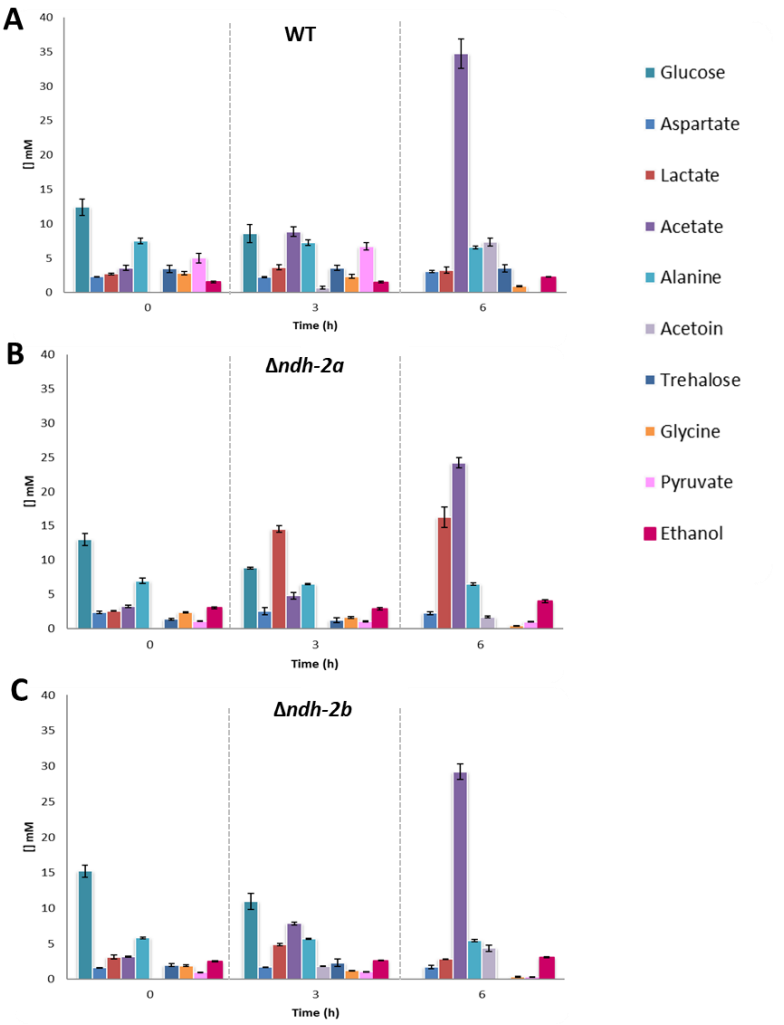

Figure 5.7 Extracellular metabolites identified by ^{1}H-NMR analysis. Bar Graphs representing the concentration of the metabolites identified in the growth *of S. aureus* from 0 to 6 hours for wild-type, Δ*ndh-2a* and Δ*ndh-2b* strains.

We first analyzed the variation of the extracellular metabolites, glucose, acetate, and lactate over 6 hours of *S. aureus* growth with glucose (approximately 14 mM) as the carbon source, in TSB medium (Figure 5.8).

The wild-type, Δ*ndh-2a* and Δ*ndh-2b* strains catabolized all the glucose present in the media between 3 and 6 hours of growth, as observed by a

decrease in glucose concentration (Figure 5.8A). This result agrees with the fact that *S. aureus*, as many other microorganisms, use the glycolytic and the pentose phosphate pathways for the catabolism of glucose (Figure 5.11)[1]. This process, glycolysis, yields two equivalents of pyruvate, generating two molecules of ATP, and reducing two molecules of NAD^+ to NADH (Figure 5.11). When totally oxidized one molecule of glucose originates three molecules of acetate.

In addition, we observe that along glucose consumption, acetate is being produced by all the strains (Figure 5.8B). By 6 hours of growth, 35 mM of acetate is produced by the wild type strain, 30 mM by the Δ*ndh-2b* mutant and 25 mM by the Δ*ndh-2a* mutant. The accumulation of acetate in the culture medium, is probably responsible for the characteristic pH decrease previously observed in all growth curves (Figure 5.3B). Another observation is that, at 6 hours of growth, acetate is still accumulating, leaving in doubt whether acetate will be consumed in the following hours, by the three strains. This doubt is risen by some studies with NCTC-8325-4 strain, showing the inability of this strain to metabolize acetate[2]. In fact, strain NCTC 8325-4 contains an 11-bp deletion in *rsbU*, the gene encoding a positive regulator of the alternative sigma factor σ^B, that plays a crucial role in regulating gene expression in *S. aureus* upon major changes in the environment. The loss of acetate catabolism lead to reduced growth yields relative to strains that do catabolize acetate, and the authors point that in certain situations, like niche adaptation, this decreased growth yield can be profitable[2].

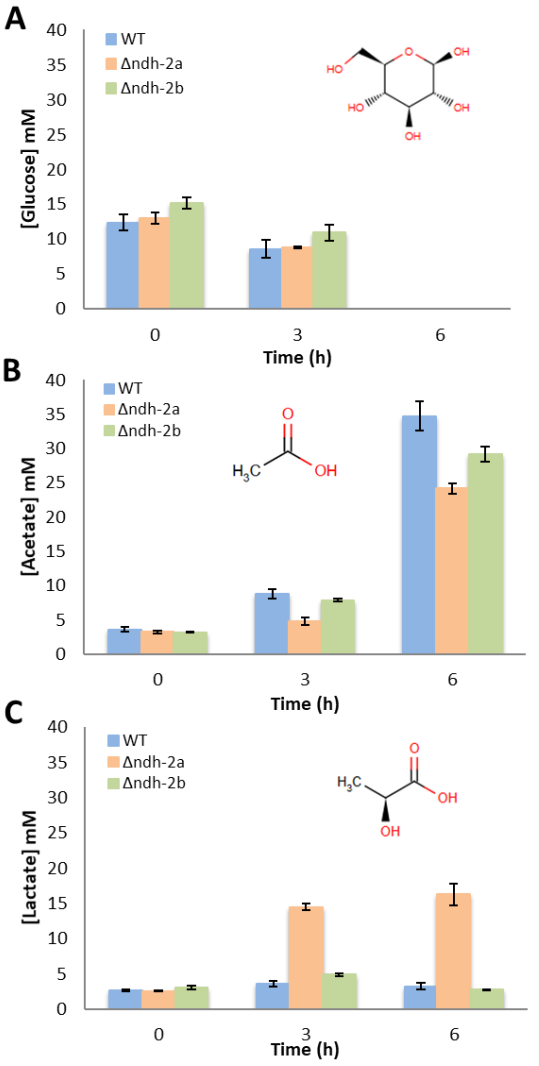

Figure 5.8 Quantification of the main extracellular metabolites, glucose (A), acetate (B) and lactate (C). *S. aureus* wild-type, Δ*ndh-2a* and Δ*ndh-2b* strains were grown in TSB under aerobic conditions, at 1.5-h intervals, an aliquot (1.5 mL) was removed and the glucose, acetate, and lactate concentrations in the culture supernatants were monitored by ^{1}H-NMR.

Lactate is produced by the three strains**,** although the WT and Δ*ndh-2b* strains produce lower amounts of this metabolite (4 mM and 5mM lactate in WT and Δ*ndh-2b,* respectively) than Δ*ndh-2a* strain and the concentration

remains approximately the same along the 6 hours of growth. The mutant strain Δ*ndh-2a* presented a higher accumulation of lactate (approximately 16 mM, 4 times higher) when comparing to the others. (Figure 5.8C). This result reveals a strong phenotype for the Δ*ndh-2a* strain that may have opted a fermentation metabolism by oxidizing glucose to lactate, in which NAD^+ regeneration occurs through NADH:pyruvate oxidoreductase, with production of lactate, to maintain the glycolytic flux. This hypothesis is strengthened by the fact that NDH-2A function is to convert NADH to NAD^+ and, in its absence, *S. aureus* resorts to fermentation to produce NAD^+, so that it can be used again in glycolysis (Figure 5.11). The high production of lactate by Δ*ndh-2a* explains the lower production of acetate by this strain in comparison to the other strains since pyruvate may be being converted into lactate instead of acetate.

In addition, we observe in the Δ*ndh-2a* mutant that the lactate concentration does not change significantly between 3 and 6 hours of growth, but acetate concentration increases in this time interval (Figure 5.8C). The excretion of acetate implies the need to regenerate NAD^+ consumed in glycolysis by the membrane respiratory chain, since NADH is not involved in the conversion of pyruvate to acetate. Therefore, acetate production is linked to aerobic metabolism, and because we observe accumulation of acetate by Δ*ndh-2a* strain from 3 to 6 hour of growth we conclude that this strain resume to respire in that time frame. If this is the case, it means that the function of NDH-2A is being replaced and that this replacement only occurs close to 6 hours of growth. This time is coincident with the reach of a pH value close to 5.5. In fact, there is a large set of genes, as the ones that codify for formate acetyltransferase or pyruvate carboxylase, that are up or down regulated at pH 5.5 [3]. We thus hypothesize that *ndh-2b* gene could also be regulated by the same process of those genes whose expression is sensitive to pH. In this case,

at 6 hours of growth, the pH value is close to pH 5.5 allowing the transcription of *ndh-2b* gene. Therefore, NDH-2B may substitute NDH-2A in these conditions, regenerating NAD^+ through the respiratory chain.

The Δ*ndh-2b* mutant strain has a minor phenotype compared to the WT strain and taking into account what was hypothesized for Δ*ndh-2a* strain, NDH-2B will not be expressed before 6 hours of growth and thus no phenotype is expected for Δ*ndh-2b* until then. Nevertheless, we observe some minor differences in Δ*ndh-2b* mutant strain that we will describe below.

We could also identify and quantify other metabolites as it is the case of acetoin which was produced at higher levels by the wild type strain (7 mM) and at low amounts by both mutant strains (Figure 5.9A). In the case of the Δ*ndh-2a* strain, acetoin was only produced after 6h of growth and in very low amounts (~ 2 mM). The Δ*ndh-2b* mutant started producing acetoin earlier, after 3h, but still the final measured concentration was approximately 4 mM. The excretion of acetoin has physiological meaning to *S. aureus* mainly in the reduction of acidification of the intracellular environment. Moreover, the production of acetoin can contribute to the regeneration of NAD^+, when converted to butanediol. Our hypothesis is that, since we found lower concentrations of acetoin in Δ*ndh-2a* mutant, this strain may already be converting acetoin into butanediol for NAD^+ regeneration. Regarding Δ*ndh-2b* mutant, this strain accumulates more acetoin in comparison to Δ*ndh-2a* mutant, however, less than the WT, suggesting again that the absence of NDH-2B also alters *S. aureus* metabolism. Unfortunately, the production of butanediol was not observed among the extracellular metabolites identified, in any of the strains studied, to further confirm our hypothesis.

Pyruvate was also produced in much higher concentrations by the wild-type strain (7 mM) and consumed after 3h of growth (Figure 5.9B). Upon

inspecting the mutants, they produced only 1 mM of pyruvate, although Δ*ndh-2b* still consumes this metabolite at 6 hours of growth, but Δ*ndh-2a* does not (Figure 5.9B). Here, we can assume that part of the pyruvate is being converted to lactate by NADH:pyruvate oxidoreductase and another part in acetate by pyruvate:quinone oxidoreductase and so we do not observe the accumulation of pyruvate in the mutant strains.

Ethanol was also identified among all the extracellular metabolites and we could observe that Δ*ndh-2a* presented slightly increased concentrations of this product of alcoholic fermentation (4 mM) when compared to the other strains (2 mM by WT and 3mM by Δ*ndh-2b*) (Figure 5.9C). This result shows again that this strain is using alternative pathways to regenerate NAD^+ since, the reduction of acetaldehyde to ethanol, that is catalyzed by the alcohol dehydrogenase (ADH), consumes NADH (Figure 5.9C and Figure 5.11).

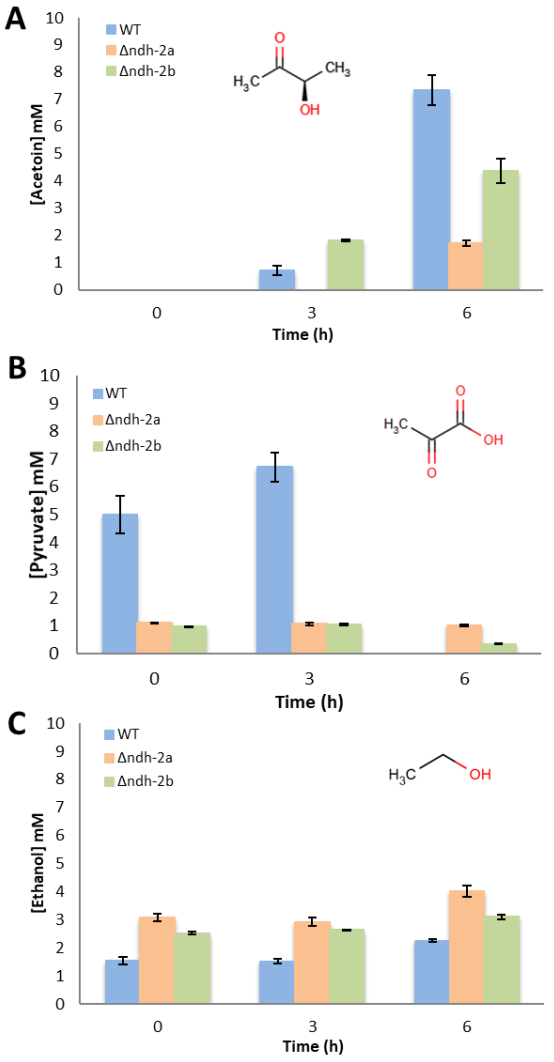

Figure 5.9 Quantification of the extracellular metabolite's acetoin (A), pyruvate (B) and ethanol (C). *S. aureus* wild-type, Δ*ndh-2a* and Δ*ndh-2b* strains were grown in TSB under aerobic conditions, at 1.5-h intervals, an aliquot (1.5 mL) was removed and the acetoin, pyruvate and ethanol concentrations in the culture supernatants were monitored by ^{1}H-NMR.

Figure 5.10 shows trehalose was consumed by the mutant strains after 6h of growth but not by the WT. It is known that *S. aureus* is able to metabolize glycolytic substrates like trehalose, maltose or sucrose in anaerobic

environments[5]. Since the mutant strains have NAD(P)H:quinone oxidoreductase activity impaired (absence of *ndh-2a* or *ndh-2b* genes), they may need to obtain additional energy from other carbohydrates, as it is the case of trehalose (Figure 5.10).

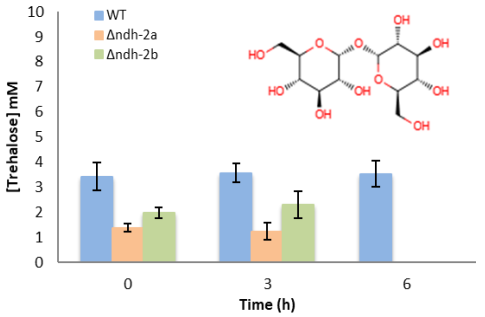

Figure 5.10 Quantification of the extracellular metabolite trehalose. *S. aureus* wild-type, Δ*ndh-2a* and Δ*ndh-2b* strains were grown in TSB under aerobic conditions, at 1.5-h intervals, an aliquot (1.5 mL) was removed and the trehalose concentration in the culture supernatant was monitored by ^{1}H-NMR.

In our study we could identify some amino acids such as alanine, aspartate, and glycine. Alanine and aspartate were not consumed by none of the strains under studied, but we observe the consumption of glycine by all the strains. We have not yet been able to observe any relevant phenotype in the mutant strains connected to amino acid metabolism (Figure S5.4).

This analysis allowed us to conclude that NAD(P)$^{+}$ regeneration is a metabolic requirement for *Staphylococcus aureus*, and when NAD(P)H:quinone oxidoreductase activity is compromised (in the absence of NDH-2s), the organism resorts to alternative pathways fermentation with production of lactate, ethanol and butanediol to proliferate and survive.

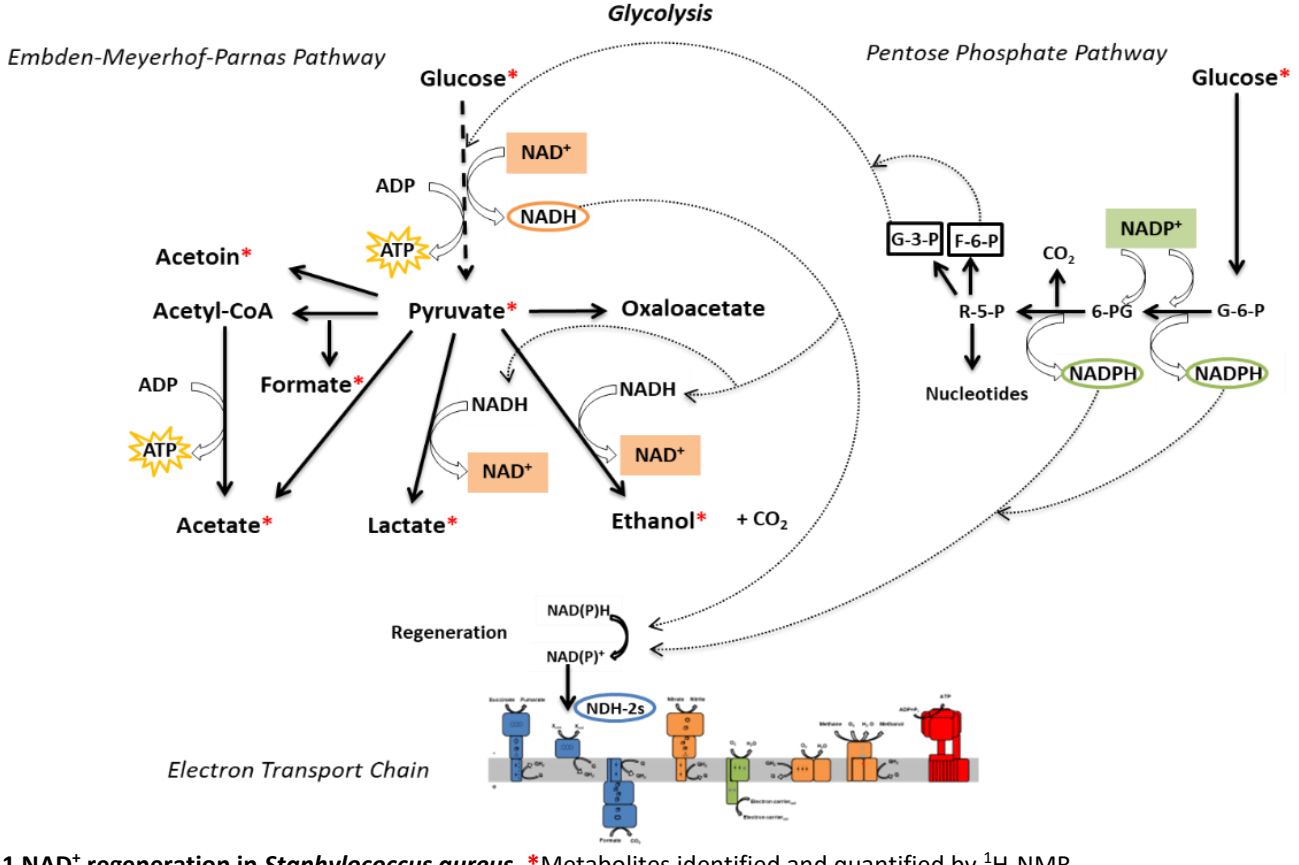

Figure 5.11 NAD$^+$ regeneration in *Staphylococcus aureus*. *Metabolites identified and quantified by ^{1}H-NMR.

5.5 Conclusion

Staphylococcus aureus is an opportunistic pathogen and has become a worldwide problem in clinical medicine due to the increased incidence of its drug resistance. For this reason, it is central to explore and understand the mechanisms behind this resistance, but also the fundamental biological features that allow *S. aureus* to live and survive. We aimed at contributing to this knowledge by exploring respiratory enzymes involved in the respiratory chain of *S. aureus*, specifically NAD(P)H:quinone oxidoreductases (NDH-2s).

This work covers the study of NDH-2s at the cellular level through the design of mNeonGreen reporter constructs expressing a C-terminal NDH-2A-mNeonGreen and an N-terminal NDH-2B-mNeonGreen and, knockout mutants (Δ*ndh-2a* and *Δndh-2b*), in order to study the localization of each enzyme and understand the impact of NDH-2s on the metabolism of *S. aureus*. We observed that NDH-2A-mNeonGreen localizes at the membrane or assembled in foci and is functionally active and NDH-2B-mNeonGreen seems to localize mostly in the cytoplasm. Cell growths of the wild-type and knockout strains showed an evident delay of the Δ*ndh-2a* strain, reaching the lowest OD_{600} value. This result agrees with the recent published study of NDH-2s from *S. aureus* that showed loss of NdhC (NDH-2 that corresponds to NDH-2A), significantly impaired staphylococcal growth when compared to wild-type bacteria[17].

Fluorescence microscopy analysis of the Δ*ndh-2a* and Δ*ndh-2b* strains showed an increase in cell volume in both mutants when compared with wild-type cells that were confirmed by calculating the volume of each cell in each phase (P1, P2 and P3) of *S. aureus* cell cycle. Herein, Δ*ndh-2a* presented more cells in P2 and P3 phases meaning that cell division may be compromised in this mutant. This result can be explained by the fact that Δ*ndh-2a* may have partially opted for a lactate fermentation metabolism, proven by the observed high

levels of lactate excretion by this strain, in which the ATP yield is lower when compared to a strain that is using the NDH-2A from the respiratory chain. Since energy is needed for cell division, Δ*ndh-2a* mutant may have cell cycle impaired due to the low ATP amount available.

We investigated the profile of extracellular metabolites among the three strains (WT, Δ*ndh-2a* and Δ*ndh-2b*) through NMR analysis where main compounds such as glucose, acetate, lactate, as well as acetoin, pyruvate, ethanol, trehalose, alanine, glycine and aspartate were identified and quantified. We conclude Δ*ndh-2a* strain adopts a metabolic strategy that goes through glycolysis and lactate excretion, maximizing the glucose uptake to obtain the most ATP, ensuring NAD^+ regeneration and allowing survival of this mutant strain. The imposed mutation renders the aerobic respiratory chain limiting, thus for glycolysis to proceed and recycling NAD^+ through alternative pathways, being lactate the main fermentation product. This condition adopted by Δ*ndh-2a* mutant agrees with the hypothesis proposed by Schurig-Briccio *et al* who stated that the inability of *S. aureus* Δ*ndhC* to maintain the supply of NAD^+ could result in the conversion of pyruvate to L-Lactate, generating NAD^+ using the lactate dehydrogenase[17]. Nevertheless, we assume NDH-2B enzyme can replace NDH-2A, since at 6h of growth and at lower pH, lactate stops accumulating but acetate concentration is still increasing. Acetate production indicates Δ*ndh-2a* mutant changes to a respiratory metabolism and NAD^+ can be regenerated by NDH-2B. The mutant strain Δ*ndh-2b*, revealed a minor phenotype compared to the wild-type, but by identifying metabolites such as trehalose, pyruvate, ethanol and acetoin, demonstrates that the NDH-2B protein plays an important cellular role in *S. aureus* metabolism, although its expression may be pH dependent and we hypothesize that this enzyme is only expressed after 6 hours of growth.

Altogether the NDH-2s knockouts provide the chance to determine how this pathogenic microorganism behaves and alters its metabolism in response to imposed constraints. Notably the loss of NDH-2A and NDH-2B result in different phenotypes emphasizing that each enzyme has unique cellular roles in the metabolism of *S. aureus*. It is worth mentioning that the NDH-2s are the major enzymes for $NAD(P)^+$ regeneration in *S. aureus*.

It is important to note that growth conditions are critical determinants of the consequences of the knockouts.

This knowledge of the metabolic adaptation strategies of *S. aureus* to environmental and bioenergetics challenges can provide clues to therapeutic strategies that interfere with the ability of the pathogen to successfully adapt when it invades different niches within its host.

5.6 Acknowledgements

We acknowledge Ana Raquel Pereira for helping with the construction of the mNeonGreen and knockout mutants and for the microscopy expriments; Pedro Fernandes and Pedro Pereira for helping with *S. aureus* cell dimensions imaging and calculations and Dr Mariana G Pinho for hosting me in her laboratory. F.V.S. and F.M.S. are recipients of fellowships by Fundação para a Ciência e a Tecnologia (PD/BD/113985/2015, PD/BD/128213/2016, respectively (within the scope of the PhD program Molecular Biosciences PD/00133/2012)).

5.7 References

[1] G.A. Somerville, B. Saïd-Salim, J.M. Wickman, S.J. Raffel, B.N. Kreiswirth, J.M. Musser, Correlation of acetate catabolism and growth yield in *Staphylococcus aureus*: Implications for host-pathogen interactions, Infect. Immun. 71 (2003) 4724–32. https://doi.org/10.1128/IAI.71.8.4724-4732.2003.

[2] C.R. Halsey, S. Lei, J.K. Wax, M.K. Lehman, A.S. Nuxoll, L. Steinke, M. Sadykov, R. Powers, P.D. Fey, Amino acid catabolism in *Staphylococcus aureus* and the function of carbon catabolite repression, MBio. 8 (2017) e01434-16. https://doi.org/10.1128/mBio.01434-16.

[3] D. Zühlke, K. Dörries, J. Bernhardt, S. Maaß, J. Muntel, V. Liebscher, J. Pané-Farré, K. Riedel, M. Lalk, U. Völker, S. Engelmann, D. Becher, S. Fuchs, M. Hecker, Costs of life-Dynamics of the protein inventory of *Staphylococcus aureus* during anaerobiosis, Sci. Rep. 6 (2016). https://doi.org/10.1038/srep28172.

[4] K.C. Strasters, K.C. Winkler, Carbohydrate metabolism of *Staphylococcus aureus*., J. Gen. Microbiol. 33 (1963) 213–29. https://doi.org/10.1099/00221287-33-2-213.

[5] S. Fuchs, J. Pané-Farré, C. Kohler, M. Hecker, S. Engelmann, Anaerobic gene expression in *Staphylococcus aureus*, J. Bacteriol. 189 (2007) 4275–4289. https://doi.org/10.1128/JB.00081-07.

[6] C. Liang, M. Liebeke, R. Schwarz, D. Zühlke, S. Fuchs, L. Menschner, S. Engelmann, C. Wolz, S. Jaglitz, J. Bernhardt, M. Hecker, M. Lalk, T. Dandekar, *Staphylococcus aureus* physiological growth limitations: Insights from flux calculations built on proteomics and external metabolite data, Proteomics. 11 (2011) 1915–35. https://doi.org/10.1002/pmic.201000151.

[7] K. Seidl, S. Müller, P. François, C. Kriebitzsch, J. Schrenzel, S. Engelmann, M. Bischoff, B. Berger-Bächi, Effect of a glucose impulse on the CcpA regulon in *Staphylococcus aureus*, BMC Microbiol. 9 (2009). https://doi.org/10.1186/1471-2180-9-95.

[8] A.R. Richardson†, G.A. Somerville†, A.L. Sonenshein†, Regulating the Intersection of Metabolism and Pathogenesis in Gram-positive Bacteria, Microbiol. Spectr. 3 (2015). https://doi.org/10.1128/microbiolspec.mbp-0004-2014.

[9] B. Görke, J. Stülke, Carbon catabolite repression in bacteria: Many ways to make the most out of nutrients, Nat. Rev. Microbiol. (2008) 613–624. https://doi.org/10.1038/nrmicro1932.

[10] P.N. Refojo, F. V. Sena, F. Calisto, F.M. Sousa, M.M. Pereira, The plethora of membrane

respiratory chains in the phyla of life, Adv. Microb. Physiol. 74 (2019) 331–414. https://doi.org/10.1016/bs.ampbs.2019.03.002.

[11] B.C. Marreiros, F. Calisto, P.J. Castro, A.M. Duarte, F. V. Sena, A.F. Silva, F.M. Sousa, M. Teixeira, P.N. Refojo, M.M. Pereira, Exploring membrane respiratory chains, Biochim. Biophys. Acta - Bioenerg. 1857 (2016) 1039–1067. https://doi.org/10.1016/j.bbabio.2016.03.028.

[12] M. Arnaud, A. Chastanet, M. Débarbouillé, New vector for efficient allelic replacement in naturally nontransformable, low-GC-content, gram-positive bacteria, Appl. Environ. Microbiol. 70 (2004) 6887–91. https://doi.org/10.1128/AEM.70.11.6887-6891.2004.

[13] J.M. Monteiro, P.B. Fernandes, F. Vaz, A.R. Pereira, A.C. Tavares, M.T. Ferreira, P.M. Pereira, H. Veiga, E. Kuru, M.S. Vannieuwenhze, Y. V. Brun, S.R. Filipe, M.G. Pinho, Cell shape dynamics during the staphylococcal cell cycle, Nat. Commun. 6 (2015). https://doi.org/10.1038/ncomms9055.

[14] M.T. Ferreira, A.S. Manso, P. Gaspar, M.G. Pinho, A.R. Neves, Effect of Oxygen on Glucose Metabolism: Utilization of Lactate in *Staphylococcus aureus* as Revealed by In Vivo NMR Studies, PLoS One. 8 (2013) e58277. https://doi.org/10.1371/journal.pone.0058277.

[15] M. Liebeke, H. Meyer, S. Donat, K. Ohlsen, M. Lalk, A metabolomic view of staphylococcus aureus and its ser/thr kinase and phosphatase deletion mutants: Involvement in cell wall biosynthesis, Chem. Biol. 17 (2010) 820–830. https://doi.org/10.1016/j.chembiol.2010.06.012.

[16] N.P. Vitko, M.R. Grosser, D. Khatri, T.R. Lance, A.R. Richardson, Expanded glucose import capability affords *Staphylococcus aureus* optimized glycolytic flux during infection, MBio. 7 (2016) e00296-16. https://doi.org/10.1128/mBio.00296-16.

[17] R.B. Schurig-Briccio, Lici A.; Solorzano, Paola K Parraga;Lencina, Andrea M; Radin, Jana N; Chen, Grischa Y; Sauer, John-Demian; Kehl-Fie, Thomas E; Gennis, Role of respiratory NADH oxidation in the regulation of *Staphylococcus aureus* virulence, EMBO Rep. (2020) e45832.

[18] B.L.M. De Jonge, Y.S. Chang, D. Gage, A. Tomasz, Peptidoglycan composition of a highly methicillin-resistant *Staphylococcus aureus* strain, J. Biol. Chem. 267 (1992) 11248–11254.

[19] I.R. Monk, I.M. Shah, M. Xu, M.W. Tan, T.J. Foster, Transforming the untransformable: Application of direct transformation to manipulate genetically *Staphylococcus aureus* and S*taphylococcus epidermidis*, MBio. 3 (2012) e00277-11.

https://doi.org/10.1128/mBio.00277-11.

5.8 Supplementary Information

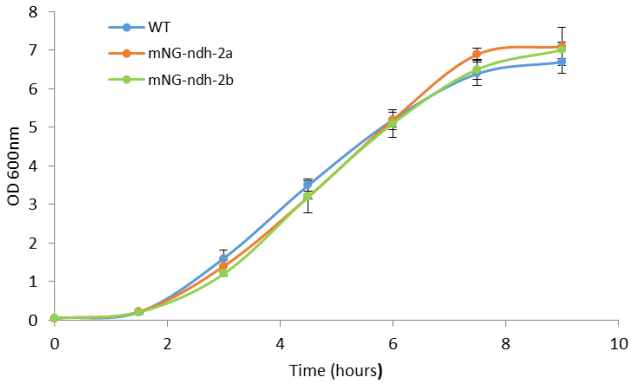

Figure S5.1 Growth of *S. aureus* wild-type strain, *ndh-2a*-mNeonGreen and *ndh-2b*-mNeonGreen fusions strains in TSB (initial OD 0.05, in aerobic conditions). The absorbance at 600 was measured and the results presented are representative of three independent experiments (respective error bars).

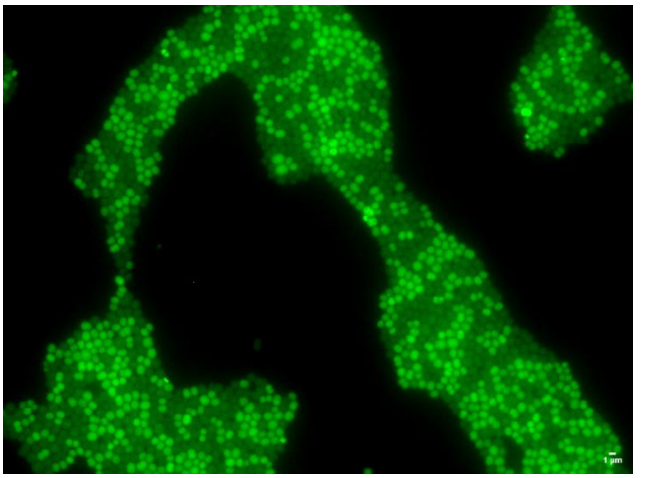

Figure S5.2 Comparison of the localization of mNeonGreen-labelled *ndh-2b* and the WT strain (without the fusion) by fluorescence microscopy. The image shows *ndh-2b*-mNeonGreen signal at the cytoplasm (cocci with more intense fluorescence) and as expected, no localization for the WT strain. Scale bar, 1 µm.

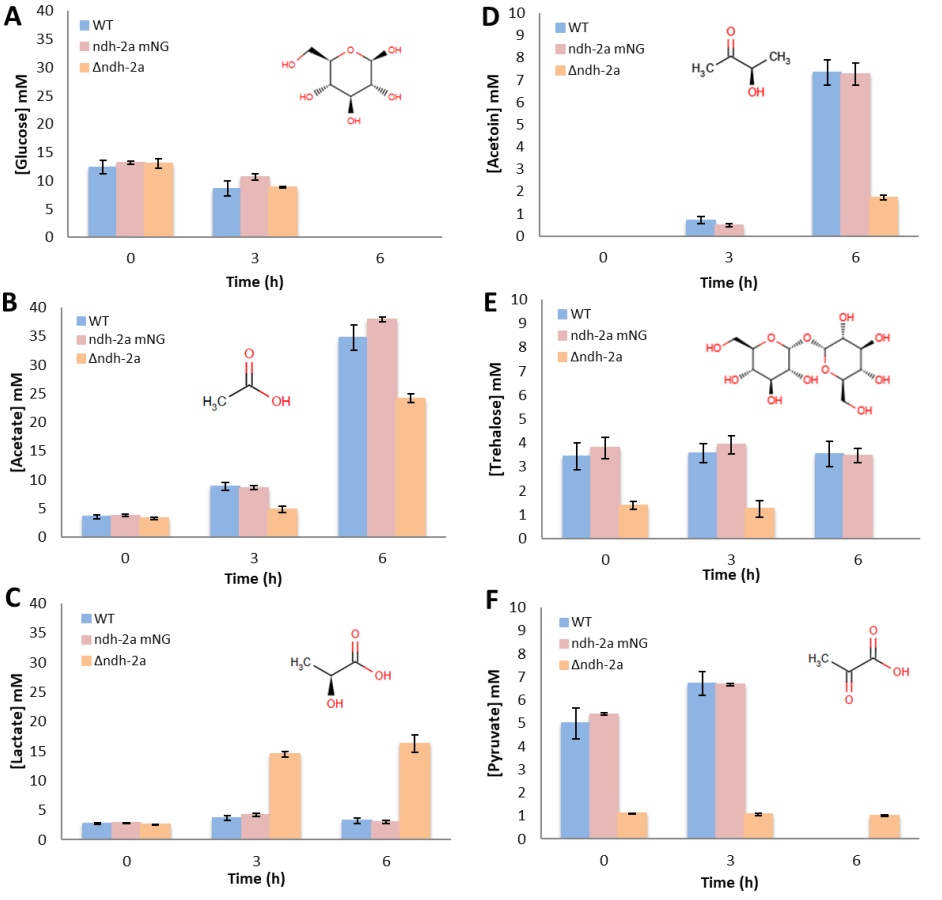

Figure S5.3 Extracellular metabolites excreted from *S. aureus* wild-type strain, WT with NDH-2A fused with mNeonGreen fluorescent protein and Δ*ndh-2a* growths under aerobic conditions, monitored by ^{1}H-NMR. This analysis was performed to prove that the fitness of the strain, with the *ndh-2a*-m-NeonGreen construct, was not affected. **(A)** Glucose **(B)** Acetate **(C)** Lactate **(D)** Acetoin **(E)** Thehalose and **(F)** Pyruvate**.**

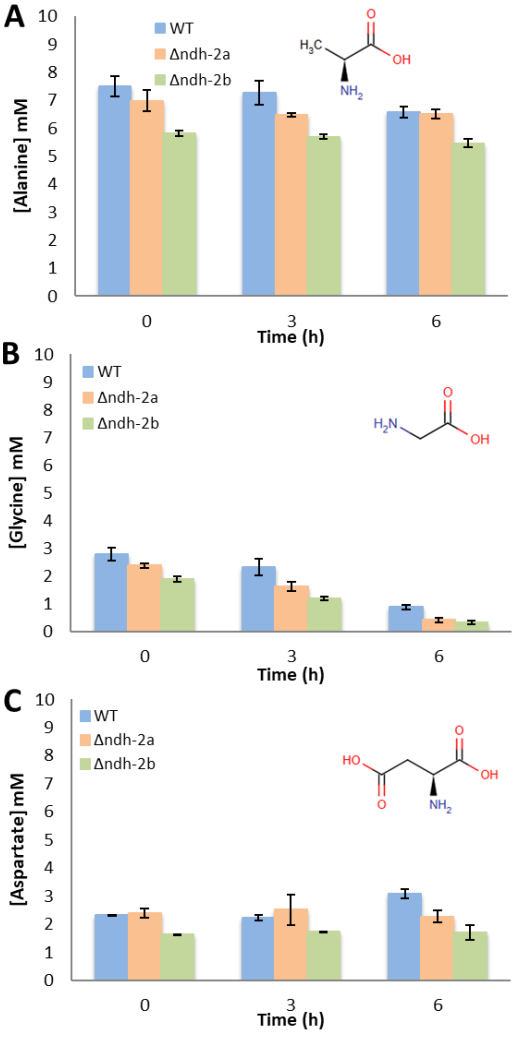

Figure S5.4 Extracellular metabolites excreted from *S. aureus* wild-type, Δ*ndh-2a* and Δ*ndh-2b* growths under aerobic conditions, monitored by ^{1}H-NMR. (A) Alanine **(B)** Glycine **(C)** Aspartate**.**

Table S5.1 Oligonucleotide primers used in this study. Bold sequences represent restriction cut sites.

Primer name	Nucleotide sequence (5'- 3')
p1pMAD-ndh2A_KO	TC**GGATCC**TCAACTGGAAAATGACCCAG
p2pMAD-ndh2A_KO	ACTTTATTTAAAGCTTAATTTCACCTAAGCTTTC
p3pMAD-ndh2A_KO	AATTAAGCTTTAAATAAAGTTTCAGCTAAAC
p4pMAD-ndh2A_KO	ATGCCATGGAACGACATTCGCAGCGCCACAC
p1pMAD-ndh2B_KO	TC**GGATCC**ACCTAAAAATTAAAATACAAATAG
p2pMAD-ndh2B_KO	GGTACTTCATTAATTAAAAAGCAATGTCAGTTC
p3pMAD-ndh2B_KO	CTTTTTAATTAATGAAGTACCCCTTTTATATG
p4pMAD-ndh2B_KO	ATG**CCATGG**TCAAATATGTCCTTAATCGTTATTG
p1pMAD-Neon-ndh2A	TGA**CGTCGA**CTCAACTGGAAAATGACCCAG
p2pMAD-Neon-ndh2A	TTTGATACCATTTAATTTCACCTAAGCTTTC
p3pMAD-Neon-ndh2A	TGAAATTAAATGGTATCAAAAGGTGAAGAAG
p4pMAD-Neon-ndh2A	ACCGCCACCAGATCCACCTCCACCTTTGTATAACTCATCCATGC
p5pMAD-Neon-ndh2A	AGGTGGATCTGGTGGCGGTGGCTCTATGGCTCAAGATCGTAAAAAAG
p6pMAD-Neon-ndh2A	ATG**CCATGG**TAATGTTTTTAGCAACACTTTC
p1pMAD-ndh2A-Neon	GAC**GTCGAC**CTAAAAAGGTAGAAACAAATC
p2pMAD-ndh2A-Neon	CCACCGCCACCAGATCCACCTCCACCGAATTTACCTTTTTTGAATG
p3pMAD-ndh2A-Neon	GGTGGATCTGGTGGCGGTGGCTCTATGGTATCAAAAGGTGAAGAAG
p4pMAD-ndh2A-Neon	TTATTTAAAGCTTATTTGTATAACTCATCCATG
p5pMAD-ndh2A-Neon	ACAAATAAGCTTTAAATAAAGTTTCAGCTA
p6pMAD-ndh2A-Neon	ATG**CCATGG**TACTATAACCACCAGAATCATAC
p1pMAD-ndh2B-Neon	GAC**GTCGAC**ATGAAAAACTTAGTTTTGTTAG
p2pMAD-ndh2A-Neon	ACCGCCACCAGATCCACCTCCACCACCATTATGATATTTATATAAC
p4pMAD-ndh2B-Neon	GCTTTTTAATTTTATTTGTATAACTCATCCATG
p5pMAD-ndh2B-Neon	ATACAAATAAAATTAAAAAGCAATGTCAGTTC
p6pMAD-ndh2B-Neon	A**CCCGGG**ATGGATGAGCAAATTGCGAAAC

p1pMAD-Neon-ndh2B	GAC**GTCGAC**TCAAATATGTCCTTAATCG
p2pMAD-Neon-ndh2B	TTTGATACCATAATGAAGTACCCCTTTTATATG
p3pMAD-Neon-ndh2B	TACTTCATTATGGTATCAAAAGGTGAAGAAG
p5pMAD-Neon-ndh2B	GGTGGATCTGGTGGCGGTGGCTCTATGAAAAACTTAGTTTTGTTA
p6pMAD-Neon-ndh2B	A**CCCGGG**TTAACCATTATGATATTTATATAAC

Table S5.2 Strains and plasmids used in this study.

Strains	**Description**	**Source or reference**
Escherichia coli		
DC10B	Δ*dcm* in the DH10B background; Dam methylation only; for cloning	[18]
Staphylococcus aureus		
RN4220	Restriction-deficient derivative of NCTC8325-4	[19]
NCTC8325-4	Wild-type strain (MSSA)	R. Novik
ndh-2a-mNeonGreen	NCTC8325-4 *ndh-2a::ndh-2a-mneongreen*	This work
ndh-2b-mNeonGreen	NCTC8325-4 *ndh-2b::ndh-2b-mneongreen*	This work
Δ*ndh-2a*	NCTC8325-4 with ndh-2a gene deleted	This work
Δ*ndh-2b*	NCTC8325-4 with ndh-2b gene deleted	This work
Plasmids	**Description**	**Source or reference**
pMAD	*E. coli-S. aureus* shuttle vector with a thermosensitive origin of replication for Gram positive bacteria; Ampr Eryr lacZ	[12]

Table S5.3 Compounds analyzed by ^{1H}-NMR with the chemical shifts and the number of protons. Assignment performed based on the Chenomx Nmr Suite software and on the Biological Magnetic Resonance Data Bank.

Compound	**Chemical Shift (ppm)**		**Protons**
α-Glucose	5.233	Doublet (3Hz)	1
β-Glucose	4.6441	Doublet (7Hz)	
Aspartate	2.78	Doublet	1
Methionine	2.12	Singlet	3
Acetate	1.91	Singlet	3
Alanine	1.47	Doublet	3
Lactate	1.31	Doublet(6.9Hz)	3
Acetoin	1.366	Doublet	3
Trehalose	5.1864	Doublet	1
Glycine	3.55	Singlet	2
Pyruvate	2.36	Singlet	3
Dymethilamine	2.74	Singlet	6
Ethanol	1.2	Triplet	3

Chapter 6

Concluding Remarks and Future Perspectives

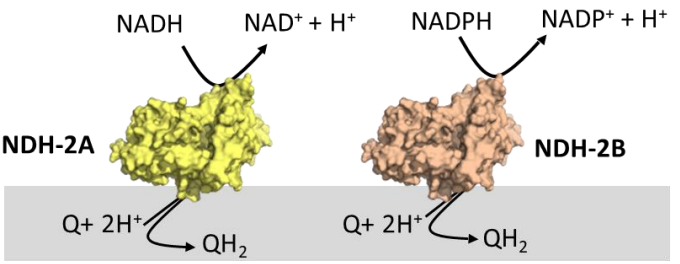

Chapter 6- Concluding Remarks and Future Perspectives

6.1 Concluding Remarks

Regeneration of pyridine nucleotides is central to the metabolism of most microorganisms. This is because almost all catabolic pathways involve NAD^+ or $NADP^+$ as metabolites. Their respective reduced forms NADH or NADPH may be oxidized by respiratory chains through different NADH:quinone oxidoreductases[1]. The energy released by oxidoreduction reactions catalyzed by several respiratory complexes is used by these to establish a transmembrane difference in electrochemical potential, whose dissipation allows the synthesis of ATP, import or export of solutes, and cell motility[2].

Three types of NADH:quinone oxidoreductases are able to regenerate $NAD(P)^+$ through the oxidation of NAD(P)H into $NAD(P)^+$ and the reduction of quinones, these are: type II NADH:quinone oxidoreductase (NDH-2), respiratory Complex I and the sodium-translocating NADH dehydrogenase (Na^+-NQR)[3].

In this thesis, the two NDH-2s of the pathogenic bacterium *Staphylococcus aureus*, NDH-2A and NDH-2B, have been deeply investigated, unraveling their molecular mechanism and their cellular role.

6.1.1 Biochemical and Biophysical investigation of NDH-2s from *Staphylococcus aureus*

The two NDH-2s from *S. aureus,* NDH-2A and NDH-2B, were functionally and structurally characterized as well as the site-directed mutants of NDH-2A, such as $E_{172}A$, $E_{172}S$, $E_{172}Q$ and $E_{172}D$. The oligomerization state of the target proteins, their reduction potential and kinetic parameters such as K_M and V_{MAX} for NADH/NADPH and for the different quinones were determined for the two *S. aureus* enzymes.

We performed extensive kinetic studies, using steady-state and fast kinetics methodologies. The catalytic mechanism, inhibition and the quinone binding site of these enzymes were controversially discussed in the literature, which motivated us to scrutinize their catalytic mechanism, including allostery, by analysing different effects such as concentration of substrates and products, temperature, pH, and concentration of other molecules as HQNO that can inhibit NDH-2s. Moreover, the interaction of NDH-2s with different quinones was investigated using fluorescence and STD-NMR spectroscopies and binding parameters were determined. Fluorescence studies allowed the analysis of the effects of the interaction of the different ligands with NDH-2s at the protein level and, on the other hand, the STD-NMR experiments provided insights into the interaction of the different ligands with NDH-2s at the ligand/substrate level and to perform competition assays between the different ligands/substrates. These studies were crutial to the clarification of the number of binding sites and solve in this way the controverse discussions in the field.

NDH-2A crystallographic structure showed to be typical of the proteins of the flavin disulfide family containing NADH and FAD binding domains and in addition a membrane domain. Our crystal structure also suggests that NADH and the quinone bind at different sites. SAXS measurements showed NDH-2A is a dimer in solution. Our sequence and structural analysis, based on the rationale that conservation of some elements reflects their structural/functional importance, identified relevant amino acid residues, as a series of conserved amino acid residues that can form a proton pathway in each dinucleotide binding domain and may conduct protons from the bulk to the quinone binding pocket. These conserved common elements of NDH-2 reinforce the observation that NDH-2s have independent substrates binding

sites and allowed us to propose the presence of a proton conducting residue at the interface of NADH and quinone pockets.

Our fluorescence and STD data showed that, indeed, NAD(P)H and quinone bind to different sites, in the two studied proteins, NDH-2A and NDH-2B. Furthermore, the data indicated that HQNO only interfered with the binding of the quinone, DMN. HQNO binding seemed not to affect the binding of NADH. These differences reinforce that NADH and quinone interact with the protein in distinct binding sites. Additionaly, we hypothezise the inhibitor, HQNO, binds to a distinct site (nor the NAD(P)H or the quinone bindind site), stabilizing a conformation with less affinity for the quinone, which is possibly also located at the si-side of the isoalloxazine ring of FAD as that of the quinone.

NDH-2A and NDH-2B showed a Michaelis-Menten behavior towards their substrates, NADH and NADPH respectively and the quinones and were both inhibited by HQNO. We observed the formation of a stable charge-transfer (CT) complex upon the reduction of NDH-2A with NADH, which disappears upon oxidation by the quinone. In contrast, we did not observe the formation of a CT complex in NDH-2B upon NADPH reduction. Moreover, we describe for NDH-2A that the presence of the CT complex controls the rate of the second half reaction, being the quinone reduction the limiting step. In NDH-2B, no CT complex is formed and the rate limiting step corresponds to NADPH oxidation. Both processes, the establishment of CT complex in NDH-2A or NADPH oxidation being the limiting step in NDH-2B, may be of equivalent physiological importance and should be further explored. We hypothesize that both processes may contribute to avoid the reduced flavin to react nonspecifically with O_2, preventing the production of ROS in vivo and in this way keeping a low quinol/quinone ratio. We conclude both enzymes have different processes to regulate enzyme reduced state, but it does not imply a different catalytic

mechanism. We proposed the first catalytic mechanism for NDH-2 family that constitutes a solid model to foster debate and inspire the design of future experimental approaches aimed at understanding the molecular mechanism of other members of the two Dinucleotide Binding Domain Flavoprotein superfamily[4]. We also proposed a 'proton gate' key role for the conserved glutamate (E_{172}) localized near the FAD cofactor and NAD(P)H binding site.

6.1.2 Cellular investigation of NDH-2s from *Staphylococcus aureus*

The cellular function of NDH-2s was explored, specifically through the investigation of the localization, by fluorescence microscopy, of the two enzymes of *S. aureus* to each a linker containing a mNeonGreen tag was fused, by its C-terminal and/or N-terminal. The function of each NDH-2 was deeply explored by phenotypic and functional studies using knockout mutants of *S. aureus*.

Our results show that the two mNeonGreen-NDH-2s localized similarly, in the cytoplasm or/and in the membrane, and this can be explained by the fact that these are monotopic enzymes that are attached to the membrane from one side but do not cross the lipid bilayer completely, having no transmembrane domains and can thus appear temporarily in the cytoplasm.

Fluorescence microscopy analysis of the knockout mutants, Δ*ndh-2a* and Δ*ndh-2b* strains showed an increase in cell volume in both mutants when compared with wild-type cells that were confirmed by calculating the volume of each cell in each phase (P1, P2 and P3) of *S. aureus* cell cycle. Herein, Δ*ndh-2a* presented most cells in P2 and P3 phases meaning that cell division might have been compromised in this mutant.

To further investigate the impact of both NDH-2s in the energetic metabolism of *S. aureus*, a thorough NMR-based metabolomics analysis was

performed. We observed that glucose is consumed equally by the WT, Δ*ndh-2a* and Δ*ndh-2b* strains. Throughout the consumption of glucose, acetate was produced by the three strains, but at different levels of concentration and at 6 hours of growth, this metabolite was still accumulating in the culture medium. Lactate was produced in higher concentrations by the mutant Δ*ndh-2a* than in the other strains, revealing a strong phenotype for this strain. We conclude Δ*ndh-2a* strain may have partially opted for fermentation metabolism by oxidizing glucose to lactate, in which NAD^+ regeneration occurs through NADH:pyruvate oxidoreductase to maintain the glycolytic flux. Nevertheless, we assume NDH-2B enzyme can replace NDH-2A in Δ*ndh-2a* strain, since at 6h of growth and at lower pH, lactate stops accumulating but acetate is produced in Δ*ndh-2a* mutant. Since NADH is not used in the pyruvate to acetate pathway, acummulation of acetate is indicative that NADH is being oxidised by the respiratory chain. So we hypothesize that this mutant changes to a respiratory metabolism and NAD^+ can be again regenerated, possibly by NDH-2B. In the case of Δ*ndh-2b* mutant strain, NAD^+ regeneration is assured by NDH-2A since the beginning of the growth.

Altogether the study of the knockouts strains provide the chance to determine how this pathogenic microorganism behaves and alters its metabolism, from respiration to fermentation, in response to imposed constraints (the absence of NDH-2A or NDH-2B). Notably the loss of NDH-2A or NDH-2B result in different phenotypes emphasizing that each enzyme has unique cellular roles in the metabolism of *S. aureus*. It is worth mentioning that the NDH-2s are the major enzymes for $NAD(P)^+$ regeneration in *S. aureus*.

6.2 Future Perspectives

This work contributed to the state of the art on Type II NADH:quinone oxidoreductases from *Staphylococcus aureus*, as they were investigated in structural, functional and cellular terms. The outputs of this thesis may also contribute to more applied areas, such as health as illustrated by the fact that NDH-2 is the only enzyme having NADH:quinone oxidoreductase activity expressed in many pathogenic organisms, such as is the case of *Staphylococcus aureus*. This observation raises the prospect for rational design of specific drugs that interact at the level of this enzyme. In this case, the recognition of the structural/functional determinant elements for the specificity of the binding site for different types of quinones, contribute to that. In addition, since NDH-2 catalyzes the same substrates of complex I, it has been suggested to replace this complex in the case of pathologies in which it is malfunctioning, as in the case of neurodegenerative diseases. In fact, complementation of complex I by NDH-2 has been demonstrated *in vivo* mammalian cells deficient in complex I[5].

As there is no structural information for NDH-2B, efforts are being made to obtain the X-ray structure to get more insights into the structure and function of this enzyme and to compare it with NDH-2A. Additionally, the co-crystallization/soaking of each enzyme (NDH-2A and NDH-2B) with the different substrates/ligands quinone, NADH/NADPH and/or HQNO is vital to unambiguously define where the substrates bind and where the inhibitor interferes. In parallel, we will proceed to deepen structural studies through in silico investigation. In fact, we are using Coarse Grained (CG) molecular dynamics (MD) simulations, which will provide information on dynamics of substrate binding events and on protein-membrane interaction. We will also

tackle the complexity of the Gram-positive membrane, as in the case of *S. aureus*, which has never been simulated before.

Pre-steady state kinetics assays of NDH-2B in the presence of the inhibitor HQNO are missing and will help to understand further deeply the mechanism of inhibition of this quinolone analog and whether it behaves in the same way as in NDH-2A.

Likewise, and since HQNO is not a specific inhibitor for NDH-2s, it also inhibits other enzymes that interact with quinones, the screening of new inhibitors and the study of their kinetic behavior will be of great importance, as these inhibitors may be new antibacterial compounds with a novel mode of action, unlike any existing antibiotic.

Regarding the catalytic mechanism of NDH-2s, hydride transfer is being investigated in our laboratory using modified nicotinamide nucleotides, in this case, NADH labelled with deuterium, [4S-^{2}H]NADH or [4R-^{2}H]NADH, synthesized accordingly with the literature[6]. We have already managed to synthesize one of the compounds ([4R-^{2}H]NADH) and now further experiments will be taken, such as the reaction of [4R-^{2}H]NADH with NDH-2 and quinone. These assays will allow, through NMR, to confirm the hydride transfer, to know which hydride is transferred to FAD and may also unravel how the quinone protonation occurs.

The investigation of the impact of knockout mutants on cell growth will be further explored by using different energy and carbon sources as lactate or acetate. Investigation of intracellular levels of metabolites, such as ATP, NAD(P)$^{+}$/NAD(P)H or acetyl-CoA will be determined using commercial kits and other intracellular metabolites will be identified by Mass spectrometry and HPLC, complementing our NMR-based metabolomics data. In fact, we also collected the intracellular metabolites from the samples obtained from the

growth curves we discussed, and which will be analyzed in the future. To further understand our NMR-based metabolomic data, we are also resorting to mathematical and computational methods to reconstruct metabolic networks of *S. aureus*, so that we can compare the WT with the mutant strains and explore our hypotheses.

Additionally, the effect of the mutations on the expression of each NDH-2 can be also assessed by quantification of mRNA transcripts using real-time PCR.

Protein expression under different conditions and at different growth stages will be evaluated by fluorescence microscopy, using promoter fusions or by flow cytometry analysis using the fluorescence tagged mNeonGreen proteins. This will enable to monitor the localization of the fluorescence target proteins during cell division and will allow addressing the relation of the energetic metabolism with other fundamental cellular processes, such as cell division and cell shape and size.

Overall, this thesis led to an incremental knowledge on NDH-2s in general and specifically on those of *Staphylococcus aureus*. The integrated molecular and cellular perspectives will certainly stimulate intense discussions within the scientific community.

6.3 References

[1] B.C. Marreiros, F. V. Sena, F.M. Sousa, A.P. Batista, M.M. Pereira, Type II NADH:quinone oxidoreductase family: phylogenetic distribution, structural diversity and evolutionary divergences, Environ. Microbiol. 18 (2016) 4697–4709. https://doi.org/10.1111/1462-2920.13352.

[2] P.N. Refojo, F. V. Sena, F. Calisto, F.M. Sousa, M.M. Pereira, The plethora of membrane respiratory chains in the phyla of life, Adv. Microb. Physiol. 74 (2019) 331–414. https://doi.org/10.1016/bs.ampbs.2019.03.002.

[3] S. Kerscher, S. Dröse, V. Zickermann, U. Brandt, The three families of respiratory NADH dehydrogenases, Results Probl. Cell Differ. (2008) 185–222. https://doi.org/10.1007/400_2007_028.

[4] B.C. Marreiros, F. V. Sena, F.M. Sousa, A.S.F. Oliveira, C.M. Soares, A.P. Batista, M.M. Pereira, Structural and Functional insights into the catalytic mechanism of the Type II NADH:quinone oxidoreductase family, Sci. Rep. 7 (2017) 42303. https://doi.org/10.1038/srep42303.

[5] B.S. Byoung, E. Nakamaru-Ogiso, T.R. Flotte, A. Matsuno-Yagi, T. Yagi, In vivo complementation of complex I by the yeast Ndi1 enzyme: Possible application for treatment of Parkinson disease, J. Biol. Chem. 281 (2006) 14250–14255. https://doi.org/10.1074/jbc.M600922200.

[6] G. Ottolina, S. Riva, G. Carrea, B. Danieli, A.F. Buckmann, Enzymatic synthesis of [4R-2H]NAD(P)H and [4S-2H]NAD(P)H and determination of the stereospecificity of 7α- and 12α-hydroxysteroid dehydrogenase, Biochim. Biophys. Acta (BBA)/Protein Struct. Mol. 998 (1989) 173–178. https://doi.org/10.1016/0167-4838(89)90270-7.

Apoio financeiro da FCT e do FSE no âmbito do Quadro Comunitário de Apoio, Bolsa nº PD/BD/113985/2015.

ITQB-UNL | Av. da República, 2780-157 Oeiras, Portugal
Tel (+351) 214 469 100 | Fax (+351) 214 411 277

www.itqb.unl.pt